Capture and Identification of a Novel Protein in the Necrotic Cell Death Pathway,

Toward Discovery of Inhibitors of Human Group III Secreted Phospholipase A2,

Lessons Learned from *In Vivo* Mouse Studies of Secreted Phospholipase A2 Clearance from Extra-Cellular Medium by the M-type Receptor

Heather Noelani Ewing

A dissertation

submitted in partial fulfillment of the

requirements for the degree of

Doctor of Philosophy

University of Washington

2017

Reading Committee:

Michael H. Gelb, Chair

Champak Chatterjee

Robert Synovec

Program Authorized to Offer Degree:

Chemistry

Abstract

Capture and Identification of a Novel Protein in the Necrotic Cell Death Pathway,
Toward Discovery of Inhibitors of Human Group III Secreted Phospholipase A2,
Lessons Learned from *In Vivo* Mouse Studies of Secreted Phospholipase A2 Clearance from Extra-Cellular Medium by the M-type Receptor

Heather Noelani Ewing

Chair of the Supervisory Committee:
Professor Michael H. Gelb
Department of Chemistry

Chapter I. Capture and Identification of a Novel Protein in the Necrotic Cell Death Pathway

The serine hydrolase inhibitors Pyrrophenone and KT195 were found to inhibit cell death induced by A23187 and H_2O_2 in mouse lung fibroblast cells. The effect of Pyrrophenone and KT195 on these processes is not due to inhibition of their known targets, cytosolic phospholipase A2 and α/β-hydrolase domaincontaining (ABHD) 6, respectively, but represents off-target effects. To identify the target/s of Pyrrophenone and KT195, several activity-based protein profiling strategies were employed which were dependent upon the synthesis of derivatives of both compounds. Ultimately, a strategy employing the use of an alkynyl derivative of KT195 to label the protein target followed by click chemistry with biotin azide, enrichment on streptavidin beads, and tryptic peptide analysis by mass spectrometry was able to identify ABHD2, a poorly

characterized enzyme, as the protein target. The results identified a novel mechanism for regulating cell death induced by A23187 and H_2O_2 that involves the serine hydrolase ABHD2.

Chapter II. Toward Discovery of Inhibitors of Human Group III Secreted Phospholipase A2

The development of inhibitors of human group III secreted phospholipase A2 (hGIII-sPLA2) is an important undertaking since this enzyme has been shown to play a role in mast cell function and maturation. Currently, no potent inhibitors of hGIII-sPLA2 have been reported. Herein, we describe the adaptation of a fluorescence-based enzyme activity monitoring method to a high-throughput screening format. The substrate is a BODIPY fluorophore containing phospholipid analogue dispersed as a minor component in non-fluorescent phospholipid vesicles to more closely resemble the natural substrate of hGIII-sPLA2. Cleavage of the BODIPY substrate leads to PLA2 dependent increase in fluorescence. The assay was optimized in both 96-well and 1536-well plate formats and uses optical detection at a wavelength outside of the UV range so as to minimize false-positive hits that result from quenching of the fluorescence. A high-throughput screen was successfully carried out on a library of 370,276 small molecules. Additionally, a panel of known sPLA2 inhibitors was screened using the 96-well plate format. Several hits were discovered, and the resulting data has been uploaded to PubChem. This study describes the first high-throughput optical screening assay for secreted phospholipase A2 inhibitors based on a phospholipid vesicle substrate.

Chapter III. Lessons Learned from *In Vivo* Mouse Studies of Secreted Phospholipase A2 Clearance from Extra-Cellular Medium by the M-type Receptor

The in vivo biological functions of many mammalian secreted phospholipase A2s (sPLA2s) remain to be elucidated, especially with respect to their non-catalytic activity. Among sPLA2 binding proteins, the best known target is the M-type receptor which is hypothesized to play a role in the removal sPLA2s from extracellular fluids such as blood. The binding properties of the full set of mouse sPLA2s to the mouse M-type receptor have been analyzed *in vitro*. Of interest, mGIIA-sPLA2, and mGX-sPLA2 were found to be high-affinity ligands of the M-type mouse receptor. To study *the in vivo* molecular mechanism by which secreted phospholipases A2 are removed from blood, mice containing or lacking the M-type receptor were injected i.v. with secreted phospholipase A2 protein that bore a radioiodine tag as a tracer. The clearance and biodistribution of the radiolabeled sPLA2 was analyzed by radioactive monitoring following the collection of successive blood samples, total excreta collection, and isolation of key organs upon euthanasia. The discovery of *in vivo* deiodination prompted the reimagining of methods to incorporate radioiodine into the sPLA2 proteins. Though we were ultimately unable to complete the study, our efforts detail approaches to avoid in future attempts.

Table of Contents

List of Figures

List of Abbreviations

1D	One-dimensional
2D	Two-dimensional
^{3}H	Tritium
AA	Arachidonic acid
ABHD2	α/β-hydrolase domain-containing 2
ABHD6	α/β-hydrolase domain-containing 6
ABPP	Activity based protein profiling
ATP	Adenosine triphosphate
BEL	Bromoenol lactone
BH	Bolton-Hunter
BOC	tert-butoxy carbonyl
BODIPY	Boron-dipyrromethene
BSA	Bovine serum albumin
BSA	Bovine serum albumin
Ca	Calcium
CDD	Collaborative Drug Discovery
cDNA	Complementary DNA
CID	Compound identifier
cPLA2	Cytosolic phospholipase A2
CRC	Concentration response curve
CsA	Cyclosporin A
CTLD	C-type lectin-like carbohydrate recognition domain
$CuSO_4$-$5H_2O$	Copper(II) sulfate penta-hydrate
CypD	Cyclophilin D
DCC	Dicyclohexyl carbodiimide
DCM	Dichloromethane
DIPEA	Diisopropylethylamine
DMAP	4-Dimethylaminopyridine
DMF	Dimethylformamide
DMSO	Dimethyl sulfoxide
DOPC	Dioleoylphosphatidylcholine
DOPG	Dioleoylphosphatidylglycerol
DUB	Deubiquitylase
EDC	1-ethyl-3-(3-dimethyl-aminopropyl)carboiimide hydrochloride
EGTA	Ethylene-bis(oxyethylenenitrilo)tetraacetic acid
ER	Endoplasmic reticulum
EtOH	Ethanol
FMN	flavin mononucleotide
HCl	Hydrogen chloride
HEPES	4-(2-hydroxyethyl)-1-piperazineethanesulfonic acid

hGIII	Human group III
HOAc	Acetic acid
HOBt	1-hydroxybenzotriazole hydrate
HPLC	High performance liquid chromatography
HTS	High throughput screening
IACUC	Institutional Animal Care and Use Committee
ICD	Isothiocyanatophenyl-*closo*-decaborate(2-) derivative
IEF	Isoelectric focusing
IMLF	Immortalized mouse lung fibroblasts
iPLA2	Calcium independent phospholipase A2
ITLC	Instant thin-layer chromatography
IYD	Iodotyrosine deiodinase
K_2CO_3	Potassium carbonate
KO	Knockout
LAH	Lithium aluminum hydride
LB	Luria broth
LC	Liquid chromatography
LDH	Lactate dehydrogenase
$LiBH_4$	Lithium borohydride
MeOH	Methanol
mGIII	mouse group III
MLF	Mouse lung fibroblasts
MLPCN	Molecular Library Probe production Center Network
MLSMR	Molecular Libraries Small Molecule Repository
MPT	Mitochondrial membrane permeability transition
MPTP	Mitochondrial membrane permeability transition pore
mRNA	messanger RNA
MS	Mass spectrometry
MsCl	Mesyl chloride
MSLCN	Molecular Library Screening Center Network
NaH	Sodium hydride
NaN_3	Sodium azide
NHS	N-Hydroxysuccinimide
NIH	National Institutes of Health
OD	Optical density
PAF-AH	Platelet activating factor acetyl hydrolase
PAINS	Pan Assay Interference Compounds
PBS	Phosphate-buffered saline
$Pd(PPh_3)_4$	Palladium triphenylphosphine
$PdCl_2(dppf)_2$	[1,1′-Bis(diphenylphosphino)ferrocene]dichloropalladium(II)
PGD2	Prostaglandin D2
PLA2	Phospholipase A2
PLA2R	Muscle-type phospholipase A2 receptor

POI	Protein of interest
POI	Protein of interest
PPh_3	Triphenylphosphine
PtO_2	Platinum dioxide
Pyr	Pyrrophenone
rpm	Revolutions per minute
rt	room temperature
SD	Standard deviation
SDS-PAGE	Sodium dodecyl sulfate polyacrylamide gel electrophoresis
SI2B	N-Succinimidyl-3-(3-iodophenyl)propionate
SIB	N-Succinimidyl-3-iiodobenzoate
sPLA2	Secreted phospholipase A2
SRIMSC	Scripps Research Institutes Molecular Screening Center
TAMRA	Tetramethylrhodamine
TBHP	*tert*-Butyl hydroperoxide
tBuOH	tert-butyl alcohol
TEA	Triethylamine
TFA	Trifluoroacetic acid
TFA	Trifluoroacetic acid
THF	Tetrahydrofuran
TLC	Thin-layer chromatography
$TMS-N_3$	Trimethylsilyl azide
Tris	Tris(hydroxymethyl)aminomethane
Ub	Ubiquitin
UBL	Ubiquitin-like protein
UV	Ultraviolet
WT	Wild-type

<u>Units</u>

°	Degree
C	Celsius
p	Pico
n	Nano
µ	Micro
m	Mili
g	Gram
M	Molar
Ci	Curie
k	Kilo
Da	Dalton
mol	Mole
L	Liter
hr	Hour

min	Minute
m	Meter
bar	Bar
dpm	Disintegrations per minute
cpm	Counts per minute
ID/g	Injected dose per gram

ACKNOWLEDGEMENTS

I would like to thank my advisor Michael H. Gelb for his support and guidance, my committee members for their advice and encouragement, and the University of Washington Chemistry Department and the National Institutes of Health for financial support throughout graduate school. My research would not have been possible without the help of numerous lab members, peers, and personnel from the departments of Chemistry, Radiation Safety, Radiation Oncology, Pharmaceutics, and Bioengineering. I would also like to thank my family and friends for their continued love and support.

DEDICATION

To all those who have empowered me to achieve my dreams, especially my son Trysten, my parents Gina and Harold, my grandmother Virginia, my cousin Carrie, my fiancé Justin, and my confidante Bridget.

Introduction

A. Phospholipase A2 Background

Phospholipids are a class of biomolecules that are integral components of cell membranes. They consist of a glycerol backbone linked to two fatty acids and a phosphodiester linkage to a polar molecule (ex. choline, ethanolamine, or inositol.)(*1*) Phospholipases are enzymes that catalyze the hydrolysis of phospholipids. Hydrolysis can occur at multiple sites resulting in four main classifications of phospholipases; A1, A2, C, D (**Figure 1**). The following work deals solely with phospholipase A2 enzymes which selectively cleave the *sn*-2 position of glycero-phospholipids producing a free fatty acid and a lysophospholipid.

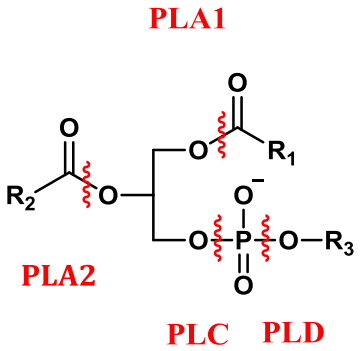

Figure 1. Classification of Phospholipases. Depiction of bond cleavage by the respective phospholipases classified as A1, A2, C, or D. The term phospholipase B applies to enzymes with both A1 and A2 activity.

Phospholipases A2 have been studied extensively since the free fatty acids and lysophospholipids they produce serve a variety of significant physiological roles. One or more of these enzymes is thought to initiate pro-inflammatory cascades by liberation of arachidonic acid (AA) from membrane phospholipids for the biosynthesis of the eicosanoids (prostaglandins and leukotrienes, among others). As a whole, PLA2 family members have been shown to

produce products that are important for signal transduction processes, lipid mediator release, lipid metabolism, and host defense.(*2*)

Phospholipases A2 are further classified into four main categories based on structural features (ex. number of disulfide bonds), size, localization, active site composition, and requirement for calcium.(*1*) These categories include cytosolic (cPLA2), secretory (sPLA2), calcium independent (iPLA2), and platelet activating factor acetyl hydrolase (PAF-AH) (**Figure 2**). Further discussion will focus on cPLA2 and sPLA2 as they are specifically applicable to this research.

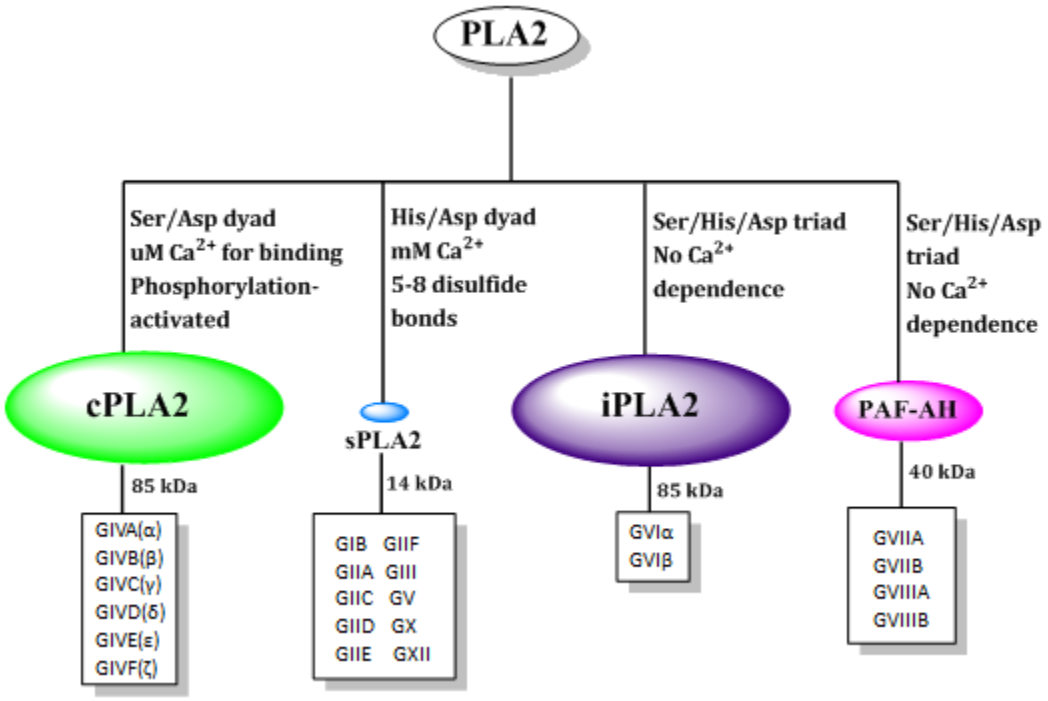

Figure 2. Phospholipase A2 (PLA2) Overview. Family tree of phospholipase A_2. Adapted from (*3*)

B. Cytosolic Phospholipases A2 (cPLA2s)

The cPLA2 family contains six members, α, β, ϒ, δ, ε, and ζ isoforms which are homologous proteins.(*4*) Cytosolic phospholipase A2 (cPLA2) are large (~85 kDa), intracellular, calcium dependent enzymes. The signature of this cPLA2 family is a conserved active site dyad composed of serine and aspartic acid.(*4*) Along with the catalytic domain, cPLA2 also contains a C2 domain referred to as the calcium binding domain. Calcium is necessary for translocation of cPLA2 from the cytosol to intracellular membranes.(*5*)

When calcium concentration in the cell reaches 0.3-1.0 μM, cPLA2 is translocated from the cytosol to intercellular membranes where catalysis takes place.(*5*) The catalytic domain contains an active site serine nucleophile contained within an GXSXG motif.(*2*) Hydrolysis of phospholipid substrates proceeds via serine hydroxyl attack of the substrate ester carbonyl group forming a stable acyl enzyme intermediate. The acyl enzyme is then hydrolyzed by water to yield the free fatty acid. After hydrolysis, cPLA2 may either dissociate from the membrane interface or bind another phospholipid substrate and repeat the catalytic cycle.(*5*)

C. Secreted Phospholipases A2 (sPLA2s)

Secreted phospholipase A2 (sPLA2) are typically relatively small (~14 kDa), extracellular enzymes that require milli molar concentrations of calcium for catalytic activity. Ten mammalian sPLA2s have been identified to date and include group IB, IIA, IIC, IID, IIE, IIF, III, V, X and XIIA.(*6*) Conserved structural features of sPLA2s include 6-8 disulfide bonds, a Ca^{2+} binding loop, and a histidine/aspartic acid catalytic dyad in the active site.(*7*) While sPLA2s do not exhibit a preference for distinct fatty acid acyl chains in the sn-2 position of

glycerophospholipids, some specificity is seen for certain head groups of the phospholipid.(*8*) The various sPLA2s exhibit distinct tissue distribution patterns and unique enzymatic properties suggesting varied biological roles.(*9*)

sPLA2 enzymes act on the lipid-water interface of aggregated phospholipids. Binding of sPLA2s to the membrane surface takes place via an interfacial recognition site made up of hydrophobic and basic residues that surround the buried active site and allow attachment of the enzyme.(*10*) The active site of sPLA2s contains a large hydrophobic channel with Ca^{2+} bound deep in the pocket. Once the phospholipid substrate is bound, hydrolysis proceeds through the activation of a water molecule via a hydrogen bond to histidine, which is adjacent to an aspartate residue. This aspartate, in concert with the calcium binding loop, creates a ligand cage for Ca^{2+}. The Ca^{2+} is essential in the catalytic cycle to stabilize the tetrahedral intermediate formed during hydrolysis of the phospholipid.(*11*)

Research on phospholipases has been a primary focus in the Gelb lab for over 30 years. As such, a number of fruitful collaborations have developed with colleagues at the forefront of this field. The following research is rooted in two such collaborations and covers three areas of study; the identification of a protein involved in necrotic cell death, the search for an inhibitor of human group III secreted phospholipase A2, and the elucidation of the role of the M-type receptor in the removal of sPLA2s from extracellular fluids.

I. Capture and Identification of a Novel Protein in the Necrotic Cell Death Pathway

A. Introduction

Necrotic cell death, or necrosis, is a prevalent form of cell death that has been implicated in a number of diseases such as cancer, cardiac disease, and neurodegenerative disorders.(*12-14*) Though originally thought to be an uncontrolled form of cell death, evidence has emerged indicating that it can be a regulated process.(*15, 16*) Hallmarks of primary necrosis include oxidative stress and calcium overload of the mitochondria. Calcium overload of the mitochondria causes irreversible opening of the mitochondrial permeability transition pore (MPTP), which leads to mitochondrial swelling, depolarization, ATP depletion and membrane permeabilization.(*17, 18*)

The molecular identity of the MPTP has yet to be elucidated however key discoveries have led to a better understanding of signaling pathways involved in pore formation.(*19*) Cyclosporin A (CsA) has been shown to block MPTP formation by targeted inhibition of Cyclophilin D (CypD), a mitochondrial peptidyl prolylisomerase, implicating CypD as a critical regulator of pore formation and necrotic cell death.(*17, 20, 21*) Furthermore, in isolated mitochondria, MPTP formation is accompanied by the release of free fatty acids which suggests that phospholipase A2 may play a role in regulating pore opening.(*22-24*)

Previous studies have implicated two PLA2s in the regulation of MPTP formation. Evidence suggests that calcium independent PLA2 (iPLA2), which localizes to the mitochondria, regulates MPTP formation based on the use of the iPLA2 inhibitor bromoenol lactone (BEL) and using mitochondria from iPLA2 knock-out mice.(*25-29*) Group IVA cytosolic PLA2 (cPLA2α) is also

thought to regulate MPTP formation and cell death by releasing arachidonic acid based on the use of the cPLA2α inhibitor Pyrrophenone.(*29-31*)

The following chapter details the synthesis of inhibitors designed to probe the possible role of PLA2s in MPTP formation and necrotic cell death. The design of inhibitors was adjusted to incorporate various strategies for the capture and identification of proteins, as the identity of a protein of interest (POI) involved in MPTP formation and necrotic cell death was explored. This work was done in collaboration with the lab of Dr. Christina Leslie at National Jewish Health who was responsible for all research conducted with the inhibitors accredited herein.

B. Development of Inhibitors

i. Synthesis of a Pyrrophenone derivative

The importance of cPLA2α in inflammatory diseases makes inhibitors of this enzyme attractive targets as agents to treat inflammatory disorders.(*32-34*) Pyrrophenone was developed as an inhibitor of cPLA2α which has since been shown to possess activity against cPLA2ζ as well.(*35, 36*) Since its discovery, Pyrrophenone has been used to probe the biological role of cPLA2α/ζ in a number of important cellular contexts.(*29, 37-39*) The synthesis of Pyrrophenone has been previously described by Seno et al.(*40*) Since Pyrrophenone was used in preliminary experiments to study the role of cPLA2α in MPTP formation and necrotic cell death, this inhibitor was chosen as a basis for chemical probe design. (*30, 31*)

Activity-based protein profiling relies on the bi-functionality of a chemical probe which is specially designed to both react with its protein target, and to be functionalized with either a

reporter tag (ex. fluorescent or radiochemical) or an affinity label (ex. biotin).(*41*) When designing the chemical scaffold of a probe it is important to place the site of attachment for the reporter distal from the enzyme-reactive moiety. Inhibition of Pyrrophenone likely proceeds via formation of a hemiketal between its ketone carbonyl and the active site serine of the enzyme making any derivitization of the N-pyrrolidine group disadvantageous (**Figure 3**).(*42-44*) Analysis of numerous derivatives of Pyrrophenone indicated that modifications to the triphenyl moiety (**Figure 3**, green) had minimal impact on its ability to inhibit cPLA2α, therefore this site was chosen for derivitization.(*45*)

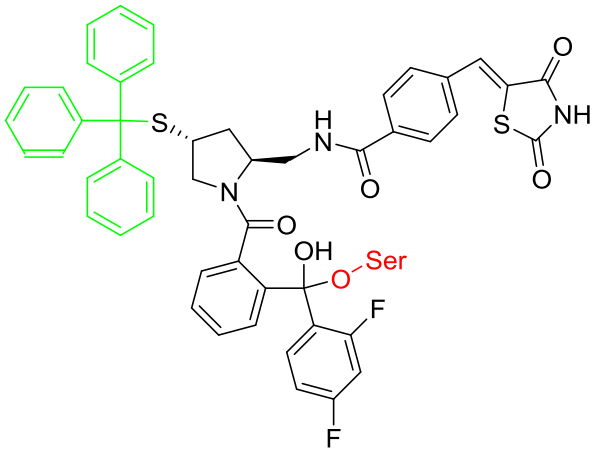

Figure 3. Pyrrophenone chemical probe modification.

The synthesis of Pyrrophenone is accomplished in ten steps and is known to tolerate the presence of a *tert*-butoxycarbonyl BOC-protected secondary amine.(*40*) Hence, we chose to incorporate a protected primary amine moiety, capable of later attachment to either a reporter or affinity label, since we knew protected amines were chemically compatible with the synthetic route to Pyrrophenone. Likewise, a BOC protecting group has been successfully used in the synthesis of Pyrrophenone, and thus the BOC group was chosen as a protecting group for the primary amine.

Retrosynthetic analysis of the triphenyl primary amine tagged Pyrrophenone derivative (**Figure 4**) resulted in two initial fragments; cis-N-Boc-4-hydroxyl-L-proline methyl ester which was commercially available (Sigma-Aldrich #654000) and a triphenyl thiol containing a protected primary amine which would require synthesis. Of note, towards the end of the synthesis, selective modification of the secondary amine of the pyrrolidine ring would need to take place without competing with coupling to the primary amine so that Pyrrophenone could be formed without compromising the ability of the probe to react with a reporter or affinity label. Removal of both BOC groups under standard acidic conditions followed by the selective protection of the primary amine with ethyl trifluoroacetate was chosen as the best method of selective modification.(*46*)

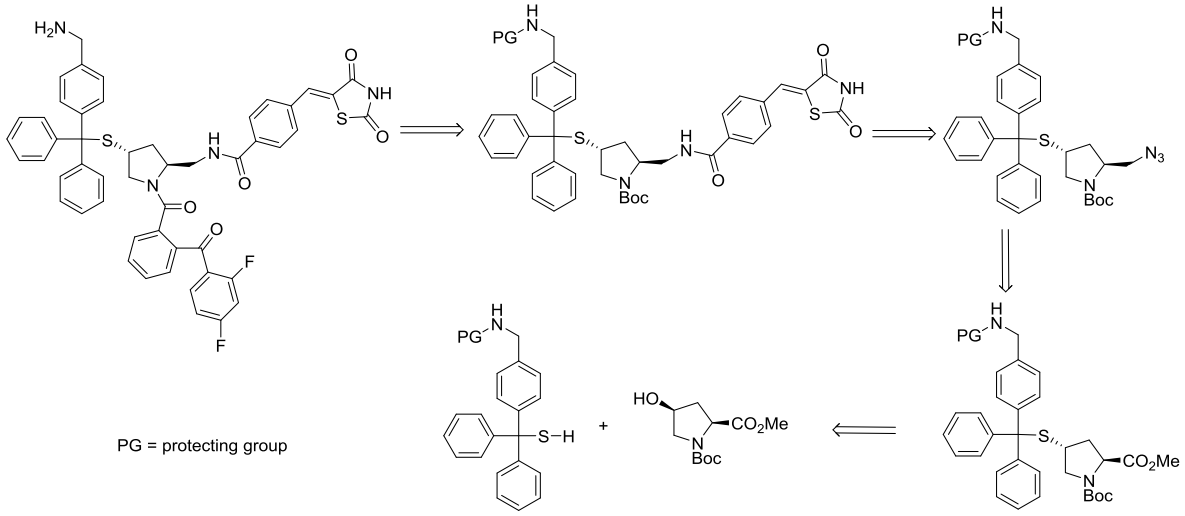

Figure 4. Retrosynthesis of amine tagged Pyrrophenone derivative.

Synthesis of the thiol fragment (**Figure 5**) began with commercially available 4-Bromobenzonitrile (Sigma-Aldrich #B58407) which reacts with n-butyllithium at -100 °C by metal-halogen exchange. The resulting lithiobenzonitrile, stable at -100 °C, can then react with

benzophenone to produce the desired alcohol **1**.(*47*) Reduction with lithium aluminum hydride yielded the primary amine **2**.(*48*) The primary amine was then masked with a BOC group to produce compound **3**. Lawesson's reagent could then be used to convert the alcohol to the desired thiol compound **4**.(*49*)

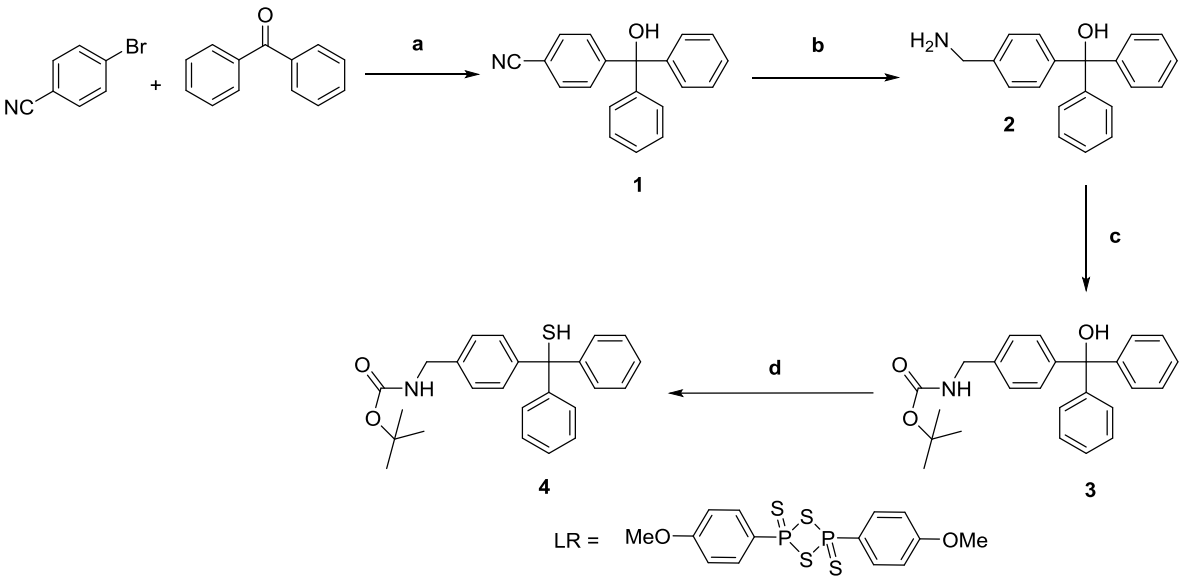

Figure 5. Synthesis of amine tagged triphenyl thiol derivative. (a) n-butyllithium, -100 °C, 5 min; (b) LAH, THF(dry), reflux, 3 hr; (c) BOC-anhydride, DIPEA, DCM, rt, overnight; (d) Lawesson's Reagent (LR), toluene, reflux, 4 hr.

Synthesis of the amine tagged Pyrrophenone derivative was then completed (**Figure 6**).(*40*) Compound **4** was reacted with the mesylate of *cis*-N-Boc-4-hydroxyl-L-proline methyl ester to produce compound **5**. The methyl ester was reduced to an alcohol with lithium borohydride. The alcohol **6** was then converted to the mesylate **7** which was reacted with sodium azide to produce the azide product **8**. A Staudinger reduction was used to convert the azide to an amine **9**, which was then coupled to 4-(2,4-dioxo-thiazolidin-5-ylidenemethyl)-benzoic acid with the aid of coupling agents 1-hydroxybenzotriazole hydrate (HOBT) and 1-ethyl-3-(3-dimethyl-aminopropyl)carboiimide hydrochloride (EDC) to produce compound **10**. Removal of both BOC

groups under acidic conditions was then followed by the selective protection of the primary amine using ethyl trifluoroacetate. With the primary amine protected, the secondary amine is subjected to standard EDC/HOBT coupling with 2-(2,4-difluorobenzoyl)benzoic acid. Then the trifluoroacetamide protecting group was removed under basic conditions to yield the desired Pyrrophenone derivative **14** containing a methyl amine extension that was then capable of being attached to a fluorescent reporter or affinity label.

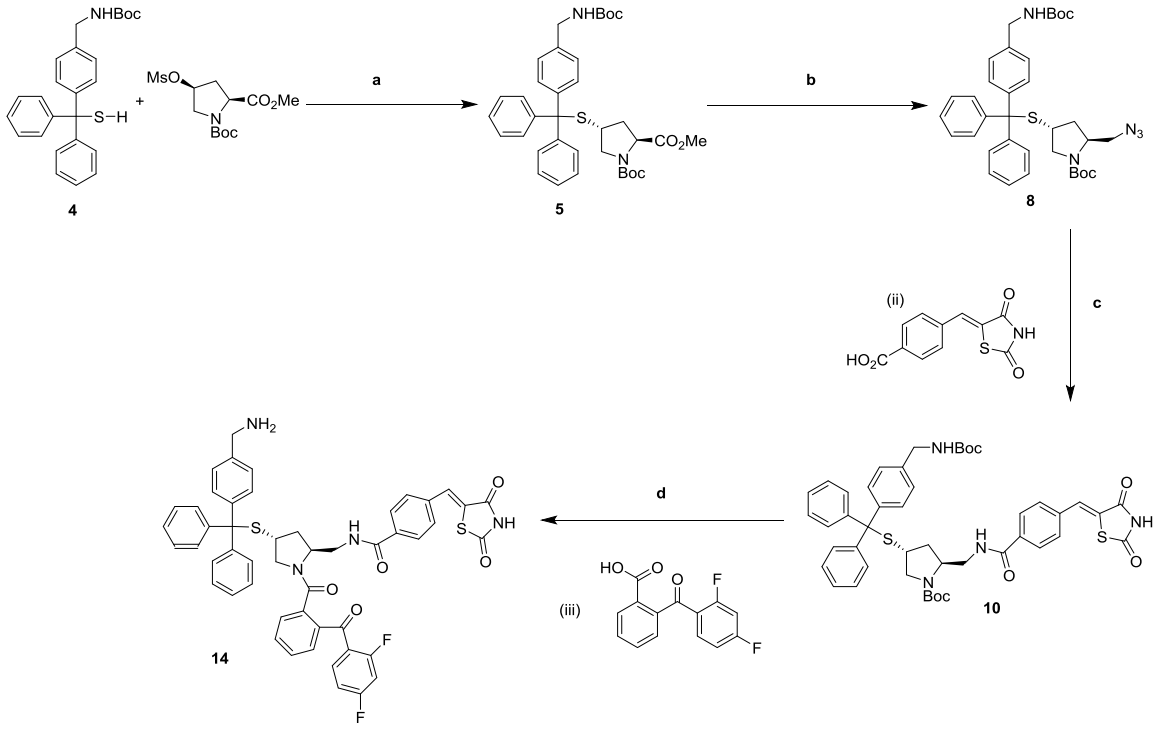

Figure 6. Synthesis of Pyrrophenone derivative. (a) NaH, DMF, 50 °C, 3 hr; (b) (i) $LiBH_4$, THF, 0 °C -rt, 3 hr; (ii) MsCl, TEA, THF, 0 °C, 1 hr; (iii) NaN_3, DMF, 80 °C, overnight; (c) (i) PPh_3, THF, H_2O, rt, overnight; (ii) EDC, HOBt, DMF, rt, 3 hr; (d) (i) 50% TFA/DCM, rt, 2 hr; (ii) TEA, CF_3CO_2ET, DMF, rt, overnight; (iii) EDC, HOBt, DMF, rt, overnight; (iv) K_2CO_3, EtOH, rt, 4 hr.

To date, Pyrrophenone had been the best option for visualization or capture of the POI in A23187-induced necrotic cell death due to its activity, potency, and cell permeability. Though we had planned to conjugate the Pyrrophenone derivative **14** to either fluorophores for

visualization or modified beads for use in pulldown experiments, we were concerned about this strategy of capture since the inhibition of cPLA2α by Pyrrophenone is likely reversible.(*50-52*) We hypothesized that the inhibition of the POI in A23187-induced necrotic cell death, possibly cPLA2α, may also be reversibly bound to our Pyrrophenone derivative, complicating visualization and/or capture strategies. At this time a novel serine hydrolase inhibitor KT195 was discovered, altering our strategy.

ii. Synthesis of KT195

KT195 is a derivative of 1,2,3-triazole urea that inhibits serine hydrolases by covalent, irreversible carbamoylation of the active serine nucleophile.(*29, 50, 51*) KT195 is a known inhibitor of α/β-hydrolase domain containing 6 (ABHD6).(*53*) Once the known targets of Pyrrophenone had been ruled out as the POI in A23187-induced necrotic cell death (see section C.iii.), inhibitors of other serine hydrolases were tested to see if they produced the same effect as Pyrrophenone. Of the many known serine hydrolase inhibitors, KT195 displayed similar inhibition of necrotic cell death to Pyrrophenone with the added feature of its irreversibility. Similarly, KT195 had chemical space known to be modifiable without compromising its target inhibition like Pyrrophenone. The synthesis of KT195 was undertaken, as previously described by Hsu et al., for use in the capture and identification of a POI in A23187-induced necrotic cell death in IMLF.(*50*)

iii. Synthesis of KT195-amine derivative

Since the mechanism of inhibition of KT195 is irreversible, we decided to move forward with POI capture strategies that incorporate KT195 as opposed to Pyrrophenone which is proposed to be a reversible inhibitor. We chose to modify the isolated phenyl ring of KT195 since previous studies had shown that introducing groups at this site did not affect inhibitory activity against ABHD6, a serine hydrolase, α/β-hydrolase domain-containing 6 and known target of KT195.(*53*) In accordance with our previous derivitization of Pyrrophenone, we also chose to attach a primary amine since we had multiple strategies in place for the end-stage fluorescent reporter and/or pulldown functionalization.

Synthesis of a KT195 inhibitor with a methyl amine extension was devised as follows (**Figure 7**).(*50*) Negishi coupling of pyridylzinc bromide with 4-bromobenzonitrile resulted in the formation of 2-(4-cyanophenyl)pyridine **15**. Reduction of the nitrile to the primary amine with LAH followed by hydrogenation of the pyridine ring with platinum oxide under hydrogen atmosphere yielded the diamine compound **16**. As previously discovered during the synthesis of the pyrrolidine-2 derivative, protection of a primary amine in the presence of a secondary amine can be accomplished with ethyl trifluoroacetate which yielded compound **17**. The urea derivative **18** was then formed when the secondary amine was reacted with triphosgene followed by treatment with 4-(4-bromophenyl)-1H-1,2,3-triazole. Suzuki coupling with 4-methoxyphenylboronic acid generated compound **19** and subsequent removal of the TFA protecting group under basic conditions yielded the final compound **20** containing a methyl amine extension that was then capable of being attached to a fluorescent reporter or affinity label.

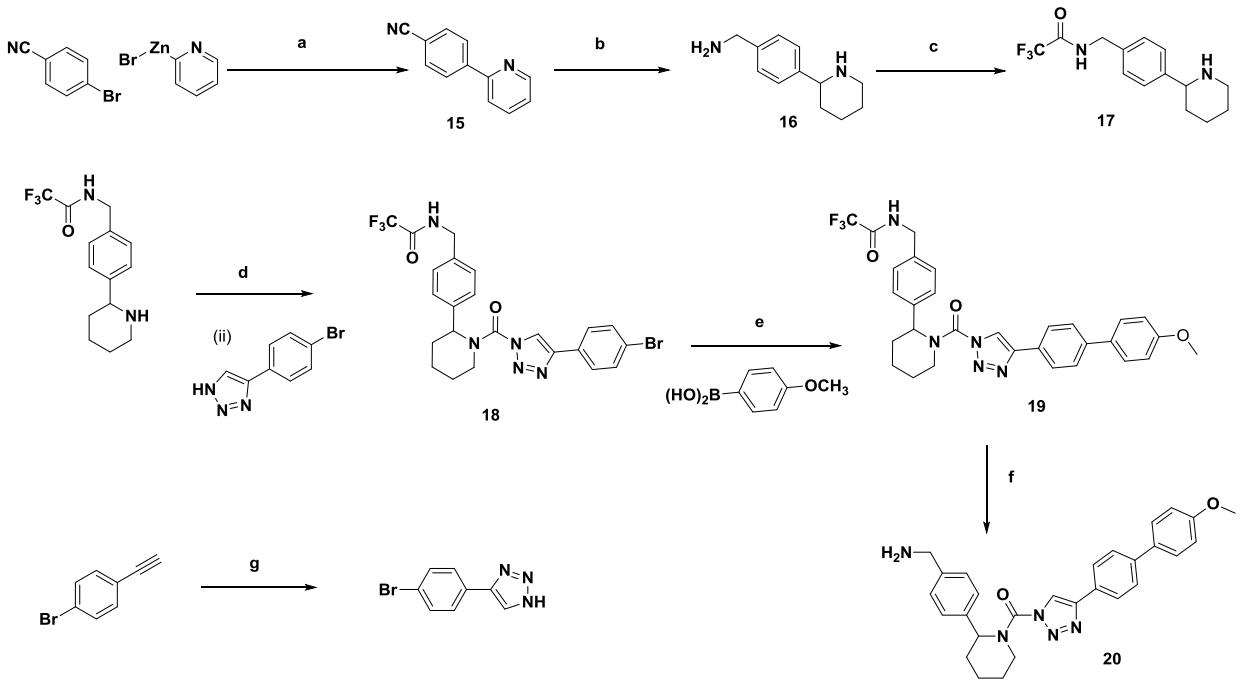

Figure 7. Synthesis of KT195-amine derivative. (a) $Pd(PPh_3)_4$, THF, 65 °C, overnight; (b) PtO_2, HCl, MeOH, H_2 balloon, rt, overnight; (c) CF_3CO_2Et, TEA, DMF, rt, 2 hr; (d) (i) Triphosgene, DIPEA, THF, 4 °C, 30 min; (ii) DIPEA, DMAP, THF, 60°C, 2 hr; (e) $PdCl_2(dppf)_2$, K_2CO_3, dioxane-H_2O, 80 °C, 1 hr; (f) K2CO3, EtOH/H_2O, rt, overnight; (g) TMS-N_3, $CuSO_4$-$5H_2O$, sodium ascorbate/H_2O, tBuOH, 100 °C, overnight.

iv. Synthesis of KT195 fluorophores

One facet of activity-based protein profiling or ABPP utilizes gel-based methods for detection of enzyme activities.(*54-57*) In this approach, KT195-amine would be conjugated to a fluorophore and incubated with A23187-induced IMLF cells, followed by resolution on a one-(1D) or two-dimensional (2D) polyacrylamide gel electrophoresis (PAGE), then the labeled enzymes would be visualized by in-gel fluorescence scanning.(*41*) Synthetic design of KT195-fluorophores focused on two aspects, linker length and type of fluorescent dye. Since the specifics of the interaction of KT195 with the POI were not known, various linker lengths were chosen for testing. BODIPY (4,4-difluoro-4-bora-3a,4a-diaza-s-indacene) dye was chosen since it is

relatively nonpolar, electrically neutral, and has low molecular weight which minimizes dye-induced perturbation of conjugate functional properties and has been shown to be cell permeable.(*58*, *59*)

Five fluorescent analogs of the KT195-amine **20** containing various linker lengths and fluorophores were synthesized. Synthesis of the five fluorescent analogs of KT195-amine **20** was accomplished by EDC/HOBT coupling to the fluorophore succinimide esters **21-25** (**Figure 8**). The TFA protected version of the KT195 derivative **19** was found to be cell permeable and blocked MPTP which looked promising (data not shown). However, none of the resulting fluorescent analogs were found to be cell permeable. Cell permeability of the fluorescent inhibitors was deemed important because interactions between the POI and the inhibitor may be disrupted in a complex mixture like cell lysate. This method of protein visualization was therefore abandoned.

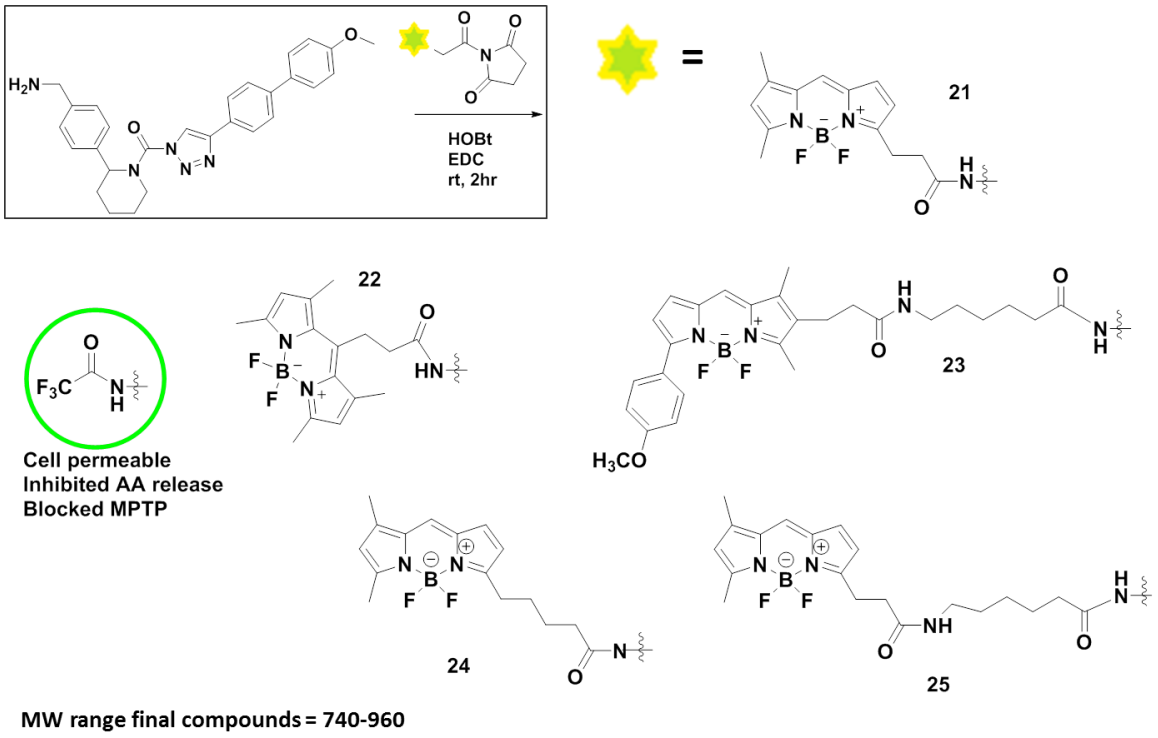

Figure 8. KT195 fluorescent probe design. For synthesis see section E.iii.

v. Synthesis of Halo KT195

A method for getting around the cell permeability of the fluorescently-labeled inhibitors was proposed by utilizing a technique in which a fusion protein is used as a linker between a fluorophore and the POI-inhibitor complex. The ASH Fluorescent Imaging Technique involves a fusion protein that contains AGT, SUMO, and HaloTag proteins termed ASH.(*60*) AGT, a mutant of O^6-alkylguanine-DNA alkyltransferase, is known to undergo an efficient self-labeling reaction with benzylguanine derivatives while HaloTag, an engineered form of Rhodococcus dehalogenases, is known to undergo a self-labeling reaction with alkylchlorides (the utility of the SUMO domain will be discussed later).(*61-64*) Therefore ASH can be labeled uniquely on both the AGT end using a chloropyrimidine derived moiety and on the Halo end using a hexylchloride

tagged moiety (**Figure 9**). For our purposes, we proposed the use of a TAMRA Fluorophore conjugated to chloropyrimidine and added a hexylchloride extension to the KT195 Derivative. The cell permeable KT195-hexylchloride derivative **26**, once bound to the POI inside cells can be fluorescently tagged by conjugation to the ASH fusion protein once cells are lysed.(*60*)

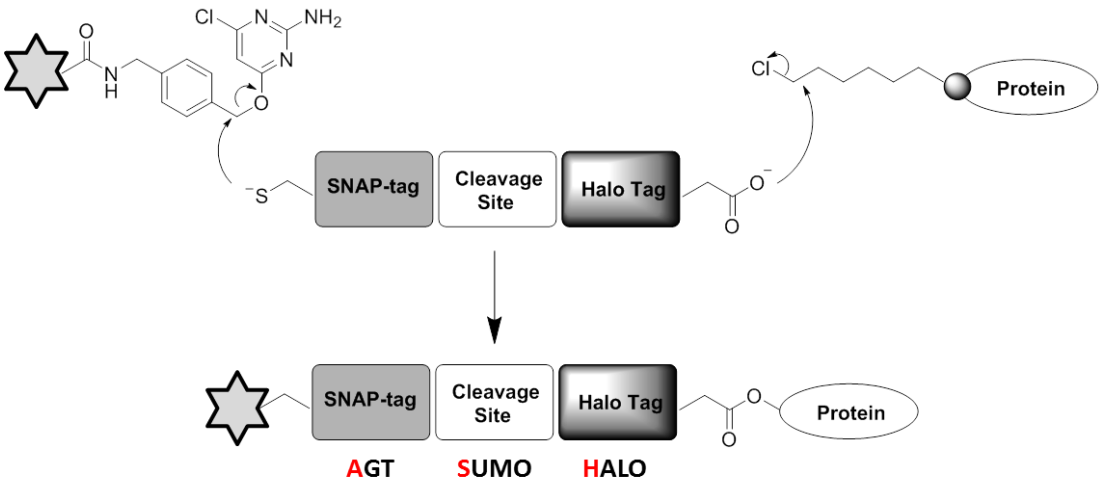

Figure 9. ASH system. Figure adapted from (*60*)

To install the hexylchloride tag on the KT195 derivative **20**, the 2-[2-(6-chlorohexoxy)ethoxy] ethanamine was reacted with succinic anhydride to obtain the carboxylic acid (**Figure 10**). Then standard EDC/HOBT coupling with the KT195-amine **20** yielded the hexylchloride tagged KT195. The KT195-hexylchloride tagged derivative **26** was found to be cell permeable and maintained similar activity to the parent compound in testing with the IMLF cells.

The work flow for the method would begin with labeling the ASH fusion protein with a TAMRA fluorophore, (we chose TAMRA because it was readily available and the proven to work with this technique).(*60*) The KT195-hexylchloride is then incubated with cells where it becomes

irreversibly bound to the POI. The cells are lysed by sonication and then incubated with the TAMRA labeled ASH. A native gel is run and bands found to contain the TAMRA fluorophore and having shifted molecular mass from the TAMRA-ASH fusion protein are isolated. An in-gel trypsin digest is performed and MS analysis can then be used to identify any POI (**Figure 10**).(*60*)

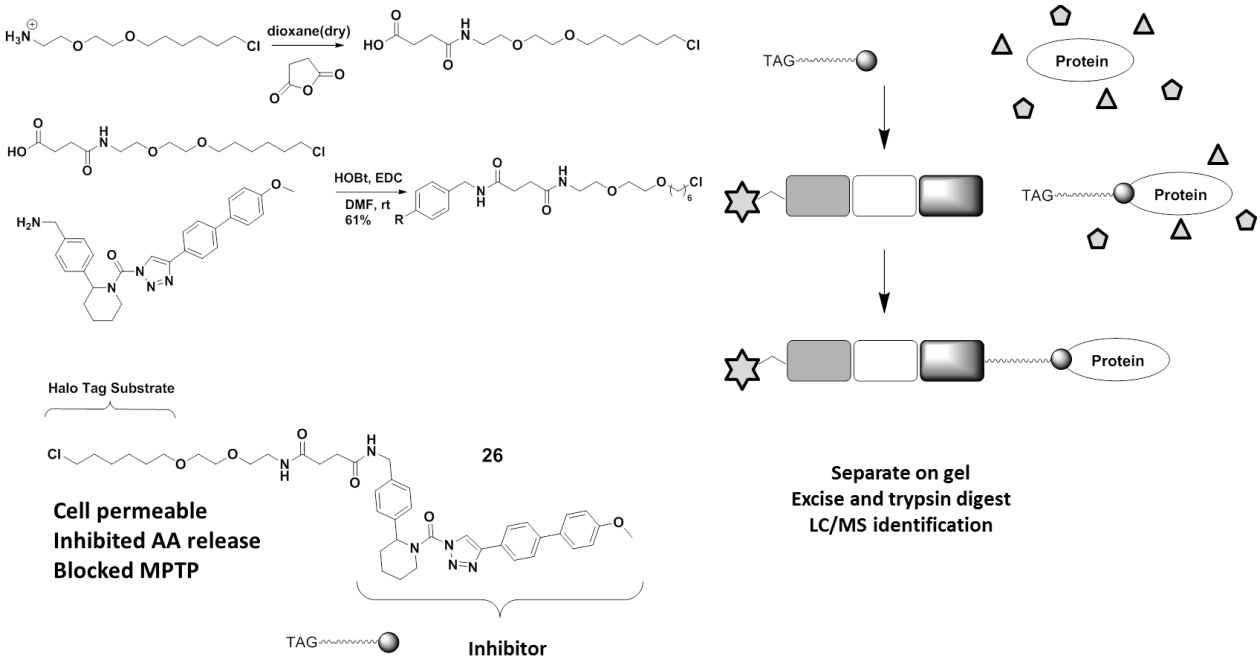

Figure 10. Synthesis of KT195-hexylchloride and work flow TAMRA labeled ASH. Figure adapted from (*60*)

The ASH technique is also amenable to protein capture via conjugation of the chloropyrimidine moiety of AGT to Sepharose beads (**Figure 11**).(*60*) This variation of the ASH technique, AS*H Pulldown System, is employed in a similar manner to the ASH Fluorescent Imaging Technique described above. Instead of conjugating the TAMRA fluorophore to the ASH fusion protein, a Sepharose bead is attached instead. Then, KT195-hexylchloride is incubated with cells

where it becomes irreversibly bound to the POI. The cells are lysed by sonication and then incubated with the AS*H fusion protein attached to Sepharose beads. A series of stringent washes using for example 1% SDS and 6M Urea would be used to disrupt any non-specific protein interactions. The selective release of captured proteins then proceeds by cleavage of the SUMO portion of the fusion protein, SUMO* which was engineered to be recognized only by its companion protease Ulp1* and not native Ulp1 proteases to prevent premature cleavage of HaloTag.(*65*) Once released, trypsin digestion followed by MS analysis would then be used to identify any POI/s (**Figure 11**).(*60, 66*)

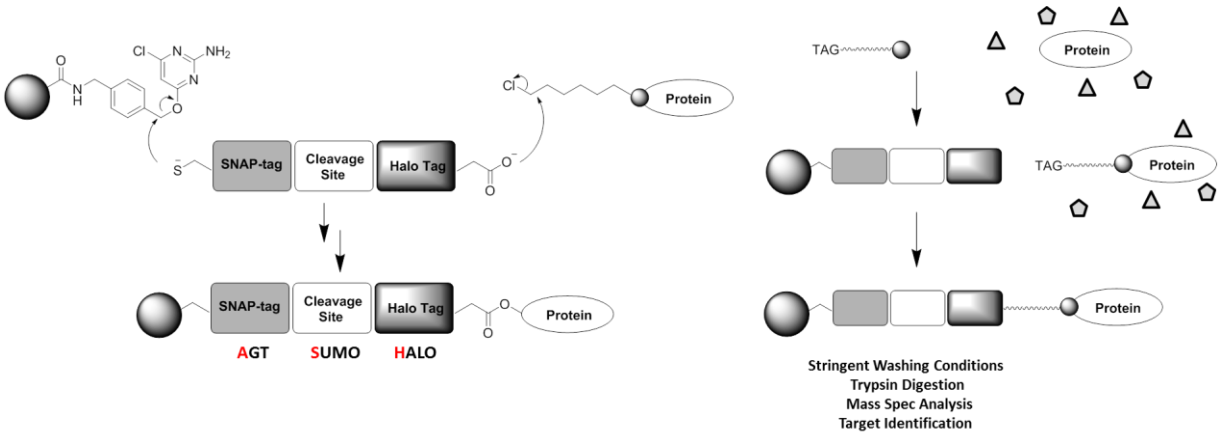

Figure 11. ASH Pulldown System. Figure adapted from (*60*)

Unfortunately, both the ASH pulldown system and the ASH TAMRA tagged system had technical difficulties that rendered them useless for this project. In the case of the ASH pulldown system, selective proteolytic cleavage of the SUMO moiety was not able to be accomplished once the fusion protein was bound to beads. This created a problem since the large fusion protein would generate a large amount of tryptic peptides that would swamp out the

peptides from the POI during MS analysis. The ASH TAMRA tagged system could not be used because when the positive control ABHD6 that KT195-hexylchloride should pull down was tested, there was a significant fluorescent band that obscured any other bands that might have been on the gel rendering analysis impossible. Further testing with these two ASH systems was abandoned.

vi. Synthesis of KT195-alkyne derivative

Success had been achieved in gel-based ABPP using an alkynylated analog of KT195 which was found to be cell permeable and maintained potency toward ABHD6, the know target of KT195.(*53*) Alkynes can react with azides in a bioorthogonal fashion via copper-catalyzed Huisgen's azide-alkyne cycloaddition (click chemistry) to visualize protein targets post-labeling providing us with new avenues for POI capture and identification.(*67, 68*) In theory, KT195-alkyne could be incubated with IMLF, followed by lysis, and then conjugated to either fluorescent dyes or affinity labels via click chemistry.(*69*) Any POI/s could then be visualized via fluorescent gel-based methods or captured and analyzed (for example via conjugation to biotin azide, followed by pulldown with streptavidin beads and LC/MS analysis of tryptic peptides).

We chose to plan a synthetic route starting with 2-(4-bromophenyl)pyridine rather than 2-(4-bromophenyl)piperidine (used in the established synthesis of KT195-alkyne) due to cost and availability. Synthesis of KT195-alkyne began with Suzuki coupling of propargyl alcohol to 2-(4-bromophenyl)pyridine (**Figure 12**).(*53*) Reduction of the alkyne by palladium hydroxide on carbon under hydrogen atmosphere followed by selective reduction (via careful monitoring) of

the pyridine ring in the presence of the phenyl ring by platinum oxide under hydrogen atmosphere and subsequent BOC protection of the piperidine moiety yields compound **30**. The primary alcohol was reacted with propargyl bromide to yield compound **32**. Urea coupling with triazole **35** then resulted in the desired KT195-alkyne derivative **36**. The other partner in the urea coupling was synthesized by Suzuki coupling of ethynyl trimethyl silane to 4-(4-bromophenyl)methoxy benzene. Removal of TMS under basic conditions and triazole formation via coupling to trimethylsilyl azide yielded compound **35** (**Figure 12**). Fortunately, KT195-alkyne inhibited necrotic cell death (LDH release) induced by A23187 in IMLF cells with similar potency to the parent KT195 inhibitor (1.5 μM vs 0.7 μM respectively) and was then successfully employed to determine the POI in A23187-induced necrotic cell death (see section C.vii.).

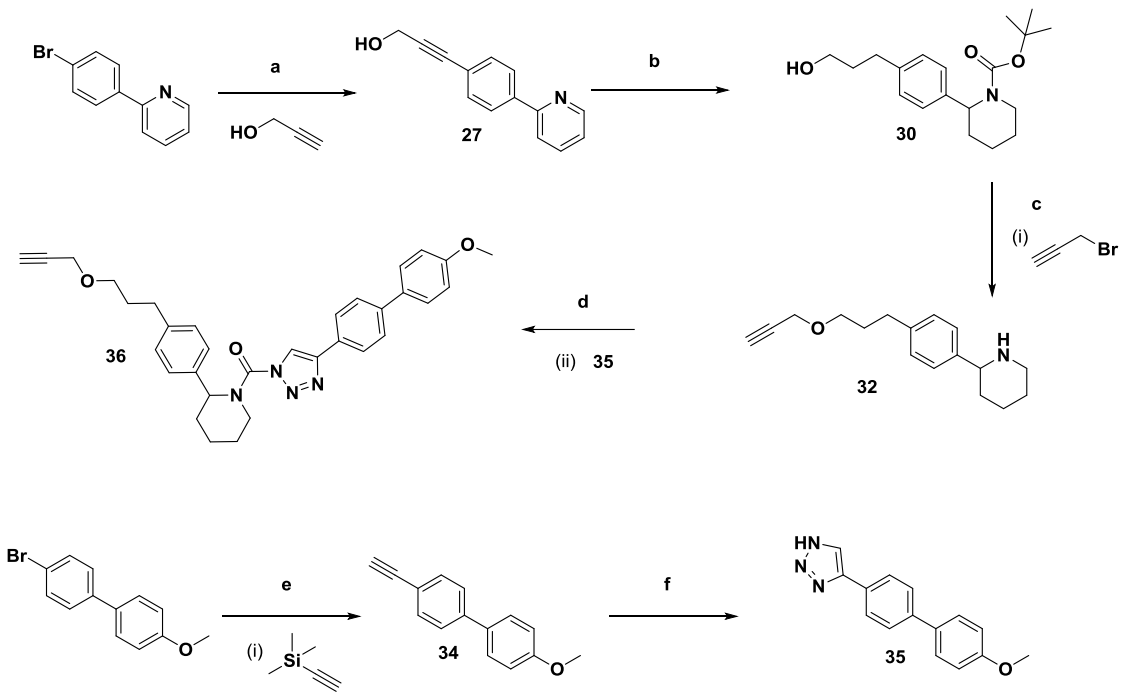

Figure 12. Synthesis of KT195-alkyne derivative. (a) $Pd(PPh_3)_4$, DBU, CuI, THF, 90 °C, 4 hr; (b) (i) $Pd(OH)_2$, MeOH, H_2 balloon, rt, overnight; (ii) PtO_2, HCl conc., MeOH, H2 balloon, rt, overnight; (iii) BOC2O, DIPEA, DCM:MeOH(1:1), rt, overnight; (c) (i) NaH, toluene, DMF, THF, 0 °C – rt, 3 hr; (ii) 50% TFA/DCM, rt, 2 hr; (d) (i) Triphosgene, DIPEA, THF, 4 °C, 30 min; (ii) DIPEA, DMAP, THF, 60 °C, 2 hr; (e) (i) $PdCl_2(PPh_3)_2$, CuI, PPh3, piperidine, 120 °C, 12 min; (ii) K_2CO_3, THF/MeOH, rt, 2 hr; (f) TMS-N_3, CuI, DMF:MeOH (9:1), 100 °C, overnight.

C. Applications of Inhibitors

i. Arachidonic acid release that accompanies A23187-induced necrotic cell death in lung fibroblasts is not mediated by cPLA2α

To probe the involvement of cPLA2α in MPTP formation and necrotic cell death, immortalized mouse lung fibroblast (IMLF) cells were obtained from cPLA2$\alpha^{+/+}$ (IMLF$\alpha^{+/+}$) and cPLA2$\alpha^{-/-}$ (IMLF$\alpha^{-/-}$) mice.(*29*) Necrotic cell death can be evidenced by markers of damage to the cell membrane. A common marker of plasma membrane damage is lactate dehydrogenase (LDH), a soluble cytoplasmic enzyme present in nearly all cells which is released into the extracellular

space when damage to the plasma membrane occurs.(*70*) The calcium ionophore A23187 is a well-known inducer of necrotic cell death due to cellular calcium overload and MPTP formation resulting in plasma membrane rupture and LDH release.(*17, 71*) A23187 was found to stimulate LDH release and ^{3}H-arachidonic acid release (to a lesser but significant extent in cPLA2α$^{-/-}$) from both cPLA2α$^{+/+}$ and cPLA2α$^{-/-}$ IMLF cells (**Figure 13**).(*29, 72*) In both cell lines, CsA and EGTA (a calcium chelating agent) inhibited LDH release which is consistent with a role for CypD-dependent MPTP formation due to calcium overload (**Figure 13**).(*29*) Taken together these data suggest that A23187-stimulated cell death and arachidonic acid release in lung fibroblasts requires extracellular calcium and is mediated by cyclophilin-D-dependent MPTP formation but does not involve cPLA2α.

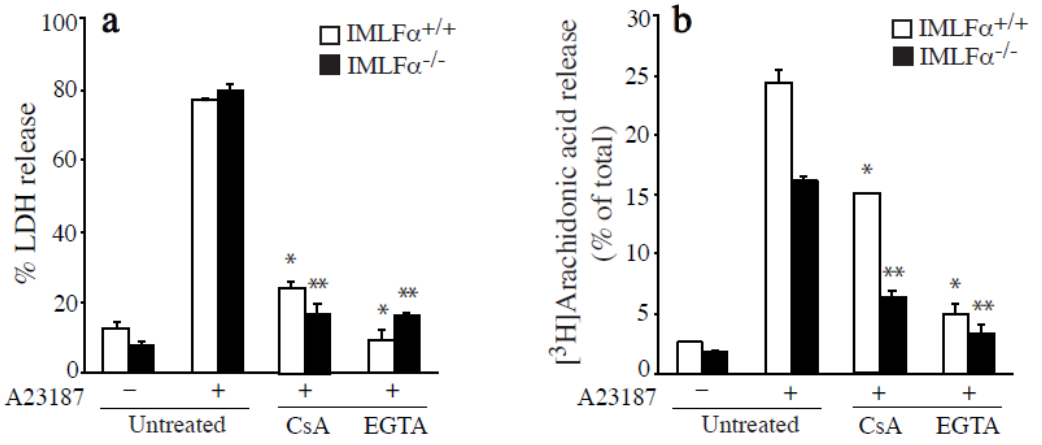

Figure 13. A23187 induces necrotic cell death and [^{3}H]arachidonic acid release independent of cPLA2α. Release of LDH (a) and [^{3}H]arachidonic acid (b) from IMLFα$^{+/+}$ (open bars) and IMLFα$^{-/-}$ (black bars) stimulated with A23187 (1 µg/ml) for 30 min was determined. Cells were treated with CsA or incubated in medium containing EGTA, for 30 min prior to stimulation with A23187. The results are from 3 independent experiments ± S.E. ($p < 0.0001$ when compared with A23187 stimulated IMLFα$^{+/+}$ (*) or IMLFα$^{-/-}$ (**) without inhibitors).(*29*)

ii. Serine hydrolase inhibitors block arachidonic acid release, MPTP formation and cell death in cPLA2α$^{-/-}$ IMLF cells

In pretreated cPLA2α$^{-/-}$ IMLF cells stimulated with A23187, both AA release (*73*) and LDH release (**Figure 14a**) were blocked by the cPLA2α inhibitors Pyrrophenone (Pry) and Wyethy-1 but not the iPLA2 inhibitor BEL which indicates that iPLA2 is not involved in A23187-induced necrotic cell death.

The effect of inhibitors on A23187-induced MPTP formation was further studied using an established method that monitors calcein fluorescence in mitochondria.(*29*, *74*) In brief, cells were pretreated with calcein, a membrane permeable fluorescent dye that is selective for calcium. Cobalt(II)chloride, which strongly quenches the fluorescence of Ca^{2+}-calcein, was then added to the culture medium. Cobalt(II)chloride is able to cross the plasma membrane of healthy cells but it is incapable of crossing an intact mitochondrial double membrane. Therefore, in healthy cells only the mitochondria are fluorescent since cobalt(II)chloride cannot cross the mitochondrial membrane and quench the Ca^{2+}-calcein. However, after MPTP formation, the mitochondrial membrane is permeable to cobalt(II)chloride, quenching the Ca^{2+}-calcein and resulting in loss of fluorescence. This technique was used on cPLA2α$^{-/-}$ IMLF cells with and without pretreatment with A23187. Cells treated with only A23187 showed a decrease in mitochondrial calcein fluorescence consistent with MPTP formation (**Figure 14b**).(*29*) However, cells pretreated with either Pry, Wyeth-1, or CsA (the known positive control) maintained robust mitochondrial calcein fluorescence and healthy cell morphology (**Figure 14b**) which indicates that both of these inhibitors block MPTP formation.(*29*)

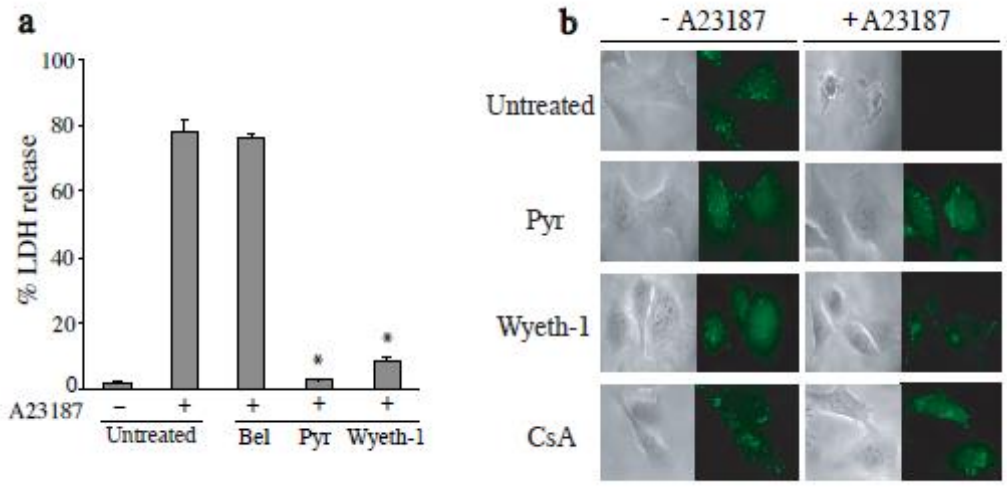

FIGURE 14. A23187-induced MPTP formation and cell death in IMLFα$^{-/-}$ are blocked by Pyrrophenone and Wyeth-1 but not bromoenolactone. (a) IMLFα$^{-/-}$ incubated with DMSO (untreated), 10 μM Pyrrophenone (Pyr), Wyeth-1, or bromoenolactone (Bel) for 30 min were stimulated with A23187 for 30 min and LDH release was determined (n = 3 ± S.E., *, $p < 0.0001$ when compared with A23187-stimulated IMLF/ without inhibitors). (b) calcein-labeled IMLFα$^{-/-}$ were treated with vehicle (DMSO), or 10 μM Pyr, Wyeth-1, or CsA for 30 min and then stimulated with A23187 for 30 min. After adding cobalt, fluorescence microscopy was used to monitor calcein fluorescence in the mitochondria, and bright field microscopy was used to evaluate cell integrity. Images are from a representative experiment and results confirmed in 3 independent experiments. Adapted from (*29*)

iii. A23187-induced cell death in primary mouse lung fibroblasts (MLF) is not mediated by cPLA2α or cPLA2ζ

Similar experiments using A23187-induced cell death were then performed on primary mouse lung fibroblasts to confirm the earlier results and to rule out other cPLA2s. Primary mouse lung fibroblast (MLF) cells were obtained from cPLA2α$^{+/+}$ (MLFα$^{+/+}$) and cPLA2α$^{-/-}$ (MLFα$^{-/-}$) mice.(*29*) MLF cells stimulated with A23187 showed more AA release from MLFα$^{+/+}$ than MLFα$^{-/-}$ but similar amounts of LDH release which were inhibited by Pyr and CsA (**Figure 15a**).(*29*) These results indicate that cPLA2α contributes to AA release but not cell death in the A23187-treated MLF cells tested.

It was previously reported that Pyr also inhibits another isoform of cPLA2, cPLA2ζ.(*75*) Primary mouse lung fibroblast (MLF) cells were also obtained from cPLA2ζ$^{+/+}$ (MLFζ$^{+/+}$) and cPLA2ζ$^{-/-}$ (MLFζ$^{-/-}$) mice.(*29*) These cells were stimulated with A23187 and no differences were observed in AA release or LHD release, or in response pre-incubation with Pyr or CsA (**Figure 15b**).(*29*) These results along with a comparison of MLF from wild type and cPLA2α/cPLA2ζ double knock-out mice confirmed that these PLA2s do not mediate cell death induced by A23187.(*29*)

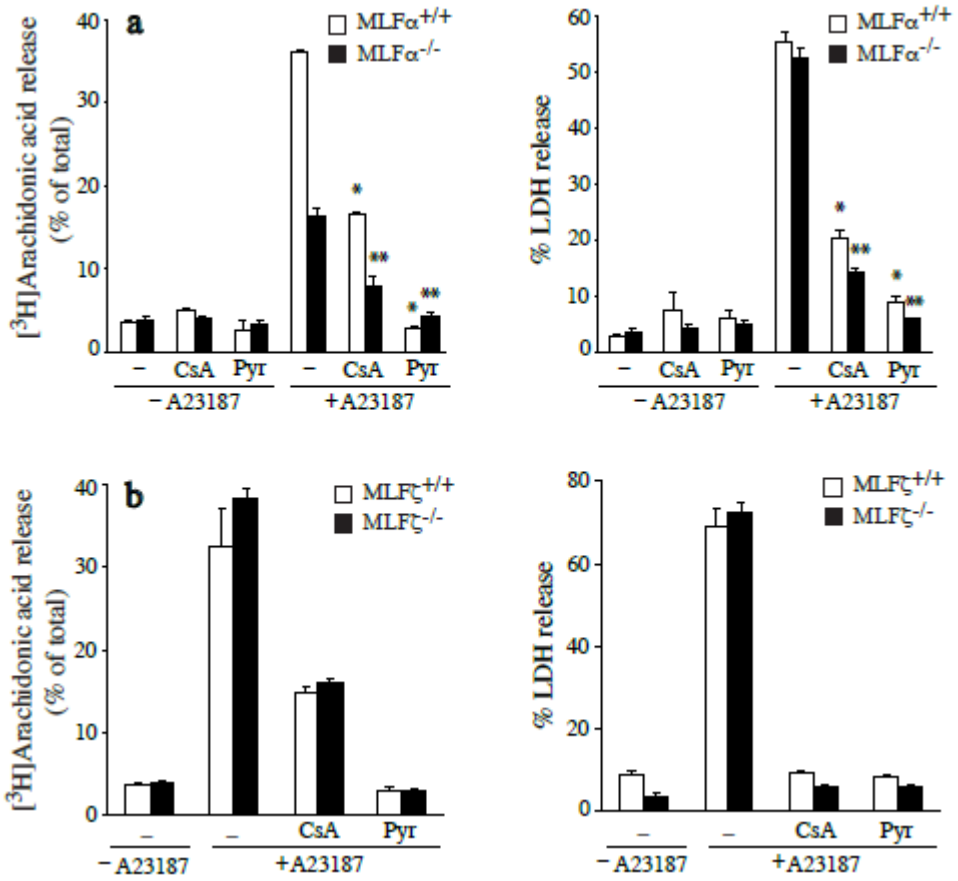

FIGURE 15. A23187-stimulated cell death and [^{3}H]arachidonic acid release occur in primary MLF and are not mediated by cPLA2ζ. (a) MLFα$^{+/+}$ (open bars) and MLFα$^{-/-}$ (black bars), or (b) MLFζ$^{+/+}$ (open bars) and MLFζ$^{-/-}$ (black bars), were stimulated with A23187 for 30 min and [^{3}H]arachidonic acid (left panels) and LDH(right panels) release was determined. Cells were treated with CsA or Pyrrophenone (Pyr) for 30 min prior to stimulation with A23187. The results in a are from 3 independent experiments ± S.E. (*, $p < 0.05$ when compared with A23187-stimulated MLFα$^{+/+}$ without inhibitors; and **, $p < 0.05$ when compared with A23187-stimulated MLFα$^{-/-}$ without inhibitors). The results in b are the average of 2 independent experiments.(*29*)

iv. Effect of Pyrrophenone and the triazole urea inhibitor KT195 on A23187-induced arachidonic acid release and cell death

Inhibition of cPLA2α by Pyrrophenone likely proceeds via formation of a hemiketal between its ketone carbonyl and the active site serine of the enzyme based on the known ability of ketones to form stable hemiketals with serine proteases and esterases.(*42-44*) To provide support for this mechanism, Pyrrophenone-OH (Pyr-OH) in which the ketone has been reduced to a secondary alcohol was tested in IMLFα$^{+/+}$ and IMLFα$^{-/-}$ assays. In cells stimulated with A23187, Pry-OH was ineffective at blocking AA release and LDH release (**Figure 16**).(*29*) These results suggest that Pry acts to prevent A23187-induced cell death by targeting a serine in the active site of a serine hydrolase.

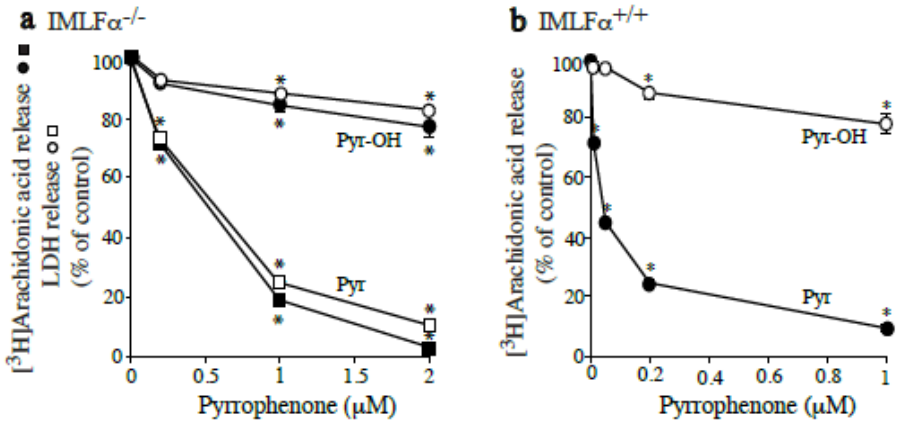

FIGURE 16. A23187-induced cell death and [^{3}H]arachidonic acid release are blocked by Pyr but not Pyr-OH. (a) Release of [^{3}H]arachidonic acid (solid symbols) and LDH (open symbols) from IMLFα$^{-/-}$ was determined 30 min after stimulation with A23187. Cells were treated with the indicated concentrations of Pyrrophenone (Pyr) or Pyrrophenone-OH (Pyr-OH) for 30 min prior to stimulation with A23187 (n = 3 ± S.E., *, $p < 0.05$ compared with A23187-stimulated IMLFα$^{-/-}$ without inhibitors). (b) release of [^{3}H]arachidonic acid from IMLFα$^{+/+}$ was determined 10 min after stimulation with 5% serum. Cells were treated with the indicated concentrations of Pyr or Pyr-OH 30 min prior to serum stimulation (n = 3 ± S.E., *, $p < 0.0001$ compared with serum-stimulated IMLFα$^{+/+}$ without inhibitors). Adapted from (*29*)

The serine hydrolase inhibitor KT195 was evaluated in IMLFα$^{-/-}$ cells stimulated with A23187. KT195 blocked both AA release and LDH release at a similar concentration as Pyr (**Figure 17**); KT195 (IC50 ~ 0.7 μM) and Pyr (IC50 ~ 0.5 μM).(*29*) These results provide further support the role for a serine hydrolase in A23187-induced cell death.

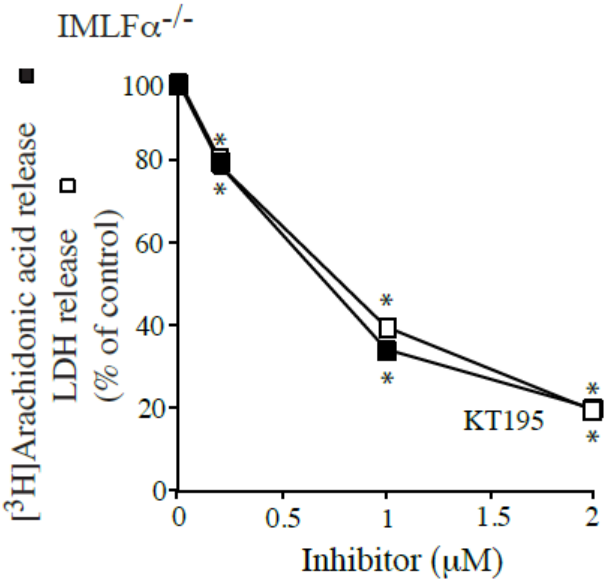

FIGURE 17. Serine hydrolase inhibitor KT195 blocks A23187-induced release of arachidonic acid and LDH. The results for IMLF are the average of 2 independent experiments. Release of [^{3}H]arachidonic acid (solid symbols) and LDH (open symbols) from IMLFα$^{-/-}$ was determined 30 min after stimulation with A23187. Cells were treated with the indicated concentrations of KT195 for 30 min prior to stimulation with A23187 (n = 3 ± S.E., *, $p < 0.05$ compared with A23187-stimulated IMLFα$^{-/-}$ without inhibitors). Adapted from (*29*)

v. Serine hydrolase inhibitors block cell death induced by H_2O_2

MLFα$^{+/+}$ and MLFα$^{-/-}$ were treated with H_2O_2 to determine whether the serine hydrolase inhibitors Pyr and KT195 blocked cell death triggered by other agents. H_2O_2 is known to trigger necrotic cell death involving cyclophilin D-dependent MPTP formation.(*71*, *76-78*) After stimulation with H_2O_2, MLFα$^{+/+}$ released slightly more AA than MLFα$^{-/-}$ (37% versus 25% respectively) and similar levels of LDH release indicating that cPLA2α does not play a role in

H_2O_2 triggered cell death (**Figure 18a**).(*29*) The inhibitors Pry, KT195 and CsA were shown to block AA release and LDH release in H_2O_2-stimulated MLFα$^{+/+}$ and MLFα$^{-/-}$ which is consistent with results from A23187 stimulation (**Figure 18a**).(*29*) A loss of calcein fluorescence in the mitochondria consistent with MPTP formation was seen upon H_2O_2 stimulation which was blocked by Pry, KT195 and CsA (**Figure 18b**) indicating that these inhibitors also block H_2O_2 triggered cell death.(*29*)

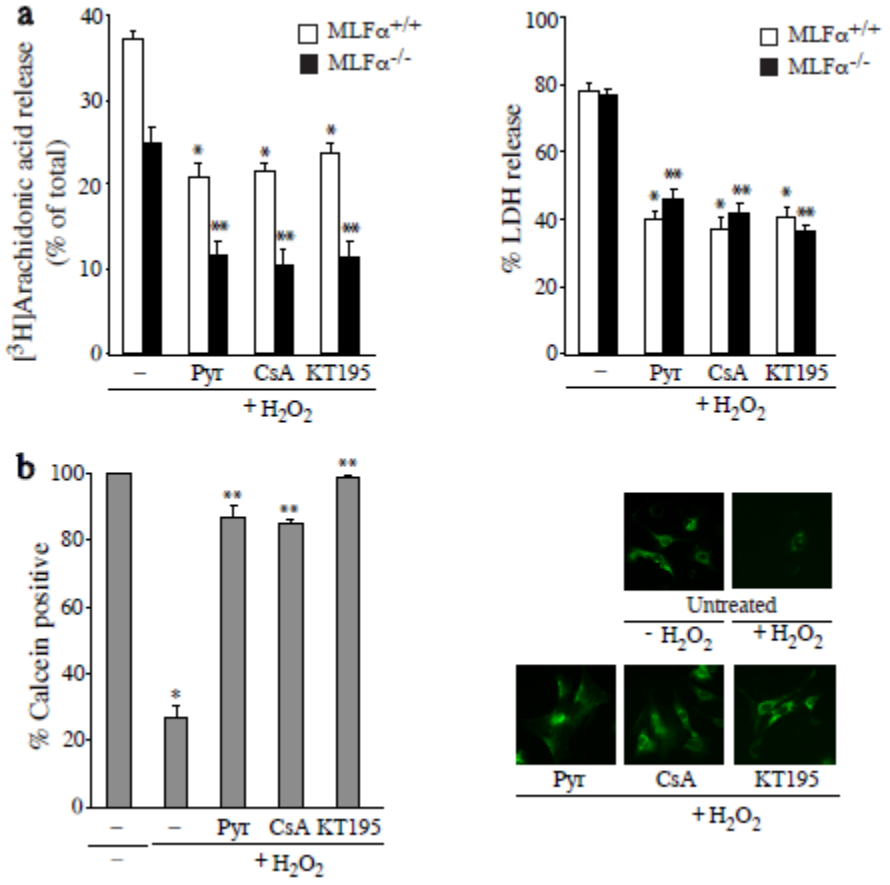

FIGURE 18. Serine hydrolase inhibitors block release of arachidonic acid and LDH from MLF stimulated with H_2O_2. (a) MLFα$^{+/+}$ (openbar) or MLFα$^{-/-}$ (black bar) were stimulated with 1 mM H_2O_2 for 18 hr and release of [^{3}H]arachidonic acid (left panel) and LDH (right panel) was determined. Cells were treated with CsA, Pyrrophenone (Pyr), or KT195 for 30 min prior to stimulation with H_2O_2.The results are from 3 independent experiments ± S.E. ($p < 0.05$ when compared with H_2O_2 stimulated MLFα$^{+/+}$ (*) or MLFα$^{-/-}$ (**) without inhibitors). (b) MLFα$^{-/-}$ were loaded with calcein prior to incubation with inhibitors for 30 min and then stimulated with 1 mM H_2O_2 for 18 hr. The results are from 3 independent experiments ± S.E. (*, $p < 0.0005$ when compared with MLFα$^{-/-}$ without H2O2; **, $p < 0.005$ when compared with H_2O_2 stimulated MLFα$^{-/-}$ without inhibitors). Images showing the effect of inhibitors on calcein fluorescence in MLFα$^{-/-}$ treated with and without H_2O_2 (right panel) are from a representative experiment and results confirmed in 2 independent experiments. Adapted from (*29*)

vi. ABHD6 Does not regulate A23187-induced cell death

KT195 is a known inhibitor of the serine hydrolase α/β-hydrolase domain-containing 6 (ABHD6), an enzyme that hydrolyzes 2-arachidonylglycerol.(*50, 79*) To rule out this known target as the protein of interest in these studies, an activity-based protein profiling (ABPP) assay was used. In this assay, IMLFα$^{-/-}$ were pretreated with KT195 or Pyr, followed by preparation of membrane proteomes that were probed with BODIPY-labeled HT-01 (a serine hydrolase reactive fluorescent probe) to detect ABHD6 (assays were also performed *in vitro*).(*50*) A strong band can be seen for both *in situ* and *in vitro* assays indicating a strong reactivity of ABHD6 with the BODIPY-labeled HT-01 probe detected by in gel fluorescence scanning (**Figure 19**,**a** and **b**).(*29*) Pyr was not able to block binding of the fluorescent probe to ABHD6 indicating that it is not an inhibitor of this enzyme (**Figure 19a**).(*29*) As expected, KT195 blocked binding of the fluorescent probe to ABHD6 both *in situ* (0.2-2 μM) and *in vitro* (IC_{50} ~ 25 nM) (**Figure 19**, **a** and **b**).(*29*) Since 0.2 μM KT195 had little to no effect on AA release or LDH release from IMLFα$^{-/-}$ cells (**Figure 17**), ABHD6 does not appear to be involved in A23187-induced cell death.

To confirm that ABHD6 is not the POI, an shRNA knockdown of *Abhd6* was performed in IMLFα$^{-/-}$ (**Figure 19**, **c** and **d**).(*29*) A23187-induced AA release and LDH release were similar in both control and ABHD6 knockdown and both were similarly inhibited by Pyr and KT195 (**Figure 19e**).(*29*) These data further support that ABHD6 does not play a role in mediating A23187-induced cell death and fatty acid release.

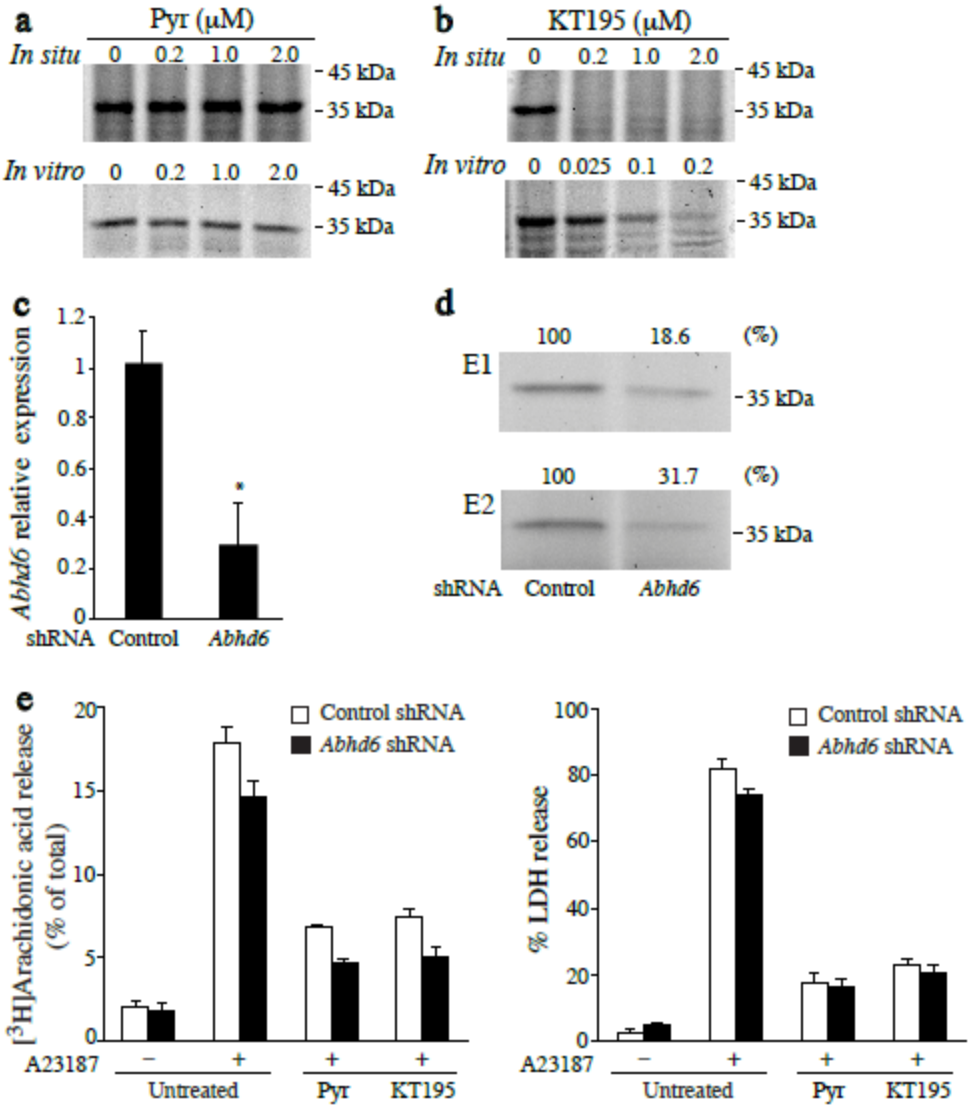

FIGURE 19. ABHD6 does not regulate A23187-induced cell death. The ability of Pyrrophenone (Pyr) (a) or KT195 (b) to bind ABHD6 was determined by competitive ABPP assay of proteomes from IMLF$\alpha^{-/-}$. The serine hydrolase inhibitors were added at the indicated concentrations either to IMLF$\alpha^{-/-}$ in situ prior to preparing membrane proteomes, or added to the proteomes in vitro, followed by incubation with BODIPY-labeled HT-01 probe. Bands were visualized on SDS polyacrylamide gels by in-gel fluorescence scanning. A representative experiment of 2–3 independent experiments is shown. (c) knockdown of Abhd6 mRNA was determined by real-time PCR analysis of RNA from IMLF$\alpha^{-/-}$ stably expressing Abhd6 shRNA or scrambled negative control. (d) knockdown of ABHD6 protein was determined by competitive ABPP assay of membrane proteomes from IMLF$\alpha^{-/-}$ stably expressing control or Abhd6 shRNA. The relative amount of BODIPY-labeled HT-01 probe binding to ABHD6 was determined by measuring the intensity of the fluorescent signal of the ABHD6 band on SDS-polyacrylamide gels using ImageQuant TL software (GE Healthcare) and expressed as the % of control. Results from two independent experiments (E1 and E2) are shown. (e) IMLF$\alpha^{-/-}$ stably expressing control or Abhd6 shRNA were treated with 2 μM Pyr or 2 μM KT195 for 30 min, stimulated with A23187 for 30 min, and then the release of [^{3}H]arachidonic acid and LDH was determined. The results are from 3 independent experiments ± S.E.(*29*)

vii. Identification of ABHD2 as the target of Pyrrophenone and KT195

Pyrrophenone and KT195 block A23187 and H_2O_2 induced necrotic cell death not by inhibiting their known targets, cPLA2α and ABHD6 respectively, but by off-target effects implicating a serine hydrolase as the target. A strategy employing chemical proteomics using copper-catalyzed azide-alkyne cycloaddition or "click" chemistry activity based protein profiling was used to identify the target(s) of these inhibitors.(*80*) Click chemistry offers a bioorthogonal approach to functionally characterize enzymes in complex biological systems and has previously been employed to identify low abundance targets.(*41, 81*) KT195-alkyne (see section B.vi.) was used as a chemical probe to covalently label the active site of the serine hydrolase protein(s) of interest in necrotic cell death in IMLF. KT195 was chosen preferentially over Pyrrophenone since it undergoes covalent, irreversible carbamoylation of active site serines whereas Pyrrophenone is a reversible inhibitor that likely acts via formation of a hemiketal between its ketone carbonyl and an active site serine nucleophile.(*50-52*) KT195-alkyne inhibited necrotic cell death (LDH release) induced by A23187 with an IC_{50} ~ 1.5 μM which is comparable to the parent compound KT195 (IC_{50} ~ 0.7 μM) (**Figure 20a**).(*29, 39*) For initial testing and to confirm labeling of KT195-alkyne the known target ABHD6, IMLF were treated with KT195-alkyne, click chemistry was employed with membrane proteomes using Rhodamine-azide, and targets were visualized in polyacrylamine gels by fluorescence scanning (**Figure 20b**).(*29, 39, 53*) As expected, a strong band at 35 kDa corresponding to the known target ABHD6 (**Figure 20b**) was visible confirming the utility of this labeling strategy.(*39*) Of interest, another major band at 48 kDa was also evident.

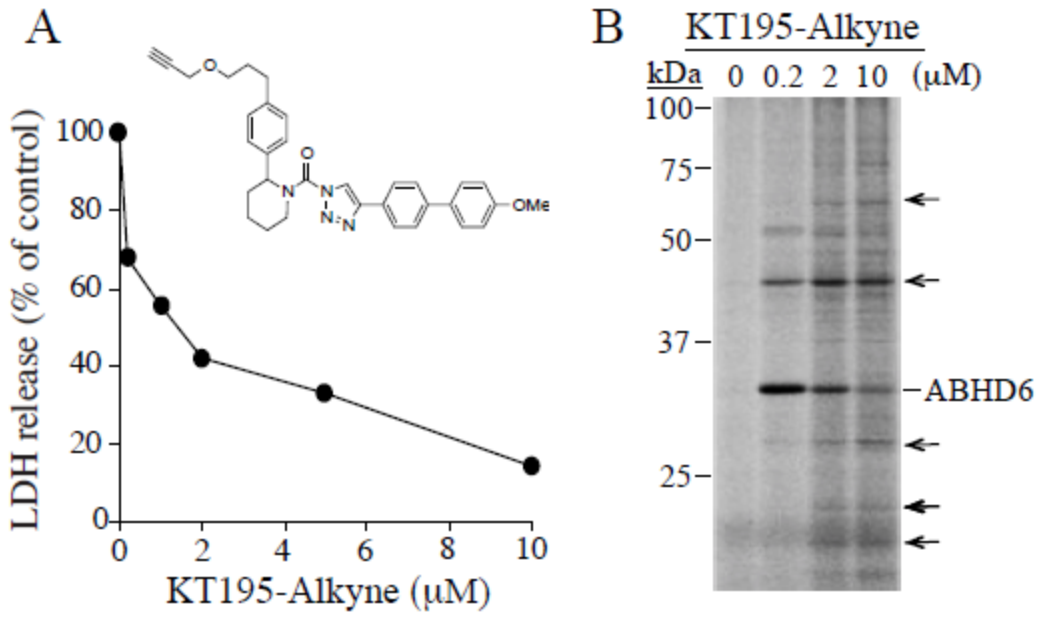

Figure 20. KT195-alkyne inhibits cell death and labels protein targets. (A) IMLF treated with KT195-alkyne were stimulated with A23187 (1 μg/ml) for 30 min and LDH release was determined. (B) Membrane proteomes were prepared from IMLF treated with KT195-alkyne (0, 0.2, 2, and 10 μM) then click chemistry carried out with Rhodamine-azide. Rhodamine-labeled proteins were separated on SDS-polyacrylamide gels and visualized by in-gel fluorescence scanning.(*39*)

To identify target(s) of the inhibitors, IMLF were treated with KT195-alkyne and click chemistry was employed in membrane and soluble proteomes using biotin azide, followed by pulldown with streptavidin beads and LC/MS analysis of tryptic peptides.(*39, 80*) The results of this pulldown are shown in **Table 1** and include several serine hydrolases along with numerous tryptic peptides from ABHD6 as expected.(*39*) Competition experiments were performed to narrow down the targets by pre-treating IMLF with either 10 μM KT195 (Exp 2, **Table 1**) or 10 μM Pyrrophenone (Exp 3, **Table 1**) prior to incubation with KT195-alkyne.(*39*) Since the POI in necrotic cell death is inhibited by both KT195 and Pyrrophenone, competitive inhibition by both compounds was required to consider a protein target for further study. As expected, KT195 but not Pyrrophenone blocked KT195-alkyne binding to the positive control ABHD6 since no

ABHD6 tryptic peptides were recovered (**Table 1**).(*39*) Competitive inhibition by both KT195 and Pyrrophenone was observed for only one protein target, ABHD2 (**Table 1**).(*39*) Encouragingly, ABHD2 has a MW of 48 kDa which corresponds to the major band labeled by Rhodamine-azide in proteomes of IMLF treated with KT195-alkyne (**Figure 20b**). Taken together, these results strongly suggest that KT195 and Pyrrophenone block A23187-induced necrotic cell death in IMLF by targeting the serine nucleophile in ABHD2.

Table 1. Proteins identified as targets of KT195-alkyne.(*39*)

Number of Experiment	Exp 1	Exp 2		Exp 3	
Competition	none	none	KT195	none	Pyr
Protein Candidates	Number of peptides				
ABHD6	16	23	0	17	20
Neutral cholesterol ester hydrolase	8	4	3	8	9
Lysosomal protective protein	4	0	2	5	2
Group XV phospholipase A2	2	3	0	4	4
ABHD11	3			4	3
Retinoid-inducible serine carboxypeptidase	2	0	1	2	2
Acyl-protein thioesterase 2	1			1	1
ADP/ATP translocase 2	1	0	1	1	2
Platelet activating factor acetylhydorlase	1			1	2
ABHD2	**1**	**3**	**0**	**1**	**0**
Non-specific lipid-transfer protein	4	1	4	1	2

The numerical values correspond to the number of tryptic peptides identified by LC-MS for each protein that was recovered in biotin-azide pull-down experiments from membrane proteomes of IMLF treated with KT-195 alkyne. In competition experiments IMLF were pretreated with KT195 (Exp 2) or pyrrophenone (Exp 3) prior to treatment with KT195-alkyne.

viii. Effect of ABHD2 knockdown

For further confirmation that ABHD2 participates in the A23187-induced necrotic cell death pathway, a RNA knockdown experiment was conducted. IMLF transfected with ABHD2 shRNA showed 72% knockdown of ABHD2 mRNA compared to control cells and less ABHD2 in Western blots (**Figure 21** inset).(*39*) When treated with A23187 to induce cell death, the

ABHD2 knockdown IMLF clone exhibited less LHD release (**Figure 21**) further implicating ABHD2 as the POI.(*39*)

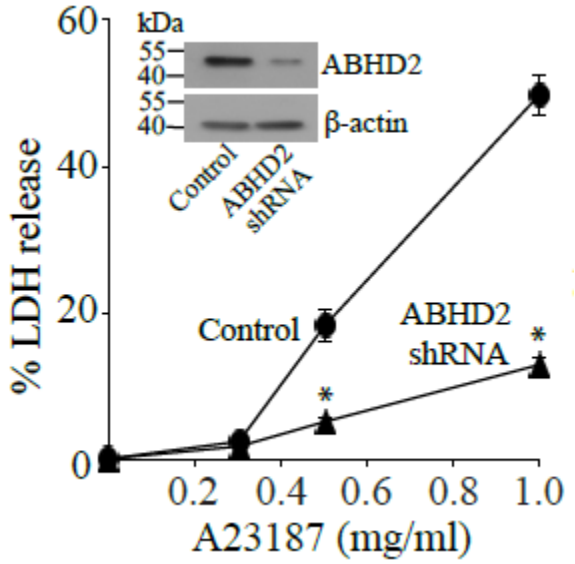

Figure 21. ABHD2 Knockdown attenuates cell death (LDH release). IMLF were transfected with lentiviruses containing ABHD2 shRNA or control vector and stable clones generated. (A) LDH release was measured from ABHD2 shRNA-knockdown IMLF (triangles) and vector controls (circles) 30 min after stimulation with the indicated concentrations of A23187 (n=3, *P<0.05). A Western blot (inset) shows that ABHD2 shRNA-knockdown IMLF express less ABHD2 than vector controls. Adapted from (*39*)

D. Conclusion

Initial observations that Pyrrophenone blocked AA release and LDH release in IMLF led to the discovery of a novel mechanism involving the serine hydrolase ABHD2 in necrotic cell death. The ABHD family of proteins contains at least 19 members including proteases, lipases, esterases, dehalogenases, peroxidases, and epoxide hydrolases making this one of the most diverse protein families known.(*82*, *83*) All family members possess and α/β-hydrolase fold and a catalytic triad composed of nucleophile-acid-histidine residues typically in a GXSXG motif (though the residues S207/D345/H376 form the catalytic triad of ABHD2).(*82-84*) Many ABHD

enzymes are predicted to be involved in lipid metabolism but are poorly characterized including ABHD2, which is widely expressed in tissues and highly conserved evolutionarily.(*39, 85*)

In this study, it was found that inhibition of ABHD2 blocks necrotic cell death in fibroblasts stimulated with A23187. Further work has shown that ABHD2 is localized to the endoplasmic reticulum but not to mitochondria or mitochondrial associated membranes.(*39*) Additionally, knockdown of ABHD2 with shRNA attenuated calcium release from the endoplasmic reticulum and mitochondrial calcium uptake. Taken together, these results describe a novel mechanism for regulating calcium transfer from the ER to mitochondria that involves the serine hydrolase ABHD2.

The previous studies were made possible by the synthesis of Pyrrophenone, KT195, and selected derivatives. Carefully chosen adaptations to these inhibitors allowed for conjugation to fluorescent dyes or affinity labels which, though not all strategies were successful, led to the discovery of ABHD2. Future work geared toward the development of small molecule, cell permeable, specific inhibitors of ABHD2 will be important for understanding its mechanistic role in regulating biological functions.(*86, 87*).

E. Experimental

i. Synthesis of Pyrrophenone derivative

Compound **1**. 4-(Hydroxydiphenylmethyl)-benzonitrile.

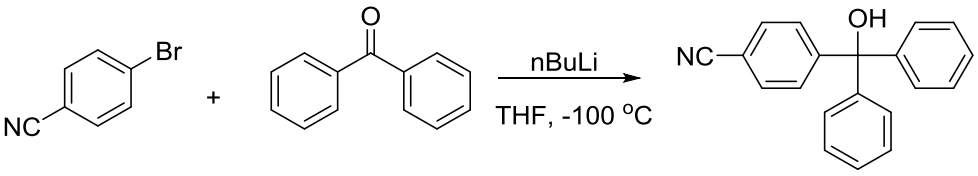

4-Bromobenzonitrile (7 g, 38.5 mmol) and dry THF (225 mL) were introduced under nitrogen atmosphere to a three-neck flask. The reaction mixture was cooled to -100 °C (diethylether/CO2). n-Butyllithium as a 2.5 M solution in hexane (15.4 mL, 38.5 mmol) was added dropwise and then the reaction mixture was stirred at -100 °C for 5min. Benzophenone (7 g, 38.5 mmol) in THF(32 mL) was added and the reaction was warmed to ambient temperature. The reaction was poured into water and extracted with diethyl ether. The aqueous layer was extracted with diethyl ether and the organic phases were pooled and dried over magnesium sulfate. TLC in 10% EtOAc/Hex, UV active. The pure product was obtained by flash chromatography in a gradient of 100% hexane to 15% ethyl acetate/hexane. [73% yield] 1H NMR (300 MHz, DMSO) δ 7.79 (d, J = 8.6 Hz, 2H), 7.42 (d, J = 8.6 Hz, 2H), 7.30 (dd, J = 13.0, 5.0 Hz, 6H), 7.20 (dd, J = 8.1, 1.6 Hz, 4H), 6.77 (s, 1H).

Compound **2**. 4-(aminomethyl)-α,α-diphenyl-benzenemethanol

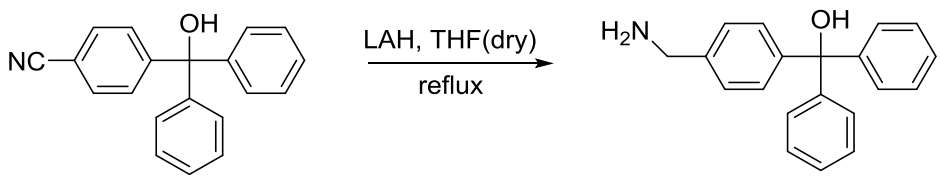

4-(Hydroxydiphenylmethyl)-benzonitrile (12.5 g, 43.8 mmol) was dissolved in dry tetrahydrofuran (200 mL). The solution was added dropwise to a stirred suspension of lithium aluminum hydride (2.5 g, 65.7 mmol) in dry THF (530 mL) under nitrogen atmosphere. The suspension was heated to reflux for 3 hours. The reaction was cooled to ambient temperature and water was added. The organic phase was collected and the aqueous phase was extracted with ethyl acetate. The organic phases were pooled, dried over sodium sulfate, and concentrated. The product was used as crude. [87% yield] 1H NMR (300 MHz, CDCl3) δ 7.37 – 7.23 (m, 14H), 3.86 (s, 2H).

Compound **3**. N-Boc-4-(Hydroxydiphenylmethyl)-benzenemethanamine

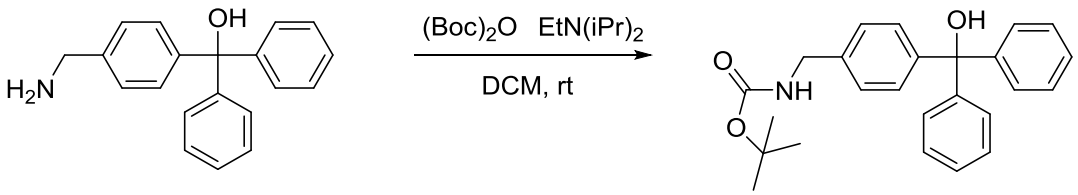

4-(Hydroxydiphenylmethyl)-benzenemethanamine (10 g, 34 mmol) dissolved in dry dichloromethane (85 mL) and N,N-diisopropylethylamine (9 mL, 51 mmol) was added. Di-tert-butyl dicarbonate (9 g, 41 mmol) was added and the reaction was stirred under nitrogen atmosphere at ambient temperature overnight. The reaction was poured into water and extracted. The aqueous phase was extracted with dichloromethane. The organic phases were pooled and washed with saturated sodium chloride solution then dried over magnesium sulfate and concentrated onto silica. The pure product was obtained by flash chromatography in a gradient of 100% hexane to 20% ethyl acetate/hexane. [74% yield] 1H NMR (300 MHz, CDCl3) δ 7.57 – 7.02 (m, 1H), 4.82 (bs, 1H), 4.32 (d, 2H), 2.77 (s, 1H), 1.45 (s, 9H).

Compound **4**. N-Boc-4-(Sulfhydryldiphenylmethyl)-benzenemethanamine

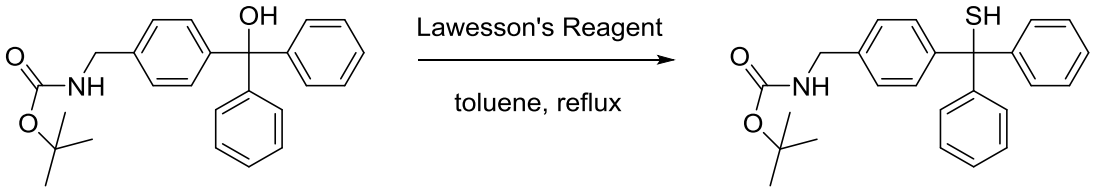

N-Boc-4-(Hydroxydiphenylmethyl)-benzenemethanamine (9.8 g, 25.2 mmol) was dissolved in toluene (840 mL) and 2,4-bis(4-methoxyphenyl)-1,3,2,4-dithiadiphosphetane-2,4-disulfide also known as Lawesson's reagent (5.6 g, 13.8 mmol) was added. The mixture was refluxed under nitrogen atmosphere for 4 hours. The reaction mixture was concentrated onto silica and the pure product was obtained by flash chromatography in a gradient of 100% hexane to 20% ethyl acetate/hexane. [69% yield] 1H NMR (300 MHz, CDCl3) δ 7.68 – 6.97 (m, 14H), 4.83 (bs, 1H), 4.36 (d, 2H), 3.14 (s, 1H), 1.55 (d, J = 1.4 Hz, 9H).

Compound **5.**

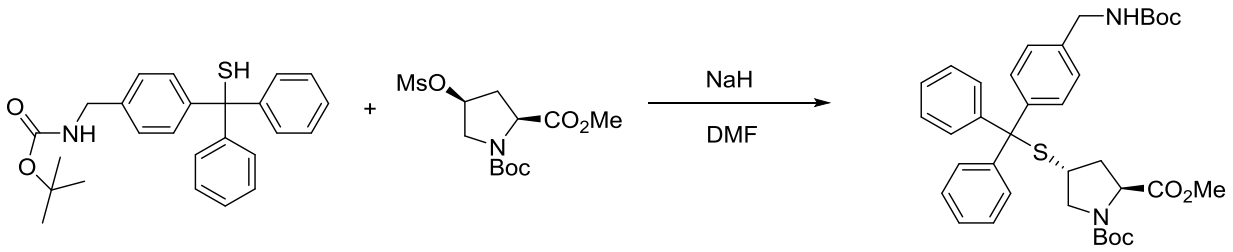

N-Boc-4-(Sulfhydryldiphenylmethyl)-benzenemethanamine (0.9 g, 2.23 mmol) was dissolved in dry DMF (2.32 mL) and cooled to 0 °C. Sodium hydride was added and the solution was stirred at 0 °C for 5 minutes. A solution of (2S,4S)-1,2-Pyrrolidinedicarboxylic acid, 4-[(methylsulfonyl)oxy]-, 1-(1,1-dimethylethyl) 2-methyl ester (0.6 g, 1.86 mmol) in dry DMF (2.32 mL) was added and the reaction was warmed to ambient temperature then heated at 50 °C

under nitrogen atmosphere for 3 hours. The reaction was poured into 1:1 ethyl acetate/water and the organic phase was extracted. The aqueous layer was extracted with ethyl acetate. The organic phases were pooled and washed with saturated sodium bicarbonate solution then dried over sodium sulfate and concentrated onto silica. The pure product was obtained by flash chromatography in a gradient of 100% hexane to 20% ethyl acetate/hexane. [50% yield] 1H NMR (300 MHz, CDCl3) δ 7.53 – 7.17 (m, 14H), 4.94 (bs, 1H), 4.31 (d, 2H), 4.24 – 4.05 (m, 1H), 3.61 (s, 3H), 3.40 (m, 1H), 2.98 (m, 2H), 1.98 – 1.69 (m, 2H), 1.47 (s, 9H), 1.37 (s, 9H).

Compound **6**.

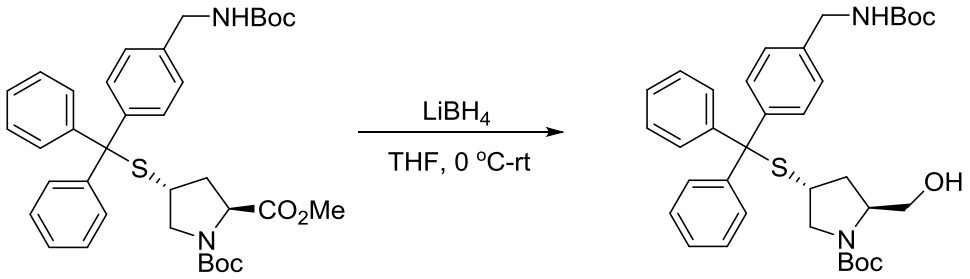

A solution of Compound **5** (4.5 g, 7.1 mmol) in dry THF (30 mL) was cooled to 0 °C in an ice bath. Lithium borohydride (0.23 g, 10.7 mmol) was added and the mixture was allowed to warm to room temperature and then stirred for 3 hours. Then, methanol (20 mL) was added and the reaction was stirred for an additional 30 min. The product was extracted from a mixture of 1:1 ethyl acetate/water. The organic layer was washed with water then washed with brine and then dried over sodium sulfate and concentrated onto silica. The pure product was obtained by flash chromatography in a gradient of 100% hexane to 30% ethyl acetate/hexane. [86% yield] 1H NMR (500 MHz, CDCl3) δ 7.58 – 7.08 (m, 14H), 4.88 (bs, 1H), 4.30 (d, 2H), 3.96 (m, 1H), 3.78 – 3.48 (m, 1H), 3.33 (dd, 2H), 3.13 – 2.72 (m, 2H), 1.79 – 1.60 (m, 2H), 1.46 (s, 9H), 1.43 (s, 9H).

Compound **7**.

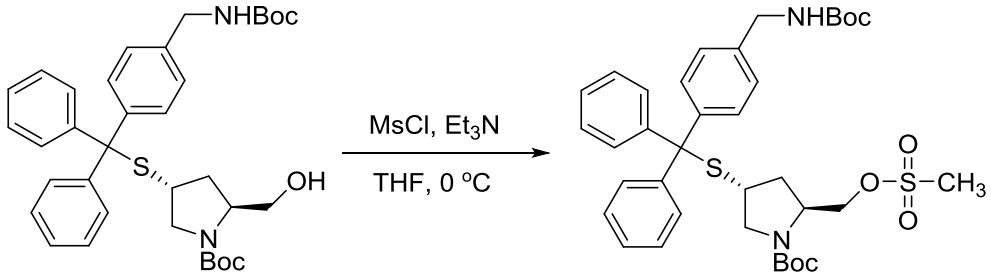

A solution of the Compound **6** (3.4 g, 5.6 mmol) in dry THF (14 mL) was prepared and triethylamine (1.1 mL, 7.9 mmol) was added. The solution was cooled on an ice bath and then methanesulfonyl chloride (0.52 mL, 6.8 mmol) was added. The mixture was stirred on the ice bath for 1 hour. The product was extracted from a mixture of 1:1 ethyl acetate/water. The organic layer was washed with brine and then dried over sodium sulfate and concentrated onto silica. The pure product was obtained by flash chromatography in a gradient of 100% hexane to 30% ethyl acetate/hexane. [87% yield] 1H NMR (500 MHz, CDCl3) δ 7.57 – 7.12 (m, 14H), 4.94 (bs, 1H), 4.30 (d, 2H), 4.02 (d, 2H), 3.90 (m, 1H), 3.81 (m, 1H), 2.96 – 2.76 (m, 5H), 1.84 – 1.63 (m, 2H), 1.45 (s, 9H), 1.43 (s, 9H).

Compound **8**.

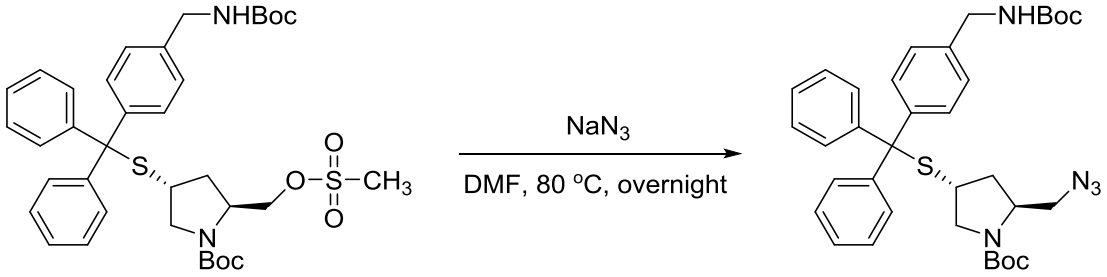

To a solution of Compound **7** (3.33 g, 4.9 mmol) in dry DMF (16 mL) was added sodium azide (0.45 g, 6.9 mmol). The solution was stirred under nitrogen atmosphere at 80 °C overnight. Water was added and the aqueous layer was extracted with diethyl ether. The organic layer was washed with water then washed with brine then dried over sodium sulfate and concentrated onto silica. The pure product was obtained by flash chromatography in a gradient of 100% hexane to 20% ethyl acetate/hexane. [61% yield] 1H NMR (500 MHz, CDCl3) δ 7.69 – 6.91 (m, 14H), 4.95 (bs, 1H), 4.33 (d, 2H), 3.81 (d, 2H), 3.50 – 2.49 (m, 5H), 1.84 – 1.63 (m, 2H), 1.45 (s, 9H), 1.43 (s, 9H).

Compound **9**.

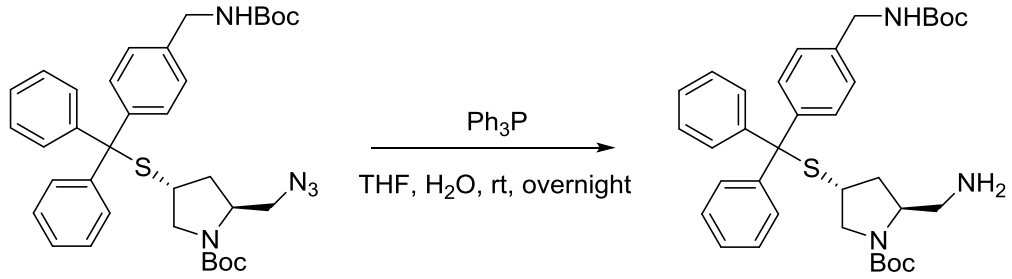

To a solution of Compound **8** (1.6 g, 2.5 mmol) in THF (13 mL) was added triphenylphosphine (2.0 g, 7.6 mmol) and water (0.4 mL). The mixture was stirred at room temperature overnight. The reaction mixture was then diluted in ethyl acetate and concentrated onto silica. The pure product was obtained by column chromatography by first eluting by products with 70% ethyl acetate/hexanes until no UV active spot is seen and then eluting the pure product with 20% methanol/chloroform. [81% yield] 1H NMR (300 MHz, CDCl3) δ 7.48 – 7.21 (m, 14H), 5.10 (bs, 1H), 4.32 (d, 2H), 3.56 – 2.64 (m, 7H), 2.0 – 1.84 (m, 2H), 1.71 – 1.06 (m, 20H).

Compound **10**.

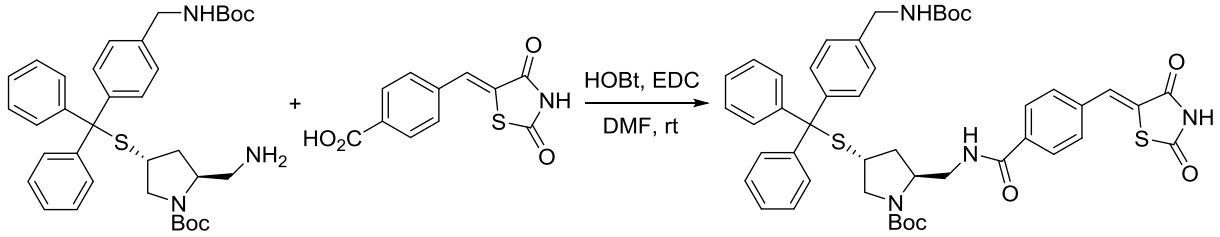

Compound **9** (1.66 g, 2.75 mmol) was dissolved in dry DMF (10 mL) and 1-hydroxybenzotriazole hydrate (0.42 g, 2.75 mmol) and 1-ethyl-3-(3-dimethyl-aminopropyl)carboiimide hydrochloride (0.47 g, 3.02 mmol) were added. A solution of 4-[(2,4-dioxo-5-thiazolidinylidene)methyl]-benzoic acid (0.68 g, 2.75 mmol) dissolved in dry dimethylformamide (5 mL) was added. The mixture was stirred at room temperature under nitrogen for 3 hours. The reaction was poured into 1:1 ethyl acetate/water and the organic layer was extracted. The aqueous phase was extracted with ethyl acetate, and then the organic phase was washed with brine and dried over sodium sulfate. The pure product was obtained by flash chromatography in a gradient of 100% chloroform to 5% methanol/chloroform. [71% yield] 1H NMR (300 MHz, CDCl3) δ 8.66 (bs, 1H), 7.91 (d, J = 8.0 Hz, 2H), 7.80 (s, 1H), 7.60 – 6.92 (m, 16H), 5.10 (bs, 1H), 4.89 (bs, 1H), 4.32 (d, 2H), 3.56 – 2.64 (m, 6H), 2.0 – 1.84 (m, 2H), 1.71 – 1.06 (m, 18H).

Compound **11**.

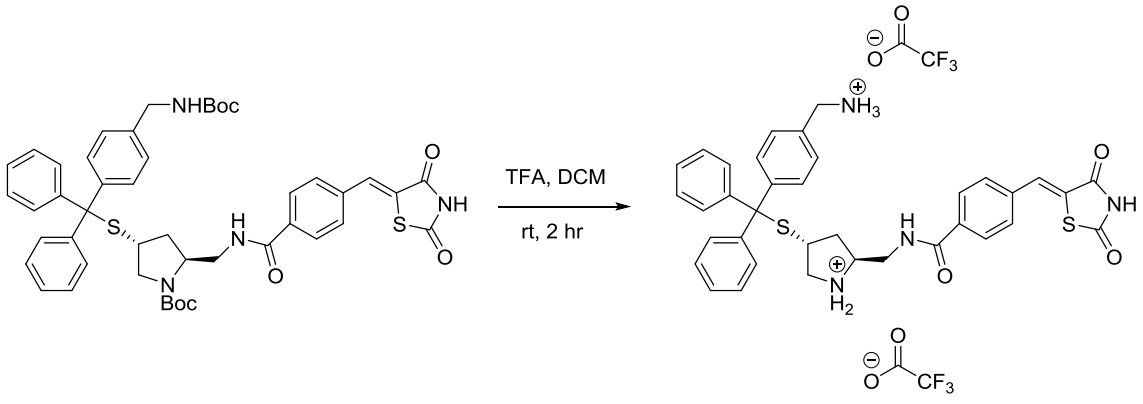

Compound **10** (0.9 g, 1 mmol) was dissolved in 50% TFA/DCM (60 mL) and stirred at room temperature for 2 hours. The solvent was evaporated off and toluene was added. The toluene was then evaporated off and this process was repeated two more times. The crude product was placed on high vac overnight and used as crude in the next step. [100% crude yield]

Compound **12**.

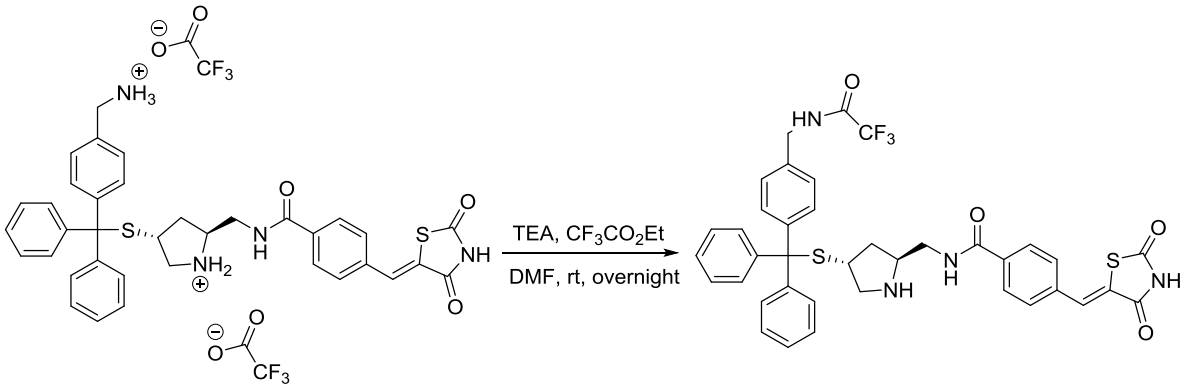

Compound **11** (0.1 g, 0.12 mmol) was dissolved in dry DMF (12 mL) and triethylamine (0.05 mL, 0.36 mmol) was added. The pH was checked and adjusted with more triethylamine if needed to reach a pH of 9. Then ethyl trifluoroacetate (0.08 mL, 0.6 mmol) was added and the reaction was stirred at room temperature overnight. The crude reaction mixture was concentrated onto silica gel without further workup and the pure product was obtained by flash chromatography in a gradient of 100% dichloromethane to 20% methanol/dichloromethane. [70% yield] 1H NMR (300 MHz, CDCl3) δ 8.66 (bs, 1H), 7.91 (d, J = 8.0 Hz, 2H), 7.80 (s, 1H), 7.60 – 6.92 (m, 16H), 5.35 (bs, 1H), 4.89 (bs, 1H), 4.37 (d, 2H), 3.56 – 2.14 (m, 7H), 2. – 1.53 (m, 2H).

Compound **13**.

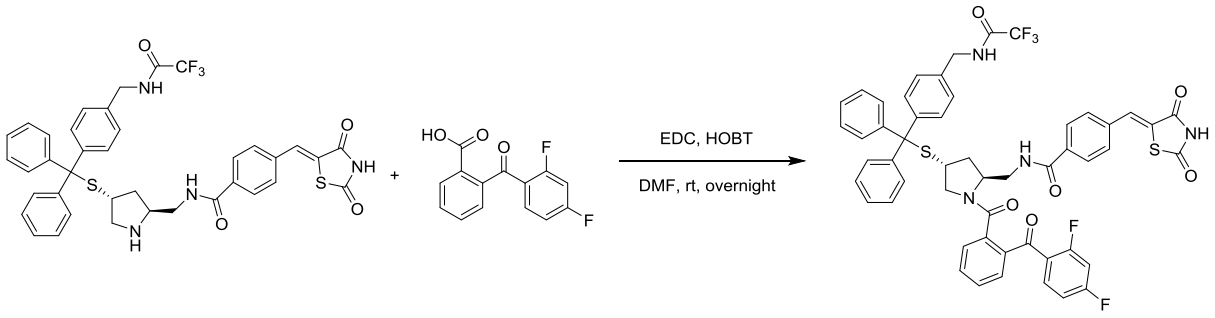

Prior to the reaction, both starting materials were evaporated from toluene 3 times and placed on high vac overnight. Compound **12** (0.66 g, 0.9 mmol), 2-(2,4-difluorobenzoyl)-benzoic acid (0.24 g, 0.9 mmol), HOBT (0.12 g, 0.09 mmol), EDC (0.15 g, 0.99 mmol) were dissolved in DMF (32 mL) and the reaction was stirred at room temperature overnight. The crude reaction mixture was concentrated onto silica gel without further workup and the pure product was obtained by flash chromatography in a gradient of 100% hexane to 100% ethyl acetate. [23% yield] 1H NMR (300 MHz, CDCl3) δ 8.14 (s, 1H), 7.91 (d, J = 8.3 Hz, 1H), 7.84 (s, 1H), 7.66 (m, 1H), 7.61 – 7.49 (m, 3H), 7.43 (d, J = 8.2 Hz, 2H), 7.35 – 7.17 (m, 8H), 7.16 – 6.92 (m, 10H), 4.86 (s, 1H), 4.44 (s, 1H), 4.23 (d, J = 5.6 Hz, 2H), 3.96 – 3.72 (m, 2H), 3.06 – 2.87 (m, 1H), 2.62 – 2.48 (m, 1H), 2.26 – 2.06 (m, 4H).

Compound **14**.

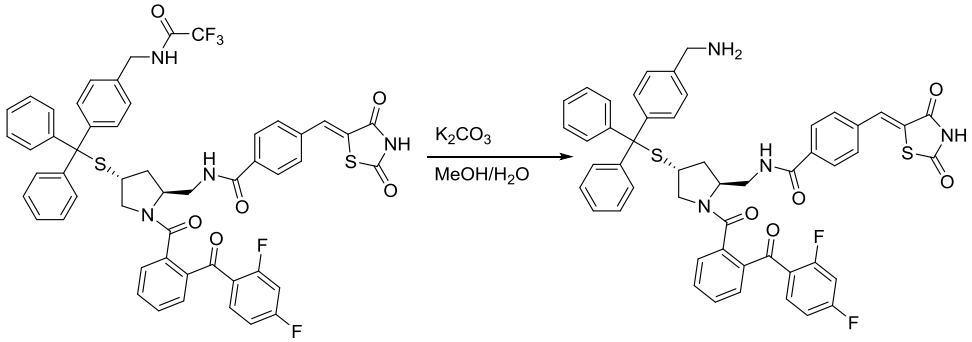

Potassium carbonate (0.1 g, 0.7 mmol) was dissolved in a 2:1 methanol/water solution (1.5 mL). Compound **13** was added and the reaction was stirred at room temperature for 4 hours. The pure product was obtained by acidification using 0.1 M HCl (2 mL, pH 4-6) followed by extraction. [60% yield] 1H NMR (300 MHz, CDCl3) δ 8.14 (s, 1H), 7.91 (d, J = 8.3 Hz, 1H), 7.84 (s, 1H), 7.66 (m, 1H), 7.61 – 7.49 (m, 3H), 7.43 (d, J = 8.2 Hz, 2H), 7.35 – 7.17 (m, 8H), 7.16 – 6.92 (m, 10H), 4.44 (s, 1H), 3.96 – 3.70 (m, 4H), 3.06 – 2.87 (m, 1H), 2.62 – 2.48 (m, 1H), 2.26 – 1.58 (m, 6H).

ii. Synthesis of KT195-amine derivative

Compound **15**. 4-(2-Pyridinyl)-benzonitrile.

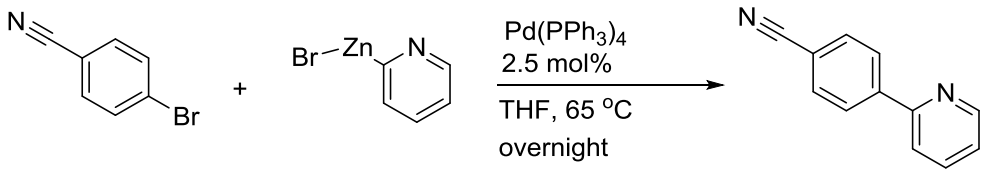

4-Bromobenzonitrile (0.5 g, 2.75 mmol) and tetrakis(triphenylphosphine)palladium(0) (0.08g, 0.025 mmol) were added to a dry rbf. 2-Pyridylzinc bromide as a 0.5 M solution in THF (8.24 mL, 4.12 mmol) was added via syringe and the mixture was heated to reflux (65 °C) overnight. Then, the crude mixture was brought up in saturate ammonium chloride soltuion and extracted with ethyl acetate. The organic phase was washed with brine, dried over magnesium sulfate, and concentrated onto silica gel. The pure product was obtained by flash chromatography using a gradient of 100% hexane to 20% ethyl acetate/hexane. [90% yield] 1H NMR (300 MHz, MeOD) δ 8.68 (d, J = 5.0 Hz, 1H), 8.17 (d, J = 8.7 Hz, 2H), 8.01 – 7.90 (m, 2H), 7.85 (d, J = 8.7 Hz, 2H), 7.43 (ddd, J = 5.9, 4.9, 2.9 Hz, 1H).

Compound **16.** 4-(2-Piperidinyl)-benzenemethanamine

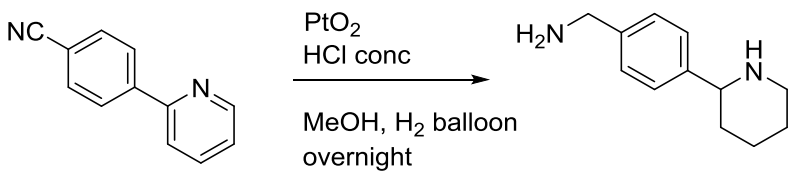

Compound **15** (0.7 g, 4 mmol) was dissolved in methanol (22.5 mL) and glacial HCl (0.5 mL) was added. Then Pt_2O (0.05 g, 0.2 mmol) was added and the reaction vessel was flushed with hydrogen gas and a balloon containing hydrogen gas was affixed to the reaction vessel so that it could stir under hydrogen atmosphere at room temperature overnight. The reaction mixture was filtered over celite and flushed with water. Then the pH was adjusted to 9 using sodium hydroxide followed by extraction with diethyl ether. The organic phase was dried over magnesium sulfate, evaporated from toluene 3 times and dried overnight. The crude product was used in the next reaction without further purification. [95% yield] 1H NMR (300 MHz, CDCl3) δ 7.33 (d, J = 8.1 Hz, 2H), 7.26 (d, J = 8.0 Hz, 2H), 3.84 (s, 2H), 3.58 (d, J = 7.7 Hz, 1H), 3.19 (d, J = 11.2 Hz, 1H), 2.88 – 2.72 (m, 1H), 1.93 – 1.41 (m, 9H).

Compound **17**.

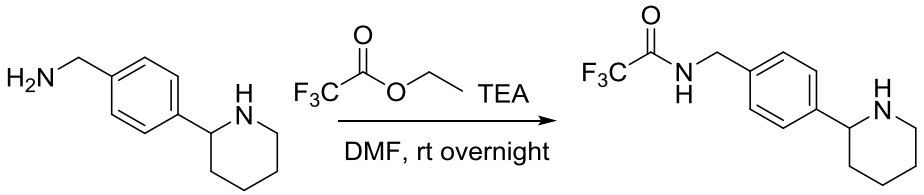

Compound **16** (0.05 g, 0.28 mmol) was dissolved in dry DMF (1 mL) then triethylamine (0.12 mL, 0.84 mmol) and ethyl trifluoroacetate (0.11 mL, 0.84 mmol) were added. The reaction mixture was stirred at room temperature for 2 hours. The crude reaction mixture was concentrated onto silica gel without further workup and the pure product was obtained by flash

chromatography in a gradient of 100% dichloromethane to 20% methanol/dichloromethane. [83% yield] 1H NMR (300 MHz, CDCl3) δ 7.39 (d, J = 8.2 Hz, 2H), 7.22 (d, J = 8.1 Hz, 2H), 6.56 (bs, 1H), 4.44 (d, J = 5.9 Hz, 2H), 3.93 (m, 1H), 3.23 (d, J = 12.3 Hz, 1H), 2.92 (m, 1H), 2.12 – 1.43 (m, 7H).

Compound **18**.

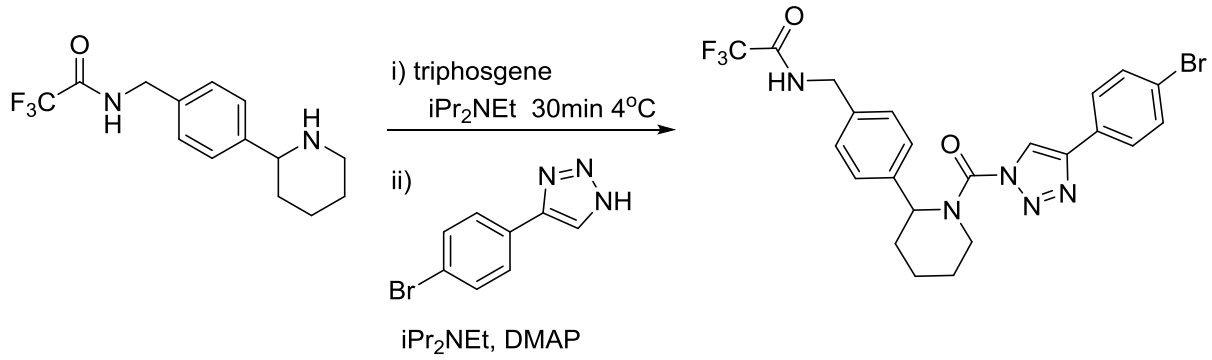

Compound **17** (0.05 g, 0.175 mmol) was dissolved in dry THF (0.5 mL) and DIPEA (0.02 mL, 0.11 mmol) and triphosgene (0.01 g, 0.035 mmol) were added. The reaction mixture was stirred at 4 °C for 30 minutes then poured into water and extracted with ethyl acetate. The organic phase was washed with water and brine, then dried over sodium sulfate. The solvent was evaporated and the crude intermdiate was used without further purification. The intermediate was dissolved in dry THF (0.5 mL) and DIPEA (0.02 mL, 0.11 mmol), DMAP (0.011 g, 0.087 mmol), and 4-(4-bromophenyl)-1H-1,2,3-triazole (0.01 g, 0.035 mmol) were added. The mixture was heated to 60 °C and stirred for 2 hours then poured into saturated aqueous ammonium chloride solution. The mixture was extracted with ethyl acetate, washed with water and brine, dried over sodium sulfate, then concentrated onto silica gel. The pure product was obtained by flash chromatography in a gradient of 100% hexane to 30% ethyl acetate/hexane. [51% yield] 1H NMR (CDCl3, 300 MHz) δ 8.40 (s, 1H), 7.75 (d, J = 8.4 Hz, 2H), 7.59 (d, J = 8.5 Hz, 2H), 7.39

(d, J = 8.2 Hz, 2H), 7.22 (d, J = 8.1 Hz, 2H), 6.56 (bs, 1H), 5.72 (s, 1H), 4.55 (d, J = 5.9 Hz, 2H), 4.11 (d, J = 13.4 Hz, 1H), 3.18 (m, 1H), 2.49 (d, J = 14.2 Hz, 1H), 2.15 (m, 1H), 1.90-1.60 (m, 4H).

Compound **19**.

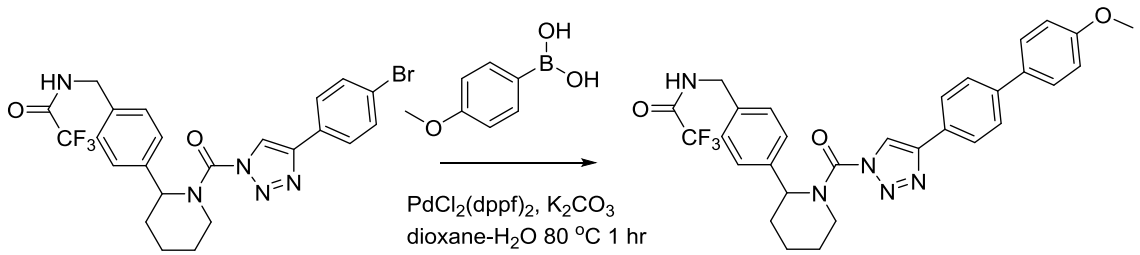

Compound **18** (0.01 g, 0.02 mmol) was dissolved in 1,4-dioxane (0.3 mL) and water (0.03 mL) was added. 4-Methoxyphenylboronic acid (0.004 g, 0.03 mmol), potassium carbonate (0.008 g, 0.06 mmol), and [1,1'-Bis(diphenylphosphino)ferrocene]dichloropalladium(II) (0.0014 g, 0.002 mmol) were added. The mixture was heated at 80 °C for 1 hour. The reaction mixture was poured into water and extracted with ethyl acetate. The organic phase was washed with brine, dried over sodium sulfate, and concentrated onto silica gel. The pure product was obtained by flash chromatography in a gradient of 100% hexane to 30% ethyl acetate/hexane. [50% yield] 1H NMR (300 MHz, CDCl3) δ 8.45 (s, 1H), 7.89 (d, J = 8.2 Hz, 2H), 7.64 (d, J = 8.4 Hz, 2H), 7.57 (d, J = 8.8 Hz, 2H), 7.46 (d, J = 8.0 Hz, 2H), 7.35 (d, J = 8.2 Hz, 2H), 7.00 (d, J = 8.8 Hz, 2H), 6.57 (bs, 1H), 5.75 (s, 1H), 4.56 (d, J = 5.8 Hz, 2H), 4.14 (d, J = 8.0 Hz, 1H), 3.87 (s, 3H), 3.09 (t, J = 11.9 Hz, 1H), 2.49 (d, J = 14.8 Hz, 1H), 2.14 (m, 1H), 1.96 – 1.47 (m, 4H).

Compound **20**.

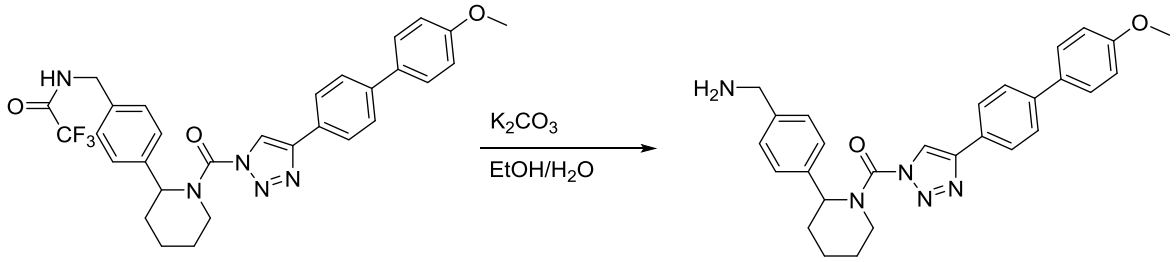

Compound **19** (11 mg, 0.02 mmol) was dissolved in ethanol (2 mL) and water (1 mL) was added. Potassium carbonate (19 mg, 0.14 mmol) was added and the reaction was stirred at room temperature overnight. The pure product was obtained by HPLC purification using methanol/water gradient of 65-90%. [54% yield] 1H NMR (300 MHz, CDCl3) δ 8.45 (s, 1H), 7.89 (d, J = 8.2 Hz, 2H), 7.64 (d, J = 8.4 Hz, 2H), 7.57 (d, J = 8.8 Hz, 2H), 7.46 (d, J = 8.0 Hz, 2H), 7.35 (d, J = 8.2 Hz, 2H), 7.00 (d, J = 8.8 Hz, 2H), 5.75 (s, 1H), 4.14 (d, J = 8.0 Hz, 1H), 3.87 (s, 3H), 3.84 (s, 2H), 3.09 (t, J = 11.9 Hz, 1H), 2.49 (d, J = 14.8 Hz, 1H), 2.14 (m, 1H), 1.96 – 1.47 (m, 6H).

5-(4-bromophenyl)-1H-1,2,3-Triazole

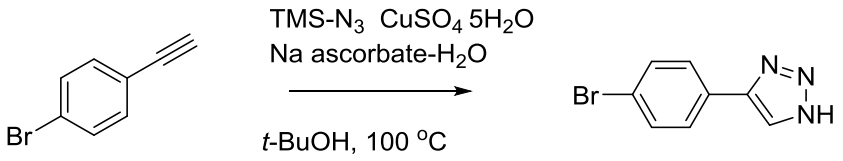

1-Bromo-4-ethynylbenzene (0.05 g, 0.28 mmol) was dissolved in t-butyl alcohol (0.4 mL). Copper(II) sulfate pentahydrate (0.007 g, 0.03 mmol) was dissolved in water (0.08 mL). Sodium ascorbate (0.027 g, 0.14 mmol) was dissolved in water (0.08 mL). All three solutions were combined in a microwave reaction tube (note a microwave is not used in this reaction but the

vessel provided a convenient way to seal the reaction during heating). Azidotrimethylsilane (0.27 mL, 2.0 mmol) was added carefully due to the toxicity of the reagent. The tube was sealed and heated at 100 °C behind a blast shield overnight. The reaction mixture was diluted with water and extracted with ethyl acetate. The organic phase was washed with brine and dried over magnesium sulfate then concentrated onto silica gel. The pure product was obtained by flash chromatography in a gradient of 100% hexane to 30% ethyl acetate hexane. [65% yield] 1H NMR (300 MHz, CDCl3) δ 11.58 (s, 1H), 7.96 (s, 1H), 7.70 (d, J = 8.5 Hz, 2H), 7.59 (d, J = 7.1 Hz, 2H).

iii. Synthesis of KT195 fluorophores

Compounds **21**-**25**.

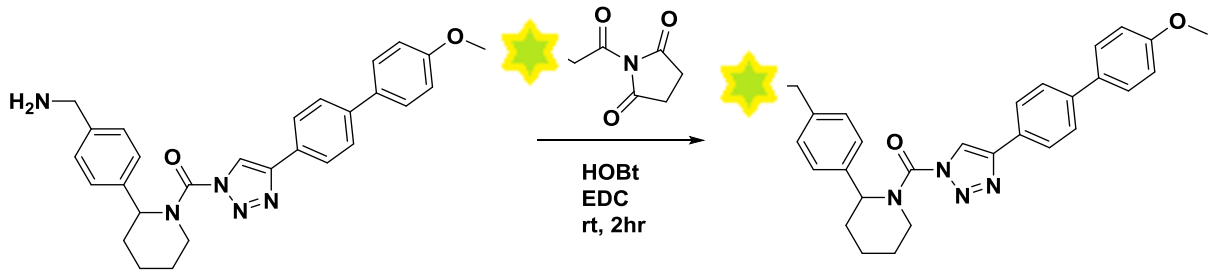

Compound **20** (1.8 mg, 0.004 mmol) was dissolved in DMF (0.5 mL) followed by addition of DIPEA (0.75 mL) and a NHS-fluorophore (0.0033 mmol). The reaction was protected from light and stirred at room temperature for 2 hours. The pure product was obtained by HPLC purification using methanol/water gradient of 65-90%. [45-77% yields]

21: [Thermo Fisher D2184] 1H NMR (300 MHz, CD2Cl2) δ 8.47 (s, 1H), 7.89 (d, J = 8.2 Hz, 2H), 7.67 (d, J = 8.4 Hz, 2H), 7.60 (d, J = 8.8 Hz, 2H), 7.35 (d, J = 8.0 Hz, 2H), 7.24 (d, J = 8.3 Hz, 2H), 7.16 (s, 1H), 7.00 (d, J = 8.8 Hz, 2H), 6.92 (d, J = 3.9 Hz, 1H), 6.29 (d, J = 4.1 Hz, 1H),

6.13 (s, 1H), 6.04 (s, 1H), 5.64 (s, 1H), 4.40 (d, J = 5.9 Hz, 2H), 4.03 (m, 1H), 3.85 (s, 3H), 3.26 (t, J = 7.5 Hz, 2H), 3.07 (t, J = 12.3 Hz, 1H), 2.66 (t, J = 7.5 Hz, 2H), 2.51 (s, 3H), 2.24 (s, 3H), 2.20 – 2.01 (m, 2H), 1.93 – 1.11 (m, 4H).

22: [Thermo Fisher D2191] 1H NMR (300 MHz, CD2Cl2) δ 8.47 (s, 1H), 7.89 (d, J = 8.1 Hz, 2H), 7.67 (d, J = 8.2 Hz, 2H), 7.59 (d, J = 8.7 Hz, 2H), 7.41 (d, J = 8.1 Hz, 2H), 7.30 (d, J = 8.1 Hz, 2H), 7.00 (d, J = 8.7 Hz, 2H), 6.09 (s, 2H), 5.88 (s, 1H), 5.66 (s, 1H), 4.44 (d, J = 5.7 Hz, 2H), 4.08 (m, 1H), 3.85 (s, 3H), 3.38 (dd, J = 15.8, 7.4 Hz, 2H), 3.09 (t, J = 12.2 Hz, 1H), 2.46 (m, 15H), 2.29 – 2.02 (m, 1H), 1.95 – 1.42 (m, 4H).

23: [Thermo Fisher D6117] 1H NMR (300 MHz, CD2Cl2) δ 8.47 (s, 1H), 7.89 (d, J = 7.9 Hz, 2H), 7.82 (d, J = 8.8 Hz, 2H), 7.67 (d, J = 8.2 Hz, 2H), 7.59 (d, J = 8.6 Hz, 2H), 7.38 (d, J = 7.8 Hz, 2H), 7.28 (d, J = 8.0 Hz, 2H), 7.13 (s, 1H), 6.97 (dd, J = 14.5, 8.9 Hz, 4H), 6.52 (d, J = 4.0 Hz, 1H), 5.86 (s, 1H), 5.64 (m, 2H), 4.36 (d, J = 5.8 Hz, 2H), 4.07 (m, 1H), 3.84 (d, J = 1.8 Hz, 6H), 3.27 – 2.94 (m, 3H), 2.72 (t, J = 7.2 Hz, 2H), 2.49 (s, 4H), 2.33 – 1.96 (m, 7H), 1.89 – 1.35 (m, 12H).

24: [Thermo Fisher D6184] 1H NMR (300 MHz, CD2Cl2) δ 8.47 (s, 1H), 7.89 (d, J = 8.0 Hz, 2H), 7.67 (d, J = 8.2 Hz, 2H), 7.63 – 7.50 (m, 2H), 7.38 (d, J = 7.8 Hz, 2H), 7.32 (d, J = 8.2 Hz, 2H), 7.12 (s, 1H), 7.05 – 6.96 (m, 2H), 6.94 (s, 1H), 6.31 (d, J = 3.7 Hz, 1H), 6.11 (s, 1H), 5.93

(s, 1H), 5.64 (s, 1H), 4.42 (d, J = 5.7 Hz, 2H), 4.03 (m, 1H), 3.85 (d, J = 2.3 Hz, 3H), 3.07 (t, J = 13.1 Hz, 1H), 2.95 (s, 2H), 2.49 (s, 3H), 2.25 (m, 5H), 2.19 – 1.98 (m, 2H), 1.91 – 1.16 (m, 8H).

25: [Thermo Fisher D6102] 1H NMR (300 MHz, CD2Cl2) δ 8.47 (s, 1H), 7.89 (d, J = 7.7 Hz, 2H), 7.67 (d, J = 8.3 Hz, 2H), 7.63 – 7.52 (m, 2H), 7.40 (d, J = 7.6 Hz, 2H), 7.32 (d, J = 8.1 Hz, 2H), 7.13 (s, 1H), 7.04 – 6.95 (m, 2H), 6.91 (s, 1H), 6.27 (s, 1H), 6.13 (s, 1H), 5.93 (s, 1H), 5.74 (s, 1H), 5.64 (s, 1H), 4.41 (d, J = 5.7 Hz, 2H), 4.03 (m, 1H), 3.85 (d, J = 2.3 Hz, 3H), 3.41 (s, 1H), 3.18 (m, 5H), 2.61 – 2.38 (m, 6H), 2.33 – 1.95 (m, 7H), 1.95 – 1.14 (m, 8H).

iv. Synthesis of Halo KT195

Compound **26**.

(i)

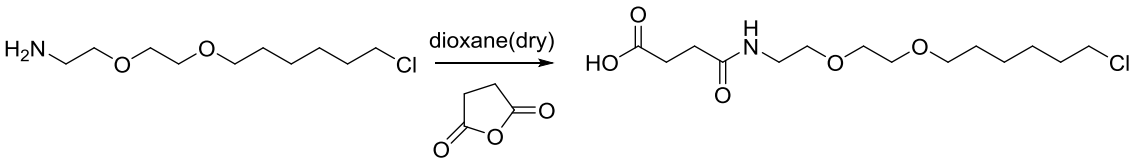

2-[2-[(6-chlorohexyl)oxy]ethoxy]-Ethanamine (0.1 g, 0.45 mmol) was dissolved in dry 1,4-dioxane (0.9 mL) and succinic anhydride (0.045 g, 0.45 mmol) was added. The reaction was refluxed at 105 °C for 5 hours. The reaction was poured into water and the pH was adjusted to 2 with 1 M HCl. The product was extracted with diethyl ether and the organic phase was washed with 0.1 M HCl, dried over magnesium sulfate, and the solvent was evaporated. . The crude product was used in the next reaction without further purification. [90% yield] 1H NMR (300 MHz, CDCl3) δ 3.83 – 3.21 (m, 12H), 2.78 – 2.53 (m, 4H), 1.93 – 1.15 (m, 8H).

(ii)

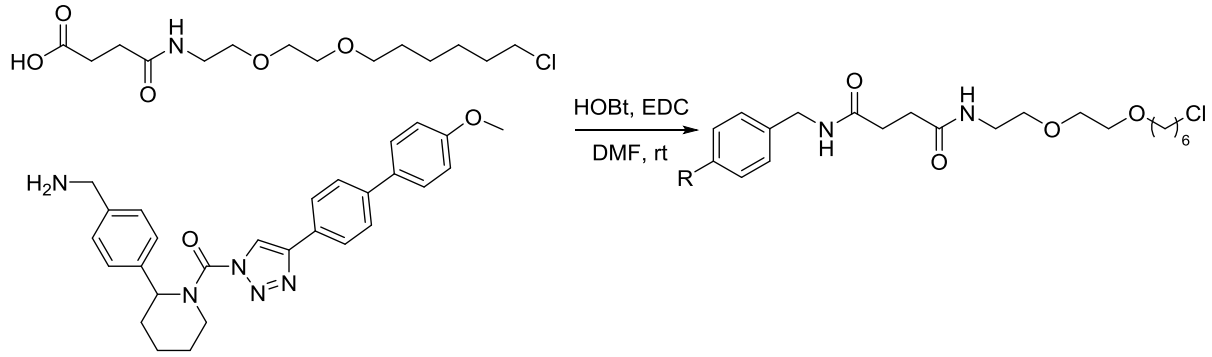

4-[[2-[2-[(6-chlorohexyl)oxy]ethoxy]ethyl]amino]-4-oxo-Butanoic acid (9.8 mg, 0.03 mmol) and compound **20** (6.4 mg, 0.014 mmol) were dissolved in DMF (1 mL). HOBT (4.2 mg, 0.027 mmol) and EDC (4.2 mg, 0.027 mmol) were added and the reaction was stirred at room temperature overnight. The pure product was obtained by HPLC purification using methanol/water gradient of 65-90%. [61% yield] 1H NMR (300 MHz, CDCl3) δ 8.45 (s, 1H), 7.91 (d, J = 8.2 Hz, 2H), 7.67 (d, J = 8.3 Hz, 2H), 7.60 (d, J = 8.7 Hz, 2H), 7.42 (d, J = 8.0 Hz, 2H), 7.33 (d, J = 8.3 Hz, 2H), 7.02 (d, J = 8.8 Hz, 2H), 6.46 (s, 1H), 6.25 (s, 1H), 5.76 (s, 1H), 4.47 (d, J = 5.7 Hz, 2H), 4.13 (s, 1H), 3.89 (s, 3H), 3.72 – 3.33 (m, 12H), 3.11 (t, J = 12.4 Hz, 1H), 2.67 – 2.43 (m, 5H), 2.32 – 2.02 (m, 1H), 1.98 – 1.17 (m, 12H).

v. Synthesis of KT195-alkyne derivative

Compound **27**.

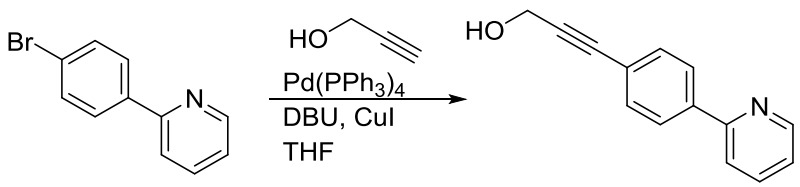

To a flame dried rbf was added dry THF (15 mL) and dry nitrogen gas was bubbled through the THF with stirring for 15 minutes. 2-(4-bromophenyl)-Pyridine (1.0 g, 4.3 mmol), propargyl alcohol (1.2 mL, 21 mmol), tetrakis(triphenylphosphine)palladium(0) (0.5g, 0.43 mmol), DBU (1.3 mL, 8.5 mmol), and CuI (0.024 g, 0.1 mmol) were added. The rbf was purged with nitrogen gas, sealed, and heated at 90 °C behind a blast sheild for 4 hours. The reaction mixture was poured into water and extracted with ethyl acetate. The organic phase was washed with water and brine, then dried over magnesium sulfate and concentrated onto silica gel. The pure product was obtained by flash chromatography in a gradient of 100% hexane to 30% ethyl acetate/hexane. [77% yield] 1H NMR (300 MHz, CDCl3) δ 8.68 (s, 1H), 7.88 (d, J = 8.6 Hz, 2H), 7.72 (m, 2H), 7.60 (d, J = 8.6 Hz, 2H), 7.33 – 7.18 (m, 1H), 4.49 (s, 2H), 3.0 (bs, 1H).

Compound **28**.

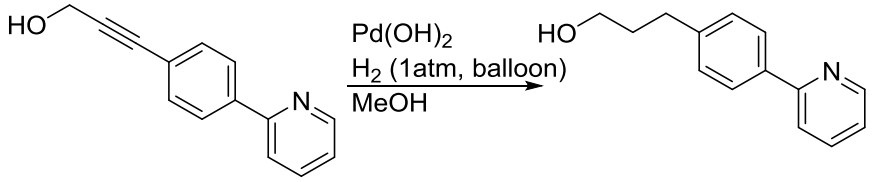

Compound **27** (2 g, 10 mmol) was dissolved in methanol (150 mL) then $Pd(OH)_2$ (1.34 g, 10 mmol) was added and the reaction was flushed with hydrogen gas then sealed placed under hydrogen atmosphere using a balloon and stirred at room temperature overnight. The reaction mixture was filtered and the solvent was evaporated. The crude product was used in the next step without further purification.

Compound **29**.

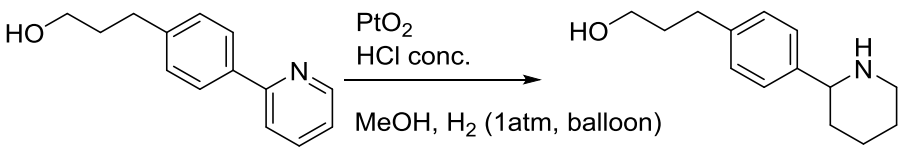

Compound **28** (2 g, 10 mmol) was dissolved in MeOH (64 mL) then glacial HCl (1.48 mL) and PtO_2 (0.11g, 0.5 mmol) were added. The flask was flushed with hydrogen gas then sealed placed under hydrogen atmosphere using a balloon and stirred at room temperature overnight. The reaction mixture was filtered and the solvent was evaporated. The crude product was used in the next step without further purification.

Compound **30**.

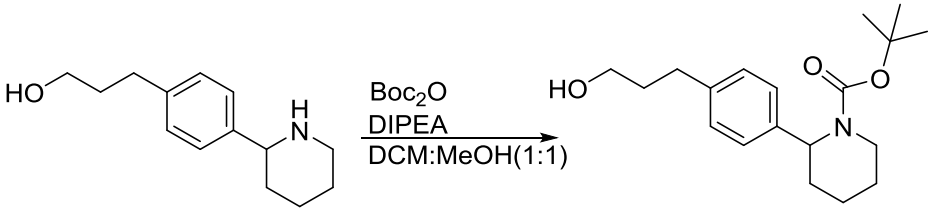

Compound **29** (2.52 g, 11.5 mmol) was dissolved in 1:1 DCM/MeOH (77 mL) and DIPEA (about 4 mL) was added until the pH was found to be 9. Then Boc_2O (7.5 g, 5 mmol) was added and the reaction was stirred at room temperature overnight. The reaction was concentrated on to silica gel without a workup and the pure product was obtained by flash chromatography in a gradient of 100% hexane to 30% ethyl acetate/hexane. [65% yield over 3 steps]

Compound **31**.

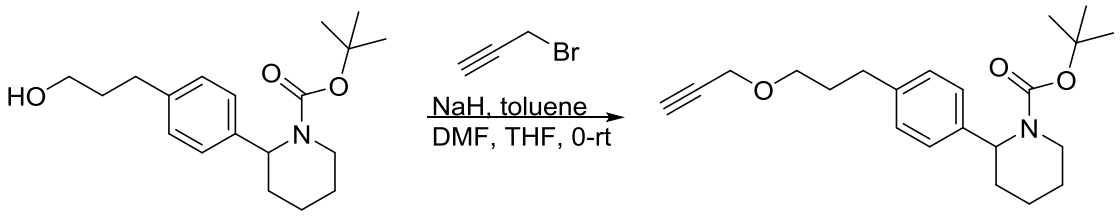

Compound **30** (2.4 g, 7.5 mmol) was dissolved in THF (63 mL) and DMF (16 mL) was added. The reaction was brought to 0 °C then treated with NaH (0.2 g, 8.3 mmol) and stirred for 30 minutes on ice. Propargyl bromide (1.25 mL, 11.3 mmol) was added and the reaction was stirred for 3 hours and allowed to warm to room temperature. The reaction mixture was then diluted with ethyl acetate and water was added slowly. The water layer was separated and extracted again with ethyl acetate. The organic phase was dried over magnesium sulfate and evaporated on to silica gel. The pure product was obtained by flash chromatography in a gradient of 100% hexane to 20% ethyl acetate/hexane. [56% yield] 1H NMR (CDCl3, 400 MHz) δ 7.19 – 7.10 (m, 4H), 5.39 (br s, 1H), 4.14 (d, J = 2.4 Hz, 2H), 4.01 and 4.05 (2 br s, rotamers, 1H), 3.53 (t, J = 6.4 Hz, 2H), 2.75 (m, 1H), 2.69 (dd, J = 8.7, 6.8 Hz, 2H), 2.42 (t, J = 2.4 Hz, 1H), 2.33 – 2.25 (m, 1H), 1.96 – 1.49 (m, 6H), 1.46 (s, 9H).(*53*)

Compound **32**.

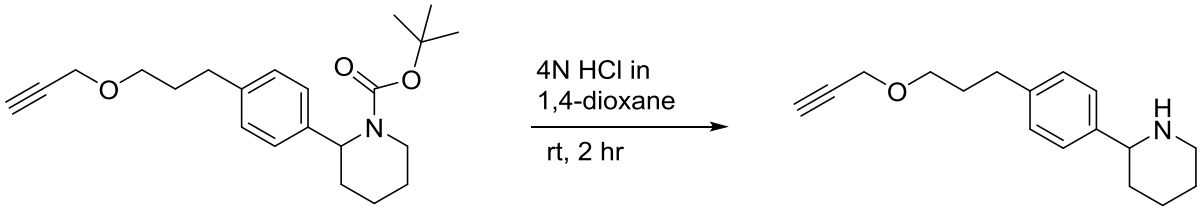

Compound **31** (1.2 g, 3.4 mmol) was treated with 4N HCl in 1,4-dioxane (52 mL) and stirred at room temperature for 2 hours. The solvent was evaporated and the crude product was used without further purification in the next reaction. [100% crude yield]

Compound **33**.

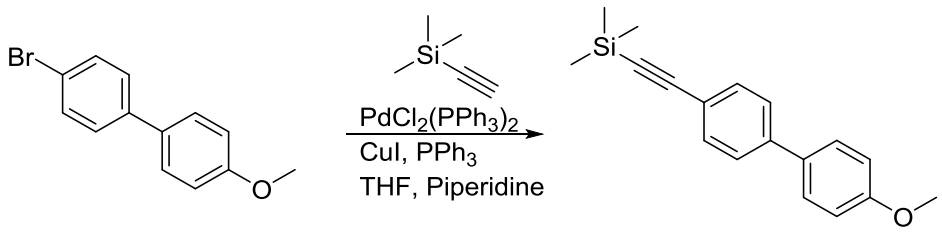

4-bromo-4'-methoxy-1,1'Biphenyl (2 g, 7.6 mmol), ethynyltrimethylsilane (1.9 mL, 13.7 mmol), bis(triphenylphosphine)palladium(II) dichloride (0.11 g, 0.15 mmol), copper(I) iodide (0.05 g, 0.3 mmol), triphenylphosphine (0.08 g, 0.3 mmol), piperidine (3 mL), and THF (4.5 mL) were added to a microwave reaction vial. The vial was purged with nitrogen gas and heated in a microwave reactor 120 °C for 12 min, max power 300 W. The reaction mixture was diluted with diethyl ether and washed with 10% sulfuric acid, then the organic phase was washed with water followed by brine. The organic phase was dried over magnesium sulfate and evaporated on to silica gel. The pure product was obtained by flash chromatography in a gradient of 100% hexane to 5% ethyl acetate/hexane. [67% yield] 1H NMR (300 MHz, CDCl3) δ 7.59 – 7.44 (m, 6H), 6.97 (d, J = 8.8 Hz, 2H), 3.85 (s, 3H), 0.26 (s, 9H).

Compound **34**.

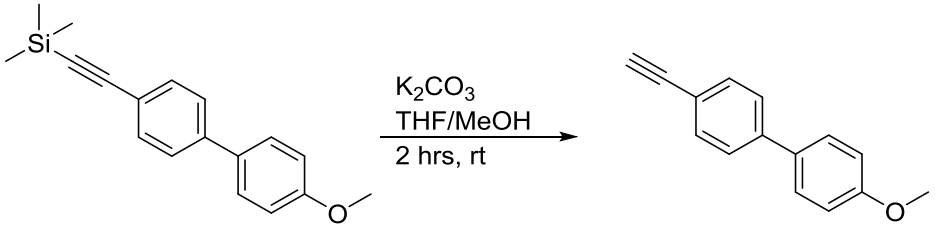

Compound **33** (2.8 g, 10 mmol) was dissolved in methanol (22 mL) and THF (50 mL) and potassium carbonate (5.5 g, 40 mmol) was added. The reaction mixture was stirred at room temperature for 2 hours then poured into water and extracted with ethyl acetate. The organic

phase was dried over magnesium sulfate and concentrated onto silica gel. The pure product was obtained by flash chromatography in 100% hexane. [95% yield] 1H NMR (300 MHz, CDCl3) δ 7.53 (m, 6H), 6.98 (d, J = 8.8 Hz, 2H), 3.86 (s, 3H), 3.11 (s, 1H).

Compound **35**.

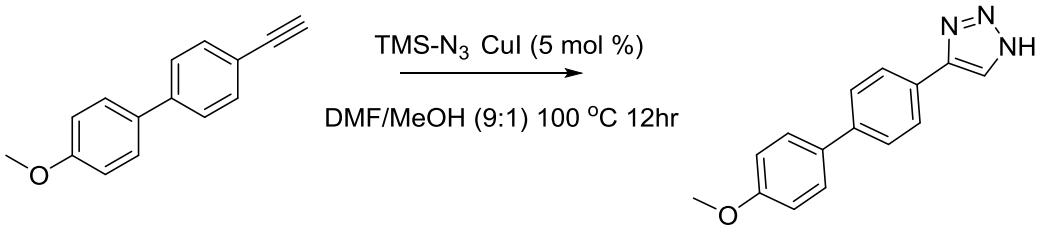

Compound **34** (0.05 g, 0.24 mmol), copper(I) iodide (0.002g, 0.01 mmol), DMF (0.43 mL), and methanol (0.05 mL) were added to a microwave reaction vial. The vial was purged with nitrogen gas and then azidotrimethylsilane (0.05 mL) was added carefully due to the toxicity of the reagent. The vial was sealed and heated at 100 °C behind a blast shield overnight. The reaction mixture was filtered through Florisil and evaporated onto silica gel. The pure product was obtained by flash chromatography in a gradient of 100% hexane to 80% ethyl acetate/hexane. [90% yield] 1H NMR (300 MHz, DMSO) δ 8.36 (s, 1H), 7.92 (d, J = 8.3 Hz, 2H), 7.69 (dd, J = 14.7, 8.6 Hz, 4H), 7.04 (d, J = 8.8 Hz, 2H), 3.81 (s, 3H).

Compound **36**.

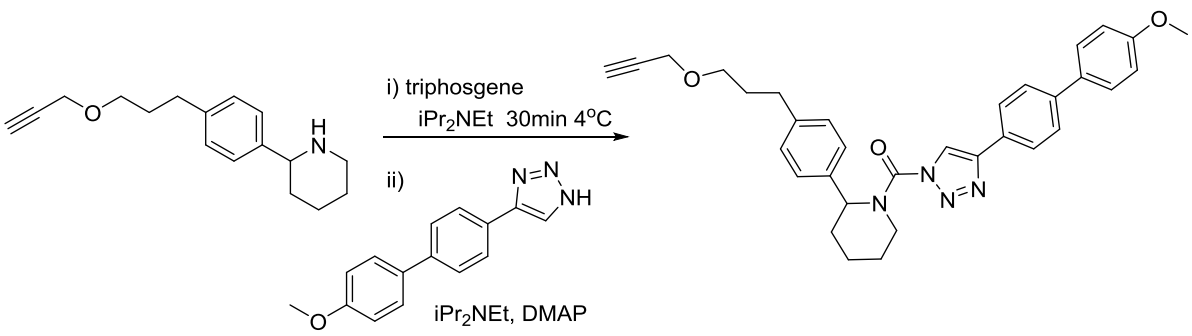

Compound **32** (0.05 g, 0.19 mmol) was dissolved in dry THF (1.5 mL) and DIPEA (0.1 mL, 0.6 mmol) and triphosgene (0.03 g, 0.09 mmol) were added. The reaction mixture was stirred at 4 °C for 30 minutes then poured into water and extracted with ethyl acetate. The organic phase was washed with water, then dried over sodium sulfate. The solvent was evaporated and the crude intermdiate was used without further purification. The intermediate was dissolved in dry THF (1.5 mL) and DIPEA (0.1 mL, 0.6 mmol), DMAP (0.023 g, 0.19 mmol), and compound **35** (0.05 g, 0.19 mmol) were added. The mixture was heated to 60 °C and stirred for 2 hours then poured into saturated aqueous ammonium chloride solution. The mixture was extracted with ethyl acetate, washed with water and brine, dried over sodium sulfate, then concentrated onto silica gel. The pure product was obtained by flash chromatography in a gradient of 100% hexane to 20% ethyl acetate/hexane. [74% yield] 1H NMR (300 MHz, CDCl3) δ 8.42 (s, 1H), 7.92 (d, J = 8.3 Hz, 2H), 7.65 (d, J = 8.4 Hz, 2H), 7.58 (d, J = 8.8 Hz, 2H), 7.42 – 7.10 (m, 4H), 7.00 (d, J = 8.8 Hz, 2H), 5.90 (s, 1H), 4.36 (d, J = 13.5 Hz, 1H), 4.15 (d, J = 2.4 Hz, 2H), 3.86 (s, 3H), 3.54 (t, J = 6.3 Hz, 2H), 3.18 (t, J = 12.3 Hz, 1H), 2.81 – 2.61 (m, 2H), 2.59 – 2.34 (m, 2H), 2.24 – 2.03 (m, 1H), 1.99 – 1.85 (m, 2H), 1.84 – 1.65 (m, 4H).

II. Toward Discovery of Inhibitors of Human Group III Secreted Phospholipase A2

A. Introduction

The cloning and expression of a cDNA coding for a human group III (hGIII) sPLA2 was first reported in 1999.(*88*) hGIII-sPLA2 was found to have a molecular weight of 55 kDa making it uniquely large among sPLA2s. It contains three domains: a central domain that displays features common to group III sPLA2s (key resides of the active site as well as the Ca^{2+} loop are conserved along with the 10 cysteines specific for GIII sPLA2s), a 130-amino acid N-terminal domain extension, and a 219-amino acid C-terminal domain extension which are functionally unknown and structurally not homologous to the other known sPLA2 proteins.(*88*)

Northern blot analysis of the tissue distribution of hGIII-sPLA2 found expression in kidney, heart, liver, and skeletal muscle tissue as well as presence at low levels in placenta and peripheral blood leukocytes. This pattern of expression is distinct from that of other human sPLA2s suggesting that this is a novel enzyme which has specific functions.(*88*)

Of particular interest, hGIII-sPLA2 has been shown to be highly expressed in mast cells.(*89*) GIII-sPLA2 was found to be secreted from both human and mouse mast cells and leads to subsequent production of prostaglandin D2 (PGD2). It is thought that PGD2 production is stimulated by arachidonic acid liberated from the *sn*-2 position of membrane phospholipids by GIII-sPLA2. The binding of PGD2 to its receptor (DP1) on the surface of mast cells then leads to mast cell maturation. Mice lacking mGIII-sPLA2 have been shown to produce immature mast cells and show a marked reduction in anaphylactic responses that are known to involve mast cell activation.(*89*) These findings suggest that inhibitors of hGIII-sPLA2 may be integral to the treatment of mast cell-mediated diseases.

Although multiple inhibitor classes for sPLA2s have been reported, so far none have been found to inhibit GIII-sPLA2.(*90*) Discovery of specific inhibitors for sPLA2s is complicated by the fact that they are interfacial enzymes that act at the lipid-water interface hence many inhibitors may act in a non-specific manner by causing desorption of the enzyme from the interface.(*91*) To date, reported assays for sPLA2s are not well suited for high throughput screening (HTS) of compound libraries due to lack of sensitivity thus requiring impractical amounts of enzyme. It is common for HTS assays to utilize fluorescence based optical readouts. Though a fluorescence-based sPLA2 assay has previously been developed, it is not appropriate for HTS because it relies on pyrene-containing phospholipids with excitation in the near-UV range and therefore optical quenching is likely to occur with a large number of test compounds in the library. Additionally, this assay incorporates a significant amount of serum albumin known to bind many drug-like molecules, rendering the assay unusable in a HTS format. (*92*)

This chapter details the results and adaptation of an assay (Thermo Fisher Scientific MP07701) for sPLA2s that has all of the properties desired for a high throughput assay: 1) The assay is sufficiently sensitive so that a reasonable amount of enzyme is needed; 2) The assay is easy to execute and miniaturize; 3) The fluorescence excitation and emission are well into the visible range where quenching is less of a problem; 4) The assay uses phospholipid vesicle substrate, thus allowing compounds to be tested in a matrix that highly resembles the natural environment of sPLA2s.(*93*)

B. Materials and Methods

i. Materials

Commercial lipids were as follows: Red/Green BODIPY PC-A2 (Life Technologies, part A10072); BODIPY Fluorescence Product (BODIPY FL C5) (Life Technologies, part D3834); dioleoylphosphatidylcholine (DOPC) (Avanti Polar Lipids, part 850375); dioleoylphosphatidylglycerol (DOPG) (Avanti Polar Lipids, part 840475). Other reagents and supplies are: Tris (Amresco, part 0497); NaCl (Macron, part 7581); $CaCl_2$ (calcium chloride pellets) (J.T. Baker, part 1313); ethylene-bis(oxyethylenenitrilo)tetraacetic acid (EGTA) (Fluka, part 03779); 96-well plates black (Perkin Elmer, part 6005279).

ii. Recombinant hGIII-sPLA2

Expression of hGIII-sPLA2 in *E. coli* has been previously described.(*88*) Inclusion bodies were isolated as described.(*9*) The inclusion body pellet was dissolved in 35 mL of 6 M guanidine-HCl, 0.3 M sodium sulfite, 50 mM Tris, pH 8.0 using a Dounce homogenizer and sonication. The mixture was treated with Thanhauser reagent. The mixture was centrifuged for 20 min at 10,000 rpm at 4°C to remove insolubles, and the supernatant was subjected to refolding using the dialysis method with refolding buffer consisting of 0.9 M guanidine-HCl, 50 mM Tris, pH 7.0, 0.8 M L-arginine, 6 mM L-cysteine, 5 mM L-methionine, 1 mM EDTA, and 0.1 M sulfobetaine SB 12. After 3 hours of refolding at room temperature, the mixture was removed from the bag and concentrated by ultracentrifugation using an YM-10 membrane. The concentrate was dialyzed against 20% acetonitrile/0.1% trifluoroacetic acid/5 mM L-methionine. The dialyzed solution was filtered to remove particulates (0.2 micron nylon-66 membrane) and submitted to

HPLC purification on a C18 Symmetry Shield column (Waters Corp.) using a gradient of 20% to 30% acetonitrile in water with 0.1% trifluoroacetic acid. Purity of hGIII-sPLA2 was estimated at 95% by SDS-PAGE. sPLA2s are very stable proteins and several previous publications have shown that they can be purified in native form using the methods described above. They have at least 5 disulfide bonds and mass spectrometry analysis of purified sPLA2s including group III sPLA2 shows that all disulfides are formed. This has been published previously.(*9, 93*)

iii. 96-well Plate hGIII-sPLA2 Inhibition Assay

Protein concentrations were measured with the Bradford dye reagent (BioRad Corp.) using bovine serum albumin as a standard. hGIII-sPLA2 solution (1 mg/mL) was stored at -80 °C and was thawed on ice prior to assay. hGIII-sPLA2 assay buffer was prepared as 50 mM Tris HCl pH 8.9, 100 mM NaCl, 1 mM $CaCl_2$. hGIII-sPLA2 stop buffer was prepared as 20 mM EGTA in 50 mM Tris-HCl, 100mM NaCl. Fresh before use, the hGIII-sPLA2 solution was diluted with hGIII-sPLA2 assay buffer to a concentration of 14 µg/mL (7 µg/mL final concentration). Test compounds were dissolved and diluted in DMSO (typical stock solution 1 mM in DMSO). Then, 1 µL of compound solution and 49 µL of enzyme solution were combined in the well of a black 96-well plate and incubated at room temperature (25 °C) for 15 minutes. To generate the control wells, hGIII-sPLA2 stop buffer (20 µL) was added to a well containing 49 µL of enzyme solution and 1 µL of DMSO. During the incubation period, the BODIPY substrate solution in a suspension of liposomes was made as follows. Red/Green BODIPY PC-A2 (1 mM in DMSO), DOPC (10 mM in ethanol), and DOPG (10 mM in ethanol) were thawed to room temperature (25 °C). Solutions containing BODIPY reagents were protected from light. Red/Green BODIPY PC-A2 (6.5 µL), DOPC (6.5 µL), and DOPG (6.5 µL) were combined in a 1.5 mL

conical polypropylene microfuge tube. The tube was flicked by hand several times to mix the substrate solution. After a brief centrifugation to bring the fluid to the bottom of the tube, 18 µL was removed and mixed with 982 µL of assay buffer, and the mixture was vortexed briefly (this gives 6 µM Red/Green BODIPY PC-A2 and 60 µM of DOPC and DOPG). This substrate solution (50 µL) was added to the well containing hGIII-sPLA2 and inhibitor after the 15 minute incubation period (see above) to start the reaction. The assay was incubated at room temperature (25 °C), protected from light, for 35 minutes. Stop buffer (20 µL per well) was then added to all wells (except for control wells in which it was already present). The assay was incubated for an additional 10 minutes, and the plate was read on a UV/VIS fluorimeter (PerkinElmer Victor^{3}V) with 485 nm excitation and 535 nm emission.

iv. 96-well Plate hGIII-sPLA2 Counterscreen Assay

Compounds that display a false positive inhibition due to quenching of the fluorescent product released by the enzyme were identified using the following counterscreen method. The assay was run as previously described along with an additional well per test compound that contained 1 µL of test compound in DMSO, 49 µL of enzyme solution, 50 µL of BOPIDY:DOPC:DOPG substrate solution (as above) but containing 300 nM BODIPY Fluorescence Product, and 20 µL stop buffer. The BODIPY Fluorescence Product was added from a 1 mM stock solution in DMSO. The amount of BODIPY FL C5 per well (150 nM) was determined by varying the concentration of BODIPY FL C5 until the fluorescence response matched that of the uninhibited enzyme.

v. 1536-Well hGIII-sPLA2 Inhibition HTS Assay

The 96-well assay was miniaturized to the 1536-well plate format. The final conditions for miniaturization, which required some modifications, are listed in **Table 2**. hGIII-sPLA2 enzyme was prepared in assay buffer (50mM Tris-HCl pH 8.9, 100 mM NaCl and 1mM $CaCl_2$) to a concentration of 2.63 μg/mL. Prior to the start of the assay, 2 μL of assay buffer were dispensed into control wells located in columns 1 thru column 3 of 1536-well black solid bottom microtiter plates. Next, 2 μL of assay buffer containing 2.63 μg/mL of hGIII-sPLA2 enzyme were dispensed into the remaining columns. Then, 37 nL of test compound in DMSO or DMSO alone (1.2% final concentration) were added to the appropriate wells using the automated GNF/Kalypsys robotic platform. Plates were incubated for 15 minutes at 25 °C. The BODIPY substrate solution in a suspension of liposomes was prepared following the same procedure as in the 96-well method. Then, the appropriate volume from the substrate solution was added and mixed in assay buffer. The lipid substrate mixture was vortexed briefly. This mixture yields a 5:5:1 DOPC:DOPG:BODIPY PC-A2 ratio. The assay started by the addition of 1 μL of 9 μM BODIPY PC-A2 substrate incorporated in liposomes containing 45 μM DOPC and 45 μM DOPG in assay buffer to all wells. Plates were centrifuged, and after 35 minutes of incubation at 25 °C, fluorescence was measured at 485nm excitation and 535nm emission using a ViewLux plate reader (PerkinElmer, Waltham, MA). Further details of this assay procedure can be found at the Pubchem AID 743126 (https://pubchem.ncbi.nlm.nih.gov/assay/assay.cgi?aid=743126) and are also listed in **Table 2**.(*93*)

vi. Screening Data

Raw fluorescent data were uploaded into the Scripps Research Institutes Molecular Screening Center (SRIMSC) HTS database (Symyx, Santa Clara, CA). Activity of each well was normalized on a per-plate basis using the following equation:

$$\%\ Inhibition = \ 100 \times \frac{Test\ well - Median\ Low\ Control}{Median\ High\ Control - Median\ Low\ Control}$$

Where Test well is defined as wells containing hGIII-sPLA2 enzyme in the presence of test compound and BODIPY PC-A2 substrate. Low Control is defined as the median of the wells containing test compounds and High Control is defined as the wells containing DMSO, BODIPY PC-A2 but, no hGIII-sPLA2.(*93*)

Data was normalized on a per plate basis, and each assay plate underwent a quality control check. A value greater than 0.5 for Z' was required before further testing.(*94*) For the primary screen, test compounds from the library were screened in singlicate at a final nominal concentration of 12.2 μM (final DMSO concentration of 1.2%). Well fluorescence was measured with a ViewLux plate reader (PerkinElmer, Waltham, MA), and the percent inhibition of each test compound was calculated on a per-plate basis. A mathematical algorithm was used to determine nominally inhibiting compounds in the primary screen. Four values were calculated to determine an interval based cutoff: (1) the average percent inhibition of all high controls tested plus three times the standard deviation of the high controls, (2) the average percent inhibition of all low controls tested minus three times the standard deviation of the low controls, (3) the average percent inhibition of all compounds tested between (1) and (2), and (4) three times their standard

deviation. The sum of two of these values, (3) and (4), was used as a cutoff parameter. Any compound that exhibited greater % inhibition than the cutoff parameter was declared active.

For dose-response experiments, the average of triplicate well data was plotted against compound concentration. A four-parameter equation describing a sigmoidal dose-response curve was fitted using Assay Explorer software (Symyx-MDL Information Systems). All further results from the screens can be found at NIH's PubChem website (http://pubchem.ncbi.nlm.nih.gov/) utilizing the AID listed in the **Table 3**.(*93*)

A two-way Venn diagram generator was used to cross compare data from the hGIII-sPLA2 confirmation and substrate counterscreen assays (**Figure 30**). Each of the assays was run at the SRIMSC and previously published in PubChem (AIDs 743126,743280, 743282, 743457 and 743455). The tool used is freely available and can be found at http://www.pangloss.com/seidel/Protocols/venn4.cgi.(*93*)

vii. Screening Library

BioFocus DPI (South San Francisco, CA) provided the Molecular Libraries Small Molecule Repository (MLSMR) library through the NIH's Roadmap Molecular Libraries Initiative. Further details regarding compound selection for this library can be found online at http://mli.nih.gov/mli/compound-repository/mlsmr-compounds/. When this assay was conducted, the library consisted of 370,276 small molecules (more than 50% in the molecular weight range 350-410 g/mol) comprised of both synthetic and natural products, from either commercial or academic sources, that can be grouped into the following categories: specialty sets of known bioactive compounds such as drugs and toxins (0.65%), focused libraries aimed at specific target

classes (2.85%), non-commercial sources (7.4%) and diversity sets covering a large area of the chemical space (89.1%).(*93*)

viii. HTS Confirmation and Tertiary Assays

The confirmation screen was run under the same conditions as the primary HTS, except that plates were assessed in triplicate and results for each compound were reported as the average percentage inhibition of the three measurements, plus or minus the associated standard deviation (Pubchem AID 743280). For titration experiments, assay protocols were identical to those described above, with the following exception that compounds were prepared in 10 point, 1:3 serial dilutions starting at a nominal test concentration of 120 μM, and assessed in triplicate using known methods (Pubchem AIDs 743457 and 743455).(*93, 95*)

C. Results and Discussion

i. Assay Principle

The structure of Red/Green BODIPY PC-A2 is shown in **Figure 22** along with the product (BODIPY FL C5) released by the action of hGIII-sPLA2. Intramolecular fluorescence energy transfer between the two fluorophores of Red/Green BODIPY PC-A2 leads to low fluorescence. Formation of the free fatty acid product leads to an increase in fluorescence due to spacial separation of the two fluorophores. Susceptibility to compound interference is always a concern and generally the higher the spectral emission of a fluorophore the less likely a compound will interfere. A key advantage of BODIPY FL C5 is that excitation and emission maxima are well into the visible range, and thus there should be minimal interference from compounds in the test

library that absorb in the UV-visible region. However the possibility of interference is still relevant but, is also concentration dependent. The substrate concentration was set at 3uM and generally as the concentration of the fluorophore increases the contribution from fluorescent compounds should be reduced. If readily available, a probe may have been chosen which emits at a longer wavelength, known to help reduce compound interference because the intensity of scatter light decreases with increasing wavelength based on the Rayleigh principle.(*96*)

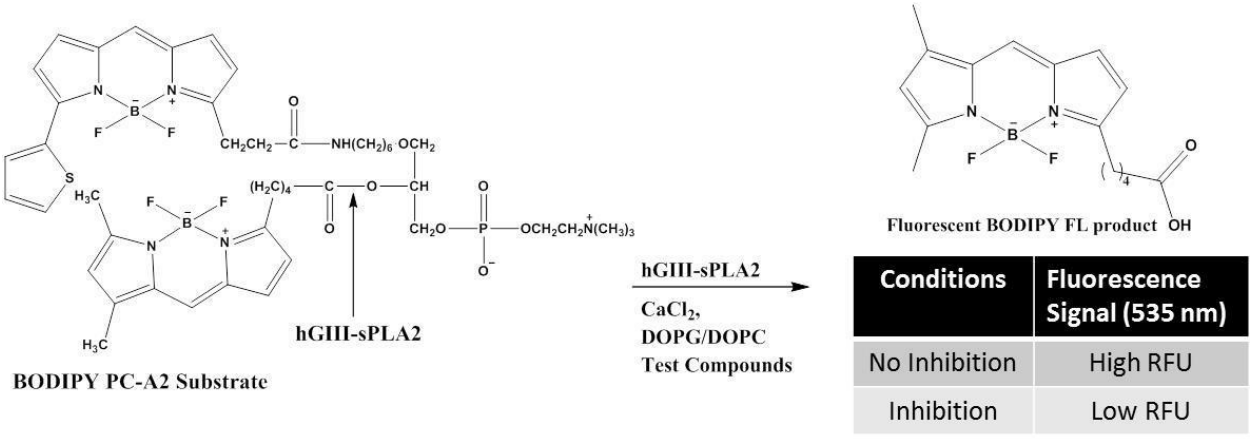

Figure 22. hGIII-sPLA2 fluorescent assay principle. Enzymatic activity of hGIII-sPLA2 was measured as an increase in fluorescent response due to cleavage of the fluorescent product, BODIPY CL F5, from the sn-2 position of Red/Green BODIPY® PC-A2. In brief, hGIII-sPLA2 enzyme is incubated with test compounds, followed by addition of the BODIPY PC-A2:DOPC:DOPG substrate mix and fluorescence is measured at a specific time point. A compound acting as an inhibitor would be identified by a decrease in fluorescent signal.(*93*)

Some of the compounds contained in the screening library may emit light in the region of our fluorescence assay response and thus lead to a false negative result. To take measures to prevent this, fluorescence would need to be measured at time zero (before addition of the enzyme) and at the endpoint of the assay. The presence of a fluorescent compound would presumably shift the fluorescence upward at both time points and to the same extent. In the high throughput screen, the fluorescence at time zero was not measured and we decided to live with the possibility of

false negatives rather than collecting twice as much fluorescent data. The results of the high throughput screen show that fluorescent compounds (compounds with negative inhibition beyond the low control + 3SD) tended to be more prevalent than putative quenchers. This was observed during the HTS campaign as 18,801 compounds had activity below 3 standard deviations plus average of the sample field; < -19.21%. Thus, by employing a signal increase assay as opposed to a signal decrease assay, we were able to avoid false positives due to the presence of fluorescent compounds.

To rule out quenchers (compounds that did not inhibit the enzymatic activity but instead quenched the fluorescence of the BODIPY FL C5 product), we developed a counter screen in which no enzyme was present. The amount of BODIPY FL C5 found to produce the same signal as that released by the uninhibited enzyme was incubated with the hits verified in the triplicate primary confirmation screen. A change in fluorescence of the enzymatic product by the library compound tells us if the compound itself reduces light emitted in the fluorescence channel of the instrument. Together with the scoring system for identifying possible hits, we now have an assay that thoroughly eliminates false positive or otherwise non-specific compounds in favor of possible true inhibitors of sPLA2s.

The following work describes the adaptation of an assay for sPLA2s to a high throughput screening platform based on phospholipids present in the form of lamellar vesicles. Some reported assays of sPLA2s rely on mixed-micelle substrate in which a small relative amount of phospholipid is dispersed in an excess of detergent as micelles. While the latter may be relevant to the action of pancreatic sPLA2 on phospholipid-bile salt mixed micelles, the group III sPLA2 acts on a cellular context and will presumably always act on phospholipids in cell membranes.

In this work we document that a high throughput assay using lamellar phospholipid vesicles is feasible.

We chose to use Red/Green BODIPY PC-A2 as a minor component in vesicles of DOPC/DOPG so that phospholipid vesicles with a well-defined lamellar structure would be formed (in case the fluorescent phospholipid did not form well-structured vesicles). A second feature is that all known mammalian sPLA2s bind tightly to the interface of vesicles that contain a critical amount of the anionic phospholipid DOPG.(*88, 97*) Tight binding to the vesicle interface is important for sPLA2 inhibitor analysis, since there are many compounds that inhibit these enzymes by the non-specific effect of causing desorption of enzyme from the interface into the aqueous phase, and we are more interested in true competitive inhibitors that bind in the active site slot of sPLA2 bound at the lipid-water interface.(*91*)

Recently there has been a report of an assay platform that incorporated sPLA2 as a reporter enzyme.(*98*) This assay screened for inhibitors of deubiquitylase (DUB) using a substrate composed of ubiquitin (Ub) or a ubiquitin-like protein (UBL) fused to the N-terminus of an sPLA2 rendering the sPLA2 inactive. Cleavage of the Ub-sPLA2 substrate by DUB released the sPLA2, which cleaved the fluorescent reporter NBD C6-HPC, generating a signal that was linear with DUB concentration. In this study, the fluorescent lipid appears to be simply dispersed from a solid into aqueous buffer. This probably leads to the formation of multi-lamellar vesicles. In contrast, in our study we used the ethanol dilution method, which is a reliable way to obtain unilamellar vesicles. In addition we did not use pure fluorescent phospholipid but rather a minor amount of the fluorescent phospholipid dispersed in non-fluorescent phospholipids that are well known to form well-defined, unilamellar vesicles. Thus our assay hopes to replicate ideal cellular conditions for sPLA2s to enable identification of true competitive inhibitors.

ii. Performance of the 96-well plate assay

To test our enzymatic assay, initial trials were performed in a 96-well assay format. **Figure 23** shows the reaction time course measured with the 96-well plate assay as a function of the amount of hGIII-sPLA2. **Figure 24** shows that the reaction progress ceases immediately following addition of EGTA, which chelates the catalytic cofactor Ca^{2+}, resulting in immediate quenching of enzymatic activity and thus a plateau in fluorescent signal. Based on these results, an amount of hGIII-sPLA2 of 0.7 µg per well and a quench time at 35 min was chosen for all fixed time point assays. **Figure 25** shows that the fluorescence in the fixed time point assay varies linearly with the amount of added hGIII-sPLA2.

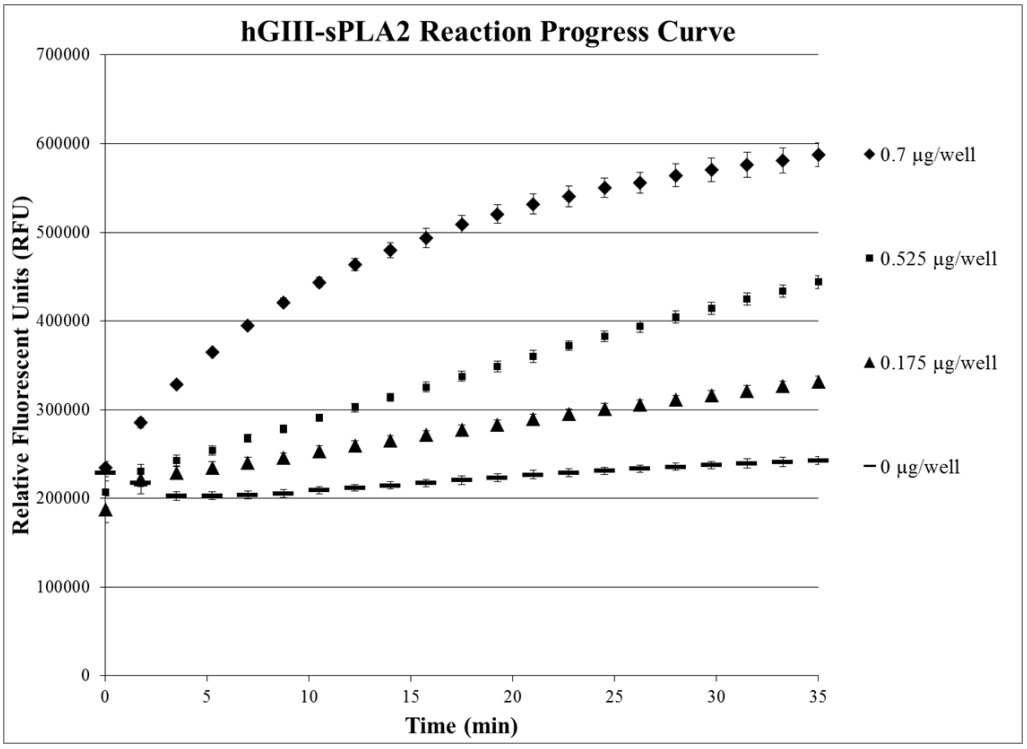

Figure 23. Reaction progress curves of various concentrations of hGIII-sPLA2 enzyme. A serial dilution of hGIII-sPLA2 was prepared in assay buffer and the reaction initiated with BODIPY PC-A2 substrate (3 µM final). Reaction progress was followed by measuring (1.75 minute intervals) the fluorescent intensity at 485 nm excitation and 535 nm emission on a PerkinElmer Victor3V imager for 35 min at room temperature (25 °C). The results plotted are the average of three wells. Error bars represent one standard deviation.(*93*)

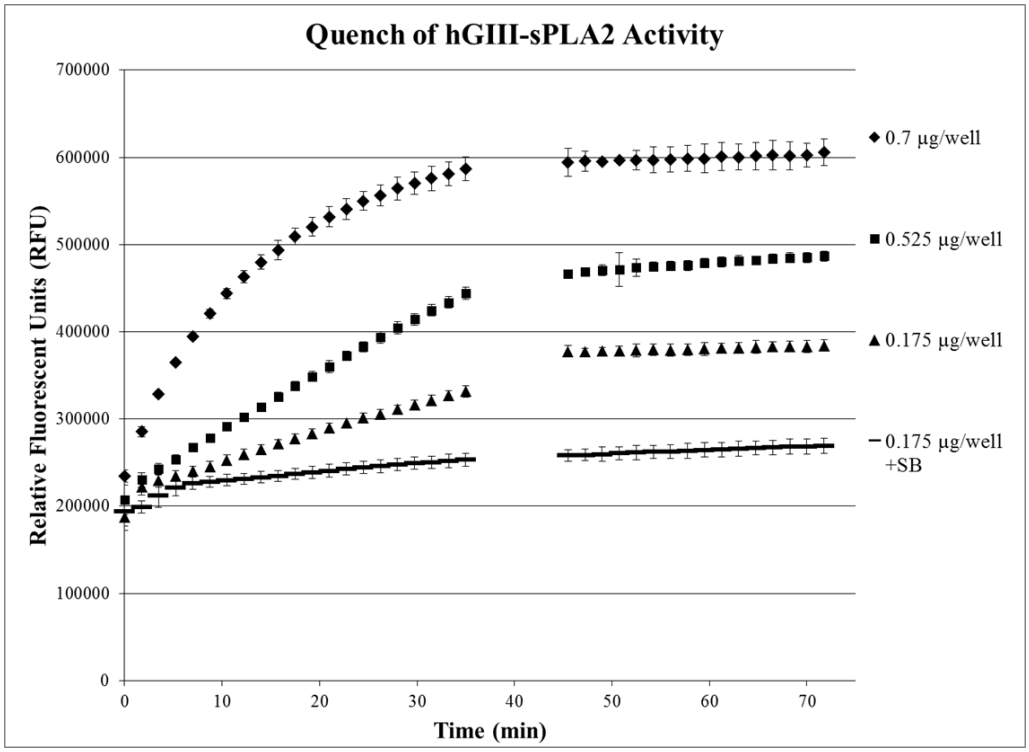

Figure 24. Reaction progress curves and quenching of activity of various concentrations of hGIII-sPLA2 enzyme. A serial dilution of hGIII-sPLA2 was prepared in assay buffer and the reaction initiated with BODIPY PC-A2 substrate (3 µM final). Reaction progress was followed by measuring (1.75 minute intervals) the fluorescent intensity at 485 nm excitation and 535 nm emission on a PerkinElmer Victor^{3}V imager for 35 min at room temperature (25 °C). At 35 minutes, the reaction was quenched by the addition of stop buffer (SB) which contained 20 mM EGTA (20 µL/well) followed by a 10 minute incubation period. The results plotted are the average of three wells. Error bars represent one standard deviation.(*93*)

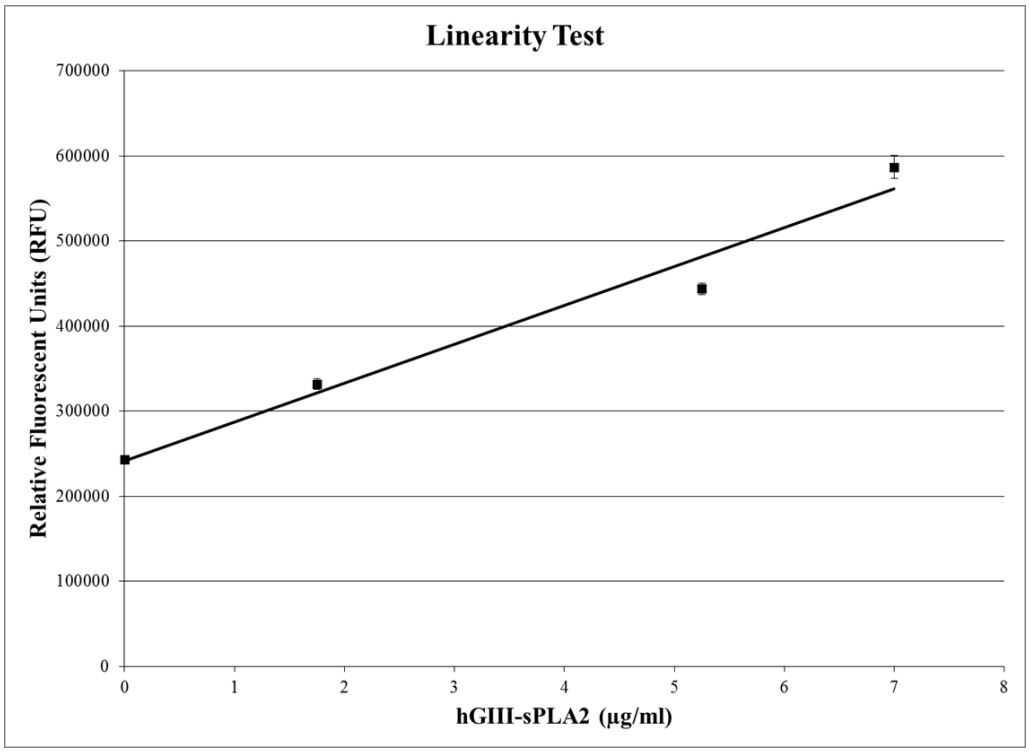

Figure 25. Dose response of fluorescence signal measured at 35 minutes after initiation of the reaction of hGIII-sPLA2 enzyme (serial dilutions in assay buffer) **with BODIPY PC-A2 substrate** (3 µM final). The results plotted are the average of three wells (R^2 = 0.967, Error bars represent one standard deviation).(*93*)

The robustness and reproducibility of the 96-well assay was examined by determining the Z' value.(*94*) The fluorescence response at 35 min of 10 replicates containing 0.7 µg of hGIII-sPLA2 per well, five pre-incubated with stop buffer, and five in which stop buffer was added at 35 min were used to determine a Z' value of 0.90, which corresponds to a high degree of reproducibility. Next, we tested the compound Indoxam, a well-known inhibitor of many sPLA2s.(*99*) This compound dose-dependently inhibited hGIII-sPLA2 in the 35-min fixed time point assay with an IC50 of 24 µM (not shown). When 24 µM Indoxam was added to the counter screen, the fluorescent signal was reduced by only 11% showing that the inhibitor blocks the action of hGIII-sPLA2 rather than quenching the fluorescence emission from the BODIPY FL C5 product. We also showed that inclusion of DMSO in the assay buffer up to 1.5% had no effect on the assay response (**Figure 26**). Finally, we demonstrated that the difference in Z'

value is minimal whether no enzyme is used as the control or enzyme plus stop buffer is used as the control, enabling us to save the use of enzyme for only testing wells in the case of the HTS (**Figure 27**).

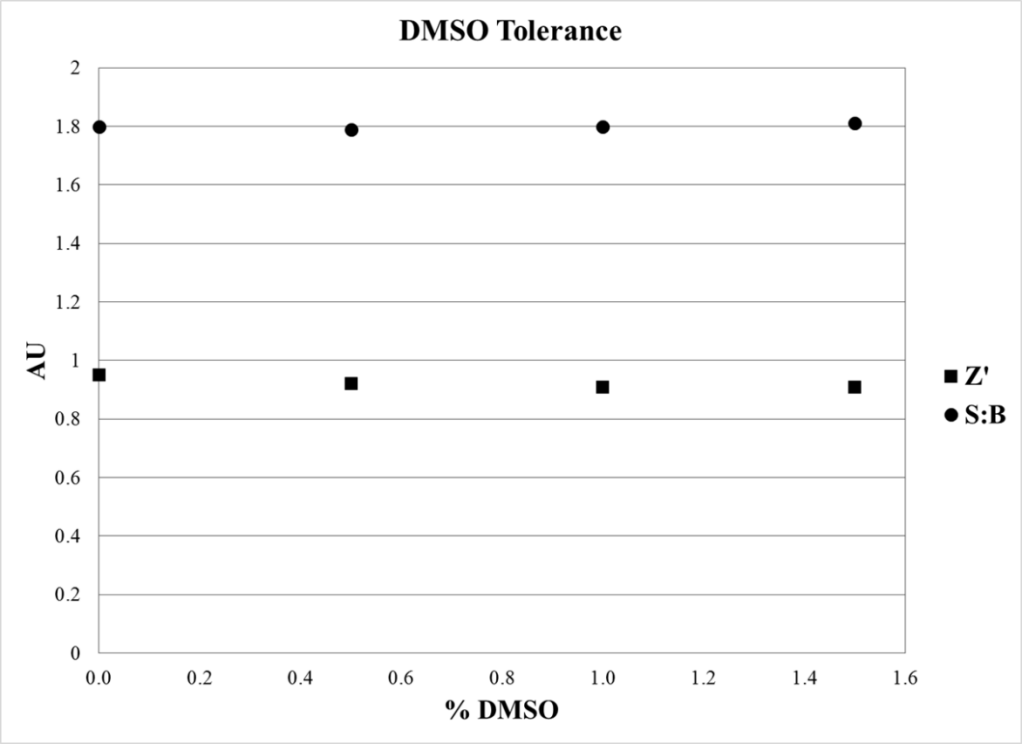

Figure 26. DMSO Tolerance 96-well Assay. The assay was performed in the 96-well plate format (n=4). hGIII-sPLA2 was prepared in assay buffer (7 µg/mL final concentration), the reaction was initiated with BODIPY PC-A2 substrate (3 µM final), and progressed for 35 min at room temperature (25 °C). At 35 minutes, the reaction was quenched by the addition of stop buffer containing 20 mM EGTA (20 µL/well) followed by a 10 minute incubation period. Control wells contained hGIII-sPLA2 and 20 mM EGTA (20 µL/well). Fluorescent intensity at 485 nm excitation and 535 nm emission was measured on a PerkinElmer Victor^{3}V imager.(*93*)

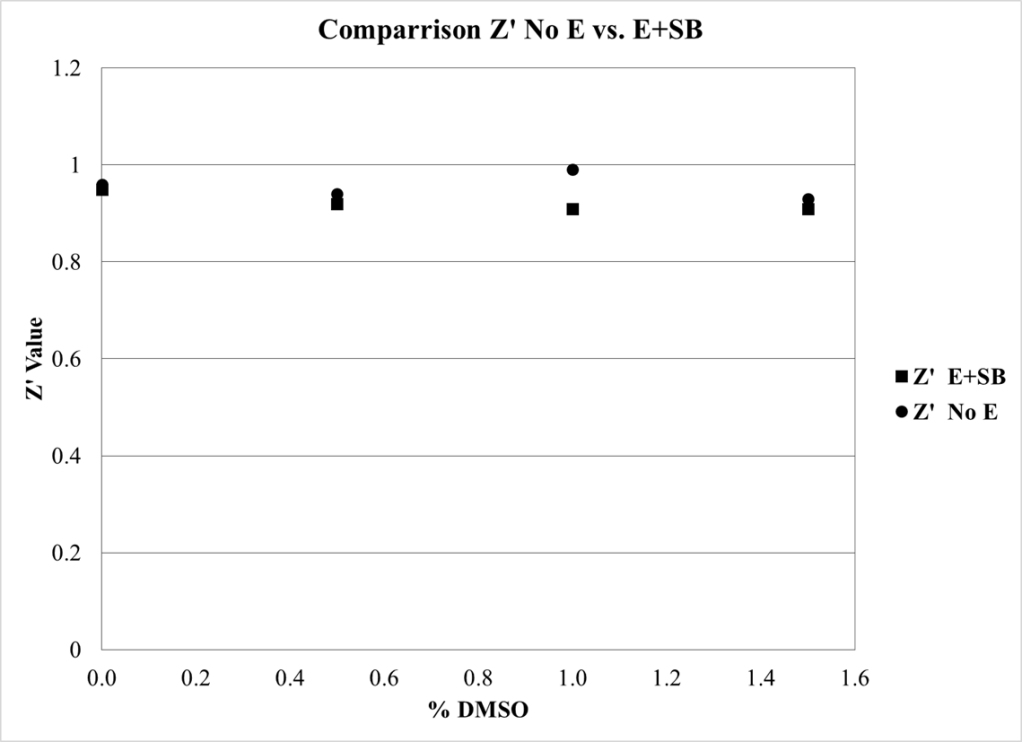

Figure 27. Z' Comparison. The assay was performed in the 96-well plate format (n=4). hGIII-sPLA2 was prepared in assay buffer (7 µg/mL final concentration), the reaction was initiated with BODIPY PC-A2 substrate (3 µM final), and progressed for 35 min at room temperature (25 °C). At 35 minutes, the reaction was quenched by the addition of stop buffer containing 20 mM EGTA (20 µL/well) followed by a 10 minute incubation period. Control wells contained either no hGIII-sPLA2 or hGIII-sPLA2 and 20 mM EGTA (20 µL/well). Fluorescent intensity at 485 nm excitation and 535 nm emission was measured on a PerkinElmer Victor^{3}V imager. It is evident from this data that the use of either no enzyme (No E) or enzyme plus stop buffer (E+SB) is an appropriate control for the assay.(*93*)

iii. hGIII-sPLA2 1536-Well Assay Optimization

Miniaturization of the assay to the 1536-well plate format (**Table 2**) required the re-optimization of the hGIII-sPLA2 enzyme concentration since it was found that the signal-to-blank was 2 fold higher than the 96-well signal-to-blank when testing at the same hGIII-sPLA2 enzyme concentration (7 µg/mL). In order to determine the optimal enzyme concentration and incubation time an enzyme titration test was performed as described in **Figure 28a**. With the goal of conserving available enzyme while maintaining or possibly increasing assay sensitivity

the enzyme concentration was reduced in the 1536 well assay to 1.75 µg/mL. At 35 minutes of incubation, the reaction was linear with respect to all enzyme concentrations tested for sPLA2 (**Figure 28b**). hGIII-sPLA2 stop buffer (20 mM EGTA in 50 mM Tris-HCl, 100 mM NaCl) was tested side-by-side with the no enzyme control in the 1536-well format and no difference was observed in the assay so in order to reduce the volume of the assay, no enzyme was used as the positive control (instead of the enzyme plus stop buffer) for the remainder of 1536-well assays. Furthermore, stop buffer was not utilized to stop the enzymatic reactions in the 1536-well format (as opposed to the 96-well format) because the plates were read immediately upon completion of the 35-minute incubation period.(*93*)

Table 2: HGIII-sPLA2 Primary and Counterscreen Assays Protocols in 1536-Well Plate Format. The *hGIII-sPLA2* primary inhibition screening and counterscreen assays were performed in the same format but the counterscreen assay employed the BODIPY Fluorescence Product to mimic the raw fluorescence signal as the uninhibited enzyme in presence of DMSO and substrate. The BODIPY fluorescence product in the substrate mix was added to the low controls and test wells. The BODIPY PC-A2 substrate mix in the absence of enzyme was added to the high controls. Details of the assay protocols can be found at PubChem.(*93*)

Order	Step	Assay Condition	Comments/Differences
1	Enzyme Mix or assay buffer dispensing	2µl/well	Final assay buffer composition: 50mM Tris-HCl pH8.9 + 100mM NaCl + 1mM CaCl2 **Primary**: Assay buffer was dispensed into the high controls and 1.75ug/mL of hGIII-sPLA2 final concentration was dispensed into the low controls and test wells **Counterscreen**: Assay buffer was dispensed into all wells
2	Compounds Addition	37nL/well	Compounds pinned at 12uM final concentration in 1.2% DMSO
3	Primary Incubation Time	15min	Room Temperature (25°C)
4	Substrate Mix Dispensing	1µL/well	**Primary**: 3uM BODIPY PC-A2, 15uM DOPC and 15uM DOPG (final assay concentrations) were dispensed into all wells. **Counterscreen**: Substrate mix as explained above was dispensed into the high controls wells. For the low controls and test wells, 25nM BODIPY Fluorescence product (final concentration) was added to the substrate mix.
5	Centrifuge plate	1 min	1,000 rpm
6	Incubation	35 minutes	Room Temperature (25°C)
7	Read fluorescence	Excitation 485 nm Emission 535 nm	EnVision reader

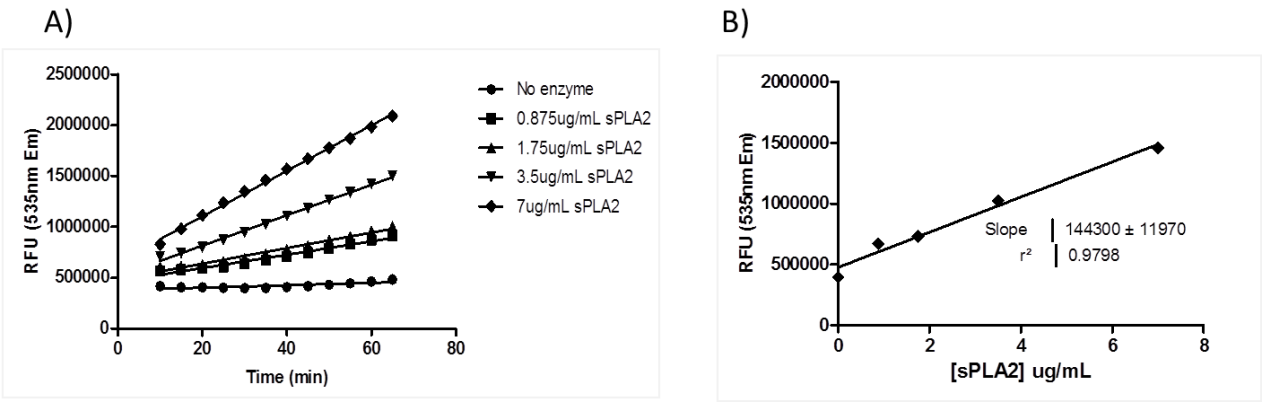

	0.875ug/mL sPLA2		1.75ug/mL sPLA2		3.5ug/mL sPLA2		7ug/mL sPLA2	
Time (min)	Z'	S:B	Z'	S:B	Z'	S:B	Z'	S:B
10	0.80	1.36	0.78	1.45	0.85	1.70	0.85	1.99
15	0.82	1.43	0.80	1.51	0.87	1.83	0.88	2.42
20	0.77	1.46	0.79	1.55	0.86	1.97	0.90	2.74
25	0.81	1.52	0.82	1.64	0.89	2.17	0.91	3.08
30	0.82	1.60	0.84	1.74	0.90	2.38	0.92	3.40
35	0.83	1.68	0.86	1.84	0.91	2.57	0.92	3.66
40	0.83	1.74	0.85	1.91	0.90	2.72	0.92	3.86
45	0.87	1.80	0.87	1.96	0.92	2.84	0.92	4.02
50	0.84	1.83	0.87	2.01	0.91	2.94	0.92	4.13
55	0.88	1.86	0.88	2.04	0.92	3.01	0.92	4.21
60	0.84	1.88	0.87	2.07	0.92	3.08	0.92	4.28
65	0.85	1.89	0.87	2.08	0.92	3.11	0.92	4.33

[sPLA2] ug/mL	Z'	S:B
0.88	0.83	1.68
1.75	0.86	1.84
3.50	0.91	2.57
7.00	0.92	3.66

Figure 28. Enzyme Titration vs. Time. A) 1536-well format assay using different enzyme concentrations over time to determine reaction linearity. Four serial dilutions of hGIII-sPLA2 were prepared in assay buffer and the reaction initiated with BODIPY PC-A2 substrate (3 µM final). Reaction progress was followed by measuring (5 minute intervals) the fluorescent intensity at 485 nm excitation and 535 nm emission on a PerkinElmer EnVision reader for 65 min at room temperature (25 °C). Linear regression analysis plot of data using mean, standard deviation and an N=32 per point; error bars are included B) sPLA2 titration was measured at 35minutes after adding the BOPIPY PC-A2 substrate (3µM final). The results plotted are the average of 32 wells. Error bars are included.(*93*)

iv. Performance of the 1536-well HTS assay

Miniaturization of the 96-well plate format to the 1536-well plate format was implemented to reduce the cost and increase the throughput of the HTS campaign. Optimization of the assay (described above) was performed to achieve the appropriate sensitivity and separation between controls. Every assay plate contained two sets of controls (N=24 per set): the high control (no enzyme) and the low control (enzyme), both controls containing DMSO (1.2% final). These controls were used to ensure hGIII-sPLA2 activity, normalize the data, and monitor the data quality by measuring Z' and signal-to-blank. Though Z' values can be artificially inflated when

using such controls, they do provide a reasonable gauge of assay robustness particularly when more appropriate small molecule or specific ligand controls are unavailable. To aid in visualization of the activity across the HTS campaign, all primary HTS data was normalized to the no enzyme control vs. enzyme, and was used to produce a scatterplot (**Figure 29**). In the interest of removing fluorescence artifacts, a counterscreen assay similar to that developed for the 96-well plate format, was implemented in 1536-well plate format. This counterscreen assay uses the BODIPY fluorescence product and measures the changes in the fluorescence signal in the absence of hGIII-sPLA2 enzyme. In order to use this assay as a counterscreen, a titration of the BODIPY Fluorescence product was performed to achieve a fluorescence signal equivalent to the completed reaction (1536-well plate format) when the enzyme was present in the reaction. The counterscreen assay was used at the HTS secondary and tertiary stages and all subsequent experiments were performed using the conditions listed in **Table 2**.(*93*)

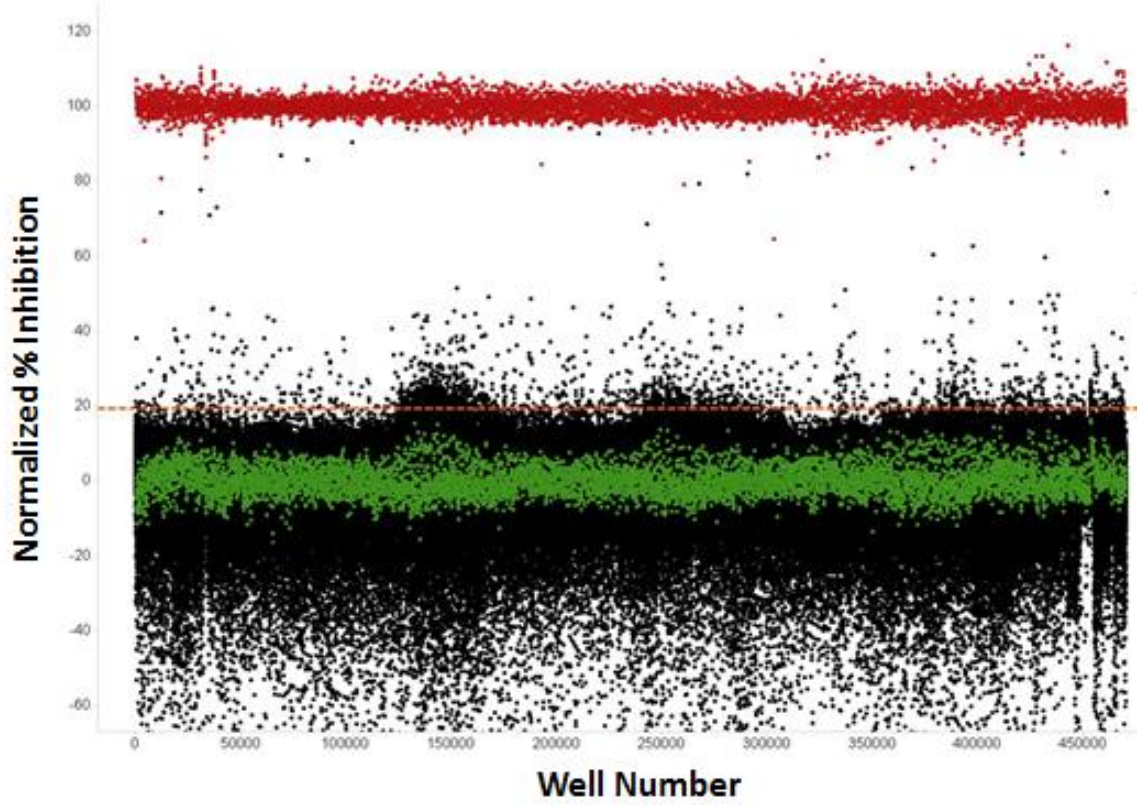

Figure 29. Primary Screen Scatterplot. Normalized percent inhibition data vs. well number were plotted in randomized order. (●) Low control wells containing enzyme, substrate, and DMSO only; (●) represent data wells containing enzyme, substrate, and compounds; and (●) represent high control wells containing substrate, no enzyme, and DMSO. The dashed line represents the hit cutoff of 19.21%, which is the average + 3 SD of the data wells. Compounds with inhibition above this line were considered primary active hits. Using the cutoff of 19.21%, 2,090 compounds were identified as hits.(*93*)

The hGIII-sPLA2 primary assay and counterscreen assay were implemented at a final assay volume of 3 µL/well in 1536-well plates. The primary assay was screened against the entire available MLSMR collection; 370,276 unique compounds were tested. All MLSMR compounds were screened at 12.2 µM. The median of the wells containing test compounds was used as a low control. Using these controls, the hGIII-sPLA2 assay demonstrated robust screening statistics. It had an average signal-to-background ratio (S/B) of 1.91 ± 0.07 and a Z' of 0.81 ± 0.04 (n=306 plates).(*93*)

v. Selection of Hits

Table 3: HTS Campaign Summary and Results. The *hGIII-sPLA2* inhibition screening campaign is summarized in Table 3. Details relative to each phase of the uHTS campaigns are shown in this table. All the data associated to each of the HTS stages are in PubChem.(*93*)

Ultra-High-Throughput Screening Campaign Summary and Results								
							Assay Statistics	
Screen type	*Target*	*Number of compounds tested*	*Number of replicates/ concentrations*	*Selection Criteria*	*Number of active compounds (Hits)*	**PubChem AID*	*Z'*	*S/B*
Primary screen	HGIII-SPLA2	370,276	1/1	%inh> 19.21%	2,090	743126	0.81 ± 0.04	1.91 ± 0.07
Confirmation	HGIII-SPLA2	1,972	3/1	%inh> 19.21%	680	743280	0.82 ± 0.03	1.68 ± 0.02
Counterscreen	BODIPY PC-A2	1,972	3/1	%inh> 5.92%	167	743282	0.90 ± 0.01	2.73 ± 0.15
Titration	HGIII-SPLA2	240	3/10	IC_{50}<10μM	1	743457	0.77 ± 0.03	2.04 ± 0.03
Counterscreen	BODIPY PC-A2	240	3/10	IC_{50}<10μM	0	743455	0.87 ± 0.01	2.94 ± 0.08

The HTS campaign to identify inhibitors of *hGIII-sPLA2* is summarized in **Table 3**. All compounds were tested at a nominal concentration of 12 μM. The primary screen identified 2,090 compounds (i.e. 0.56% of the total library) as active compounds where an active compound is described as exhibiting a percent inhibition greater than the nominal hit cutoff of 19.21%. This cutoff was chosen using the interval based method to take advantage of eliminating extreme outliers in activity, either positive or negative, thus preserving the less active compounds closer to the baseline for further study.(*100*) Of the 2,090 compounds identified as active, 1,972 were available from the MLSMR for testing in the confirmation and counterscreen stages (**Figure 30**). Inhibitory activity was confirmed and fluorescence artifacts were eliminated by retesting the 1,972 available compounds in triplicate in two different assays: (1) the original

primary assay and (2) the substrate fluorescence counterscreen assay. The hGIII-sPLA2 inhibitor confirmation assay performance was consistent with an average Z' of 0.82 ± 0.03 and a signal-to-blank of 1.68 ± 0.02. The primary assay hit-cutoff was applied to the confirmation assay which was 19.21%. The counterscreen assay performance was robust with an average Z' of 0.90 ± 0.01 and a signal-to-blank of 2.73 ± 0.15. A method to determine a cutoff for the counterscreen which would rule out fluorescence artifacts while preserving compound displaying inhibitory effects was needed. The cutoff for the counterscreen used to qualify active compounds was the average percent inhibition of all wells containing DMSO only plus three times their standard deviation (5.92%) (Pubchem AID 743282). Using this method 167 compounds (8.47% of the 1,972 compounds tested) were identified as exhibiting at least moderate fluorescence quenching. This result validates the effectiveness of using the BODIPY PC-A2 as a probe as it was minimally affected by fluorescent artifacts.(*93*)

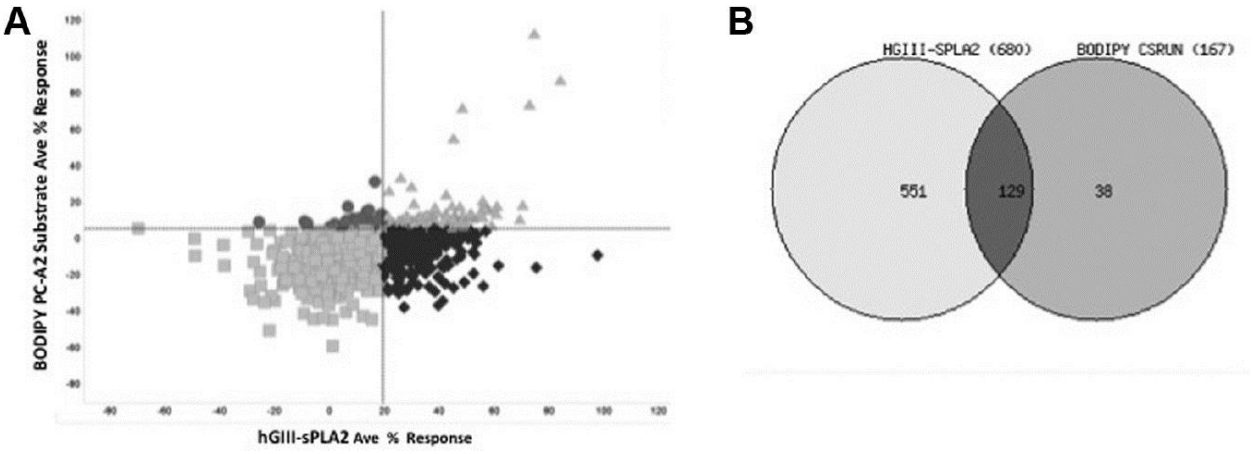

Figure 30. Comparison of hGIII-sPLA2 confirmation and substrate counterscreen results. (A) Correlation plots of activity of the secondary data results (n = 1972) from hGIII-SPLA2 confirmation assay (x-axis) and BODIPY substrate counterscreen assay (y-axis) are shown. The horizontal dashed line represents the BODIPY substrate activity cutoff (5.92%) while the vertical dashed line represents the hGIII-sPLA2 activity cutoff (19.21%). Compounds with inhibition above this line were considered active hits. Diamonds indicate active compounds in the primary assay. Triangles indicate compounds active in both assays. Circles indicate active compounds in the counterscreen assay. Squares indicate inactive compounds in both assays. (B) Venn diagram was performed with the 680 active compounds in hGIII-sPLA2 vs. 167 counterscreen actives. In total, 551 compounds appear to be active in the primary assay while 129 compounds overlap between primary and counterscreen assays.(*93*)

The confirmation screen in combination with the counterscreen yielded 551 compounds with confirmed activity against hGIII-sPLA2 that were not active in the counterscreen (680 confirmed inhibitors minus the 129 of those compounds that were found to exhibit fluorescence quenching, see **Table 3**). Confirmed and counterscreen inactive compounds identified at this stage were prioritized for concentration response curve (CRC) studies (275 compounds). This number was limited as part of the MLSMR effort. To facilitate compound selection for titration studies, the 551 compounds were classified into 84 clusters based on their most common substructure.(*101*) Based on this analysis, 61 clusters were represented in the final compound selection for dose response (73%). Under these criteria, 275 compounds were selected for IC_{50} titration, of which 240 compounds were available for further testing. **Figures 30** and **31** provide a summary of this data.(*93*)

The CRCs for the 240 compounds were determined via testing in triplicate 10 point three fold serial dilution format against both primary and counterscreen assays.(*95*) The dose response and counterscreen assays yielded satisfactory performance with an average Z' of 0.77±0.03 and a S:B of 2.04±0.03 for primary assay and Z' of 0.87±0.01 and a S:B of 2.94±0.08 for counterscreen assay. Taking a closer look at individual CRCs allowed for better examination of individual compound inhibition profiles between the primary and counterscreen assays, allowing for the removal of fluorescence artifacts such as CID "5399788", a possible fluorescence quencher based on similar inhibition in the primary and counterscreen assays (Appendix A.). To identify non-specific compounds that appear as hits in this biochemical HTS assay, additional analysis such as promiscuity and identification of Pan Assay Interference Compounds (PAINS) values were undertaken.(*102*) Of the 240 compounds analyzed at this stage, 45 compounds were considered PAINS which equates to ~18% of the total compounds tested. Promiscuity data

analysis was performed by analyzing how many times a compound is considered active over the total of screened MLPCN PubChem assays. It was found that a majority of the compounds (209) have low promiscuity (i.e. were active in ≤10% of the assays tested). As routine for the Roadmap initiative dose response results, compounds that yielded IC_{50} values below 10 μM are considered "active". Unfortunately, this HTS campaign produced only one compound that had an IC_{50} < 10 μM and was inactive in the counterscreen assay. However, there are 72 compounds with an IC_{50} > 10 μM in the primary assay that exhibited an average maximum response > 50% in the primary assay and <50% in the counterscreen assay. Of those, there are 16 compounds with IC_{50} values between 10-30 μM with more than 3 fold selectivity between primary and counterscreen assays (Appendix A.). Representive compounds for the top six most populated clusters were of interest for further characterization in low throughput assays and structure activity relationship (SAR) studies (**Figure 31**).(*93*)

	A	B	C	D	E	F
Structure	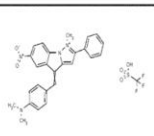	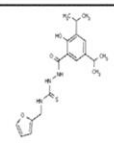	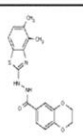	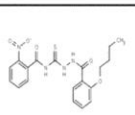	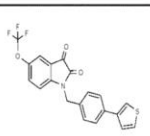	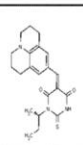
Dose Response Curves	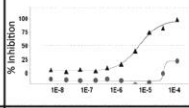	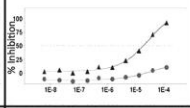	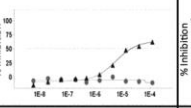	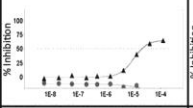	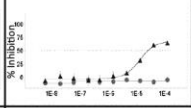	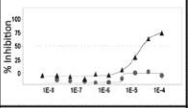
CID	404404	2211008	12005954	3138378	45281797	2927522
IC50 (uM)	6.1	18.8	20.5	20.8	25.5	25
Raw IC50 (uM)	6.2	29.0	5.7	10.5	13.1	16.4
IC50 (uM) Counterscreen	>121.8E-6	>121.8E-6	>121.8E-6	>121.8E-6	>121.8E-6	>121.8E-6
Averaged Max Response ± Standard Deviation	97.8 ± 2.7	91.9 ± 2.4	62.1 ± 2.7	64.7 ± 1	64.8 ± 4	74.4 ± 2.2
Cluster ID	10	3	20	2	7	22
# compounds	14	38	6	24	3	1

Figure 31. Compound dose-response curves. Normalized percent inhibition data (y-axis) were plotted vs. the log concentration in molar units on the x-axis. (▲) represent hGIII-sPLA2 fluorescence primary assay curve and (•) represent substrate counterscreen curve. Representive compounds for the top six most populated clusters (A–F) are

shown with their structures, averaged maximum percent response, and the IC_{50} values. All these compounds have an activity >50% in the hGIII-sPLA2 primary assay and low activity (<50%) in the counterscreen assay. For cluster A, compound CID 404404 was identified as a hit with an IC_{50} <10 μM. For cluster B, compound CID 2211008 displayed high activity based on the averaged maximum response (92%) but with a final IC_{50} >10 μM (18.8 μM). Compounds named CID 12005954, 3138378, 45281797, and 2927522 had an averaged maximum response between 60% and 75% with an IC_{50} in the range of 20 to 30 μM (C–F). Note: Raw IC_{50} data were obtained by fitting nonnormalized data to provide a point of reference compared to IC_{50} data. Compounds that do not reach high levels of inhibition compared to the controls can still be fairly active so long as they exhibit an upper and lower asymptote. All these compounds have some structure-activity relationship based on the number of compounds represented in each cluster number assigned by the clustering algorithm; all results are provided in the supplemental section.(*93*)

vi. Evaluation of Hits

A subset of hits obtained from the high throughput screen (**Figure 31**) was tested in an orthogonal assay to confirm sPLA2 inhibition. The hits chosen were representative of each of the 6 primary scaffold clusters of sPLA2 and all were among the 16 compounds that had purported IC_{50} between 10 and 30 μM. A well-established assay for PLA2 activity on [^{3}H]-oleic acid labeled *E. coli* membranes (see section E) was employed for this purpose.(*103*) This assay measures the release of radiolabeled oleic acid from autoclaved membranes derived from *E. coli* that have been grown in the presence of tritiated-oleci acid. After incubation with sPLA2, membranes are centrifuged and released [^{3}H]-oleic acid in the supernatant is measured by scintillation counting. It should be noted that compound E (**Figure 31**) was not available for further testing. The data confirm that compounds A, C, D, and F are inhibitors of hGIII-sPLA2 (**Table 4**). Compound B was not found to inhibit hGIII-sPLA2 in this assay.

Table 4. Inhibition of hGIII-sPLA2 by inhibitors A, B, C, D, and F in [^{3}H]-oleic acid labeled *E. coli* membrane assay. A final concentration of 2.5 μg/mL (hGIII-sPLA2) was chosen based on the results of the linearity test (**Figure 35**). Test compounds were dissolved and diluted in DMSO. Compound A was tested over a range of concentrations from 0.6-40 μM. Compounds B and F were tested over a range of concentrations from 6.25-100 μM. Compounds C and D were tested over a range of concentrations from 2.5-80 uM. hGIII-sPLA2 was prepared in PLA2 activity buffer (7.5 μg/mL) and allowed to incubate with the various inhibitors for 15 minutes. The reaction was initiated with addition of [^{3}H]-oleic acid labeled *E. coli* membranes and progressed for 30 min at 37 °C. At 30 minutes, the reaction was quenched by the addition of PLA2 stop buffer (300 μL/tube) followed by a 10 minute incubation period. Disintegrations per minute (dpm) were measured on a Beckman LS 6500 scintillation counter. All assays used to determine IC_{50} values were performed in triplicate.(*93*)

IC50 (μM) [^{3}H]-Oleic Acid Assay	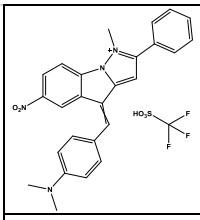	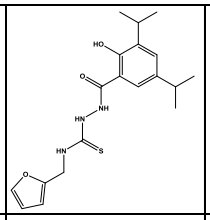	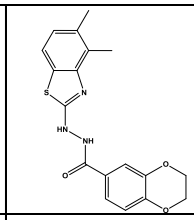	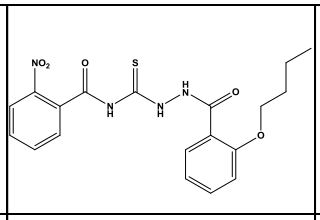	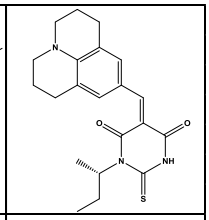
	A	**B**	**C**	**D**	**F**
hGIII-sPLA2	5	>100	21	18	43

The subset of hits obtained from the high throughput screen (**Figure 31**) were further analyzed for specificity by testing their ability to inhibit two other mammalian sPLA2s, human group IIA and human group X sPLA2s (**Table 5**). The data show that compounds C, and D are selective for group III sPLA2 over groups IIA and X sPLAs. This suggests that they are not promiscuous compounds that work by non-specific mechanisms such as destruction of phospholipid vesicle structure. Compounds A and F are pan-specific, active on all three sPLA2s, and are therefore less interesting for further evaluation as targeted inhibitors of hGIII-sPLA2.

Table 5. Percent inhibition of hGIIA-sPLA2, and hGX-sPLA2 by inhibitors A, B, C, D, and F. The assay was performed in the 96-well plate format in triplicate. Test compounds were dissolved and diluted in DMSO. The sPLA2 enzymes were prepared in assay buffer (1.75 μg/mL final concentration) and allowed to incubate with the various inhibitors for 15 minutes. The reaction was initiated with BODIPY PC-A2 substrate (3 μM final) and progressed for 35 min at room temperature (25 °C). At 35 minutes, the reaction was quenched by the addition of stop buffer containing 20 mM EGTA (20 μL/well) followed by a 10 minute incubation period. Fluorescent intensity at 485 nm excitation and 535 nm emission was measured on a PerkinElmer Victor^{3}V imager.(*93*)

% Inhibition	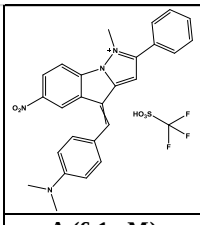	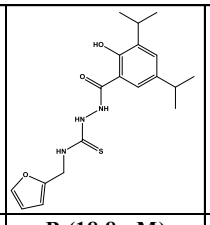	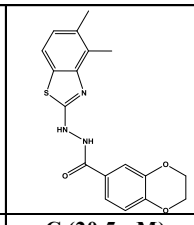	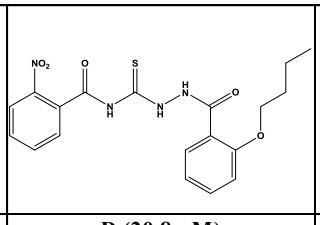	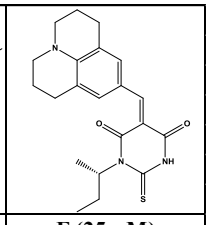
	A (6.1 μM)	**B (18.8 μM)**	**C (20.5 μM)**	**D (20.8 μM)**	**F (25 μM)**
hGIIA-sPLA2	95, 99, 91	12, 23, 17	0, 0, 0	0, 16, 7	93, 95, 87
hGX-sPLA2	61, 50, 73	0, 0, 0	0, 0, 0	0, 0, 0	82, 77, 76

The logP value for each compound was calculated using Collaborative Drug Discovery (CDD) software (**Table 6**). All compounds satisfied Lipinski's rule for oral drug bioavailability. The compounds were also tested for solubility in water and assay buffer by visual inspection over a range (10-100 μM) of concentrations (Supplemental Table 6). All compounds were observed to be soluble under assay conditions at their IC_{50} concentrations.

Table 6. Physical Properties of Compounds A, B, C, D, and F. The logP values were calculated using Collaborative Drug Discovery (CDD) software. The solubility of hit compounds was tested at 10, 25, 50, and 100 μM by visual inspection. DMSO stock solutions of compounds were dissolved in water or assay buffer (1 mL) to the listed concentrations without exceeding 1% DMSO. Compounds were considered soluble if the solution remained clear. Presence of precipitate or cloudiness present in solution indicated lack of solubility. Results in water were identical to results in assay buffer (50 mM Tris-HCL, pH 8.9, 100 mM NaCl, 1 mM $CaCl_2$). IC_{50} values shown for comparison are for inhibition of hGIII-sPLA2 (Figure 4). [Note: Solubility in the range of 25 > 50 indicates that the compound was found to be soluble at 25 μM but not at 50 μM therefore the solubility of the compound lies in the range of 25-50 μM.].(*93*)

Physical Properties	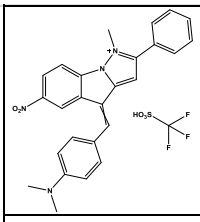	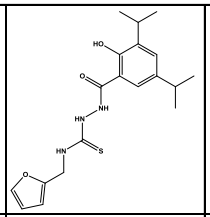	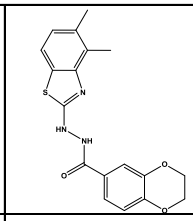	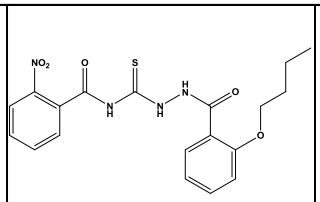	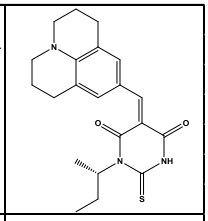
	A (IC_{50}=6.1 μM)	**B (IC_{50}=18.8 μM)**	**C (IC_{50}=20.5 μM)**	**D (IC_{50}=20.8 μM)**	**F (IC_{50}=25 μM)**
cLogP	2.68	4.64	4.29	3.74	4.27
Solubility(μM)	> 100	25 > 50	25 > 50	25 > 50	25 > 50

vii. Testing of Gelb lab inhibitor panel

Previous studies in the Gelb lab have sought to find inhibitors that are specific for each member of the sPLA2 family.(*99*, *104*) hGIII-sPLA2 has been absent from these studies because until recently, the expression and purification hGIII-sPLA2 had not produced catalytically active enzyme in sufficient quantity for testing. Having developed a fluorescent assay for hGIII-sPLA2, the full panel of inhibitors could now be tested.

Compounds (130 total) containing indole core structures were assayed. All compounds were tested at 10 μM (n = 3) following the 96-well Plate hGIII-sPLA2 Inhibition Assay (Section

B.iii.). The demonstrated sPLA2 inhibitors Indoxam, methyl Indoxam, isobutyl Indoxam, and LY315920 showed moderate inhibition, as anticipated, of 20-43% at 10 µM (**Figure 32**).

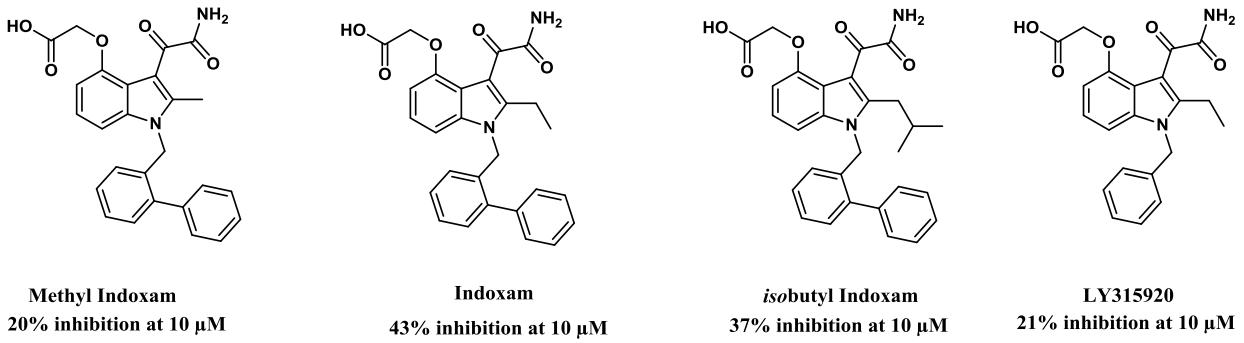

Figure 32: Known sPLA2 Inhibitors

The Scaffold 1 series (27 total compounds) contained no compounds with greater than 10% inhibition at 10 µM (**Figure 32**). The Scaffold 2 series (41 total compounds) contained no compounds with greater than 17% inhibition at 10 µM (**Figure 33**). The Scaffold 3 series (62 total compounds) contained only one compound with greater than 20% inhibition at 10 µM (**Figure 33**). RO013109A displayed 46% inhibition at 10 µM (**Figure 34**). However RO013109A was found to be an inhibitor of hGIIA-sPLA2 with an IC_{50} of 40 ± 2 µM in previous studies and will therefore not be a selective inhibitor of hGIII-sPLA2.(*105*)

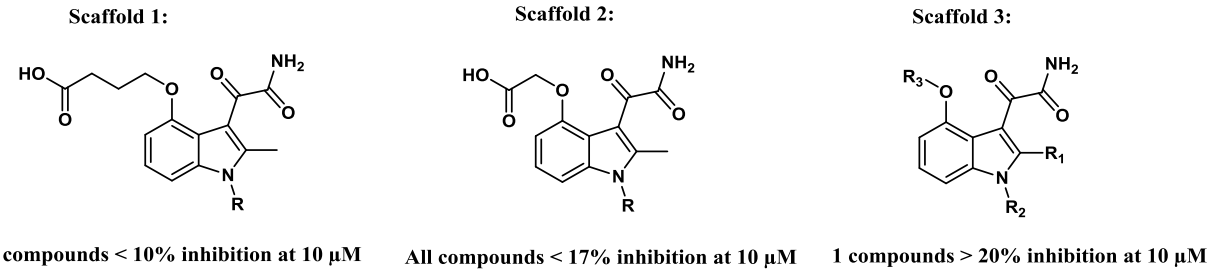

Figure 33: Indole Core Scaffolds.

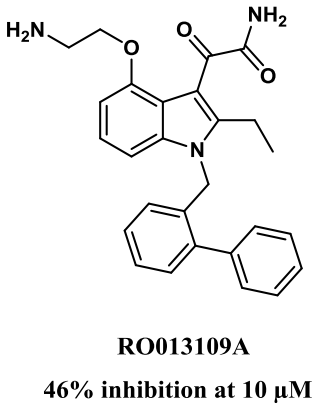

Figure 34: Scaffold 3 Series Compound found to have > 20% inhibition at 10 µM.

Though we do not rule out further testing in the future as new ideas and/or compounds arise in the literature or by other means, at this time we have decided to stop continual work on this project. We have published our assay protocol and all information obtained during HTS.(*93*)

D. Conclusion

This chapter describes the first high throughput optical screening assay for secreted phospholipase A2 inhibitors based on a phospholipid vesicle substrate. The screen displayed acceptable statistics and allowed us to carry out a successful analysis of a large library of

compounds. A few hits emerged that will set the stage for a medicinal chemistry campaign in attempts to develop the first potent inhibitor of hGIII-sPLA2.

E. [^{3}H]-Oleic Acid Labelled E. Coli Membrane Assay

Labeling of E. coli membranes with [^{3}H]-oleic acid(103):

A single colony of an *E. coli* strain was used to prepare a 10 mL overnight pre-culture in Luria Broth (LB), w/ or w/o ampicillin, which was grown to an OD_{600nm} of 2-3 undiluted. The pre-culture was then diluted in 100 mL of fresh LB to an OD_{600nm} of 0.05 and 2.5 mCi of [^{3}H]-oleic acid was added. Cells were then grown for 4.5-5 hours at 37 °C with vigorous shaking (200-230 rpm) to an OD_{600nm} of 1. The culture was spun down for 15 minutes at 4000 rpm at room temperature. A 50 μL aliquot of the supernatant was saved for quantification of incorporated oleic acid. The remaining supernatant was discarded and the pellet was resuspended in 50 mL of LB. The cells were grown for an additional 30 minutes at 37 °C under shaking to allow any remaining unincorporated labeled oleic acid to get incorporated into phospholipids. The culture was spun down again for 15 minutes at 4000 rpm at room temperature. Another 50 μL aliquot was saved for later quantification. The supernatant was discarded and the pellet was suspended in 50 mL of washing buffer (0.1 M Tris/HCl pH8.0, 1 mM EDTA containing 0.5% fatty acid free BSA). The culture was spun down again for 15 minutes at 4000 rpm at room temperature. Another 50 μL aliquot was saved for later quantification. The supernatant was discarded and the pellet was suspended in 2 mL of washing buffer without BSA. A 2 μL aliquot was saved for counting and the remaining solution was transferred to a Pyrex glass tube. The glass tube was

covered with aluminum foil as a cap and autoclaved for 20 minutes at 120 °C at 1.5 bar. After autoclaving, a 2 µL aliquot was saved for counting and the remaining solution was transferred into two Eppendorf tubes. The Pyrex tube was then rinsed with 1 mL of washing buffer which was combined with the 2 mL solution. The solution was sun down for 1 minute at 13,200 rpm at room temperature using a bench microcentrifuge. A 10 µL aliquot of the supernatant was saved for later quantification. The remaining supernatant was discarded at each pellet was resuspended in 1.5 mL of washing buffer. This washing process was then repeated five more times. On the final wash, the pellet was resuspended in 5 mL of washing buffer and a 2 µL aliquot was used for quantification of incorporated oleic acid. The solution was then diluted to 200,000 dpm/µL, portioned into 30 µL aliquots, and stored at -20 °C. The supernatant aliquots collected over the course of the labeling were then counted and used to calculate the percentage of radioactivity in the final 2 µL aliquot collected versus the input amount. The typical incorporated radioactivity is more than 30-40% of the input radioactivity added.

PLA2 assay:

Protein concentrations were measured with the Bradford dye reagent (BioRad Corp.) using bovine serum albumin as a standard. hGIII-sPLA2 solution (1mg/mL) was stored at -80 °C and thawed on ice prior to assay. The required amount of radioactivity (200,000 dpm of [^{3}H]-oleic acid labeled membranes/reaction x the number of reactions) was diluted into an Eppendorf tube and brought up to 1.5 mL with PLA2 activity buffer (0.1 M Tris/HCl pH 8.0, 10 mM CaCl2, 0.1% BSA). The solution was spun down for 1.5 minutes at 13,200 rpm at room temperature. The

supernatant was discarded and the pellet was carefully resuspended in 150 μL of PLA2 activity buffer and transferred to a glass vial. The solution was brought up in PLA2 activity buffer to the volume required for the total number of reactions (100 μL x the number of reactions). Two 100 μL aliquots were counted to ensure the radioactivity was about 200,000 dpm/100 μL. The volume was adjusted as necessary and the substrate solution was used within the next couple of hours.

Fresh before use, the hGIII-sPLA2 solution was diluted with PLA2 activity buffer to a concentration of 7.5 μg/mL (2.5 μg/mL final concentration). Test compounds were dissolved and diluted in DMSO (typical stock solution 1-10 mM in DMSO). Then, 1.5 μL of compound solution and 48.5 μL of enzyme solution were combined in a 1.5 mL Eppendorf tube and incubated at room temperature (25 °C) for 15 minutes. To generate the control tubes, PLA2 stop buffer (300 μL, 0.1 M EDTA, 0.2% fatty acid free BSA) was added to a tube containing 48.5 μL of enzyme solution and 1.5 μL of DMSO.

After the 15 minute incubation period, the reaction was started by adding 100 μL of the [^{3}H]-oleic acid labeled membranes to each Eppendorf tube containing the enzyme solution. The assay was incubated at 37 °C for 35 minutes. PLA2 stop buffer (300 μL) was then added to all the Eppendorf tubes (except for control tubes in which it was already present). The tubes were spun down for 3 minutes at 13,200 rpm at room temperature (25 °C).

For each tube, 300 μL out of 450 μL was carefully removed from the reaction mixture without disturbing the pellet. Each 300 μL sample was combined with 1.5 mL of scintillation fluid (Ecoscint part LS-271), vortexed briefly, and incubated at room temperature for 10 minutes prior

to counting (Beckman LS 6500). The total released radioactivity (dpm) equals 450/300 x Counts (dpm) given by the 300 μL sample of supernatant.

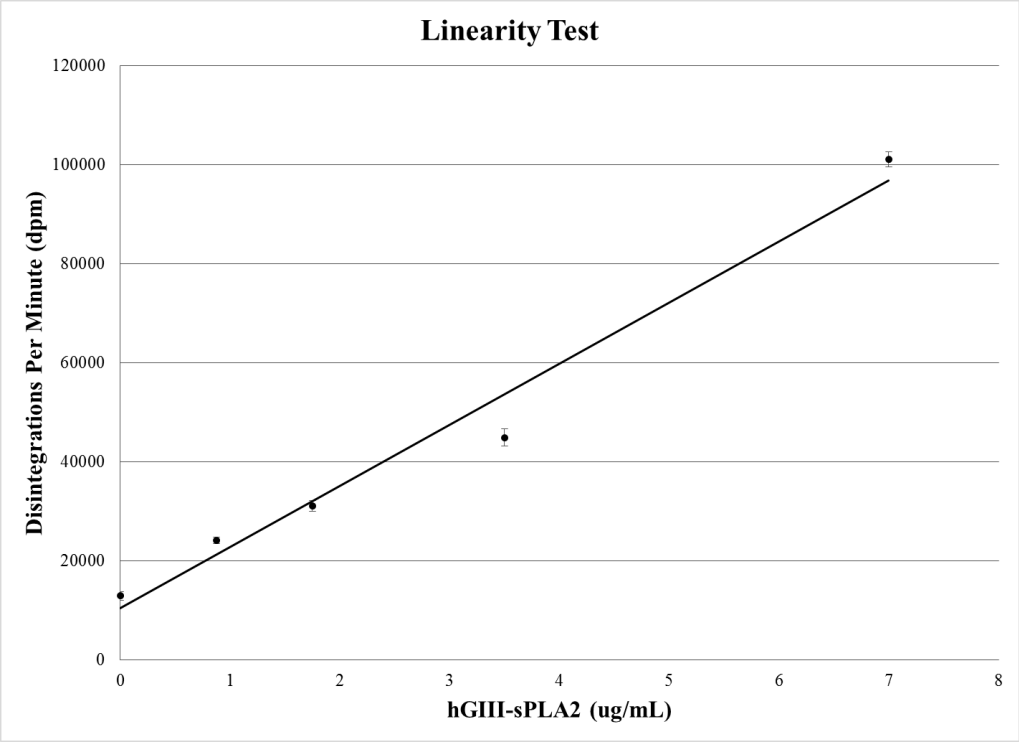

Figure 35. Dose response of radioactivity (dpm) measured at 30 minutes after initiation of the reaction of hGIII-sPLA2 enzyme (serial dilutions in PLA2 activity buffer) with [^{3}H]-oleic acid labeled E. coli membranes. The results plotted are the average of three wells (R^2 = 0.977, Error bars represent one standard deviation).(*93*)

III. Lessons Learned from *In Vivo* Mouse Studies of Secreted Phospholipase A2 Clearance from Extra-Cellular Medium by the M-type Receptor

A. Introduction

Although significant knowledge has been accumulated at the molecular and cellular levels, the *in vivo* biological functions of many mammalian secreted phospholipase A2s (sPLA2s) has yet to be fully understood especially with respect to their non-catalytic activity.(*9, 106-109*) Evidence suggests that mammalian sPLA2s may be bifunctional proteins capable of acting as either enzymes, ligands, or both.(*110-118*) This hypothesis may explain why some sPLA2s (IID, IIE, IIF, III, XIIA, and XIIB) display specific distribution patterns and lower enzymatic activities than other sPLA2s (IB, IIA, V, and X) suggesting that they have non-redundant functions distinct from catalytic activity.(*97, 106, 118-121*) Among sPLA2 binding proteins, the best known target is the M-type (Muscle-type, PLA2R) receptor.(*111*) Despite this knowledge, the biological role of the M-type receptor with regard to sPLA2 function remains obscure.(*110*)

The M-type receptor is a 180 kDa protein that was first identified in rabbit skeletal muscle cells hence, the "M" stands for muscle.(*122*) Since then, expression of the M-type receptor has been found in several tissues including lung, kidney, spleen, and colon from various mammalian species.(*110, 111, 118*) The M-type receptor is a type I membrane glycoprotein and its structural components include a single transmembrane domain, a short cytoplasmic tail, and a large extracellular region composed of an N-terminal cysteine-rich region, a fibronectin-like type II domain, and a tandem repeat of eight distinct C-type lectin-like carbohydrate recognition domains (CTLDs).(*118, 123*) Structure-function studies have indicated that the fifth CTLD (CTLD5) domain of the M-type receptor likely participates in sPLA2 binding.(*110, 111*) Studies also indicate that sPLA2 residues from the Ca^{2+} loop and interfacial binding domain are involved

in binding to the M-type receptor, and that upon binding to the receptor, the sPLA2s enzymatic activity is inhibited.(*110, 111*)

Though the biological role of the M-type receptor remains to be elucidated, a comparison of the tissue distribution of various mouse sPLA2s and the mouse M-type receptor clearly indicates co-localization in multiple tissues which suggests that interactions between the M-type receptor and one or more mouse sPLA2s are likely to occur *in vivo* under different physiological or physiopathological settings.(*118, 124-126*) One possibility is that the M-type receptor acts as a negative regulator of sPLA2 by both inhibiting sPLA2 activity through binding to the soluble secreted receptor and by withdrawing sPLA2 from the extracellular medium through the membrane bound receptor, which has both endocytic properties and sPLA2 inhibitory activity.(*111*) *In vitro* studies on transfected cells or cells endogenously expressing the receptor clearly supported this view.(*127, 128*) However, *in vivo* studies using receptor-deficient mice were inconclusive.(*129, 130*) Additionally, soluble forms of the M-type receptor have been identified that, upon binding sPLA2, block enzymatic activity.(*110, 111*) To further complicate the issue, studies suggest that the sPLA2-receptor interaction has a strict species dependence.(*124, 131-133*)

The binding properties of the full set of mouse sPLA2's to the mouse M-type receptor were analyzed *in vitro*.(*118*) Of interest to this project, mGIIA, and mGX were found to be high-affinity ligands of both the membrane-bound and soluble forms of the receptor ($K_{0.5}$ of 0.3 to 1.2 nM, where $K_{0.5}$ is defined as the concentration of sPLA2 competitor that inhibits 50% of the specific binding of the venom sPLA2 OS1 which binds to the receptor with pM afinity).(*118*) The sPLA2 mGIID was unable to bind either the membrane bound or the soluble M-type mouse receptor ($K_{0.5}$ >300 nM, maximal concentration assayed).(*118*) Based on these results, the

sPLA2s mGIIA, mGX, and mGIID were chosen as candidates for an *in vivo* study using M-type receptor deficient mice with the goal of better understanding the role of the M-type receptor in the removal and degradation of sPLA2s from the bloodstream.

B. Pilot study

In brief, to study the molecular mechanism by which secreted phospholipases A2 are removed from the extracellular fluid such as blood, mice containing or lacking the M-type secreted phospholipase A2 receptor (PLA2R) would be injected intravenously (i.v.) with secreted phospholipase A2 protein that bears a tracer. At various time points post injection, a blood sample would be taken so that the amount of sPLA2 remaining in the blood could be measured. Excreta would also be collected to track any excretion of sPLA2 from the body over the complete length of the experiment. Following a full time course, mice would be euthanized and any remaining tracer would then be measured in various mouse tissues via dissection to determine end-point biodistribution. Upon identification of target tissues, degradation studies would take place to determine if the sPLA2 had been broken down upon internalization. We chose mGIIA and mGX sPLA2s as positive controls since *in vitro* tests showed that both sPLA2s were found to be high affinity ligands of PLA2R. We also chose to test mGIID as a negative control since *in vitro* tests showed that this sPLA2 was unable to bind PLA2R.

i. Labeling of sPLA2s

To follow the blood clearance, biodistribution, and degradation of sPLA2s in a mouse model we needed to label the sPLA2s with a tracer that: (1) caused minimal perturbation of the protein's function *in vivo*; (2) could be detected at low (nM) concentrations; (3) had a lifetime capable of

lasting for the full duration of the experiment (as yet unknown as this was a pilot study but presumably on a scale from hours to days). We chose Iodine-125 as a tracer due to its small molecular mass consisting of a single atom, high specific activity, 60 day half-life, and familiarity since this tracer was used for labeling of sPLA2s by our collaborators to study M-type receptor binding *in vitro*.(*118, 127, 134*)

All sPLA2 proteins were prepared as previously described.(*118*) We chose to begin our study by labeling mGIIA-sPLA2 since the protein was most readily available in high quantities and it exhibited high-binding to PLA2R *in vitro* to provide proof of concept. Radiolabeling of mGIIA-spLA2 was accomplished by the lactoperoxidase method (section E.i.) using Na-I^{125} as the source of free iodine.(*135*) This method uses lactoperoxidase in the presence of trace hydrogen peroxide to oxidize radioactive iodine $^{125}I^-$ to produce reactive species $^{125}I_2$ or $^{125}I^+$. These reactive species substitute directly into tyrosine residues of the protein.(*136*) The oxidation was terminated by dilution, and purification of the radio-labeled protein then took place using a desalting column. SDS-PAGE was run on samples from column fractions found to contain Iodine-125 (via gamma counter) to determine the presence of radio-labeled sPLA2. Fractions containing the radio-labeled protein were pooled and labeling efficiency was determined based on the amount of Iodine-125 incorporated into the protein. The radio labeled sPLA2 protein was injected as a solution in sterile saline containing 0.1% bovine serum albumin (BSA) to prevent protein from adhering to the walls of the syringe.

To closely mimic physiological concentrations of sPLA2s in the serum of C57BL/6 mice used to generate the PLAR-/- line, we planned to keep levels close to 5 ng/mL sera.(*137*) Additionally, in order to measure the clearance of the radio-labeled sPLA2 protein *in vivo*, radioactivity per µL of blood must be sufficiently high enough to measure using a gamma counter. We planned to

inject each mouse with approximately 500,000 cpm which would require 2.3 ng of sPLA2 protein based on previous labeling efficiency found for the lactoperoxidase method (3000 cpm/fmol). Each blood sample taken would be approximately 20 µL (justification for amount described below) which even when taking into account the total volume of each mouse (about 20 g) would contain approximately 500 cpm/sample, a sufficient value for detection purposes as background counts for I-125 are approximately 50 cpm.

ii. Route of injection

Typical routes of intravenous injection in mice include retro-orbital venous sinus and lateral tail-vein injection. Retro-orbital injection must be done under anesthesia and involves addition of fluids (liquid specimens) to the venous sinus bed behind the eye. Tail-vein injection is typically performed without anesthesia and involves direct insertion of a small gauge needle into the lateral tail-vein of a restrained mouse. Both methods require adequate training and each have their own pros and cons. Retro-orbital injection is requires less training to become proficient and may improve overall delivery by providing a more consistent target than the tail vein, especially in darker pigmented mice such as those used in this study where tail vein visualization is particularly difficult.(*138, 139*) However, partially missed injections can be harder to detect visually and data may be skewed as a result. The learning curve for swift accomplishment of tail-vein injections is high especially since mice are not sedated and the depth and angle of needle insertion have to be taught via practice. However, once mastered, it is immediately evident if tail-vein injection is successful due to fluid build-up in the tail if the injection was missed. We first mastered and employed retro-orbital injection due to recommendation by the Veterinary Services Division.

iii. Blood collection strategies

We chose three commonly used sources for repeated blood draws which included the tail vein (primary source), saphenous vein (secondary source), or pedal vein (tertiary source).(*140*) In all cases, the mouse would be placed in a restraint, the vein punctured with a needle, and blood collected into a capillary tube with markings (µL). Blood samples were stored in sealed tubes and gamma counting took place after completion of the experiment. The total volume of blood that can be safely taken from an experimental animal is 10% or less of the total blood volume. As a result, to obtain 10 or more sample draws from a mouse that has a calculated total blood volume of 2 mL, the blood draw sample should be at most 20 µL.

As this was a pilot study, we were uncertain of the time it would take to clear the secreted phospholipase A2 protein from the blood. We worked with Veterinary Services to develop three possible collection strategies as follows:

(1) 2-5 day total experiment duration: Blood (20 µL) would be taken 2 times per day, every day, for 2-5 days. Total blood drawn would not exceed 0.2 mL or 10% total blood volume.

(2) 8 hour total experiment duration: Blood (20 µL) would be taken at 10 time points spaced out over the 8 hour period (example: 10 min, 30 min, 1 hr, 2 hr, 3 hr, 4 hr, 5 hr, 6 hr, 7 hr, 8 hr). Total blood drawn would not exceed 0.2 mL or 10% total blood volume.

(3) 2 hour total experiment duration: Blood (20 µL) would be taken at 10 time points spaced out over the 2 hour period (example: 30 sec, 1 min, 5 min, 10 min, 30

min, 45 min, 1 hr, 1.25 hr, 1.5 hr, 2 hr). Total blood drawn would not exceed 0.2 mL or 10% total blood volume).

Since we did not know the clearance rate of the sPLA2 proteins we decided to use the 8 hour total experiment duration as our preliminary approach. In this way we could minimize the total number of mice used because from this experiment we would be able to tell if we should proceed with the 8 hour experiment or if a shorter (2hr total duration) or longer (2-5 day total duration) was more applicable.

iv. Excreta collection

To fully track the removal of radio-labeled protein from mice it is necessary to collect and test their excreta. Proteins are removed from the blood via catabolism during passage through the kidneys and liver after which remaining peptidyl moieties are excreted into the urine and bile which ends up in feces.(*141, 142*) We chose to passively collect excreta as in particular the forced expression of urine from mice is nontrivial.(*143*) To collect all excreta over an experimental period, mice must be housed individually. We were able to obtain metabolic cages to house the mice which not only kept them in isolation but also allowed for collection of excreta since the bottom of the cage consisted of wire mesh with a collection tray underneath. We lined the collection tray with filter paper to absorb any urine while feces were collected as a solid mass. Amounts collected were combined (urine separate from feces) and counted via a gamma counter.

v. Organ collection and biodistribution

As this was a pilot study, we chose to collect all major organs (ovaries/testies, bladder, large intestine, ceecum, small intestine, stomach, spleen, liver, kidneys, heart, lungs, and brain) to evaluate biodistribution. Upon completion of the 8 hr experiment, mice were euthanized by carbon dioxide asphyxiation and all major organs were removed, placed into pre-weighed tubes and radioactivity was measured. The percent of injected dose per gram tissue (% ID/g tissue) was then determined.

The flow diagram for the pilot study (**Figure 36**) depicts the proposed experimental outline for this study. We would first evaluate one sPLA2 using the 8 hr experimental time frame and based on the blood clearance and biodistribution results over this period (i.e. was all of the radio-labeled sPLA2 removed from the blood), we could determine if either the 2 hr or 2-5 day experiment was more appropriate for analysis.

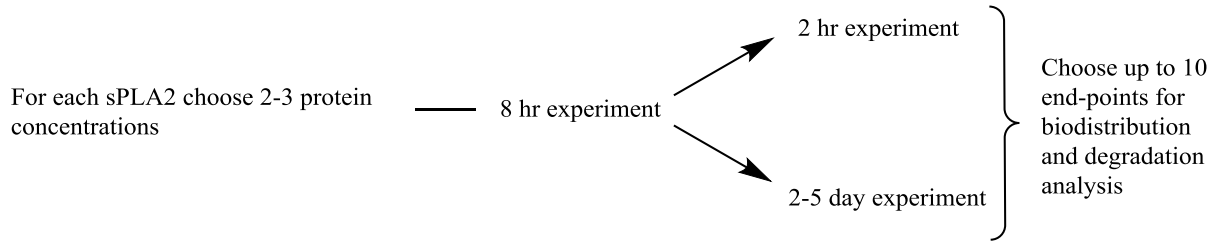

Figure 36. Experimental Flow Diagram.

C. Results and discussion

i. Preliminary results: blood clearance study

Labeling of mGIIA-sPLA2 was accomplished by using the lactoperoxidase method (Method E.i.) with a radiochemical yield of 61% and a specific activity of 1200 cpm/fmol. Mice, wild type (WT, n=3) and PLAR2-/- (KO, n=3) were matched for age and gender. Mice were injected i.v. (retro-orbital) with ^{125}I-mGIIA-sPLA2 such that the final total blood volume (tbv) concentration would be 0.2 nM (ex. For a 20 g mouse, tbv = 1.2 mL, we would inject 240 fmol which is approximately 3 ng of sPLA2, about 300,000 cpm). This was calculated based on the established total blood volume equaling approximately 6% of total body weight in mice. Mice were housed individually in metabolic cages post injection. Blood was collected via puncture of the tail vein at 6 time intervals (based on tbv and the restriction of only being able to collect up to 10% tbv in each experiment according to IACUC rules and regulations). We chose more early time-points in case rapid removal occurred so that we would know if a 2 hr study was appropriate.

Results of this preliminary blood clearance study can be seen in **Figure 37**. From these data it is evident that the ^{125}I-mGIIA-sPLA2 rapidly disappeared from blood by the first time-point at 5 minutes in both WT and PLA2R-/- mice. This result seems to indicate that under these

conditions, vascular PLA2R does not play a role in the clearance of circulating sPLA2-mGIIA.

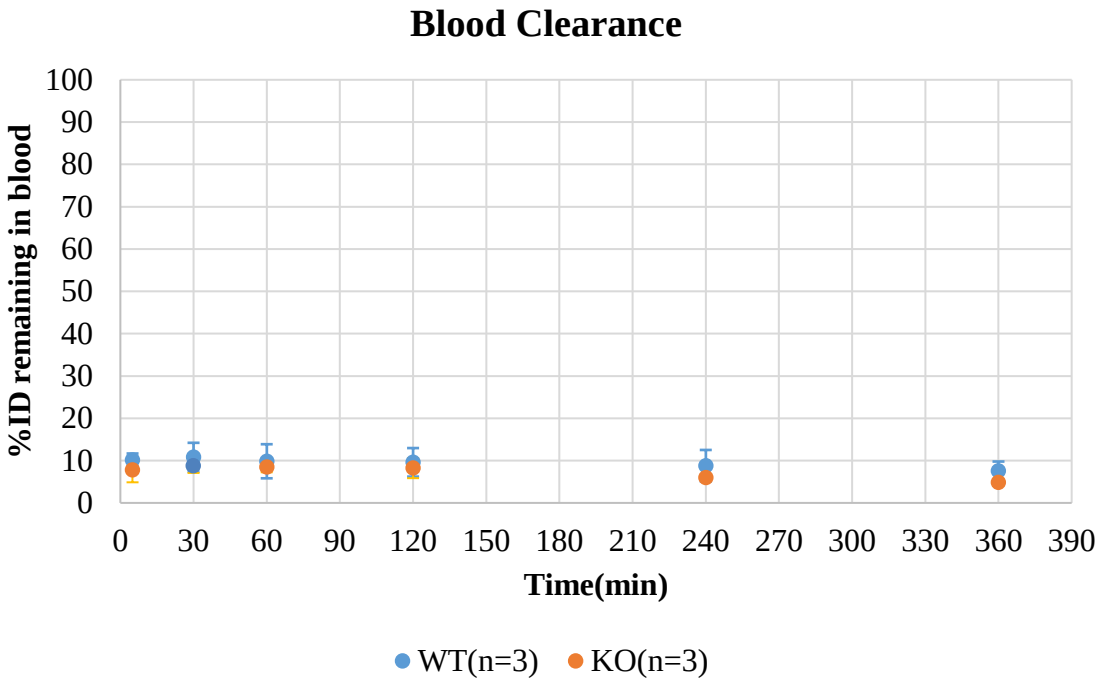

Figure 37. Blood Clearance. WT or PL2R-/- mice were matched for age and gender and injected retro-orbitally with ^{125}I-mGIIA-sPLA2 at 0.2 nM tbv. At the indicated times, blood (20 µL) was withdrawn from the tail vein and counted with a gamma counter. Data points represent the average (n=3) with error bars ± SD.

ii. Preliminary results: biodistribution study

The biodistribution of ^{125}I-mGIIA-sPLA2 was studied in both WT and PLA2R-/- mice at 6 intervals over an 8 hour time period (5 min, 15 min, 30 min, 1 hr, 6 hr, and 8 hr) and at 2 concentrations of protein in mice (0.2 and 2.0 nM tbv concentration, note for the 2.0 nM concentration lactoperoxidase labeling was carried out at 1:10 concentration of Na^{125}I according to Method E.i). The most interesting result to come out of these preliminary data was the number of counts we saw building up in the stomach. At 8 hours over two different concentrations of radio-labeled sPLA2 injected we saw a dramatic buildup of the percent

injected dose in the stomach (**Figure 38**). This result was more polarized than we had anticipated seeing and it raised some interesting questions.

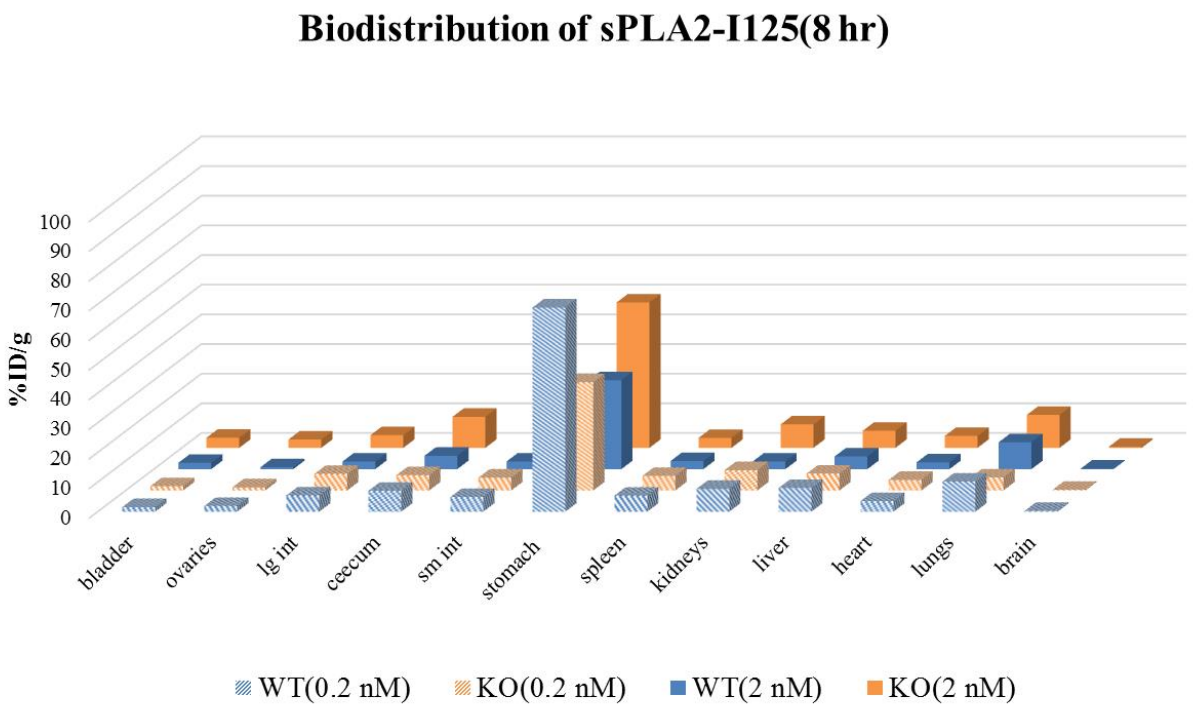

Figure 38. Biodistribution of ^{125}I-mGIIA-sPLA2 8 hrs post injection. WT or PLA2R -/- mice were injected (retro-orbitally) with ^{125}I-mGIIA-sPLA2 at the tbv shown. At 8 hr post injection, mice were euthanized via carbon dioxide asphyxiation and their organs were removed and analyzed with a gamma counter. Data represents the values for individual mice.

We had been using exclusively the retro-orbital route for injection and we postulated that if the injection was not entirely entering the blood system (potentially due to a missed injection) it could be possible to have it drain from the sinuses down the throat and into the stomach which would be one explanation of these peculiar results. To test this hypothesis, we needed to compare retro-orbital injection to another route of injection so we chose tail-vein injection. Some time was needed to become proficient at tail-vein injection which was made difficult in

our case due to the fact that the PLA2R-/- mice were C57BL/6 mice having a highly pigmented coat and skin which made visualization of the lateral tail vein more difficult. We injected WT and PLA2R-/- mice (2 nM) both retro-orbitally and via tai-vein and sacrificed them after 1 hr (this time point was chosen because it showed considerable build up in the stomach during time-point studies and was an easier time frame to conduct multiple experiments in). We found that %ID/g of the stomach were similarly high for both routes of injection (**Figure 39**) ruling out the route of injection as a possible reason for buildup of counts in the stomach.

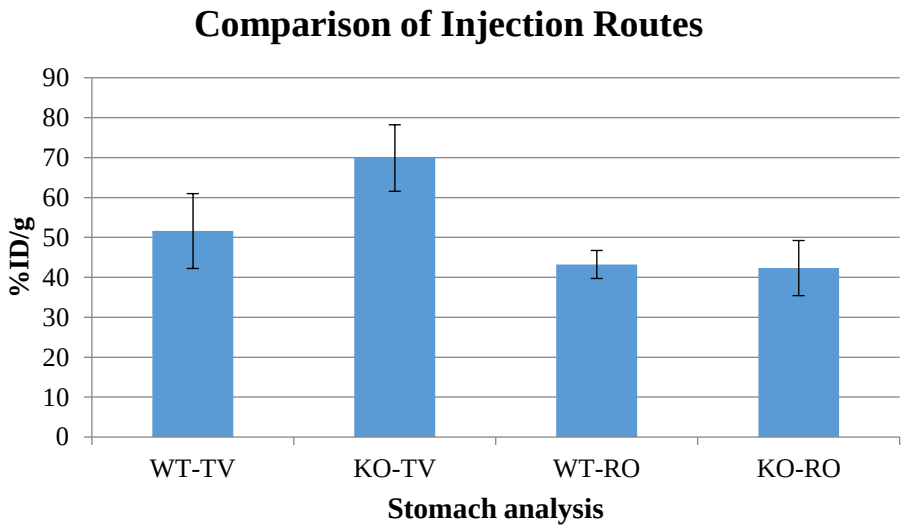

Figure 39. Comparison of Injection Routes. WT and KO mice were injected via either retro-orbital (RO) or tail vein (TV) with ^{125}I-mGIIA-sPLA2 at 2 nM tbv. At 1 hr post injection, mice were euthanized via carbon dioxide asphyxiation and their organs were removed and analyzed with a gamma counter (stomach data shown). Data represents the average (n=2) per column with error bars ± SD.

We also excised the eye sockets of the 4 mice used for retro-orbital injection in this study and found that in one case 13% ID/g remained in the eye socket (**Figure 40**) therefore we chose to move forward using only tail vein injections to ensure more accurate results.

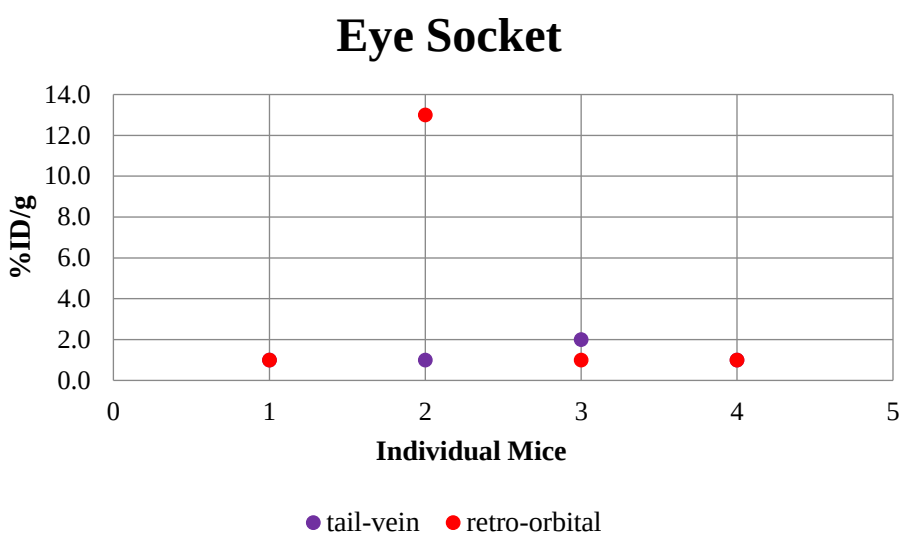

Figure 40. Eye Socket Data. WT and KO mice were injected via either retro-orbital (RO) or tail vein (TV) with ^{125}I-mGIIA-sPLA2 at 2 nM tbv. At 1 hr post injection, mice were euthanized via carbon dioxide asphyxiation and their organs were removed and analyzed with a gamma counter (eye socket data shown). Data represents individual mice.

Since we had been counting the organs as whole tissues we also went back and analyzed the contents of the stomach vs the stomach tissue and found that the counts were primarily coming from the contents (on average 85% of counts were from contents and 15% of counts were from tissue). High counts in the contents of the stomach were consistent regardless of injection route or strain of mice. We then delved into the literature to see if there was any precedent for finding a buildup of radioactivity in the stomach during similar radio-labeled biodistribution studies.

iii. Loss of iodine *in vivo*

Iodotyrosine deiodinase (IYD) with its cofactor flavin mononucleotide (FMN) catalyzes deiodination of mono- and diiodotyrosine for iodide salvage during thyroid hormone synthesis.(*144*, *145*) Mammalian IYD is found in the thyroid, liver, and kidneys and contains an

N-terminal membrane anchor, an intermediate domain, and a large C-terminal catalytic domain.(*146*) The amide nitrogen of A126 of IYD provides a key active site interaction by coordinating to the phenolic OH group of iodinated tyrosine residues.(*145, 147*) Free iodine released from the tyrosine residues of radio-iodinated proteins by IYD readily diffuses out of the liver and into the bloodstream.(*148, 149*) Evidence of high activity in the stomach typically results from transport of free iodine from the blood into the gut lumen by Na/I symporters in the gastric mucosa and thus indicates that free iodine must have been liberated from the radio-labeled protein.(*148, 149*) Based on these findings, we believe that the high counts we saw in the stomach of mice in our pilot study so far are likely due to deiodination by IYD.

iv. Bolton-Hunter technique for radio-labeling

In instances where the direct iodination of the tyrosine residues of proteins results in deiodination *in vivo*, one alternative is introduction of iodine via the Bolton-Hunter (BH) reagent. Use of the BH reagent has shown increased *in vivo* radiolabel stability over direct iodination in several studies.(*150-155*) The BH reagent (**Figure 41**) contains a tyrosine-like moiety appended to a succinimidyl ester by a 2 carbon linker which is introduced to free amino groups in a protein (typically the ε-amino group of lysine residues or potentially N-terminal α-amines).(*152*) The BH reagent is also commercially available (PerkinElmer #NEX120250UC).

All of the sPLA2s used in this study have multiple lysine residues (7-16) available for conjugation to the BH reagent. We chose to introduce Iodine-125 into mGIIA-sPLA2 using the BH reagent with the hopes of lowering *in vivo* deiodination by IYD in our study.

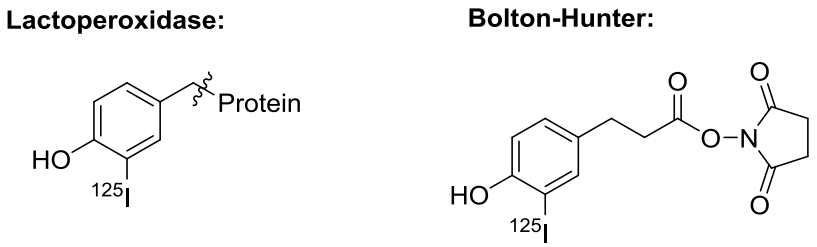

Figure 41. Structure Comparison Bolton-Hunter Reagent.

The BH reagent was successfully coupled to mGIIA-sPLA2 (section E.ii.) with a labeling efficiency of 26% and a specific activity of 250 cpm/fmol. Mice wild type (WT, n=3) and PLAR2-/- (KO, n=3) were matched for age and gender. Mice were injected i.v. (tail-vein) with ^{125}I-BH-mGIIA-sPLA2 such that the final total blood volume (tbv) concentration would be 2 nM. After one hour, mice were euthanized by carbon dioxide asphyxiation and all major organs (including the thyroid) were collected. Stomach contents were removed and counted separately from stomach tissue. The lactoperoxidase method of protein labeling showed a 2.5 fold increase over the BH method in overall counts coming from the stomach tissue and contents of both WT and KO mice to a similar extent (**Figure 42**) Additionally, values for uptake in the thyroids collected from both WT and KO mice compared well with literature values for BH labeling in biodistribution studies.(*150*) However, we did observe a 10 fold increase in the %ID/g in the small intestine for the BH method over the lactoperoxidase method which was a concern since the small intestine is the next organ in the digestive pathway.

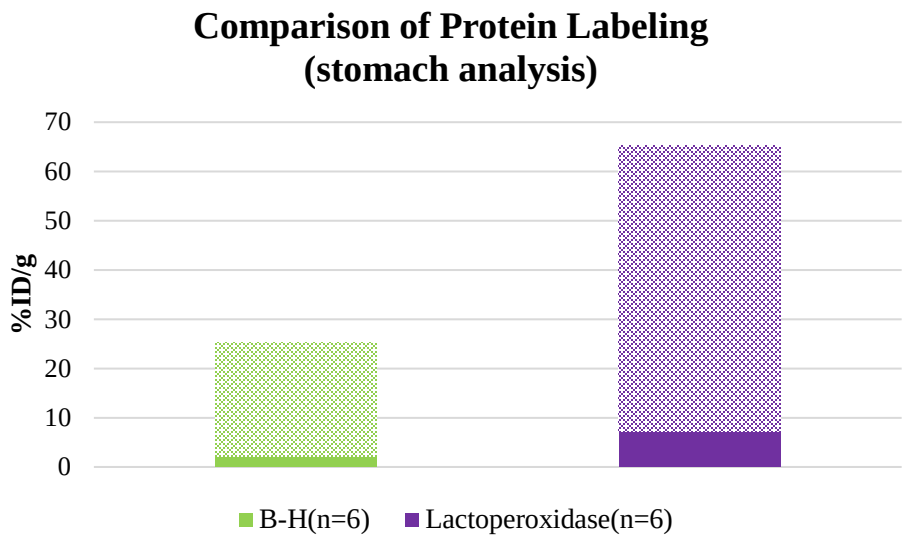

Figure 42. Analysis of stomach tissue from Lactoperoxidase and Bolton-Hunter trials. WT and KO mice were injected via tail vein with either ^{125}I-BH-mGIIA-sPLA2 (green) or ^{125}I-mGIIA-sPLA2 (purple) at 2 nM tbv. At 1 hr post injection, mice were euthanized via carbon dioxide asphyxiation and their organs were removed and analyzed with a gamma counter (stomach data shown). Data represents the average of 6 mice per column. The cross hatched area represents counts from the contents of the stomach and solid area represents counts from the tissue alone.

While researching methods to combat deiodination *in vivo*, we came across the reagent N-succinimidyl-3-[^{125}I]iodobenzoate (SIB) which had superior reduction of loss of iodide. A comparison of %ID/g values for the stomach tissue (among other organs) of mice labeled with SIB was drastically improved over both the BH method and the lactoperoxidase method (**Figure 43**).(*156*) We therefore chose to explore this method of labeling.

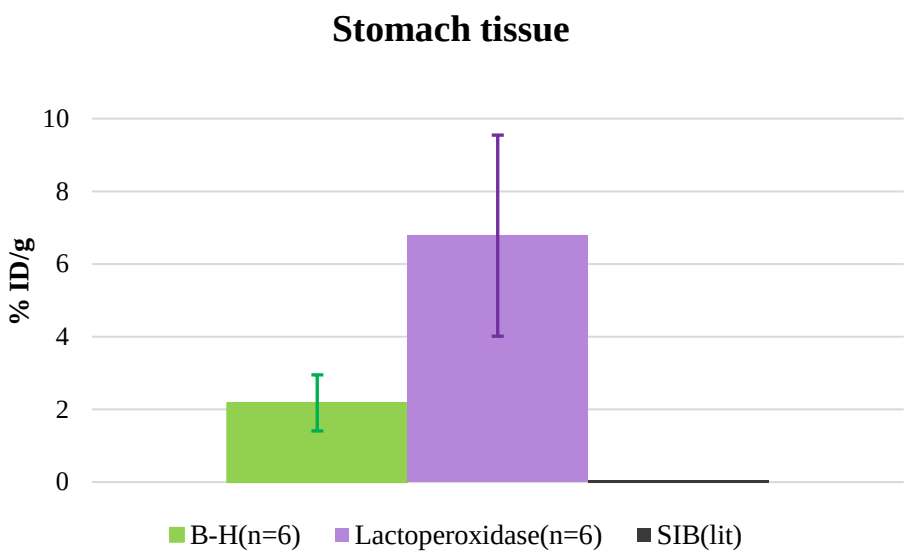

Figure 43. Comparison of %ID/g from stomach tissue. WT and KO mice were injected via tail vein with either ^{125}I-BH-mGIIA-sPLA2 (green) or ^{125}I-mGIIA-sPLA2 (purple) at 2 nM tbv. At 1 hr post injection, mice were euthanized via carbon dioxide asphyxiation and their organs were removed and analyzed with a gamma counter (stomach tissue only data shown). Data represents the average (n=6) with error bars ± SD. Literature value for SIB labeled protein found in stomach at 1hr(0.77 %ID/g).(*156*)

v. N-succinimidyl-3-iodobenzoate derivatives for radio-labeling

N-succinimidyl-3-(4-hydroxy-3-[^{125}I]iodophenyl)propionate (Bolton-Hunter reagent) was used as the basis for the design of other protein iodination reagents such as N-succinimidyl-3-[^{125}I]iodobenzoate (SIB) with the goal of reducing *in vivo* deiodination (**Figure 44**).(*157-159*) One major modification was the removal of the phenolic hydroxyl group. It was speculated that *in vivo* deiodination by dehalogenases could be reduced by structural divergence from that of naturally occurring thyroid hormones which, being iodinated derivatives of the amino acid tyrosine, contain a phenolic hydroxyl group.(*160-162*) Additionally, the two-carbon spacer between the aromatic ring and the activated ester was removed in order to increase protein coupling yields by minimizing competitive hydrolysis.(*150*)

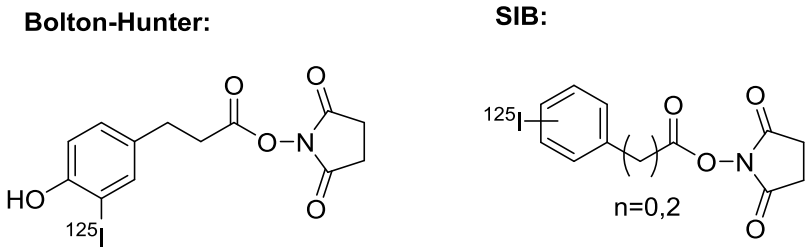

Figure 44. Structural comparison of BH and SIB reagents.

Synthesis of SIB (**Figure 45**, section E.iii.) was accomplished from *m*-bromobenzoic acid by first undergoing lithium halogen exchange followed by a transmetalation reaction where lithium was exchanged for tributyl tin (compound **37**). Installation of the NHS ester with DCC and N-hydroxysuccinimide resulted in formation of N-succininidyl-3-(tri-*n*-butylstannyl)-benzoate (compound **38**). SIB was then prepared from compound **38** via electrophilic destannylation (section E.iv.).(*157, 163*)

Radioiodination of compound **38** was accomplished using t-butyl hydroperoxide as the oxidant followed by isolation of the labeled product SIB by chromatography using a silica gel Sep-Pak column (section E.iv.). Thin-layer chromatography (TLC) analysis of radiolabeled SIB produced a ^{125}I-positive spot that co-migrated with cold-SIB (compound **39**) indicating that radio-labeling had been accomplished.(*163*)

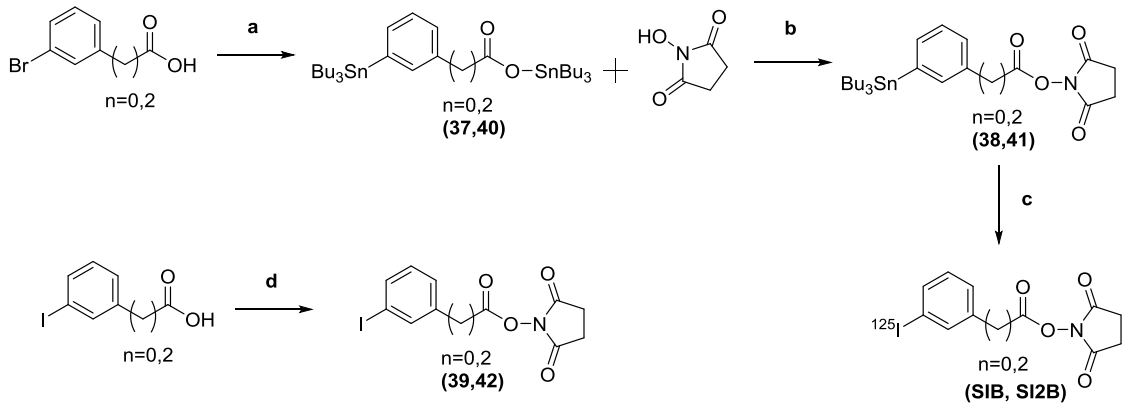

Figure 45. Synthesis of N-succinimidyl-3-[125I]-benzoate derivative. (a) (i) n-BuLi, THF, -78 °C, 30 min; (ii) $(n\text{-}Bu)_3SnCl$, overnight; (b) DCC, THF, rt, overnight; (c) $Na^{125}I$, TBHP, HOAc, CHCl3, see section E.iv.; (d) N-hydroxysuccinimide, DCC, THF, rt, overnight.(155)

Coupling of SIB to mGIIA-sPLA2 was attempted in borate buffer under mildly alkaline conditions followed by purification on a PD-10 size exclusion column (section E.iv.). We observed a single peak in the expected region for radio-labeled mGIIA-sPLA2 by gamma counting. However, when we analyzed the peak using SDS-PAGE and cold-mGIIA-sPLA2 as a standard, less than 10% of the counts loaded were coming from the sPLA2 band. The majority of counts were found in the lowest portion of the gel and therefore likely associated with uncoupled SIB or the corresponding carboxylic acid product of its hydrolysis.

Since we had previous success with coupling to the Bolton-Hunter reagent, we decided to synthesize an analog of SIB that contained the two-carbon spacer N-succinimidyl-3-(3-[^{125}I]iodophenyl)propionate (SI2B). Synthesis of SI2B was accomplished using the same synthetic pathway as SIB (**Figure 45**, compounds **40, 41**, section E.iii.) from 3-(3-bromophenyl)propionic acid.

Radioiodination of compound **41** was accomplished using t-butyl hydroperoxide as the oxidant followed by isolation of the labeled product SI2B by chromatography using a silica gel Sep-Pak

column (section E.iv.). Thin-layer chromatography (TLC) analysis of radiolabeled SI2B produced a ^{125}I-positive spot that co-migrated with cold-SI2B (compound **42**) indicating that radio-labeling had been accomplished. EAH Sepharose beads displaying primary amine groups were incubated with SI2B and after multiple rounds of washing were found to retain 36% of the counts loaded indicating that the SI2B reagent was capable of labeling primary amines.

Introduction of SI2B to proteins was also investigated under "cold" conditions using non-radio-labeled SI2B (compound **42**). Mass spectrometry was used to follow the reaction of SI2B with mGIIA-sPLA2 and coupling was observed in a stoichiometric and time-dependent manner. However when we attempted to reproduce these conditions in the "hot" lab we were unable to obtain radio-labeled protein. We observed a single peak in the expected region for radio-labeled mGIIA-sPLA2 by gamma counting. However, when we analyzed the peak using SDS-PAGE and cold-mGIIA-sPLA2 as a standard, less than 10% of the counts loaded were coming from the sPLA2 band. Though we explored the pH dependence, time dependence, and the ratio of SI2B to protein, we were unable to obtain radiolabeled protein and we were at a loss as to how to proceed. We then reached out to one of the pioneers of N-succinimidyl iodobenzoate derivatives for use in radio-iodination, Dr. Scott Wilbur at UW Radiation Oncology for advice.

vi. *closo*-Decaborate(2-) conjugates for radio-labeling

.Dr. Wilbur's lab had since moved away from the use of SIB derivatives due to the discovery of *closo*-decaborate(2-) conjugates.(*164*) Isothiocyanatophenyl-*closo*-decaborate(2-) derivative (ICD, **Figure 46**) was found to be advantageous over the previously used N-succinimidyl iodobenzoate (SIB) derivative since conjugation of ICD to proteins takes place prior to radio-

labeling which allowed for direct labeling of the ICD-protein conjugate, simplifying the radio-labeling procedure and providing higher radiochemical yields than the 2-step labeling procedure used to prepare the SIB derivatives. Additionally, the iodinated *closo*-decaborate conjugate has shown equivalent *in vivo* stability toward deiodination in comparison with N-succinimidyl iodobenzoate derivatives.(*164*)

ICD Labeling:

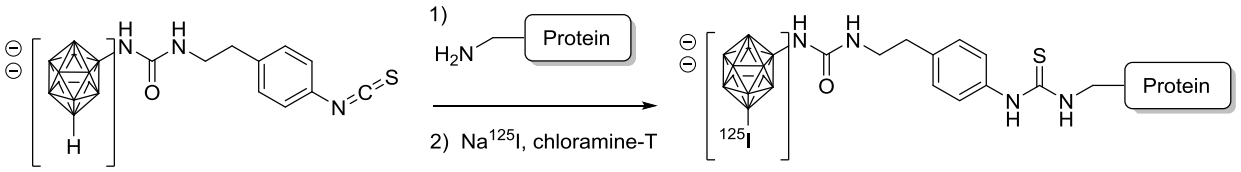

Figure 46. Isothiocyanatophenyl-*closo*-decaborate(2-) conjugate.

We chose to label mGX-sPLA2 at this time because 100 ug of protein was required for labeling and our stock of mGIIA-sPLA2 had been depleted by previous experimentation with the N-succinimidyl iodobenzoate derivatives and lactoperoxidase labeling. ICD was synthesized in the Wilbur lab and this compound was provided for our use.(*164*) Conjugation of ICD to mGX-sPLA2 proceeded overnight at room temperature in HEPES buffer at pH 8.6 followed by purification by size-exclusion chromatography.(*164*) Coupling of ICD to the protein can be confirmed by isoelectric focusing (IEF) analysis due to the addition of a 2^- charge on the boron cage moiety. IEF analysis showed a significant change in PI, and while the actual number of conjugates is not readily obtained, the shift of bands from unmodified protein standard indicated that conjugation of ICD to mGX-sPLA2 had been accomplished.

Iodination of the ICD-mGX-sPLA2 conjugate with $Na^{125}I$ was accomplished in 30 seconds at room temperature using chloramine-T as the oxidant followed by chromatography using a silica gel Sep-Pak column to isolate the radio-labeled protein. Results of ITLC analysis of the purified protein fractions were consistent with successful radioiodination (40% radiochemical yield).

Since the coupling of ICD represented a significant addition to the sPLA2 protein, we conducted an *in vitro* receptor binding study to investigate if radiolabeling using this method perturbed receptor binding. Binding of radio-labeled ICD-mGX-sPLA2 to the soluble recombinant mouse M-type receptor (R&D Systems #5367-PL) was tested under equilibrium conditions (section E.v.). mGX-sPLA2 was previously shown to bind to the soluble receptor with low nM affinity ($K_{0.5}$ = 1.2 nM).(*118*) We tested affinity of radio-labeled ICD-mGX-sPLA2 (2 nM) with and without the soluble receptor (0 or 20 nM soluble PLA2R) under equilibrium conditions and no specific binding was observed. It is likely that the addition of ICD perturbed the natural affinity of mGX-sPLA2 for the soluble receptor and therefore we cannot use radio-labeled ICD-mGX-sPLA2 to study the relationship of sPLA2 to PLA2R *in vivo*.

D. Conclusion

The design of a pilot study using an *in vivo* mouse model to follow the clearance, biodistribution, and degradation of sPLA2s with respect to the presence or absence of the M-type receptor was developed and approved by the Institutional Animal Care and Use Committee at the University of Washington. This type of study had not been previously attempted in our lab and we learned numerous new techniques including safety and handling of Iodine-125, mouse handling, mouse monitoring and health, retro-orbital and tail-vein injection routes, various blood sampling routes

and techniques, organ dissection, and multiple radio-labeling techniques to enact this pilot study. We were disappointed that we were ultimately unable to find a radio-labeling strategy which would allow us to study the role of PLA2R binding in the clearance and degradation of sPLA2s *in vivo*. Future work in this area will hinge on the ability to radio-label sPLA2s using a tracer with minimal biological degradation that also does not perturb binding to PLA2R.

E. Experimental

i. Procedure for sPLA2 iodination with lactoperoxidase

CAUTION: Working with Iodine-125 is a health hazard. Labeling procedure must be done in a fume hood in an area approved by radiation safety.

Labeling of sPLA2 with Iodine-125:

Reagents:

sPLA2: mGIIA, mGX, mGIID. (Initial work done with mGIIA-sPLA2)

NaH_2PO_4 [Sigma S3139-500G]

Lactoperoxidase [Sigma L2005-25MG]

Hydrogen peroxide solution [Sigma 216763-100ML]

Iodine-125 [Perkin Elmer NEZ033A001MC], store in fume hood at RT

Preparation of buffers and solutions:

NaH_2PO_4 (1M, pH 6.5, 100 mL):

Dissolve 12.0g NaH_2PO_4 in Milipore water and adjust pH to 6.5 (final volume 100 mL)

NaH_2PO_4 (0.1M, pH 6.5, 10 mL):

dilute 1/10 from 1M stock solution NaH_2PO_4

$1\ mL\ 1\ M\ NaH2PO4 + 9\ mL\ milipore\ water$

Lactoperoxidase solution (0.05 µg/µL, 400 µL):

Start by dissolving 2 mg of lactoperoxidase in 0.1M NaH_2PO_4 (1 mL)

Add 10 µL of lactoperoxidase (2mg/ml solution) to 390 µL of 0.1M NaH_2PO_4 [40-fold dilution]

H_2O_2 solution (1/40,000 dilution of 30%, 400 mL):

10 µL 30% H_2O_2 solution in 400 mL of milipore water [1/40,000 dilution]

sPLA2 solution (100 µM in 1xPBS):

Weigh approximately 0.5 mg of sPLA2-mGIIA and dissolve in 0.25 mL of PBS(1x)

Test a few µL of this solution using UV-Vis A_{280nm}

Calculate the concentration based on $\Sigma_{1\%} = 8.4$ for mGIIA

Dilute to make 100 µM final concentration based on calculation

Procedure:

Iodination:

Final volume: ~60 µL

Incubation 2x10 min/RT

Typical labeling efficiency 3000 cpm/fmol

Add in order:

1. 9 µL Water
2. 6 µL NaH_2PO_4 (1 M, pH 6.5) ie 0.1M final conc.
3. 5 µL sPLA2 (100 µM), ie 0.5 nmol (7 µg) of sPLA2-mGIIA
4. 10 µL 125-INa, ie 0.5 nmol free iodine (note: for 1:10 labeling this was reduced to 0.05 nmol in the same volume)
5. 10 µL Lactoperoxidase solution (0.05 µg/µL freshly diluted 40-fold from 2 mg/mL stock) ie 0.5 µg Lactoperoxidase
6. 10 µL H_2O_2 (1/40,000 dilution freshly made)
7. Incubate 10 min at RT
8. Add another 10 µL H_2O_2 (1/40,000 dilution freshly made)
9. Incubate 10 min at RT
10. Dilute to 500 µL in 1xPBS/BSA 0.1%
11. Purify using PD10 desalting column with 1xPBS/BSA 0.1% as elution buffer. Initially, collect 1x3 mL fractions followed by approximately 40 x 0.5 mL fractions. Take 5 µL from each fraction and count using I-125 program (1 min duration). Look for two peaks; one initial peak from the radio-labeled sPLA2 and a later peak from the remaining free iodine. For at least the first time working with a particular sPLA2, run an SDS-PAGE gel on the initial fractions by loading 5 µL of each fraction per lane, and a sPLA2 standard lane then stain with Coomassie Blue. Cut out each band at 14,000 and count using I-125 program. Compare cpm to the cpm from 5 µL not loaded on the gel to get a rough determination of how many cpm come directly from radio-labeled sPLA2.

12. Pool fractions containing radio-labeled sPLA2 (61% radiochemical yield) and store at -20 °C.

ii. Procedure for sPLA2 radio-iodination with Bolton-Hunter reagent

Reagents:

Bolton-Hunter Reagent (N-succinimidyl-3-(4-hydroxy-3-[^{125}I]iodophenyl)propionate) [250 µCi NEX120250UC]

Pierce™ 20X Borate Buffer [Thermo Fisher #28341]

Sephadex G-25 in PD-10 Desalting Columns [GE Life Sciences # 17085101]

Procedure:

1. The Bolton-Hunter reagent comes in a solution of benzene which was evaporated off in the iodine-hood by parafilming the top of the container and using dry nitrogen gas filled balloons to gently blow off the benzene using the charcoal trap (included) as the out-port.
2. 20 µL of 0.1 M Borate buffer was added directly to the reagent container
3. 10 µg of mGIIA (1 µg/µl) as a solution in water was added directly to the reagent container
4. The vial was vortexed and incubated for 40 minutes with occasional vortexing
5. Then, 200 µl of 0.2 M Glycine in 0.1 M Borate buffer was added, the solution was vortexed, and incubated for 5 min

6. The solution was loaded onto a G25 Sephadex PD10 column (pre-washed with 0.1% BSA in PBS)
7. The vial was washed with 500 µL of 0.1% BSA in PBS which was also loaded onto the column
8. The labeled protein was eluted with 0.1% BSA in PBS (500 µl fractions)
9. Fractions (5 µL from each) were tested for presence of protein via gamma counter using the I-125 program (1 min duration)
10. An SDS-PAGE gel was run to confirm that counts were coming from the sPLA2 band as previously described (section E.i.)
11. Fractions containing radio-labeled sPLA2 (26% radio-labeling efficiency) were pooled and stored at -20 °C.

iii. Synthesis of N-succinimidyl-3-iodobenzoate derivatives

Compounds **37**/**40**.

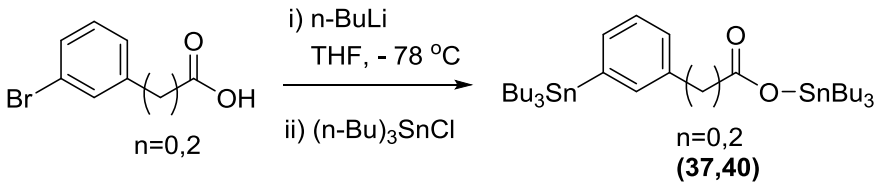

3-Bromobenzoic acid or 3-bromobenzenepropanoic acid (7.5 mmol) was dissolved in dry THF (45 mL) and the flask was cooled to -78 °C in a dry ice/acetone bath. n-BuLi 1.6 M in hexane (16.4 mmol) was added slowly over 15 minutes while keeping the temperature at -78 °C then the reaction was stirred at that temperature for an additional 30 minutes. Then tri-n-butyltin chloride

(16.4 mmol) was added slowly over 10 minutes and the reaction was stirred for 30 minutes while keeping the temperature at -78 °C. Then a balloon filled with nitrogen gas was affixed and the reaction was stirred at overnight and allowed to warm to room temperature. The reaction mixture was diluted with ethyl acetate and water was added slowly. The water layer was extracted with ethyl acetate and the organic phase was washed with brine and dried over sodium sulfate. The solvent was evaporated and the compound was used as crude in the next step without further purification.

Compounds **38**/**41**.

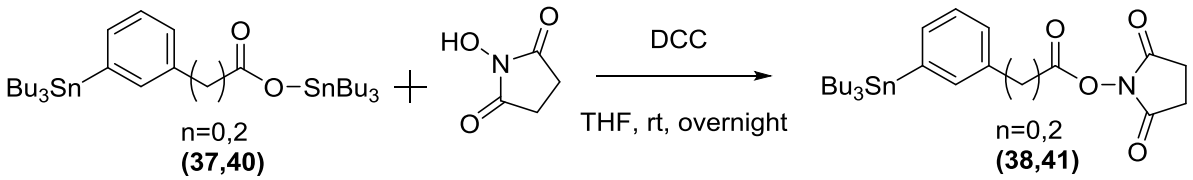

Compound **37** or **40** (2.0 mmol) was dissolved in dry THF (20 mL) and N-hydroxysuccinimide (2.4 mmol) and DCC (1.9 mmol) were added. The reaction was stirred under nitrogen atmosphere at room temperature overnight then filtered through filter paper and concentrated onto silica gel. The pure product was obtained by flash chromatography in a gradient of 100% hexane to 30% ethyl acetate/hexane. The purified product was aliquoted and stored at -20 °C to prevent hydrolysis of the NHS ester. [30% yield over two steps] **38** 1H NMR (300 MHz, DMSO) δ 8.12 (s, 1H), 8.03 (dd, J = 6.4, 1.5 Hz, 1H), 7.91 (d, J = 7.2 Hz, 1H), 7.62 (t, J = 7.5 Hz, 1H), 2.90 (s, 4H), 1.61 – 1.44 (m, 6H), 1.29 (dd, J = 14.7, 7.3 Hz, 6H), 1.14 – 1.05 (m, 6H), 0.85 (t, J = 7.3 Hz, 9H). **41** 1H NMR (300 MHz, CDCl3) δ 7.42 – 7.20 (m, 4H), 7.15 (d, J = 7.4 Hz,

1H), 3.03 (dd, J = 12.2, 4.5 Hz, 2H), 2.97 – 2.88 (m, 2H), 2.85 (s, 4H), 1.62 – 1.45 (m, 6H), 1.33 (dd, J = 14.7, 7.3 Hz, 6H), 1.11 – 0.99 (m, 6H), 0.89 (t, J = 7.3 Hz, 9H).

Compounds **39**/**42**.

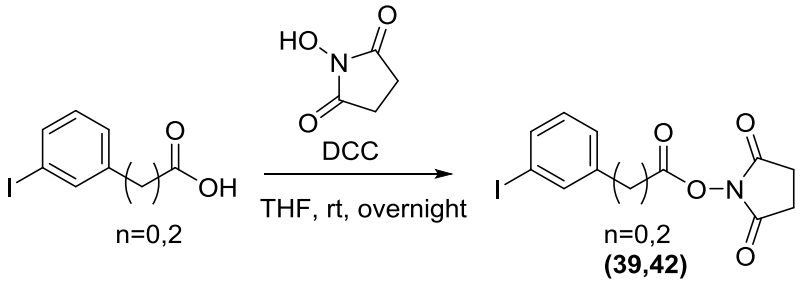

3-Iodobenzoic acid or 3-iodobenzenepropanoic acid (8 mmol) was dissolved in dry THF (20 mL) and N-hydroxysuccinimide (8.8 mmol) and DCC (7.6 mmol) were added. The reaction was stirred under nitrogen atmosphere at room temperature overnight then filtered through filter paper and concentrated onto silica gel. The pure product was obtained by flash chromatography in a gradient of 100% hexane to 30% ethyl acetate/hexane. The purified product was aliquoted and stored at -20 °C to prevent hydrolysis of the NHS ester. [85-90% yield] **39** 1H NMR (300 MHz, DMSO) δ 8.35 (s, 1H), 8.21 (d, J = 7.1 Hz, 1H), 8.11 (d, J = 7.7 Hz, 1H), 7.46 (t, J = 7.8 Hz, 1H), 2.90 (s, 4H). **42** 1H NMR (300 MHz, DMSO) δ 7.70 (s, 1H), 7.58 (d, J = 7.8 Hz, 1H), 7.33 (d, J = 7.7 Hz, 1H), 7.10 (t, J = 7.7 Hz, 1H), 3.02 (t, J = 7.0 Hz, 2H), 2.90 (t, J = 7.1 Hz, 2H), 2.80 (s, 4H).

iv. Radio-labeling and conjugation of N-succinimidyl-3-iodobenzoate derivatives

CAUTION: Working with Iodine-125 is a health hazard. Labeling procedure must be done in a fume hood in an area approved by radiation safety. Lead aprons, double gloves, eye protection, and lab coat are required.

Radio-labeling:

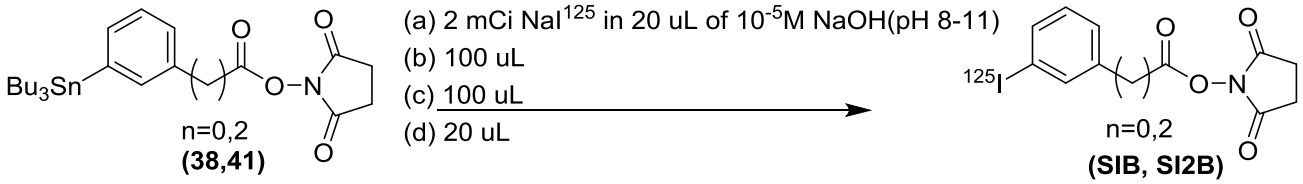

Reaction time = 1 hour

Temperature = room temp (25 °C)

Total volume = 240 µL

Reagents:

Na-I^{125} in 10^{-5} M NaOH pH (8-11), specific activity 17 Ci/mg, [PerkinElmer NEZ033A002MC]

TBHP, *tert*-butyl hydrogen peroxide, 70 wt% solution in H_2O [458139 Sigma-Aldrich]

STB/ST2B [section E.iii.]

Sephadex G-25 in PD-10 Desalting Columns [GE Life Sciences # 17085101]

2000 mg silica column cartridge [Varian, SI 1210-2037]

Procedure:

Solution **b**: 6 mg acetic acid in 100 µL of $CHCl_3$ [make 200 µL total]

Solution **c**: 9 mg TBHP and a few crystals of Na_2SO_4 in 100 µL $CHCl_3$

$$9mgTBHP \times \frac{100mgSolution}{70mgTBHP} \times \frac{1mLSolution}{0.93gSolution} \times \frac{1000uL}{1mL} \cong 14uL$$

So, 14 µL of 70 wt% TBHP solution + 86 µL of $CHCl_3$, then add a few crystals of Na_2SO_4

[Make 200 µL total]

Solution **d**: STB/ST2B (1.5 mg, 0.003 mmol) in 20 µL of $CHCl_3$ [just add 20 µL $CHCl_3$ to vial and add all other components to vial containing STB/ST2B]

To a glass vial containing a stir-bar were added,

1) 100 µL solution (**b**)
2) 100 µL solution (**c**)
3) 20 µL solution (**d**)
4) 20 µL Na-I^{125} in 10^{-5} M NaOH (pH 8-11)

Stir at room temp for 1 hour. Transfer to a silica column and purify.

Purification:

- Prepare 2000 mg silica column cartridge by wetting with 25% EtOAc/Hex
- Load reaction mixture and rinse vessel with same solvent
- Run solvent through column, collecting 1.0 mL fractions and take out 5 µL from each fraction for counting
- Count tubes and determine which contain SIB/SI2B [Note: STB/ST2B should elute in tubes 5-7 followed by SIB/SI2B tubes 15-30]
- 92% radiochemical yield

[In parallel, run a trial column as follows: to a small amount of I-125 (1 µL), add 5 µL of solutions **b** & **c**. Then right before columning, add 2 mg of cold-SI2B in $CHCl_3$. Run on a column exactly as previously described. Follow by TLC and note when cold-SI2B is eluted. Run samples on the gamma counter to test if the free iodide elutes at the same time as cold-SIB, if so then re-column SIB/SI2B.]

Labeling of mGIIA with N-succinimidyl-3-iodobenzoate derivatives:

1. Tubes found to contain SIB/SI2B were evaporated in the hood overnight (TLC in the morning showed no product degradation). Tubes shown by gamma counting to contain SIB/SI2B will be pooled into a glass vial, washed with $CHCl_3$, then dried down with a delicate stream of air (TLC again to prove no degradation).
2. 50 µL milli-Q water was added to the glass vial containing SIB/SI2B, then mGIIA was added to a final concentration of 10 µg/50 µL.

3. The reaction was incubated at room temperature for (tried everything from 30 min to overnight) with periodic vortexing.
4. Protein purification took place by loading the whole sample on a PD10 column and eluting with 0.1% BSA in PBS and collecting 0.5 mL samples. mGIIA is expected to elute in tubes 5-7 corresponding to 3-4.5 mL.
5. An SDS-PAGE gel was run to confirm that counts were coming from the sPLA2 band as previously described (section E.i.).
6. All fractions containing radio-labeled sPLA2 will be pooled and stored at -20 °C. Prior to animal work, stock radio-labeled sPLA2 should be aliquoted into single-use portions and the radioactivity of each portion should be measured individually to control for variation in the amount injected.

v. Radio-lableing with *closo*-Decaborate(2-) conjugates

Procedure:

To 35 μL of mGX-sPLA2 at 5 μg/μL in PBS was added 180 μL HEPES buffer (100 mM with 150 mM NaCl, pH 8.6) followed by 5 equivalents (18 μg) of ICD at 7 μg/μL in DMSO. The reaction was run overnight at room temperature with gentle tumbling. In the morning, the reaction mixture was eluted over a size-exclusion (PD-10) column using PBS as eluant. The protein containing fractions were combined and concentrated in Vivaspin 6 centrifugal filters (30 kDa MWCO) to yield 70 μg of the ICD-mGX conjugate.

The ICD-mGX conjugate was evaluated on an IEF gel to determine changes in charge (isoelectric point, pI). IEF analyses were conducted on a Novex PowerEase 500 instrument with the XCell II chamber using Invitrogen (Novex) precast gels, pH 3−7 (1.0 mm thick × 12 wells), running under the standard IEF program. The protein was stained with GelCode Blue Stain (Pierce). IEF standards were from Serva Electrophoresis GmbH: pH 10.7, cytochrome C; 9.5, ribonuclease A; 8.3, 8.0, 7.8, lectin; 7.4, 6.9, myoglobin; 6.0, carbonic anhydrase; 5.3, 5.2, γ-lactoglobulin; 4.5, trypsin inhibitor; 4.2, glucose oxidase; 3.5, amyloglucosidase.

ICD-mGX 30 μg at 0.7 μg/μL in PBS was added 50 μL of sodium phosphate (0.5 M, pH 7.2) followed by 10 μL of Na[125I]I (2.0 mCi in 0.1 N NaOH). To that solution was added 7 μL of a 1 mg/mL solution of chloramine-T in H_2O. After 30 seconds at room temperature the reaction was quenched with 3.5 μL of a 10 mg/mL solution of sodium metabisulfite in H_2O. The reaction mixture was then eluted over a Sephadex G-25 size-exclusion column (PD-10) using PBS as the eluant. Protein fractions were combined to yield 0.80 mCi (40% radiochemical yield) on 24 μg of [^{125}I]ICD-mGX.

vi. Receptor binding protocol

Materials:

Recombinant Mouse PLA2R1 [R&D Systems #5367-PL]

Whatman Grade GF/C Glass Microfiber Filters [GE Life Sciences #1822-024]

Whatman Grade GF/F Glass Microfiber Filters [GE Life Sciences #1822-024]

Cellulose Acetate (CA) Membrane Filters [Steriltech Corp. # CA04525100]

Vacuum filtration manifold, Millipore® model 1225

Procedure:

Aliquots of the receptor were made by adding 500 µL of 1xPBS to the vial containing the receptor then 100 µL aliquots were made in glass vials (5x100 µL) and stored in the -80 °C freezer (stable for 3 months under these conditions).

5% PEI solution:

- Measure out 50% PEI solution into a falcon tube
- Add 100mM Tris, pH 7.4
- Titer solution to pH 7.4 and then make 5% solution in same buffer and re-check pH

10% BSA solution:

- Weigh out BSA and put in 50 mL falcon tube
- Add binding buffer slowly and let sit to dissolve, no mixing
- Once up to 20mL then adjust pH to 7.4

Receptor solution:

- 100 ng/µl stored in 100 µL aliquots in -80 °C taken out just prior to use (do not freeze/thaw multiple times)
- Dilute with binding buffer binding buffer [20 mM Tris-HCL (pH 7.4), 140 mM NaCl, 2 mM $CaCl_2$, 0.1% BSA] to desired concentration

Protein solution:

- Protein solution (various concentration) is diluted in binding buffer (see above) to the desired concentration

Combine Receptor + Protein solutions (1:1, not to exceed 500 µL) and incubate for 1 hour at room temperature.

During incubation, the various filters should be soaked in either 5% PEI solution (GF/C or GF/F) or 10% BSA solution (CA).

Once incubation was complete, the solutions were rapidly filtered using the vacuum manifold. The tubes were washed with 200 µL wash buffer [20 mM Tris-HCL (pH 7.4), 140 mM NaCl] and this was also applied to the filter under vacuum. Radioactivity remaining on filters (associated with the receptor/protein bound complex which would be retained on the filter) was assessed using a gamma counter I-125 program (1 minute duration).

vii. *In vivo* mouse pilot study protocol

Procedure:

1. Mice were housed in a social environment until the start of the experiment to reduce stress.
2. Mice were weighed and their total blood volume (6% weight) was calculated. The injection volume was then calculated based on the target molarity of sPLA2 in the mouse and the concentration of radio-labeled sPLA2 solution prepared.
3. Mice were injected intravenously with the labeled sPLA2 by one of two methods:

a. Retro-orbital injection: Mice were placed in a chamber and anesthetized with isoflurane gas (3%) for a couple of minutes until visible signs of alertness and response to pain stimuli were absent. Mice were removed from the chamber and placed on a flat, well-lit surface and their noses were placed in a cone that continued to provide them with isoflurane. Mice were positioned on their side and the index finger of the non-dominant hand was used to pull the skin above the eye taut while the thumb was used to pull down the skin below the eye such that the eye was bulging out of its socket. The pre-loaded syringe (not to exceed 1/2" in length and 27.5 gauge or smaller) bevel down was inserted approximately at a 45° angle to the eye, lateral to the medial inner corner of the eye, through the conjunctival membrane where the needle will be positioned behind the globe of the eye in the retrobulbar sinus. Carefully, without moving the needle in any direction, the syringe was depressed slowly as to not flood the sinus until all of the solution was injected. It is essential that you remove the needle at the exact same angle of entry as to not tear the sinus on the way out. As the needle was removed, the fingers used to pull back the eye were moved toward the sight of injection and slight pressure was applied and held for 30 seconds. Upon removal of fingers, no visible blood or fluid should be present around the eye if the injection was successful. Mice were then removed from the isoflurane nose cone, transferred to a metabolic cage, and watched for signs of recovery. The mouse should return to normal activity levels and the eye should show no signs of trauma (swelling, blood, scratching at the eye). Note, the start time of the experiment was marked as soon as the injection was complete.

b. Tail-vein injection: In a well-lit area, mice were placed in a full-body restraint containing a hole where the tail protruded. The tail was wiped with an alcohol swab and then a heat pack was applied to the tail to dilate the blood vessels. The tail was positioned using the non-dominant hand horizontally over the fingers and gripped tightly between the thumb and index finger such that the lateral tail vein was on top. A pre-loaded syringe (27-30 gauge) was inserted bevel up as low as possible towards the tip of the tail and with the needle positioned horizontally to the vein. The vein is very superficial and requires the needle to be inserted with very little angle to penetrate the vein without poking through it. The plunger was then depressed slowly to begin the injection and if the needle was successfully inserted into the tail vein there was no resistance and the red blood in the tail vein was visibly replaced by a clear solution. The needle was withdrawn and a small amount of pressure is applied to the injection site with gauze. Once the injection was complete, mice were moved to a metabolic cage for the duration of the experiment. Note, the start time of the experiment was marked as soon as the injection was complete.

4. Blood collection was accomplished from the tail vein though the saphenous and pedal veins were reserved as backup sites for blood collection should the tail vein become collapsed though this did not occur. At various times indicated, mice were removed from metabolic cages and placed in a full-body restraint. The tail vein was punctured with a needle (26-28 gauge) and a droplet of blood was formed by milking the tail vein with the index and thumb of the non-dominant hand. The blood (20 µL) was then collected with a capillary tube containing markings for either 5, 10, or 20 µL which were then placed in

gamma tubes for counting. Pressure was applied to the site with gauze to halt any bleeding and the mouse was returned to the metabolic cage.

5. After injection of the radiolabeled protein, mice were monitored for signs of pain and distress. In mice, these signs include changes in activity such as abnormally low or high states of activity or restlessness, changes in body condition including weight loss, respiratory distress, changes in grooming such as a messy coat, change in skin color of the paws or mucus membranes, and behavioral cues such as hiding in the corner of the cage, self-mutilation, or vocalization. Mice were monitored periodically throughout the duration of the experiment (for example, 8 hour experiment/once per hour). If signs of distress were observed then personnel from Veterinary Services would be notified and mice would be treated or euthanized.
6. Upon completion of the experiment, mice were euthanized by carbon dioxide asphyxiation (30%, 6 minutes). Mice were transferred to a well-lit area and positioned on their backs with arms and legs splayed. A Y-incision was made to the outer coat of fur running from either shoulder down the full length of the torso. The thin layer of skin encasing the organs of the abdominal cavity was then punctured and removed to expose the area. The bladder was punctured and contents were collected then the organ was removed and the tissue was washed with saline, patted dry and placed in a gamma counting tube. The remaining abdominal organs were then removed starting with the ovaries or testes and followed by the large intestine, ceecum, small intestine, stomach, spleen, kidneys, and liver. The contents were removed from the stomach and collected separately from the stomach tissue in all later experiments. Then, the chest cavity was opened with scissors and the heart and lungs were collected. The thyroid was collected

by careful dissection of the neck. Then the outer coat of the mouse was pulled back and up over the head to expose the skull. The spinal cord was severed at the base of the skull and two lateral incisions were made around the perimeter of the skull to expose the brain which was removed as a single piece. All organs were placed in gamma tubes for counting.

7. Excreta, urine and feces, were collected passively over the course of the experiment paying close attention to any emissions during blood sampling and collecting all liquids via absorption onto filter paper or tissues and collecting solids which were all placed in gamma tubes for counting.

List of References:

1. A. Aloulou, Y. B. Ali, S. Bezzine, Y. Gargouri, M. H. Gelb, Phospholipases: an overview. *Methods Mol Biol* **861**, 63-85 (2012).
2. M. H. Gelb, G. Lambeau, PLA_2: A Short Phospholipase Review. 2003.
3. S. B.P., University of Washington, (2006).
4. M. Ghosh, D. E. Tucker, S. A. Burchett, C. C. Leslie, Properties of the Group IV phospholipase A2 family. *Prog Lipid Res* **45**, 487-510 (2006).
5. C. C. Leslie, Properties and regulation of cytosolic phospholipase A2. *J Biol Chem* **272**, 16709-16712 (1997).
6. R. H. Schaloske, E. A. Dennis, The phospholipase A2 superfamily and its group numbering system. *Biochim Biophys Acta* **1761**, 1246-1259 (2006).
7. M. Murakami, Y. Taketomi, C. Girard, K. Yamamoto, G. Lambeau, Emerging roles of secreted phospholipase A2 enzymes: Lessons from transgenic and knockout mice. *Biochimie* **92**, 561-582 (2010).
8. E. A. Dennis, J. Cao, Y. H. Hsu, V. Magrioti, G. Kokotos, Phospholipase A2 enzymes: physical structure, biological function, disease implication, chemical inhibition, and therapeutic intervention. *Chem Rev* **111**, 6130-6185 (2011).
9. A. G. Singer *et al.*, Interfacial Kinetic and Binding Properties of Complete Set of Human and Mouse Groups I, II, V, X, and XII Secreted Phospholipases A_2. *J. Biol. Chem.* **277**, 48535-48549 (2002).
10. J. E. Burke, E. A. Dennis, Phospholipase A2 structure/function, mechanism, and signaling. *J Lipid Res* **50 Suppl**, S237-242 (2009).
11. G. Lambeau, M. H. Gelb, Biochemistry and physiology of mammalian secreted phospholipases A2. *Annu Rev Biochem* **77**, 495-520 (2008).
12. C. P. Baines, The cardiac mitochondrion: nexus of stress. *Annu Rev Physiol* **72**, 61-80 (2010).
13. D. J. Surmeier, J. N. Guzman, J. Sanchez-Padilla, Calcium, cellular aging, and selective neuronal vulnerability in Parkinson's disease. *Cell Calcium* **47**, 175-182 (2010).
14. E. Noch, K. Khalili, Molecular mechanisms of necrosis in glioblastoma: the role of glutamate excitotoxicity. *Cancer Biol Ther* **8**, 1791-1797 (2009).
15. C. Piot *et al.*, Effect of cyclosporine on reperfusion injury in acute myocardial infarction. *N Engl J Med* **359**, 473-481 (2008).
16. L. Duprez, E. Wirawan, T. Vanden Berghe, P. Vandenabeele, Major cell death pathways at a glance. *Microbes Infect* **11**, 1050-1062 (2009).
17. A. P. Halestrap, A pore way to die: the role of mitochondria in reperfusion injury and cardioprotection. *Biochem Soc Trans* **38**, 841-860 (2010).
18. J. W. Elrod *et al.*, Cyclophilin D controls mitochondrial pore-dependent Ca(2+) exchange, metabolic flexibility, and propensity for heart failure in mice. *J Clin Invest* **120**, 3680-3687 (2010).
19. A. Rasola, M. Sciacovelli, B. Pantic, P. Bernardi, Signal transduction to the permeability transition pore. *FEBS Lett* **584**, 1989-1996 (2010).
20. M. Crompton, H. Ellinger, A. Costi, Inhibition by cyclosporin A of a Ca2+-dependent pore in heart mitochondria activated by inorganic phosphate and oxidative stress. *Biochem J* **255**, 357-360 (1988).
21. E. J. Griffiths, A. P. Halestrap, Protection by Cyclosporin A of ischemia/reperfusion-induced damage in isolated rat hearts. *J Mol Cell Cardiol* **25**, 1461-1469 (1993).
22. D. R. Pfeiffer, P. C. Schmid, M. C. Beatrice, H. H. Schmid, Intramitochondrial phospholipase activity and the effects of Ca2+ plus N-ethylmaleimide on mitochondrial function. *J Biol Chem* **254**, 11485-11494 (1979).

23. K. M. Broekemeier, D. R. Pfeiffer, Inhibition of the mitochondrial permeability transition by cyclosporin A during long time frame experiments: relationship between pore opening and the activity of mitochondrial phospholipases. *Biochemistry* **34**, 16440-16449 (1995).
24. J. L. Blum *et al.*, Profiling of fatty acids released during calcium-induced mitochondrial permeability transition in isolated rabbit kidney cortex mitochondria. *Toxicol In Vitro* **25**, 1001-1006 (2011).
25. G. R. Kinsey, J. McHowat, K. S. Patrick, R. G. Schnellmann, Role of Ca2+-independent phospholipase A2gamma in Ca2+-induced mitochondrial permeability transition. *J Pharmacol Exp Ther* **321**, 707-715 (2007).
26. K. M. Broekemeier, J. R. Iben, E. G. LeVan, E. D. Crouser, D. R. Pfeiffer, Pore formation and uncoupling initiate a Ca2+-independent degradation of mitochondrial phospholipids. *Biochemistry* **41**, 7771-7780 (2002).
27. S. D. Williams, R. A. Gottlieb, Inhibition of mitochondrial calcium-independent phospholipase A2 (iPLA2) attenuates mitochondrial phospholipid loss and is cardioprotective. *Biochem J* **362**, 23-32 (2002).
28. S. H. Moon *et al.*, Genetic ablation of calcium-independent phospholipase A(2)γ (iPLA(2)γ) attenuates calcium-induced opening of the mitochondrial permeability transition pore and resultant cytochrome c release. *J Biol Chem* **287**, 29837-29850 (2012).
29. B. Yun *et al.*, Serine hydrolase inhibitors block necrotic cell death by preventing calcium overload of the mitochondria and permeability transition pore formation. *J Biol Chem* **289**, 1491-1504 (2014).
30. L. Scorrano, D. Penzo, V. Petronilli, F. Pagano, P. Bernardi, Arachidonic acid causes cell death through the mitochondrial permeability transition. Implications for tumor necrosis factor-alpha aopototic signaling. *J Biol Chem* **276**, 12035-12040 (2001).
31. D. Penzo *et al.*, Arachidonic acid released by phospholipase A(2) activation triggers Ca(2+)-dependent apoptosis through the mitochondrial pathway. *J Biol Chem* **279**, 25219-25225 (2004).
32. N. Uozumi *et al.*, Role of cytosolic phospholipase A2 in allergic response and parturition. *Nature* **390**, 618-622 (1997).
33. N. Uozumi, T. Shimizu, Roles for cytosolic phospholipase A2alpha as revealed by gene-targeted mice. *Prostaglandins Other Lipid Mediat* **68-69**, 59-69 (2002).
34. J. V. Bonventre *et al.*, Reduced fertility and postischaemic brain injury in mice deficient in cytosolic phospholipase A2. *Nature* **390**, 622-625 (1997).
35. K. Seno *et al.*, Pyrrolidine inhibitors of human cytosolic phospholipase A(2). *J Med Chem* **43**, 1041-1044 (2000).
36. F. Ghomashchi *et al.*, Interfacial kinetic and binding properties of mammalian group IVB phospholipase A2 (cPLA2beta) and comparison with the other cPLA2 isoforms. *J Biol Chem* **285**, 36100-36111 (2010).
37. P. Zizza *et al.*, Phospholipase A2IVα regulates phagocytosis independent of its enzymatic activity. *J Biol Chem* **287**, 16849-16859 (2012).
38. B. Yun, H. Lee, H. Ewing, M. H. Gelb, C. C. Leslie, Off-target effect of the cPLA2α inhibitor pyrrophenone: Inhibition of calcium release from the endoplasmic reticulum. *Biochem Biophys Res Commun* **479**, 61-66 (2016).
39. B. Yun *et al.*, Regulation of calcium release from the endoplasmic reticulum by the serine hydrolase ABHD2. *Biochem Biophys Res Commun*, (2017).
40. K. Seno *et al.*, Pyrrolidine inhibitors of human cytosolic phospholipase A2. Part 2: synthesis of potent and crystallized 4-triphenylmethylthio derivative 'pyrrophenone'. *Bioorg Med Chem Lett* **11**, 587-590 (2001).

41. B. F. Cravatt, A. T. Wright, J. W. Kozarich, Activity-based protein profiling: from enzyme chemistry to proteomic chemistry. *Annu Rev Biochem* **77**, 383-414 (2008).
42. I. P. Street *et al.*, Slow- and tight-binding inhibitors of the 85-kDa human phospholipase A2. *Biochemistry* **32**, 5935-5940 (1993).
43. M. H. Gelb, J. P. Svaren, R. H. Abeles, Fluoro ketone inhibitors of hydrolytic enzymes. *Biochemistry* **24**, 1813-1817 (1985).
44. E. Barbayianni *et al.*, 2-Oxoamide inhibitors of phospholipase A2 activity and cellular arachidonate release based on dipeptides and pseudodipeptides. *Bioorg Med Chem* **17**, 4833-4843 (2009).
45. K. Seno, M. Ohtani, F. Watanabe, USPTO, Ed. (U.S., 2000), vol. 6,147,100.
46. B. T. Golding, R. J. Griffin, A. Mitchinson, M. C. O'Sullivan, New routes to polyamine analogues. *Biochem Soc Trans* **22**, 391S (1994).
47. W. E. Parham, L. D. Jones, Elaboration of Bromoarylnitriles. *The Journal of Organic Chemistry* **41**, 1187-1191 (1976).
48. M. Di Antonio *et al.*, Quinone methides tethered to naphthalene diimides as selective G-quadruplex alkylating agents. *J Am Chem Soc* **131**, 13132-13141 (2009).
49. T. Nishio, Direct conversion of alcohols into thiols. *Journal of the Chemical Society, Perkin Transactions 1*, 1113-1117 (1993).
50. K. L. Hsu *et al.*, DAGLβ inhibition perturbs a lipid network involved in macrophage inflammatory responses. *Nat Chem Biol* **8**, 999-1007 (2012).
51. A. Adibekian *et al.*, Click-generated triazole ureas as ultrapotent in vivo-active serine hydrolase inhibitors. *Nat Chem Biol* **7**, 469-478 (2011).
52. T. Ono *et al.*, Characterization of a novel inhibitor of cytosolic phospholipase A2alpha, pyrrophenone. *Biochem J* **363**, 727-735 (2002).
53. K. L. Hsu *et al.*, Discovery and optimization of piperidyl-1,2,3-triazole ureas as potent, selective, and in vivo-active inhibitors of α/β-hydrolase domain containing 6 (ABHD6). *J Med Chem* **56**, 8270-8279 (2013).
54. Y. Liu, M. P. Patricelli, B. F. Cravatt, Activity-based protein profiling: the serine hydrolases. *Proc Natl Acad Sci U S A* **96**, 14694-14699 (1999).
55. D. Kidd, Y. Liu, B. F. Cravatt, Profiling serine hydrolase activities in complex proteomes. *Biochemistry* **40**, 4005-4015 (2001).
56. M. P. Patricelli, D. K. Giang, L. M. Stamp, J. J. Burbaum, Direct visualization of serine hydrolase activities in complex proteomes using fluorescent active site-directed probes. *Proteomics* **1**, 1067-1071 (2001).
57. D. Greenbaum *et al.*, Chemical approaches for functionally probing the proteome. *Mol Cell Proteomics* **1**, 60-68 (2002).
58. Y. Liu *et al.*, Wortmannin, a widely used phosphoinositide 3-kinase inhibitor, also potently inhibits mammalian polo-like kinase. *Chem Biol* **12**, 99-107 (2005).
59. Y. Liu, N. Jiang, J. Wu, W. Dai, J. S. Rosenblum, Polo-like kinases inhibited by wortmannin. Labeling site and downstream effects. *J Biol Chem* **282**, 2505-2511 (2007).
60. J. L. Brigham, B. G. Perera, D. J. Maly, A hexylchloride-based catch-and-release system for chemical proteomic applications. *ACS Chem Biol* **8**, 691-699 (2013).
61. G. V. Los *et al.*, HaloTag: a novel protein labeling technology for cell imaging and protein analysis. *ACS Chem Biol* **3**, 373-382 (2008).
62. T. Gronemeyer, C. Chidley, A. Juillerat, C. Heinis, K. Johnsson, Directed evolution of O6-alkylguanine-DNA alkyltransferase for applications in protein labeling. *Protein Eng Des Sel* **19**, 309-316 (2006).

63. A. Keppler *et al.*, Labeling of fusion proteins of O6-alkylguanine-DNA alkyltransferase with small molecules in vivo and in vitro. *Methods* **32**, 437-444 (2004).
64. A. Keppler *et al.*, A general method for the covalent labeling of fusion proteins with small molecules in vivo. *Nat Biotechnol* **21**, 86-89 (2003).
65. L. Liu, J. Spurrier, T. R. Butt, J. E. Strickler, Enhanced protein expression in the baculovirus/insect cell system using engineered SUMO fusions. *Protein Expr Purif* **62**, 21-28 (2008).
66. M. Golkowski *et al.*, Rapid profiling of protein kinase inhibitors by quantitative proteomics. *Medchemcomm* **5**, 363-369 (2014).
67. A. E. Speers, G. C. Adam, B. F. Cravatt, Activity-based protein profiling in vivo using a copper(i)-catalyzed azide-alkyne [3 + 2] cycloaddition. *J Am Chem Soc* **125**, 4686-4687 (2003).
68. A. E. Speers, B. F. Cravatt, Profiling enzyme activities in vivo using click chemistry methods. *Chem Biol* **11**, 535-546 (2004).
69. A. E. Speers, B. F. Cravatt, Activity-Based Protein Profiling (ABPP) and Click Chemistry (CC)-ABPP by MudPIT Mass Spectrometry. *Curr Protoc Chem Biol* **1**, 29-41 (2009).
70. J. F. Burd, M. Usategui-Gomez, A colorimetric assay for serum lactate dehydrogenase. *Clin Chim Acta* **46**, 223-227 (1973).
71. T. Nakagawa *et al.*, Cyclophilin D-dependent mitochondrial permeability transition regulates some necrotic but not apoptotic cell death. *Nature* **434**, 652-658 (2005).
72. M. Ghosh *et al.*, Role of cytosolic phospholipase A(2) in prostaglandin E(2) production by lung fibroblasts. *Am J Respir Cell Mol Biol* **30**, 91-100 (2004).
73. M. Ghosh *et al.*, Function, activity, and membrane targeting of cytosolic phospholipase A(2)zeta in mouse lung fibroblasts. *J Biol Chem* **282**, 11676-11686 (2007).
74. V. Petronilli *et al.*, Transient and long-lasting openings of the mitochondrial permeability transition pore can be monitored directly in intact cells by changes in mitochondrial calcein fluorescence. *Biophys J* **76**, 725-734 (1999).
75. M. R. Wieckowski, C. Giorgi, M. Lebiedzinska, J. Duszynski, P. Pinton, Isolation of mitochondria-associated membranes and mitochondria from animal tissues and cells. *Nat Protoc* **4**, 1582-1590 (2009).
76. A. M. McGee, C. P. Baines, Complement 1q-binding protein inhibits the mitochondrial permeability transition pore and protects against oxidative stress-induced death. *Biochem J* **433**, 119-125 (2011).
77. A. V. Vaseva *et al.*, p53 opens the mitochondrial permeability transition pore to trigger necrosis. *Cell* **149**, 1536-1548 (2012).
78. C. P. Baines *et al.*, Loss of cyclophilin D reveals a critical role for mitochondrial permeability transition in cell death. *Nature* **434**, 658-662 (2005).
79. W. R. Marrs *et al.*, The serine hydrolase ABHD6 controls the accumulation and efficacy of 2-AG at cannabinoid receptors. *Nat Neurosci* **13**, 951-957 (2010).
80. J. W. Chang, A. B. Cognetta, M. J. Niphakis, B. F. Cravatt, Proteome-wide reactivity profiling identifies diverse carbamate chemotypes tuned for serine hydrolase inhibition. *ACS Chem Biol* **8**, 1590-1599 (2013).
81. T. Kambe, B. E. Correia, M. J. Niphakis, B. F. Cravatt, Mapping the protein interaction landscape for fully functionalized small-molecule probes in human cells. *J Am Chem Soc* **136**, 10777-10782 (2014).
82. M. Nardini, B. W. Dijkstra, Alpha/beta hydrolase fold enzymes: the family keeps growing. *Curr Opin Struct Biol* **9**, 732-737 (1999).
83. C. C. Lord, G. Thomas, J. M. Brown, Mammalian alpha beta hydrolase domain (ABHD) proteins: Lipid metabolizing enzymes at the interface of cell signaling and energy metabolism. *Biochim Biophys Acta* **1831**, 792-802 (2013).

84. D. L. Ollis *et al.*, The alpha/beta hydrolase fold. *Protein Eng* **5**, 197-211 (1992).
85. A. J. Edgar, J. M. Polak, Cloning and tissue distribution of three murine alpha/beta hydrolase fold protein cDNAs. *Biochem Biophys Res Commun* **292**, 617-625 (2002).
86. D. A. Bachovchin, B. F. Cravatt, The pharmacological landscape and therapeutic potential of serine hydrolases. *Nat Rev Drug Discov* **11**, 52-68 (2012).
87. M. J. Niphakis, B. F. Cravatt, Enzyme inhibitor discovery by activity-based protein profiling. *Annu Rev Biochem* **83**, 341-377 (2014).
88. E. Valentin, F. Ghomashchi, M. H. Gelb, M. Lazdunski, G. Lambeau, Novel human secreted phospholipase A(2) with homology to the group III bee venom enzyme. *J Biol Chem* **275**, 7492-7496 (2000).
89. Y. Taketomi *et al.*, Mast cell maturation is driven via a group III phospholipase A2-prostaglandin D2-DP1 receptor paracrine axis. *Nat Immunol* **14**, 554-563 (2013).
90. H. M. Garcia-Garcia, P. W. Serruys, Phospholipase A2 inhibitors. *Curr Opin Lipidol* **20**, 327-332 (2009).
91. M. K. Jain, W. Yuan, M. H. Gelb, Competitive inhibition of phospholipase A2 in vesicles. *Biochemistry* **28**, 4135-4139 (1989).
92. C. C. Leslie, M. H. Gelb, Assaying phospholipase A2 activity. *Methods Mol Biol* **284**, 229-242 (2004).
93. H. Ewing *et al.*, Fluorometric High-Throughput Screening Assay for Secreted Phospholipases A2 Using Phospholipid Vesicles. *J Biomol Screen* **21**, 713-721 (2016).
94. J. H. Zhang, T. D. Chung, K. R. Oldenburg, A Simple Statistical Parameter for Use in Evaluation and Validation of High Throughput Screening Assays. *J Biomol Screen* **4**, 67-73 (1999).
95. T. Spicer *et al.*, Identification of Potent and Selective Inhibitors of the Plasmodium falciparum M18 Aspartyl Aminopeptidase (PfM18AAP) of Human Malaria via High-Throughput Screening. *J Biomol Screen* **19**, 1107-1115 (2014).
96. T. C. Turek-Etienne *et al.*, Evaluation of fluorescent compound interference in 4 fluorescence polarization assays: 2 kinases, 1 protease, and 1 phosphatase. *J Biomol Screen* **8**, 176-184 (2003).
97. A. G. Singer *et al.*, Interfacial kinetic and binding properties of the complete set of human and mouse groups I, II, V, X, and XII secreted phospholipases A2. *J Biol Chem* **277**, 48535-48549 (2002).
98. B. Nicholson *et al.*, Characterization of ubiquitin and ubiquitin-like-protein isopeptidase activities. *Protein Sci* **17**, 1035-1043 (2008).
99. R. C. Oslund, N. Cermak, M. H. Gelb, Highly specific and broadly potent inhibitors of mammalian secreted phospholipases A2. *J Med Chem* **51**, 4708-4714 (2008).
100. F. Madoux *et al.*, Development of high throughput screening assays and pilot screen for inhibitors of metalloproteases meprin α and β. *Biopolymers* **102**, 396-406 (2014).
101. T. Kawabata, Build-up algorithm for atomic correspondence between chemical structures. *J. Chem. Inf. Model* **51**, 1775-1778 (2011).
102. J. B. Baell, G. A. Holloway, New substructure filters for removal of pan assay interference compounds (PAINS) from screening libraries and for their exclusion in bioassays. *J Med Chem* **53**, 2719-2740 (2010).
103. R. Franson, P. Patriarca, P. Elsbach, Phospholipid metabolism by phagocytic cells. Phospholipases A2 associated with rabbit polymorphonuclear leukocyte granules. *J Lipid Res* **15**, 380-388 (1974).
104. B. P. Smart *et al.*, Inhibition of the complete set of mammalian secreted phospholipases A(2) by indole analogues: a structure-guided study. *Bioorg Med Chem* **12**, 1737-1749 (2004).

105. R. C. Oslund, M. H. Gelb, Biochemical characterization of selective inhibitors of human group IIA secreted phospholipase A(2) and hyaluronic acid-linked inhibitor conjugates. *Biochemistry* **51**, 8617-8626 (2012).
106. E. Valentin, G. Lambeau, Increasing molecular diversity of secreted phospholipases A(2) and their receptors and binding proteins. *Biochim Biophys Acta* **1488**, 59-70 (2000).
107. R. S. Koduri *et al.*, Bactericidal properties of human and murine groups I, II, V, X, and XII secreted phospholipases A(2). *J Biol Chem* **277**, 5849-5857 (2002).
108. M. Murakami, I. Kudo, Secretory phospholipase A2. *Biol Pharm Bull* **27**, 1158-1164 (2004).
109. C. M. Mounier *et al.*, Arachidonic acid release from mammalian cells transfected with human groups IIA and X secreted phospholipase A(2) occurs predominantly during the secretory process and with the involvement of cytosolic phospholipase A(2)-alpha. *J Biol Chem* **279**, 25024-25038 (2004).
110. K. Hanasaki, H. Arita, Phospholipase A2 receptor: a regulator of biological functions of secretory phospholipase A2. *Prostaglandins Other Lipid Mediat* **68-69**, 71-82 (2002).
111. G. Lambeau, M. Lazdunski, Receptors for a growing family of secreted phospholipases A2. *Trends Pharmacol Sci* **20**, 162-170 (1999).
112. E. Boilard, S. G. Bourgoin, C. Bernatchez, M. E. Surette, Identification of an autoantigen on the surface of apoptotic human T cells as a new protein interacting with inflammatory group IIA phospholipase A2. *Blood* **102**, 2901-2909 (2003).
113. M. Triggiani, F. Granata, A. Frattini, G. Marone, Activation of human inflammatory cells by secreted phospholipases A2. *Biochim Biophys Acta* **1761**, 1289-1300 (2006).
114. K. Tada, M. Murakami, T. Kambe, I. Kudo, Induction of cyclooxygenase-2 by secretory phospholipases A2 in nerve growth factor-stimulated rat serosal mast cells is facilitated by interaction with fibroblasts and mediated by a mechanism independent of their enzymatic functions. *J Immunol* **161**, 5008-5015 (1998).
115. M. J. Bidgood, O. S. Jamal, A. M. Cunningham, P. M. Brooks, K. F. Scott, Type IIA secretory phospholipase A2 up-regulates cyclooxygenase-2 and amplifies cytokine-mediated prostaglandin production in human rheumatoid synoviocytes. *J Immunol* **165**, 2790-2797 (2000).
116. L. Fuentes, M. Hernández, M. L. Nieto, M. Sánchez Crespo, Biological effects of group IIA secreted phosholipase A(2). *FEBS Lett* **531**, 7-11 (2002).
117. S. Beck *et al.*, Potentiation of tumor necrosis factor alpha-induced secreted phospholipase A2 (sPLA2)-IIA expression in mesangial cells by an autocrine loop involving sPLA2 and peroxisome proliferator-activated receptor alpha activation. *J Biol Chem* **278**, 29799-29812 (2003).
118. M. Rouault *et al.*, Recombinant production and properties of binding of the full set of mouse secreted phospholipases A2 to the mouse M-type receptor. *Biochemistry* **46**, 1647-1662 (2007).
119. M. Rouault, J. G. Bollinger, M. Lazdunski, M. H. Gelb, G. Lambeau, Novel mammalian group XII secreted phospholipase A2 lacking enzymatic activity. *Biochemistry* **42**, 11494-11503 (2003).
120. I. Muñoz-Sanjuán, A. H. Brivanlou, Induction of ectopic olfactory structures and bone morphogenetic protein inhibition by Rossy, a group XII secreted phospholipase A2. *Mol Cell Biol* **25**, 3608-3619 (2005).
121. M. Murakami *et al.*, Cellular distribution, post-translational modification, and tumorigenic potential of human group III secreted phospholipase A(2). *J Biol Chem* **280**, 24987-24998 (2005).
122. G. Lambeau, A. Schmid-Alliana, M. Lazdunski, J. Barhanin, Identification and purification of a very high affinity binding protein for toxic phospholipases A2 in skeletal muscle. *J Biol Chem* **265**, 9526-9532 (1990).
123. K. Hanasaki, Mammalian phospholipase A2: phospholipase A2 receptor. *Biol Pharm Bull* **27**, 1165-1167 (2004).

124. L. Cupillard *et al.*, Both group IB and group IIA secreted phospholipases A2 are natural ligands of the mouse 180-kDa M-type receptor. *J Biol Chem* **274**, 7043-7051 (1999).
125. E. Valentin, F. Ghomashchi, M. H. Gelb, M. Lazdunski, G. Lambeau, On the diversity of secreted phospholipases A(2). Cloning, tissue distribution, and functional expression of two novel mouse group II enzymes. *J Biol Chem* **274**, 31195-31202 (1999).
126. K. Hamaguchi *et al.*, Induction of distinct sets of secretory phospholipase A(2) in rodents during inflammation. *Biochim Biophys Acta* **1635**, 37-47 (2003).
127. E. Zvaritch, G. Lambeau, M. Lazdunski, Endocytic properties of the M-type 180-kDa receptor for secretory phospholipases A2. *J Biol Chem* **271**, 250-257 (1996).
128. Y. Yokota *et al.*, Clearance of group X secretory phospholipase A(2) via mouse phospholipase A(2) receptor. *FEBS Lett* **509**, 250-254 (2001).
129. K. Hanasaki, Y. Yokota, J. Ishizaki, T. Itoh, H. Arita, Resistance to endotoxic shock in phospholipase A2 receptor-deficient mice. *J Biol Chem* **272**, 32792-32797 (1997).
130. S. Tamaru *et al.*, Deficiency of phospholipase A2 receptor exacerbates ovalbumin-induced lung inflammation. *J Immunol* **191**, 1021-1028 (2013).
131. K. Hanasaki, H. Arita, Characterization of a high affinity binding site for pancreatic-type phospholipase A2 in the rat. Its cellular and tissue distribution. *J Biol Chem* **267**, 6414-6420 (1992).
132. P. Ancian, G. Lambeau, M. G. Mattéi, M. Lazdunski, The human 180-kDa receptor for secretory phospholipases A2. Molecular cloning, identification of a secreted soluble form, expression, and chromosomal localization. *J Biol Chem* **270**, 8963-8970 (1995).
133. Y. Morioka *et al.*, Mouse group X secretory phospholipase A2 induces a potent release of arachidonic acid from spleen cells and acts as a ligand for the phospholipase A2 receptor. *Arch Biochem Biophys* **381**, 31-42 (2000).
134. G. Lambeau *et al.*, Structural elements of secretory phospholipases A2 involved in the binding to M-type receptors. *J Biol Chem* **270**, 5534-5540 (1995).
135. J. J. Marchalonis, An enzymic method for the trace iodination of immunoglobulins and other proteins. *Biochem J* **113**, 299-305 (1969).
136. M. Rouault *et al.*, Neurotoxicity and other pharmacological activities of the snake venom phospholipase A2 OS2: the N-terminal region is more important than enzymatic activity. *Biochemistry* **45**, 5800-5816 (2006).
137. L. I. Eerola *et al.*, Analysis of expression of secreted phospholipases A2 in mouse tissues at protein and mRNA levels. *Biochim Biophys Acta* **1761**, 745-756 (2006).
138. W. PINKERTON, M. WEBBER, A METHOD OF INJECTING SMALL LABORATORY ANIMALS BY THE OPHTHALMIC PLEXUS ROUTE. *Proc Soc Exp Biol Med* **116**, 959-961 (1964).
139. J. E. Price, R. F. Barth, C. W. Johnson, A. E. Staubus, Injection of cells and monoclonal antibodies into mice: comparison of tail vein and retroorbital routes. *Proc Soc Exp Biol Med* **177**, 347-353 (1984).
140. S. Parasuraman, R. Raveendran, R. Kesavan, Blood sample collection in small laboratory animals. *J Pharmacol Pharmacother* **1**, 87-93 (2010).
141. W. Strober, T. A. Waldmann, The role of the kidney in the metabolism of plasma proteins. *Nephron* **13**, 35-66 (1974).
142. L. Tang, A. M. Persky, G. Hochhaus, B. Meibohm, Pharmacokinetic aspects of biotechnology products. *J Pharm Sci* **93**, 2184-2204 (2004).
143. B. T. Kurien, N. E. Everds, R. H. Scofield, Experimental animal urine collection: a review. *Lab Anim* **38**, 333-361 (2004).
144. S. E. Rokita, J. M. Adler, P. M. McTamney, J. A. Watson, Efficient use and recycling of the micronutrient iodide in mammals. *Biochimie* **92**, 1227-1235 (2010).

145. A. Phatarphekar, J. M. Buss, S. E. Rokita, Iodotyrosine deiodinase: a unique flavoprotein present in organisms of diverse phyla. *Mol Biosyst* **10**, 86-92 (2014).
146. M. D. Roldán, E. Pérez-Reinado, F. Castillo, C. Moreno-Vivián, Reduction of polynitroaromatic compounds: the bacterial nitroreductases. *FEMS Microbiol Rev* **32**, 474-500 (2008).
147. J. M. Buss, P. M. McTamney, S. E. Rokita, Expression of a soluble form of iodotyrosine deiodinase for active site characterization by engineering the native membrane protein from Mus musculus. *Protein Sci* **21**, 351-361 (2012).
148. M. Josefsson, T. Grunditz, T. Ohlsson, E. Ekblad, Sodium/iodide-symporter: distribution in different mammals and role in entero-thyroid circulation of iodide. *Acta Physiol Scand* **175**, 129-137 (2002).
149. V. Awasthi, G. Meinken, K. Springer, S. C. Srivastava, P. Freimuth, Biodistribution of radioiodinated adenovirus fiber protein knob domain after intravenous injection in mice. *J Virol* **78**, 6431-6438 (2004).
150. G. Vaidyanathan, M. R. Zalutsky, Protein radiohalogenation: observations on the design of N-succinimidyl ester acylation agents. *Bioconjug Chem* **1**, 269-273 (1990).
151. S. H. Song *et al.*, Distribution and pharmacokinetic analysis of angiostatin radioiodine labeled with high stability. *Nucl Med Biol* **32**, 845-850 (2005).
152. A. E. Bolton, W. M. Hunter, The labelling of proteins to high specific radioactivities by conjugation to a 125I-containing acylating agent. *Biochem J* **133**, 529-539 (1973).
153. A. E. Bolton, V. Lee-Own, R. K. McLean, G. S. Challand, Three different radioiodination methods for human spleen ferritin compared. *Clin Chem* **25**, 1826-1830 (1979).
154. C. J. van der Laken *et al.*, Radiolabeled interleukin-8: specific scintigraphic detection of infection within a few hours. *J Nucl Med* **41**, 463-469 (2000).
155. J. Russell *et al.*, Iodination of annexin V for imaging apoptosis. *J Nucl Med* **43**, 671-677 (2002).
156. P. K. Garg, K. L. Alston, P. C. Welsh, M. R. Zalutsky, Enhanced binding and inertness to dehalogenation of alpha-melanotropic peptides labeled using N-succinimidyl 3-iodobenzoate. *Bioconjug Chem* **7**, 233-239 (1996).
157. M. R. Zalutsky, A. S. Narula, A method for the radiohalogenation of proteins resulting in decreased thyroid uptake of radioiodine. *Int J Rad Appl Instrum A* **38**, 1051-1055 (1987).
158. D. S. Wilbur *et al.*, Development of a stable radioiodinating reagent to label monoclonal antibodies for radiotherapy of cancer. *J Nucl Med* **30**, 216-226 (1989).
159. L. A. Khawli, A. I. Kassis, Synthesis of 125I labeled N-succinimidyl p-iodobenzoate for use in radiolabeling antibodies. *Int J Rad Appl Instrum B* **16**, 727-733 (1989).
160. M. C. Gershengorn, D. Glinoer, J. Robbins, in *The Thyroid Gland,* M. DeVisscher, Ed. (Raven Press, New York

1980), pp. 81-121.
161. J. Koehrle, M. Auf'mkolk, H. Rokos, R. D. Hesch, V. Cody, Rat liver iodothyronine monodeiodinase. Evaluation of the iodothyronine ligand-binding site. *J Biol Chem* **261**, 11613-11622 (1986).
162. R. C. Smallridge *et al.*, 3',5'-diiodothyronine to 3'-monoiodothyronine conversion in the fed and fasted rat: enzyme characteristics and evidence for two distinct 5'-deiodinases. *Endocrinology* **108**, 2336-2345 (1981).
163. G. Vaidyanathan, M. R. Zalutsky, Preparation of N-succinimidyl 3-[*I]iodobenzoate: an agent for the indirect radioiodination of proteins. *Nat Protoc* **1**, 707-713 (2006).
164. D. S. Wilbur *et al.*, Reagents for astatination of biomolecules. 6. An intact antibody conjugated with a maleimido-closo-decaborate(2-) reagent via sulfhydryl groups had considerably higher

kidney concentrations than the same antibody conjugated with an isothiocyanato-closo-decaborate(2-) reagent via lysine amines. *Bioconjug Chem* **23**, 409-420 (2012).

Appendix

A. hGIII-sPLA2 HTS Titration Results

Supplemental Table 3. hGIII-sPLA2 HTS Titration Results. All compounds tested at the dose response stage results are shown on Supplemental Table 3 for the primary and counterescreen assays. Structures and numerical assay results for all 240 tested compounds along with the clustering data analysis and other relevant cheminformatics information are included on this table.(*93*)

Sample ID	Cluster ID	PubChem CID	Structure	Dose Response Curves HGIII-SPLA2 = purple BODIPYPC-A2 =green	HGIII-SPLA2 INH Final IC50, uM	HGIII-SPLA2 Max % Response ± Standard Deviation	BODIPYPC-A2-SUBSTRATE INH Final IC50, Molar	BODIPYPC-A2-SUBSTRATE Max % Response ± Standard Deviation
SR-01000880485-1	10	404404	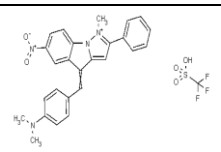	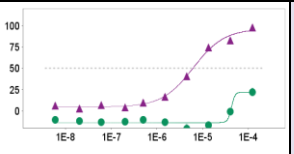	6.13	97.8 ± 2.7	>122	22.1 ± 4.9
SR-01000699586-1	3	2211008	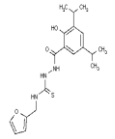	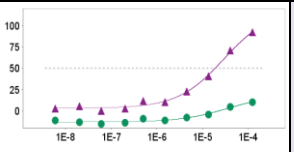	18.76	91.9 ± 2.4	>122	10.4 ± 0.9
SR-01000711569-1	3	12006125	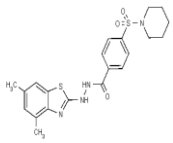	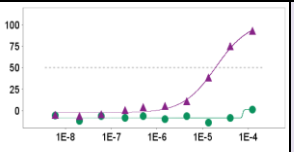	19.04	92.6 ± 2.1	>122	1.3 ± 0.9
SR-01000880338-1	32	395175	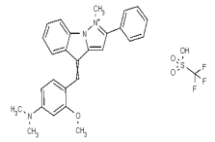	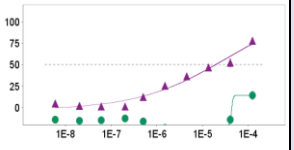	19.2	77.7 ± 3.8	>122	14.3 ± 5.5
SR-01000711735-1	20	12005954	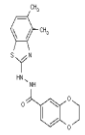	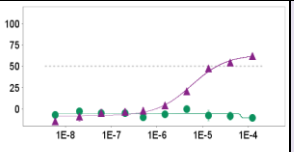	20.55	62.1 ± 2.7	>122	-0.5 ± 1.6
SR-01000369437-2	2	3138378	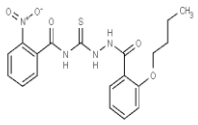	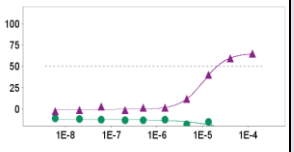	20.85	64.7 ± 1	>122	-10.9 ± 0.8
SR-01000711512-1	3	12006134	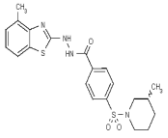	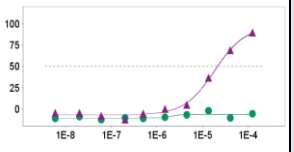	21.32	89.2 ± 2.6	>122	-2.1 ± 2.1
SR-01000714953-1	3	1790538	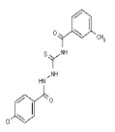	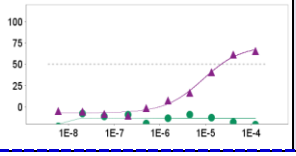	21.87	65.4 ± 3.5	>122	-7.9 ± 0.7

SR-01000638948-2	3	3806162	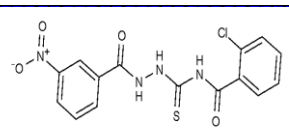	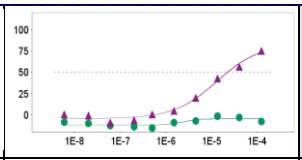	22.31	75.1 ± 2.9	>122	-1.4 ± 2.7
SR-01000705782-1	12	1879980	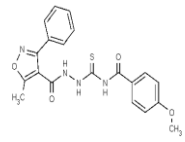	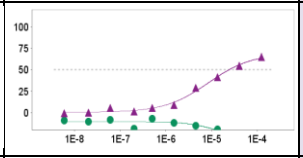	24.23	64.5 ± 4.3	>122	-7.1 ± 2.3
SR-01000732119-2	10	12871037	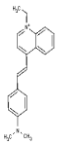	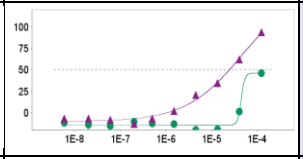	24.59	93.5 ± 1.7	>122	45.9 ± 2.6
SR-01000721243-1	3	12006166	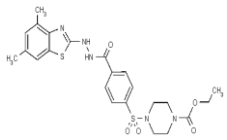	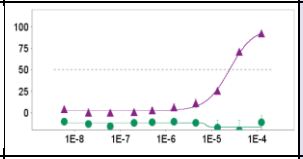	24.61	91.8 ± 1.8	>122	-10.3 ± 2.1
SR-01000720927-1	22	2927522	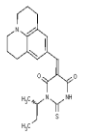	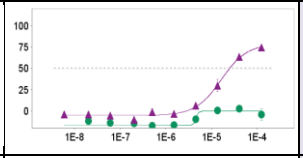	24.96	74.4 ± 2.2	>122	2.7 ± 3.6
SR-01000937009-1	7	45281797	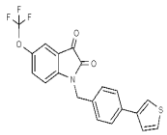	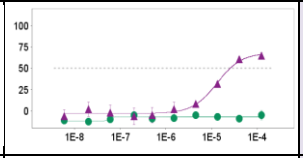	25.49	64.8 ± 4	>122	-4.8 ± 6.3
SR-01000721250-1	3	12006204	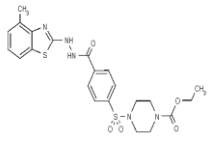	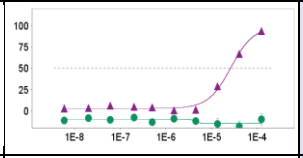	25.88	93.2 ± 0.8	>122	-7.9 ± 1.1
SR-01000711655-1	20	15944883	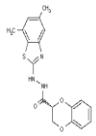	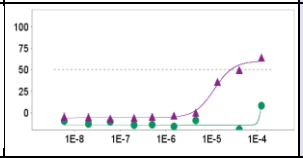	26.18	63.9 ± 3.3	>122	8.2 ± 3.2
SR-01000435887-2	10	16196127	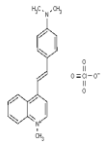	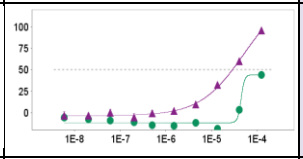	28.63	95.7 ± 2.2	>122	44 ± 0.7
SR-01000435887-3	10	12605846	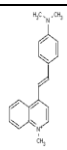	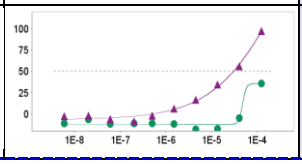	30.1	97.1 ± 2.5	>122	35.5 ± 1.8

SR-01000816123-1	25	16244880	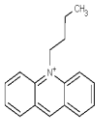	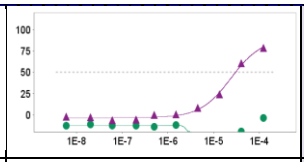	30.25	78.7 ± 1.5	>122	-3.4 ± 4.7
SR-01000771542-1	9	16240951	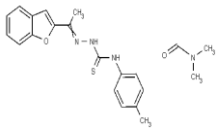	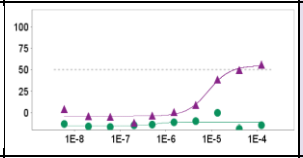	31.82	55.8 ± 4.4	>122	-0.4 ± 1
SR-01000886707-1	57	4042376	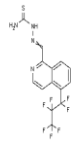	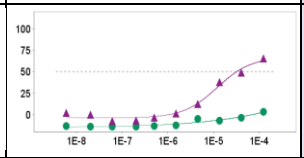	31.93	65.1 ± 1.8	>122	3.3 ± 1.9
SR-01000936277-1	7	45281794	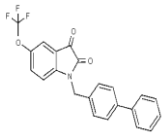	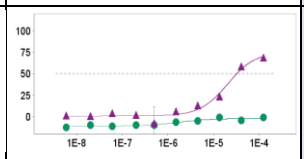	31.97	68.7 ± 1.8	>122	-1 ± 2.9
SR-01000810942-1	4	5498930	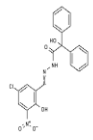	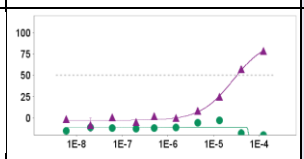	32.48	78.2 ± 0.7	>122	-2.9 ± 1.9
SR-01000696770-2	10	5702759	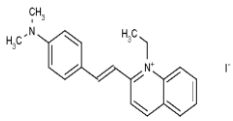	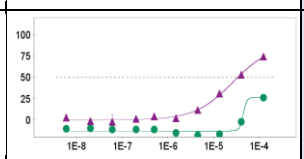	33.99	73.9 ± 1.2	>122	26.3 ± 1.3
SR-01000360777-2	2	1933094	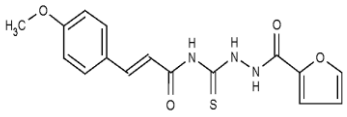	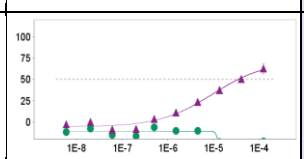	34.89	62.4 ± 6.6	>122	-6.1 ± 0.9
SR-01000713819-1	2	5021903	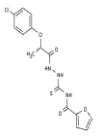	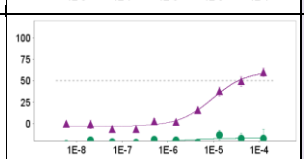	34.91	59.7 ± 5.4	>122	-13.3 ± 6.1
SR-01000882266-1	10	395179	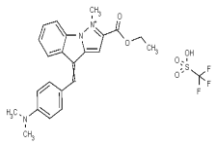	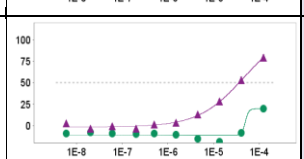	36.13	79.1 ± 3.4	>122	19.6 ± 1.8
SR-01000315082-2	2	1933179	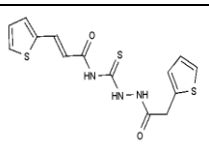	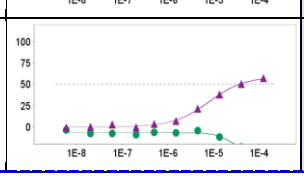	36.97	56.9 ± 1.4	>122	-3.6 ± 0.5

SR-01000707915-1	36	4417395	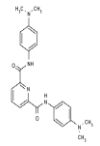	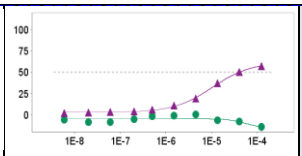	40.05	57.1 ± 3.9	>122	0.6 ± 1.1
SR-01000877278-2	10	16955	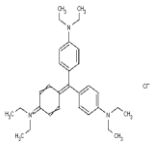	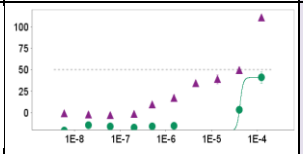	>40.59	110.7 ± 2.3	>122	41 ± 7.3
SR-01000930748-1	8	4429485	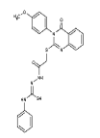	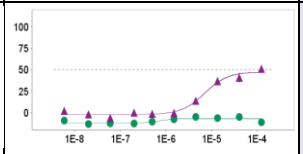	>40.60	50.5 ± 4.1	>122	-5 ± 0.6
SR-01000032366-2	2	2344236	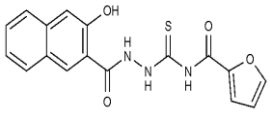	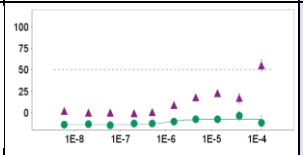	>40.61	54.9 ± 7.2	>122	-3.7 ± 5.9
SR-01000763175-1	4	6279054	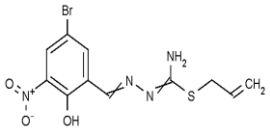	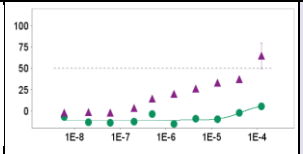	>40.61	64.7 ± 17	>122	5.3 ± 2.2
SR-01000701028-1	9	3529475	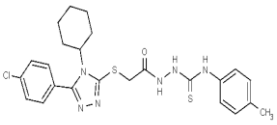	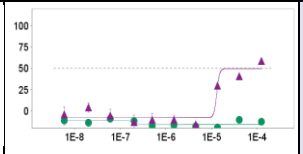	>40.61	58.7 ± 2.9	>122	-9.2 ± 3.5
SR-01000882358-1	10	392756	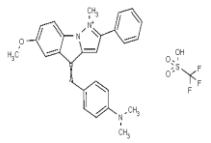	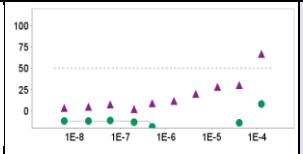	>40.63	66.6 ± 0.7	>122	8 ± 0.8
SR-01000826043-1	19	4316178	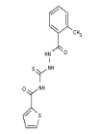	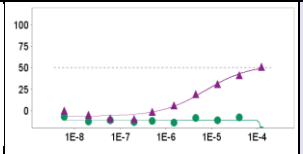	>40.63	50.8 ± 3.6	>122	-7.3 ± 0.3
SR-01000710886-1	14	5882673	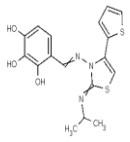	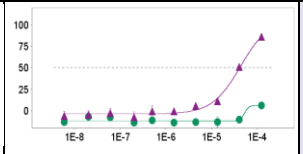	41.32	85.7 ± 3.2	>122	6.1 ± 0.3
SR-01000760446-1	10	16682266	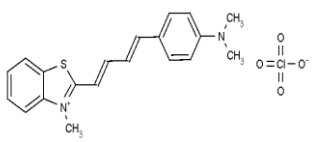	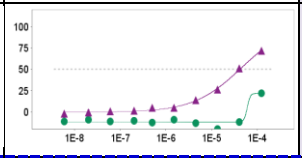	41.63	71.7 ± 2.3	>122	21.8 ± 2.4

SR-01000826021-1	4	6070340	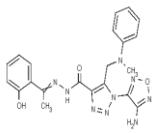	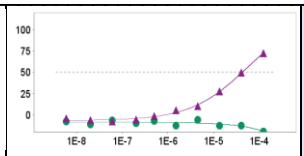	42.46	72.3 ± 4.1	>122	-5.8 ± 1.6
SR-01000679083-1	38	1620644	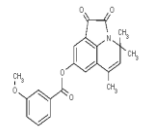	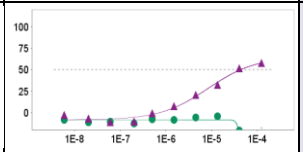	43.19	57.4 ± 2.6	>122	-4 ± 1.9
SR-01000770656-1	3	1933177	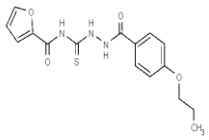	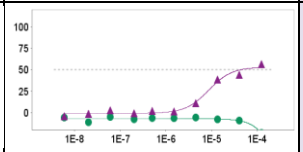	44.04	56.3 ± 3	>122	-5 ± 1.2
SR-01000705882-1	9	1304063	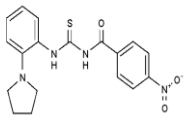	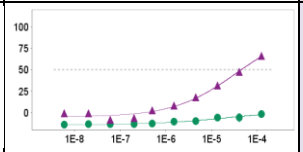	44.63	65.8 ± 1.9	>122	-1.8 ± 3.5
SR-01000720505-1	18	1212523	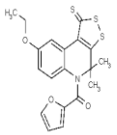	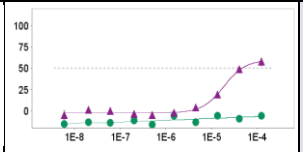	46.17	57.4 ± 5.3	>122	-5.4 ± 1.3
SR-01000720453-1	23	6182613	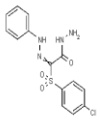	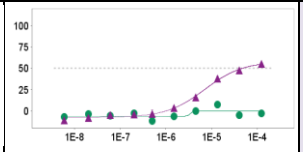	47.32	55.1 ± 0.8	>122	7.4 ± 1.7
SR-01000676776-2	41	2320031	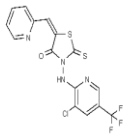	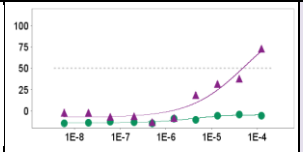	47.84	72.8 ± 3	>122	-4 ± 0.2
SR-01000821320-1	3	1566194	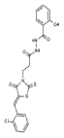	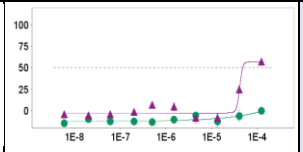	48.02	56.9 ± 1.4	>122	-0.4 ± 2.6
SR-01000759977-1	14	6282071	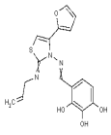	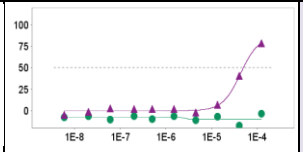	49.56	78.5 ± 2.7	>122	-3.3 ± 2.1
SR-01000739557-1	14	16195963	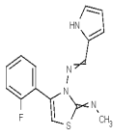	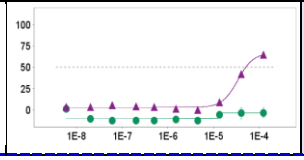	50.62	64.4 ± 3.1	>122	1.4 ± 2.9

SR-01000682758-1	34	2256906	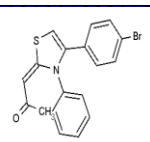	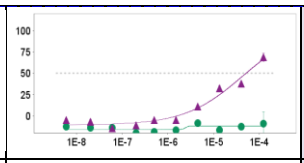	51.17	68.7 ± 5.2	>122	-8.7 ± 1.8
SR-01000359739-2	3	1728278	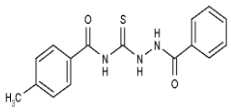	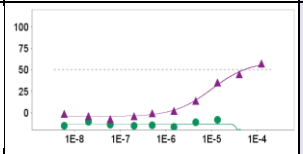	51.58	57 ± 2.8	>122	-8.2 ± 0.4
SR-01000075650-9	51	5154	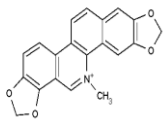	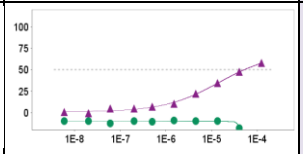	51.83	57.4 ± 3.4	>122	-9 ± 2.2
SR-01000276995-2	2	2207723	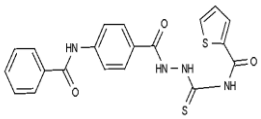	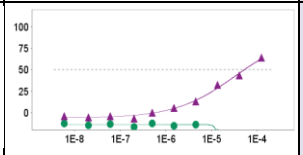	51.92	63.6 ± 1.8	>122	-12.4 ± 2.2
SR-01000721059-1	20	15944897	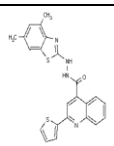	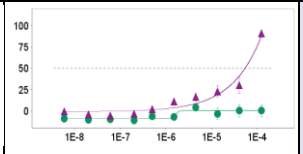	53.92	90.5 ± 3.9	>122	4.3 ± 2.5
SR-01000760630-1	12	1882124	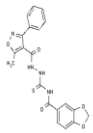	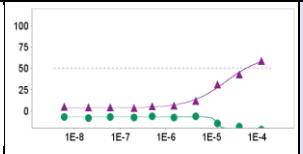	56.58	58.7 ± 0.4	>122	-6.1 ± 0.8
SR-01000930600-1	36	1990867	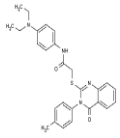	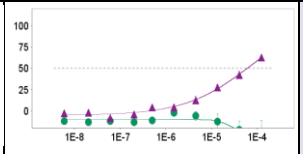	60.29	62.4 ± 2.2	>122	-2.3 ± 1.6
SR-01000297920-2	2	2234389	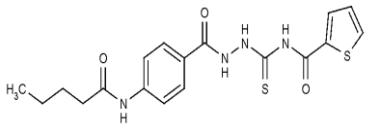	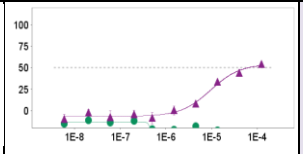	63.48	54.1 ± 3.3	>122	-11.2 ± 3.6
SR-01000314174-2	2	3138383	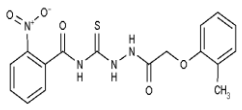	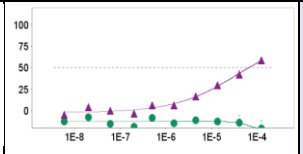	64.88	58.7 ± 2.8	>122	-7.4 ± 1.8
SR-01000765485-1	3	6578678	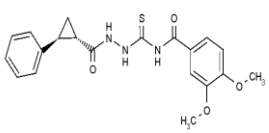	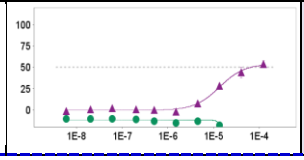	65.84	53.8 ± 4	>122	-10.3 ± 1

SR-01000822978-1	3	1933044	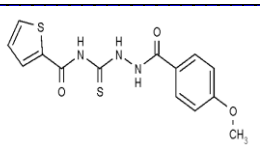	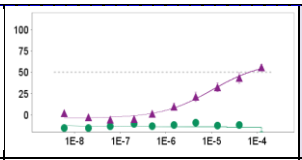	66.27	55.7 ± 3.5	>122	-9.1 ± 1.3
SR-01000882315-1	10	392754	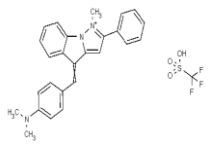	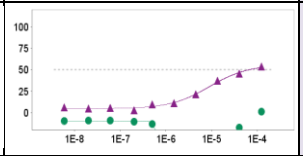	66.82	53.3 ± 0.7	>122	1 ± 1.4
SR-01000776412-1	2	1885341	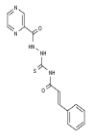	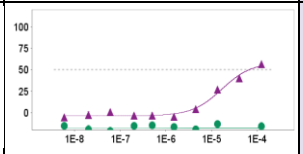	66.84	56.1 ± 1.1	>122	-13.2 ± 3.8
SR-01000736108-1	35	7066857	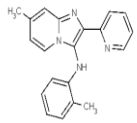	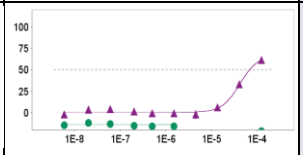	67.9	61 ± 2.2	>122	-12.1 ± 1.6
SR-01000880518-1	10	404406	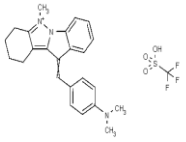	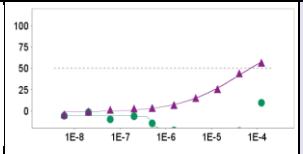	71.1	56.6 ± 1.7	>122	9.6 ± 1.3
SR-01000599166-2	66	5848270	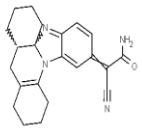	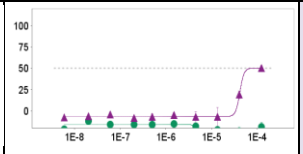	72.67	50.3 ± 3	>122	-12 ± 1.3
SR-01000699636-1	69	1559281	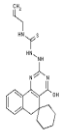	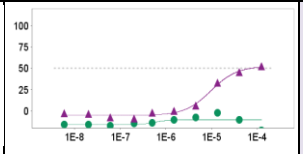	73.11	52.2 ± 3.2	>122	-2.3 ± 0.8
SR-01000839209-1	3	1790688	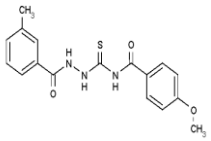	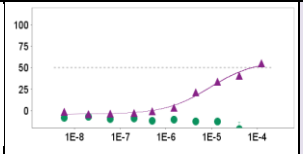	75.74	55.2 ± 1.2	>122	-7.2 ± 0.8
SR-01000439018-2	32	761632	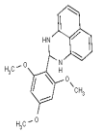	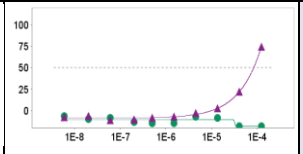	83.13	74 ± 1.1	>122	-6.5 ± 1.4
SR-01000692964-2	68	602897	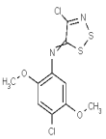	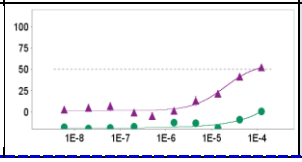	92.15	51.9 ± 3	>122	0.5 ± 1.9

SR-01000748527-1	40	1714948	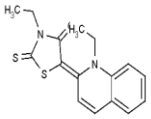	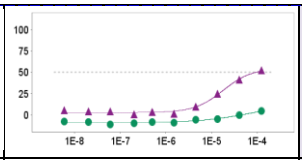	94.13	51.9 ± 0.9	>122	4.4 ± 1.6
SR-01000856371-1	36	9329256	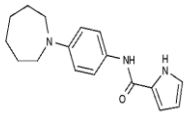	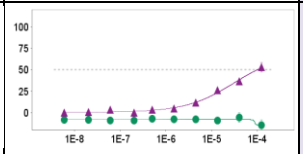	100	52.7 ± 6	>122	-5.6 ± 6.2
SR-01000705196-1	20	7110074	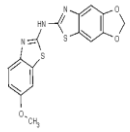	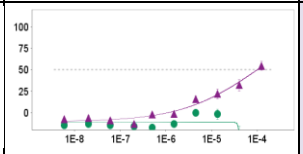	100	54.6 ± 5.5	>122	-0.3 ± 2.7
SR-01000706957-1	28	898647	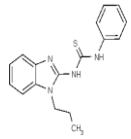	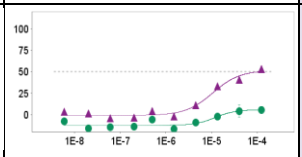	112	53.2 ± 3.7	>122	5.7 ± 4.6
SR-01000716256-1	2	3568622	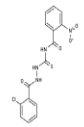	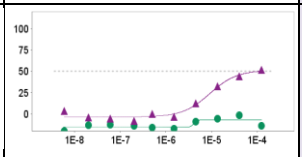	115	51.6 ± 1.9	>122	-1.8 ± 2.5
SR-01000534920-2	5	1825238	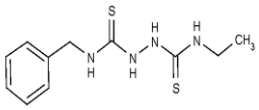	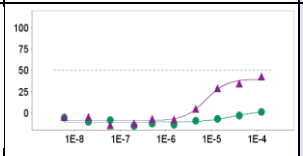	>122	42.5 ± 1.3	>122	1 ± 2.7
SR-01000635908-2	10	707007	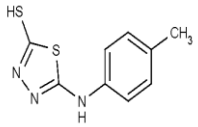	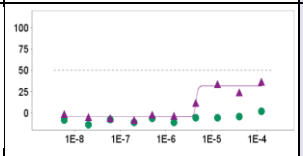	>122	36.5 ± 2.1	>122	1.9 ± 2.4
SR-01000880384-1	4	6145975	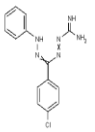	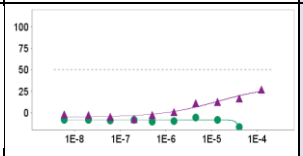	>122	26.8 ± 1.9	>122	-5.7 ± 0.9
SR-01000714832-1	17	843654	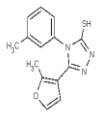	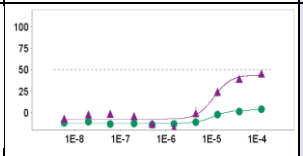	>122	45.5 ± 3.4	>122	4 ± 1.2
SR-01000822821-1	9	2373391	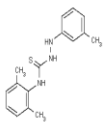	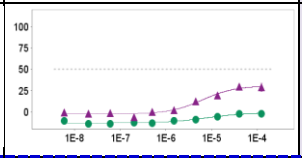	>122	29.3 ± 3.5	>122	-1.9 ± 0.6

SR-01000744439-1	17	951890	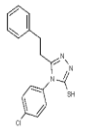	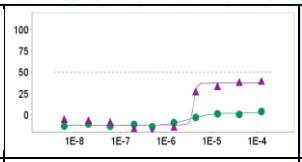	>122	39.6 ± 1.1	>122	4 ± 0.6
SR-01000771198-1	10	291365	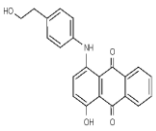	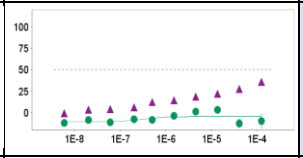	>122	35.8 ± 3.2	>122	3.2 ± 2
SR-01000769378-1	19	5158617	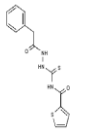	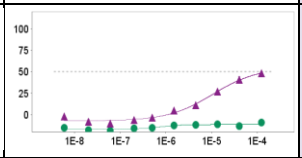	>122	48.1 ± 2	>122	-9.3 ± 1.9
SR-01000757708-1	4	6535036	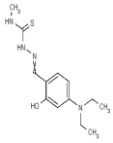	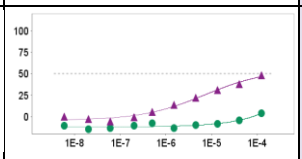	>122	48.1 ± 3.2	>122	3.9 ± 2.4
SR-01000681337-1	9	2230147	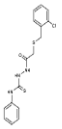	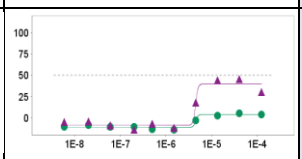	>122	45.3 ± 1.6	>122	5.6 ± 2.2
SR-01000759632-1	42	9583312	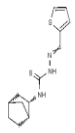	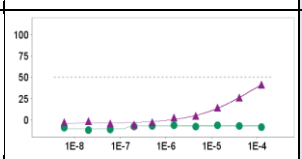	>122	41.2 ± 2.9	>122	-6.1 ± 1.8
SR-01000358139-2	9	1124396	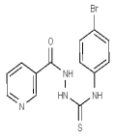	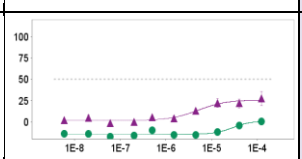	>122	27.7 ± 9.3	>122	0.5 ± 2.1
SR-01000711474-1	28	886439	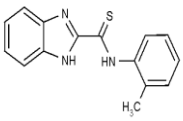	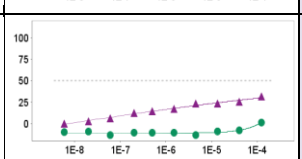	>122	31.7 ± 2.2	>122	1.5 ± 0.9
SR-01000723105-1	17	2454984	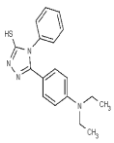	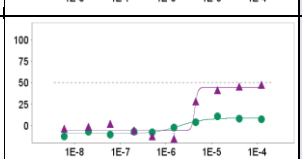	>122	47.3 ± 1.6	>122	10.7 ± 1.2
SR-01000846247-1	3	1790571	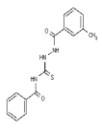	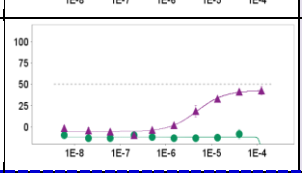	>122	42.5 ± 5.1	>122	-8.4 ± 6.3

SR-01000674048-1	1	842888	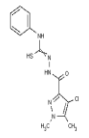	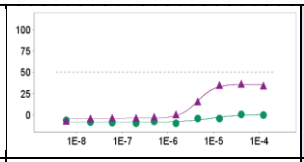	>122	36.3 ± 2.5	>122	0.8 ± 0.3
SR-01000768105-1	4	5939927	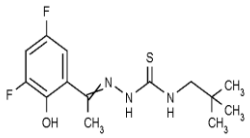	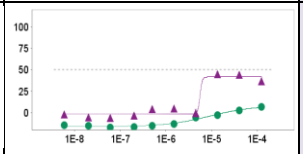	>122	44.4 ± 3.3	>122	6.8 ± 2.1
SR-01000710059-1	9	843691	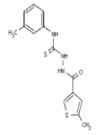	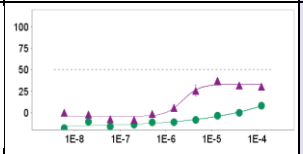	>122	37 ± 3	>122	8.1 ± 1.9
SR-01000707717-1	3	4108003	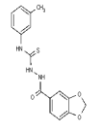	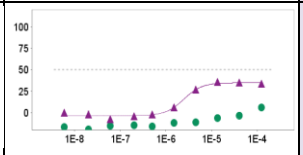	>122	35.6 ± 2.5	>122	6 ± 1.5
SR-01000715762-1	15	843677	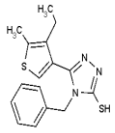	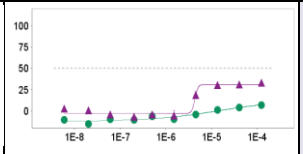	>122	32.7 ± 2.9	>122	7.1 ± 1.2
SR-01000803689-1	77	6401797	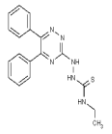	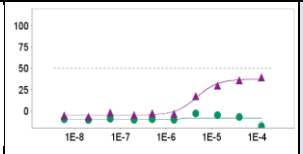	>122	39.1 ± 4.2	>122	-3.1 ± 0.5
SR-01000094742-2	60	3240793	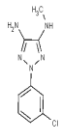	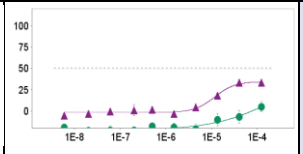	>122	33 ± 4.5	>122	4.9 ± 6.3
SR-01000076001-10	16	4212	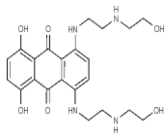	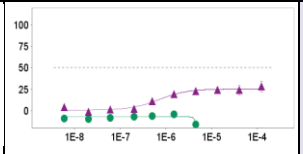	>122	28.3 ± 7.1	>122	-4 ± 0.9
SR-01000772212-1	30	16681813	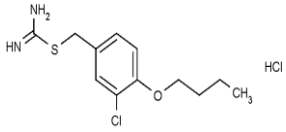	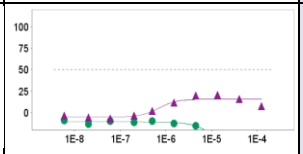	>122	20.6 ± 1.3	>122	-8.9 ± 0.6
SR-01000041911-2	3	2424240	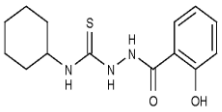	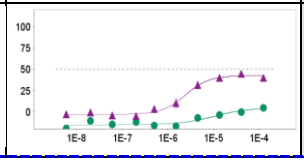	>122	44.6 ± 2.3	>122	5 ± 1.8

SR-01000359740-2	2	1728282	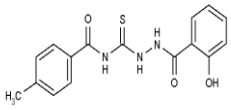	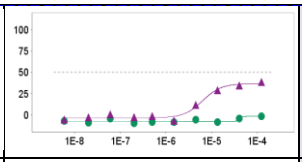	>122	38.5 ± 0.4	>122	-1.8 ± 1.2
SR-01000835258-1	51	24819048	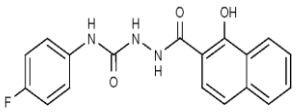	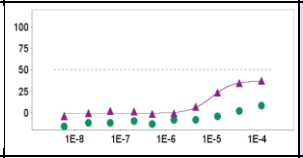	>122	37 ± 2.5	>122	8.4 ± 1.2
SR-01000699504-1	17	1543050	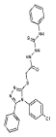	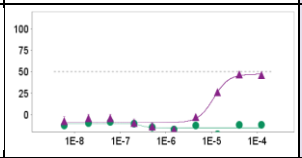	>122	46.9 ± 0.4	>122	-8.4 ± 1.8
SR-01000835262-1	51	24818763	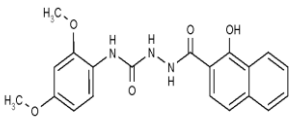	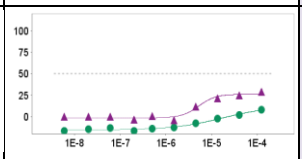	>122	28.8 ± 4	>122	7.9 ± 1.2
SR-01000731117-1	5	2928736	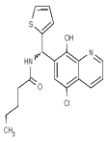	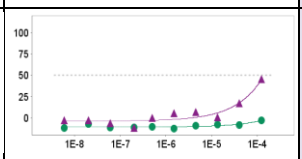	>122	45.2 ± 3.5	>122	-2.8 ± 0.9
SR-01000401273-2	2	2830220	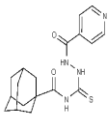	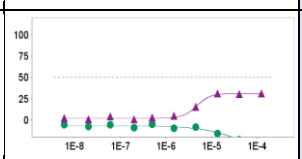	>122	30.9 ± 1.3	>122	-5.3 ± 0.9
SR-01000692527-1	30	11957158	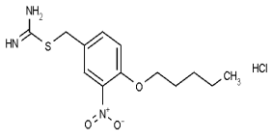	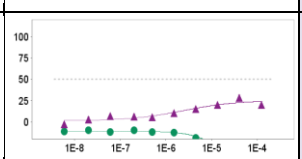	>122	28.1 ± 4	>122	-9.5 ± 1.1
SR-01000738918-1	3	1478046	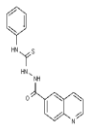	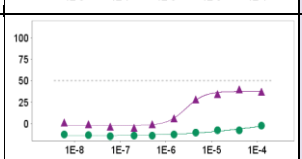	>122	39.8 ± 3.3	>122	-2.5 ± 1.2
SR-01000711692-1	20	4524998	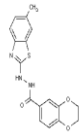	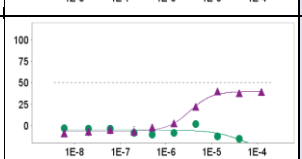	>122	39.6 ± 2.2	>122	1.9 ± 3.3
SR-01000084100-2	37	3525345	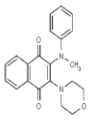	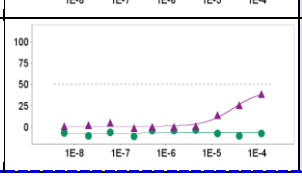	>122	38.2 ± 1.6	>122	-3.3 ± 0.4

SR-01000820782-1	4	5884815	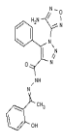	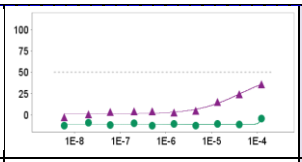	>122	35.8 ± 1.8	>122	-4.3 ± 1.5
SR-01000561175-2	28	1306043	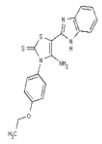	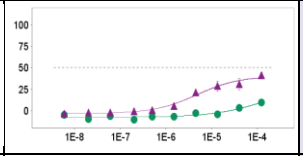	>122	41.2 ± 4	>122	9.5 ± 3.2
SR-01000681611-1	1	4413964	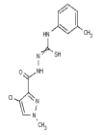	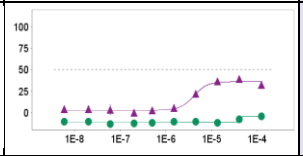	>122	38.9 ± 2.8	>122	-4.2 ± 0.7
SR-01000834396-1	36	16564446	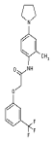	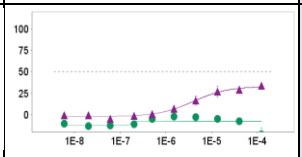	>122	33.4 ± 2.7	>122	-2.2 ± 1.1
SR-01000080771-2	16	16189280	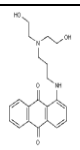	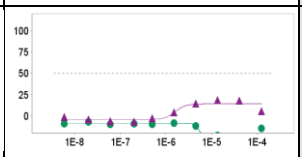	>122	18.2 ± 1.6	>122	-6.7 ± 0.8
SR-01000698057-1	5	15945829	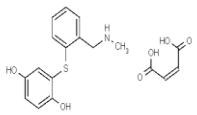	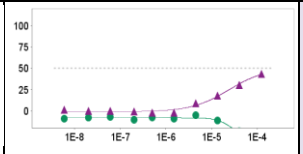	>122	43.3 ± 1.1	>122	-5.2 ± 3
SR-01000820607-1	4	5809179	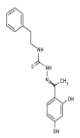	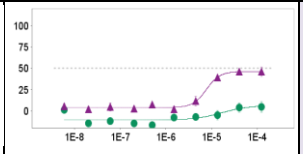	>122	46.1 ± 6.2	>122	4.9 ± 6.8
SR-01000696135-1	17	1839039	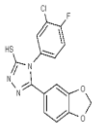	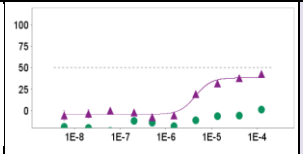	>122	42.5 ± 0.7	>122	1.3 ± 2.7
SR-01000710577-1	28	797526	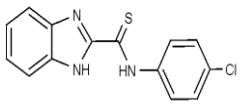	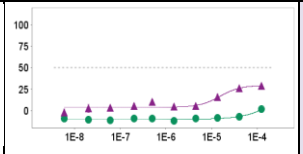	>122	29.1 ± 2.2	>122	1.6 ± 3
SR-01000688863-1	12	16413079	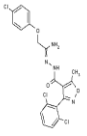	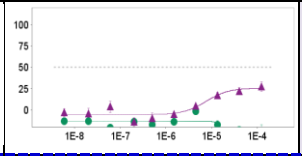	>122	27.2 ± 6	>122	-1.8 ± 1.2

SR-01000702010-1	17	2039982	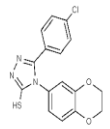	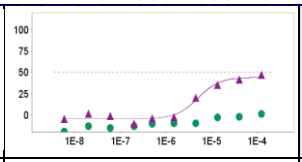	>122	46.6 ± 3.5	>122	0.9 ± 1.6
SR-01000681134-1	1	842822	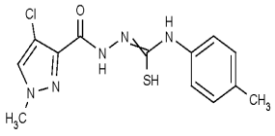	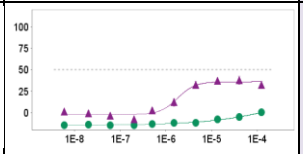	>122	37.8 ± 5.1	>122	0.2 ± 1.2
SR-01000684065-1	1	842824	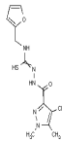	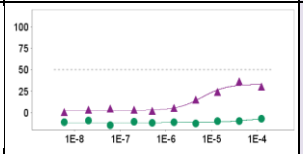	>122	36.1 ± 0.7	>122	-7.1 ± 0.9
SR-01000718618-1	57	4388531	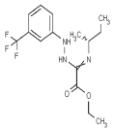	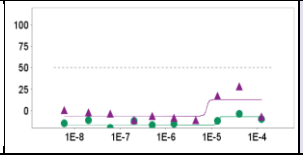	>122	28.2 ± 1.7	>122	-3.9 ± 0.1
SR-01000694750-1	44	2954577	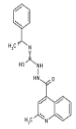	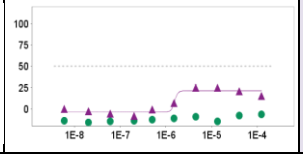	>122	24.5 ± 4.7	>122	-6.5 ± 0.8
SR-01000761287-1	12	1884111	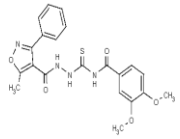	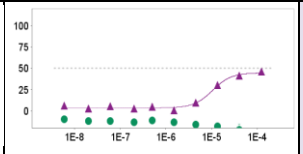	>122	45.7 ± 3.3	>122	-9.6 ± 0.5
SR-01000831389-1	51	24819050	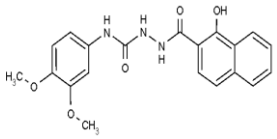	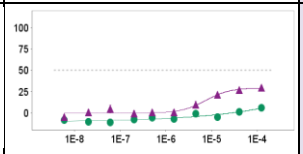	>122	29.7 ± 2.7	>122	5.9 ± 0.7
SR-01000777361-1	9	9672020	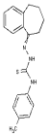	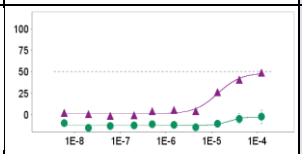	>122	48.5 ± 3.4	>122	-2.5 ± 9
SR-01000307223-2	15	1474810	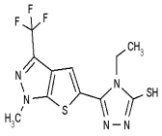	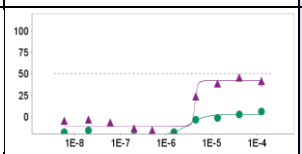	>122	45.3 ± 3.5	>122	5.8 ± 3.4
SR-01000711214-1	16	3744961	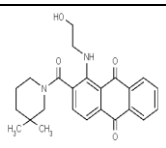	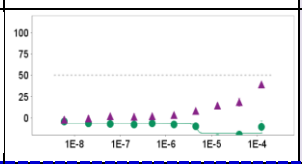	>122	39.2 ± 1.8	>122	-4 ± 0.8

SR-01000719913-1	9	5220035	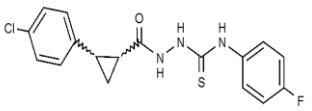	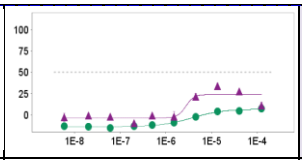	>122	33.9 ± 3.4	>122	7.4 ± 4.3
SR-01000837852-1	3	24819610	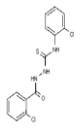	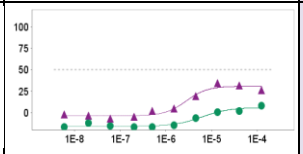	>122	34.4 ± 1.6	>122	8.1 ± 1.6
SR-01000698256-1	9	2207479	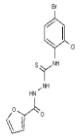	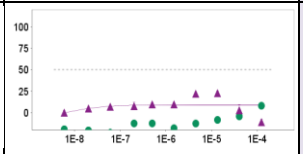	>122	22.6 ± 3	>122	7.9 ± 1.7
SR-01000462853-2	65	738764	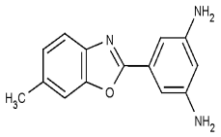	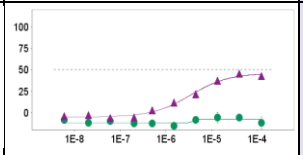	>122	45.1 ± 2.2	>122	-5.7 ± 7
SR-01000725167-1	2	3137369	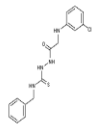	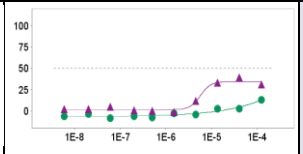	>122	38.9 ± 1.1	>122	13 ± 1.8
SR-01000761165-1	38	5888222	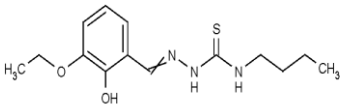	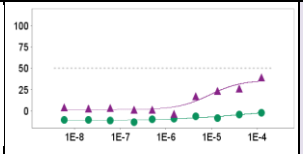	>122	38.9 ± 1.7	>122	-2 ± 2.9
SR-01000715772-1	3	998415	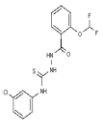	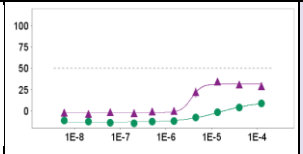	>122	34.6 ± 1.7	>122	8.8 ± 1.2
SR-01000702253-1	3	2307981	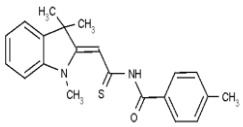	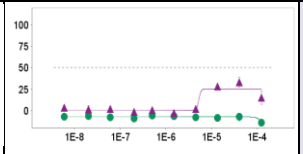	>122	33.2 ± 6.5	>122	-5.7 ± 1.5
SR-01000690164-1	2	2766604	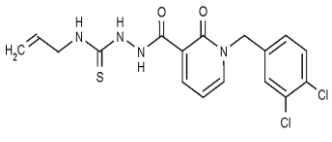	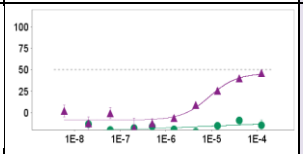	>122	45.8 ± 4.2	>122	-8.9 ± 4.4
SR-01000706072-1	2	1880649	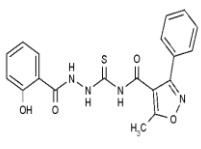	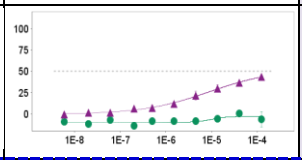	>122	43.4 ± 2.4	>122	0.6 ± 3.5

SR-01000715575-1	1	1229795	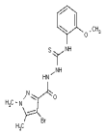	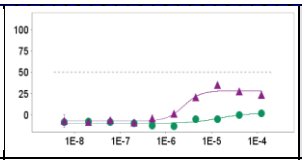	>122	35 ± 2.6	>122	1.6 ± 2.8
SR-01000714791-1	43	3776314	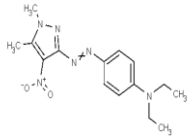	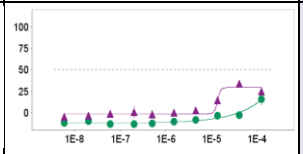	>122	33.8 ± 4	>122	15.5 ± 6.6
SR-01000703598-1	36	2358826	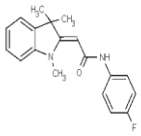	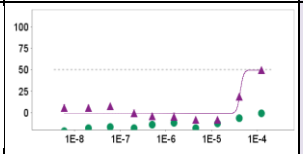	>122	49.7 ± 1.8	>122	-0.6 ± 1.7
SR-01000636557-2	3	2810212	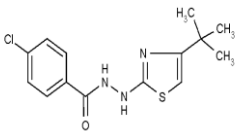	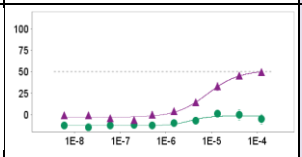	>122	49.4 ± 2.1	>122	1 ± 1.2
SR-01000900285-1	13	51360629	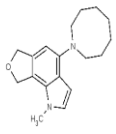	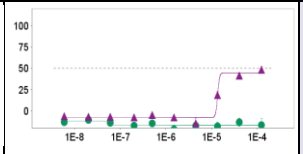	>122	47.9 ± 4.8	>122	-10.6 ± 1.5
SR-01000704228-1	4	5457268	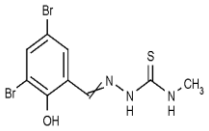	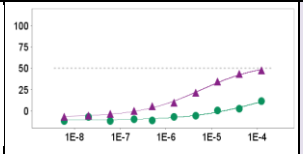	>122	47.7 ± 1.4	>122	11.3 ± 1.6
SR-01000276240-2	2	970143	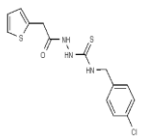	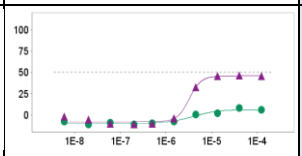	>122	46 ± 1.8	>122	8.1 ± 1
SR-01000360608-2	2	3145862	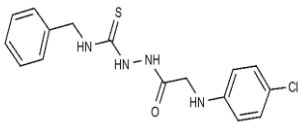	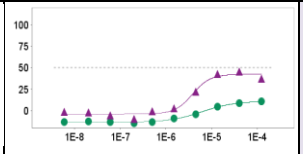	>122	45.5 ± 1.2	>122	10.7 ± 1.4
SR-01000358825-2	2	5763840	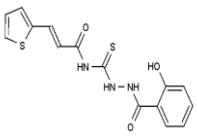	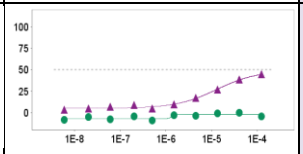	>122	44.3 ± 3.1	>122	0 ± 1.8
SR-01000710106-1	3	1790658	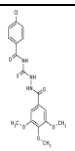	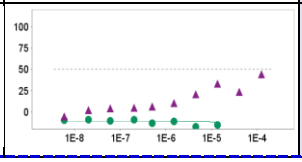	>122	43.8 ± 1.2	>122	-9.1 ± 2.1

SR-01000705061-1	29	822683	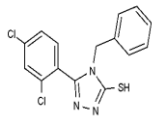	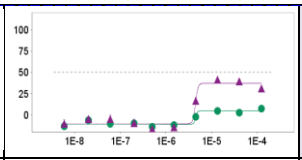	>122	40.9 ± 1.6	>122	7.2 ± 1.8
SR-01000837634-1	51	24818767	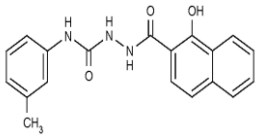	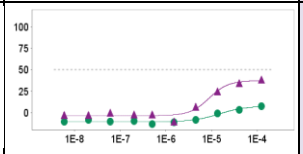	>122	38.5 ± 1.8	>122	7.7 ± 0.4
SR-01000676650-1	1	996712	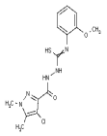	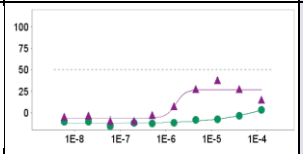	>122	37.5 ± 3.9	>122	3 ± 1.7
SR-01000689134-1	1	842689	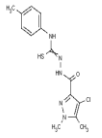	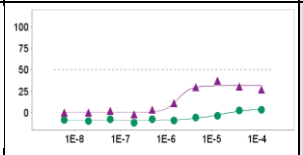	>122	37 ± 2.5	>122	3.5 ± 1.7
SR-01000718186-1	28	2850397	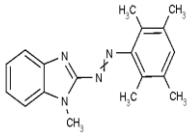	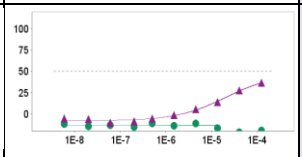	>122	36.3 ± 1.6	>122	-11 ± 0.4
SR-01000810650-1	4	5348300	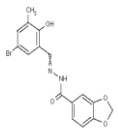	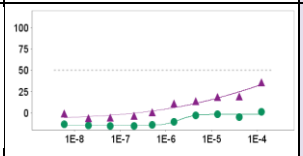	>122	35.6 ± 2.3	>122	1.4 ± 4
SR-01000275080-2	9	2204733	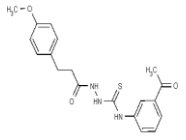	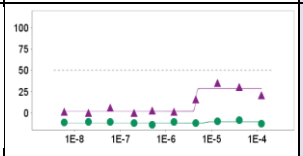	>122	35.1 ± 2.3	>122	-8.7 ± 1.6
SR-01000706596-1	9	985461	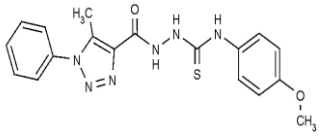	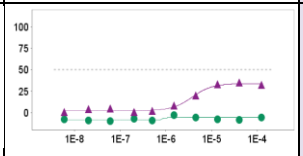	>122	34.7 ± 1.6	>122	-2.7 ± 0.9
SR-01000005109-2	59	7090639	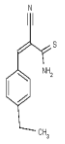	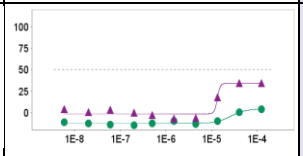	>122	34.2 ± 2	>122	4 ± 0.7
SR-01000828896-1	3	1213598	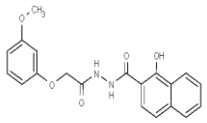	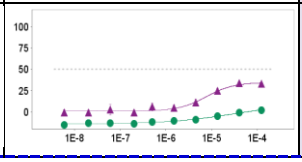	>122	33.4 ± 2.7	>122	2.2 ± 1.6

SR-01000782359-1	9	1166045	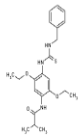	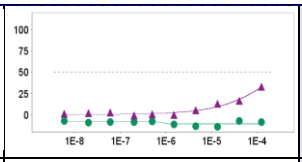	>122	32.8 ± 1.6	>122	-7.1 ± 0.1
SR-01000220091-2	3	870364	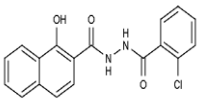	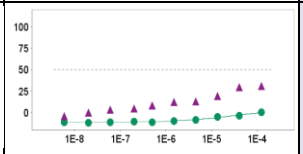	>122	30.6 ± 2.4	>122	0.2 ± 1.2
SR-01000683108-1	51	704287	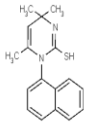	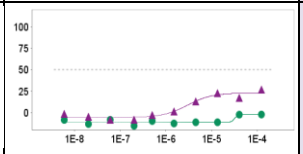	>122	26.6 ± 1.1	>122	-1.9 ± 0.9
SR-01000369729-2	2	1932924	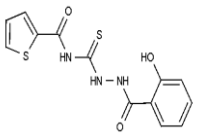	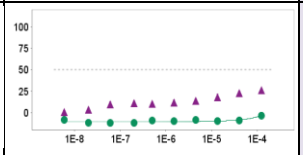	>122	25.7 ± 2.3	>122	-3.3 ± 1.8
SR-01000706901-3	4	6508320	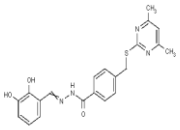	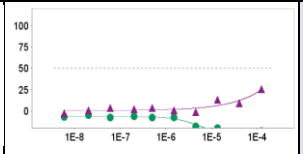	>122	25.3 ± 2.5	>122	-4.9 ± 1.6
SR-01000693906-2	55	2828115	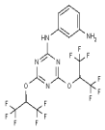	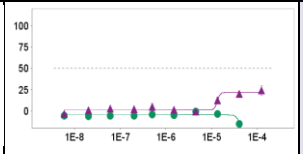	>122	23.9 ± 6.1	>122	-0.6 ± 1.9
SR-01000936681-1	7	53338863	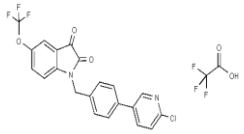	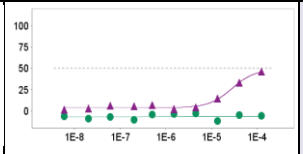	>122	45.8 ± 1.1	>122	-3 ± 0.8
SR-01000729721-1	3	4415017	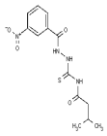	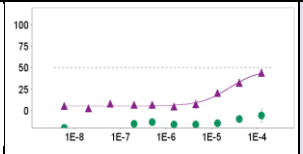	>122	43.8 ± 4.8	>122	-5.4 ± 8.5
SR-01000760515-1	3	3702769	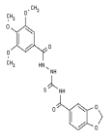	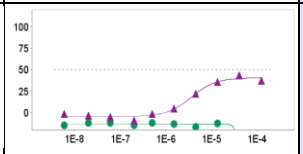	>122	43.5 ± 2	>122	-11.8 ± 3
SR-01000716292-1	3	998556	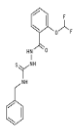	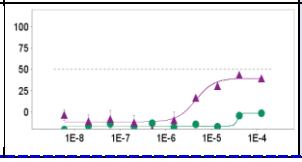	>122	43.1 ± 2.1	>122	-1.5 ± 2.2

SR-01000718688-1	45	2297665	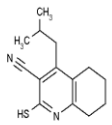	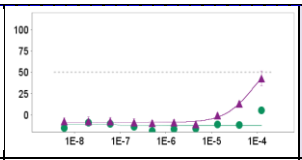	>122	42.6 ± 9.6	>122	5.4 ± 2.5
SR-01000076001-9	16	5458171	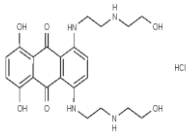	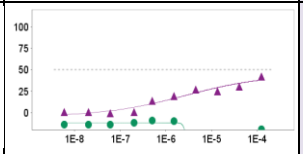	>122	42.2 ± 1.4	>122	-9.3 ± 1.5
SR-01000627353-1	29	676284	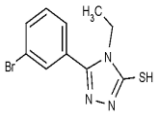	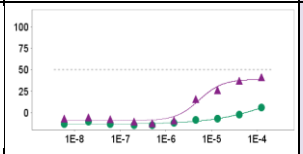	>122	41.3 ± 3.1	>122	5.8 ± 0.6
SR-01000741586-1	15	2764891	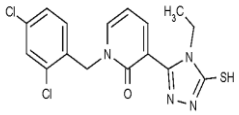	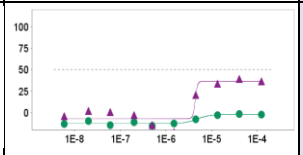	>122	39.4 ± 1.9	>122	-1.6 ± 1.4
SR-01000607876-1	32	2141781	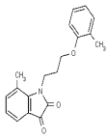	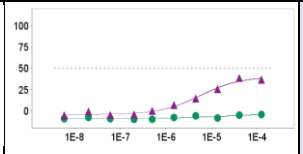	>122	38.1 ± 1.4	>122	-4 ± 4.3
SR-01000708225-1	9	843638	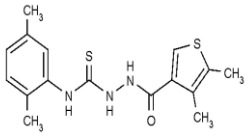	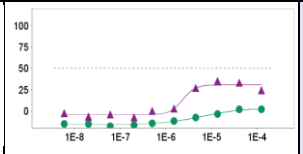	>122	34.8 ± 1.4	>122	1.9 ± 1.9
SR-01000736565-1	41	2476054	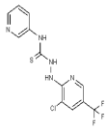	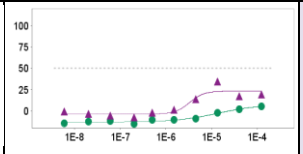	>122	34.3 ± 3	>122	5.2 ± 0.9
SR-01000678750-1	9	2204959	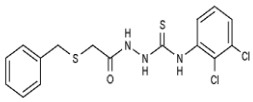	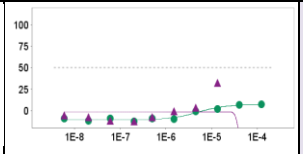	>122	32.3 ± 1.4	>122	7.3 ± 2.2
SR-01000709656-1	2	3554999	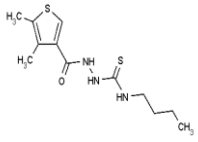	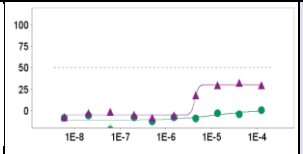	>122	32.1 ± 0.9	>122	0.6 ± 1.9
SR-01000690146-1	16	304457	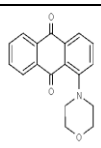	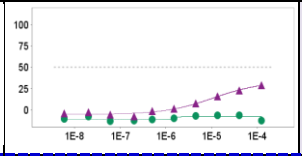	>122	29 ± 1.3	>122	-6.2 ± 0.9

SR-01000770474-1	9	950308	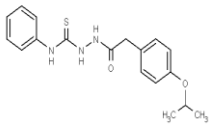	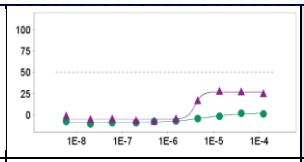	>122	28.1 ± 2.4	>122	2 ± 0.5
SR-01000702723-1	21	5760296	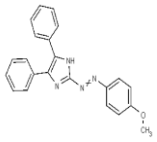	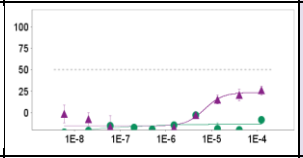	>122	25.8 ± 5.9	>122	-3.1 ± 3.1
SR-01000726172-1	24	5464544	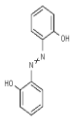	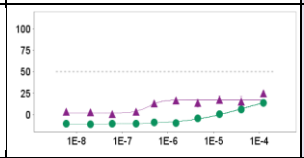	>122	24.3 ± 3.2	>122	14 ± 0.2
SR-01000743735-1	11	3898532	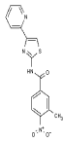	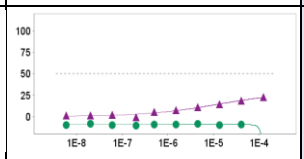	>122	22.8 ± 1.2	>122	-8.1 ± 0.5
SR-01000773609-1	47	3352410	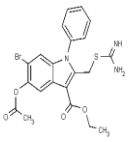	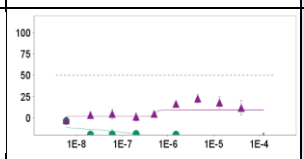	>122	22.7 ± 5.2	>122	-3.4 ± 2.1
SR-01000708865-1	16	3544983	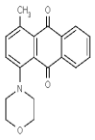	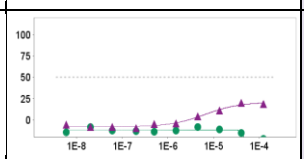	>122	19.9 ± 1	>122	-8.1 ± 1.3
SR-01000735684-1	9	1485012	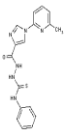	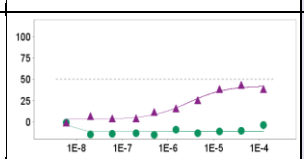	>122	43.3 ± 4.1	>122	-0.5 ± 1.1
SR-01000749125-1	9	842815	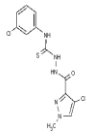	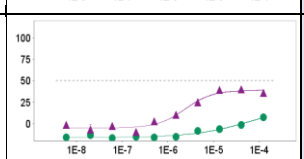	>122	39.9 ± 2.5	>122	7.3 ± 2.2
SR-01000716912-1	9	985458	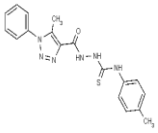	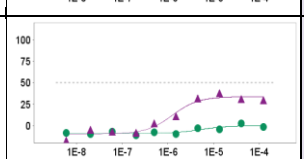	>122	37.8 ± 1.9	>122	2.6 ± 2.1
SR-01000930043-1	29	4063236	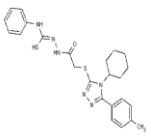	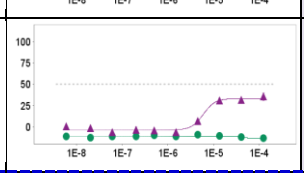	>122	35.4 ± 4.9	>122	-9 ± 0.8

SR-01000718284-1	9	2327853	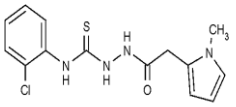	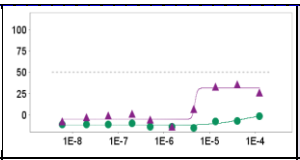	>122	35.4 ± 1.5	>122	-1.3 ± 2.6
SR-01000749456-1	9	7103604	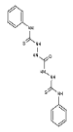	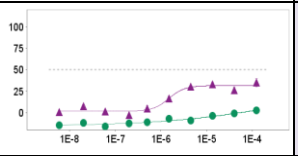	>122	35.2 ± 5.5	>122	2.9 ± 1.7
SR-01000757490-1	5	2976904	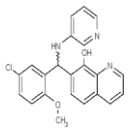	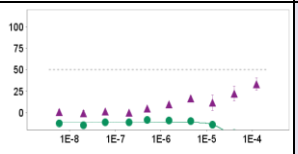	>122	33.2 ± 8	>122	-8.5 ± 1.2
SR-01000615311-1	13	204319	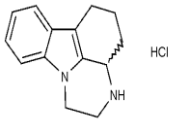	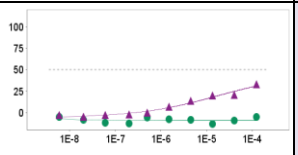	>122	32.9 ± 1.3	>122	-5.1 ± 1.2
SR-01000453998-2	5	3129248	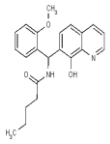	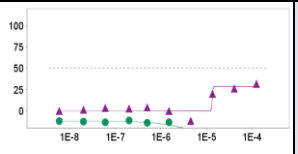	>122	31.4 ± 4	>122	-11.1 ± 0.2
SR-01000276669-2	3	970389	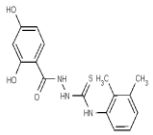	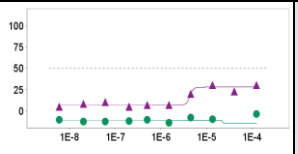	>122	30.3 ± 1.2	>122	-3.7 ± 0.2
SR-01000692831-1	33	979678	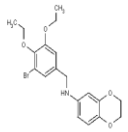	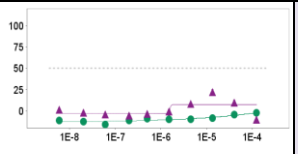	>122	21.7 ± 3.7	>122	-2.2 ± 3.5
SR-01000886951-1	36	282598	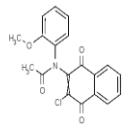	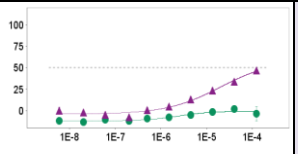	>122	46.8 ± 0.7	>122	2.1 ± 1
SR-01000770370-1	9	11900269	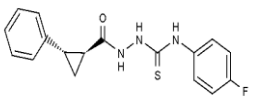	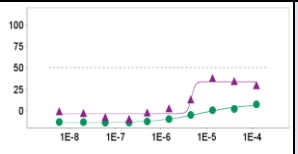	>122	37.9 ± 1.6	>122	7.1 ± 0.7
SR-01000418110-2	17	764370	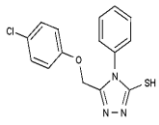	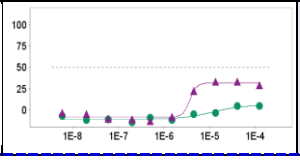	>122	33.1 ± 2	>122	4.6 ± 1

SR-01000827868-1	3	1929796	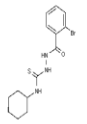	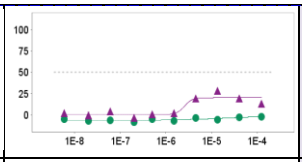	>122	28.1 ± 0.3	>122	-1.9 ± 0.5
SR-01000361106-2	3	1932975	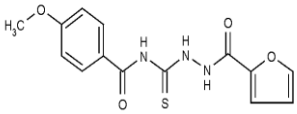	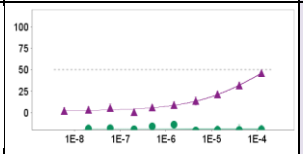	>122	46 ± 1.1	>122	-13.9 ± 2.8
SR-01000285369-2	3	2964264	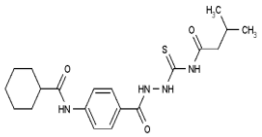	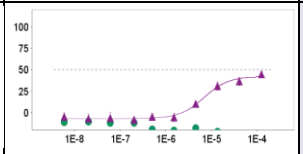	>122	44.6 ± 4	>122	-10.2 ± 0.5
SR-01000833722-1	1	2743312	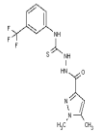	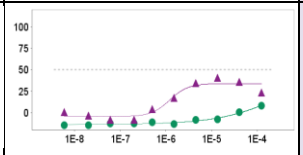	>122	40.6 ± 0.2	>122	8.1 ± 0.6
SR-01000721234-1	20	5147260	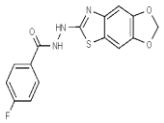	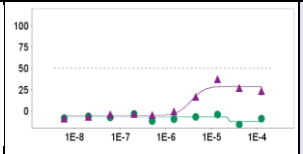	>122	37.3 ± 1.6	>122	-3.3 ± 1.4
SR-01000314503-2	9	773605	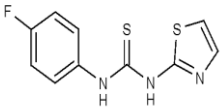	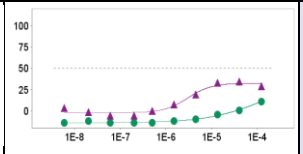	>122	34 ± 2	>122	11.1 ± 1.5
SR-01000788119-1	15	2946562	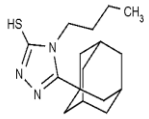	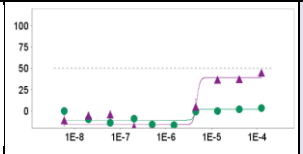	>122	44.5 ± 0.1	>122	3.5 ± 2.7
SR-01000597871-3	13	2829432	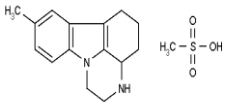	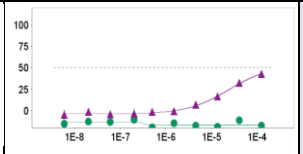	>122	42.7 ± 3.2	>122	-10.4 ± 1.3
SR-01000361280-2	2	3138360	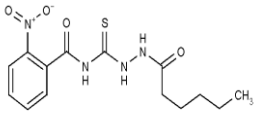	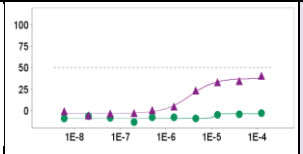	>122	40.5 ± 0.8	>122	-2.8 ± 1.6
SR-01000085782-2	15	843022	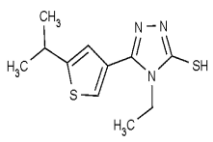	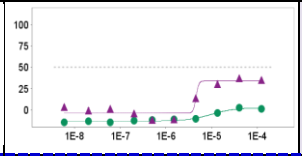	>122	37.3 ± 1.3	>122	2.5 ± 1

SR-01000702911-1	39	6859297	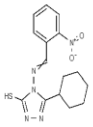	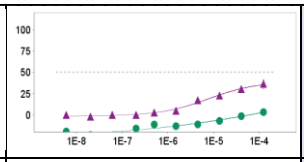	>122	36.1 ± 6	>122	3.2 ± 2.9
SR-01000832888-1	51	24818770	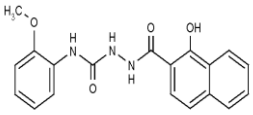	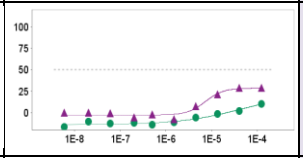	>122	28.7 ± 0.4	>122	10.3 ± 2.2
SR-01000704533-1	6	827779	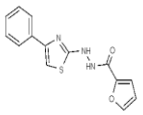	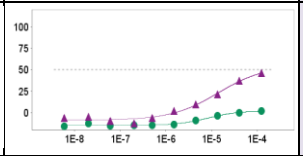	>122	46.2 ± 3.7	>122	2 ± 2.3
SR-01000768737-1	4	56642948	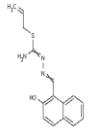	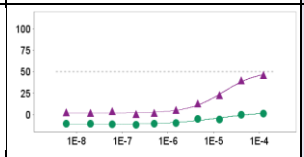	>122	46.1 ± 1	>122	1.4 ± 0.8
SR-01000009095-2	3	5191672	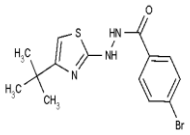	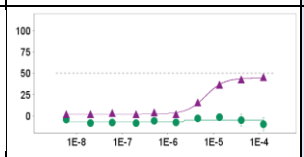	>122	45.5 ± 2.5	>122	-1.2 ± 3.2
SR-01000607277-2	54	5771294	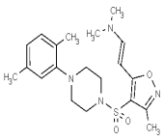	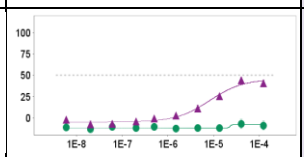	>122	44.2 ± 3.4	>122	-7.1 ± 6.4
SR-01000683873-1	1	842837	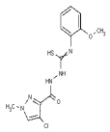	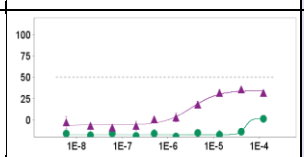	>122	35.7 ± 2.5	>122	1.6 ± 4.3
SR-01000803668-1	76	754776	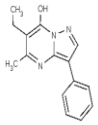	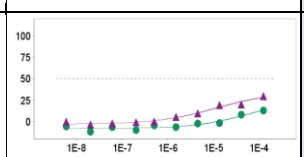	>122	29.6 ± 3.4	>122	13.1 ± 0.3
SR-01000295108-2	3	1251521	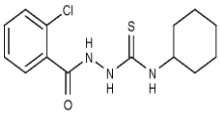	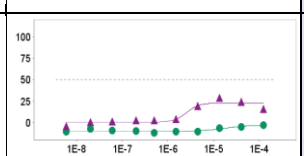	>122	28.7 ± 1.9	>122	-2.8 ± 0.5
SR-01000880129-1	30	235014	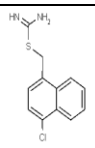	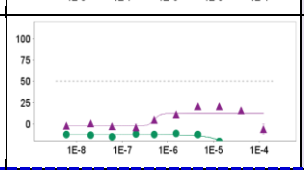	>122	20.8 ± 1.8	>122	-11.5 ± 0.2

SR-01000702344-1	21	2326682	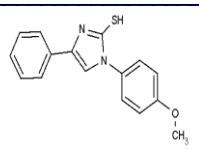	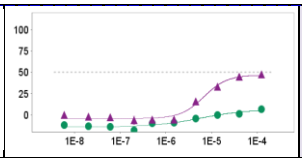	>122	47.1 ± 1	>122	6.5 ± 1.1
SR-01000275798-2	3	969905	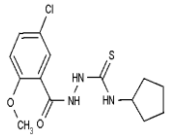	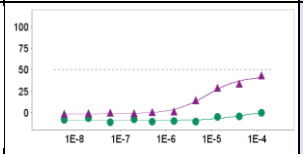	>122	43 ± 1.4	>122	0 ± 1.4
SR-01000326072-2	2	3138342	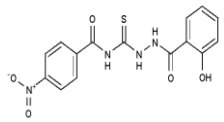	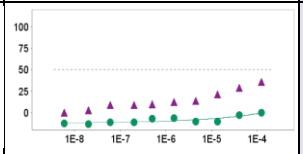	>122	36 ± 2.3	>122	0.1 ± 1.6
SR-01000723319-1	1	842656	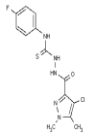	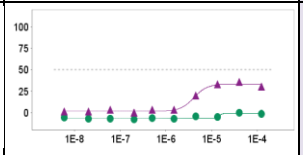	>122	35.6 ± 1	>122	0 ± 1.1
SR-01000361107-2	3	1933277	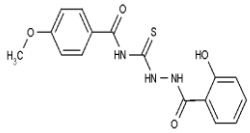	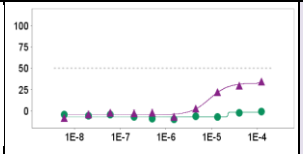	>122	34.2 ± 2.4	>122	-0.6 ± 3.3
SR-01000834653-1	78	1231795	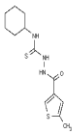	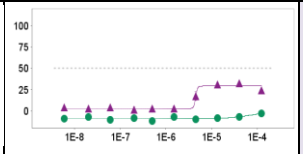	>122	32.5 ± 0.9	>122	-3.1 ± 0.2
SR-01000807218-1	3	1549394	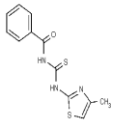	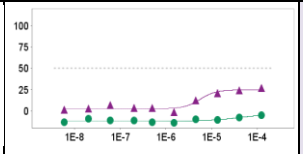	>122	26.8 ± 3.1	>122	-5.2 ± 1
SR-01000295427-2	3	1252003	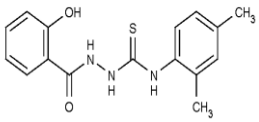	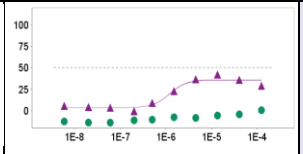	>122	41.9 ± 1.5	>122	0.5 ± 1.9
SR-01000837965-1	3	5202474	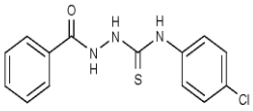	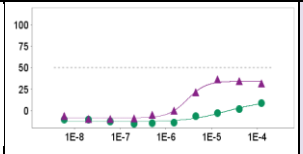	>122	36.1 ± 2	>122	8.7 ± 1
SR-01000931119-1	1	6037354	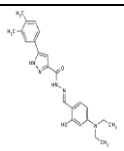	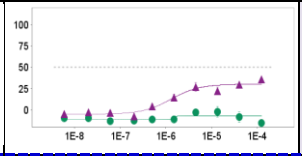	>122	35.6 ± 1.1	>122	-2.2 ± 6.8

SR-01000877149-1	17	794134	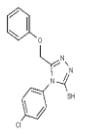	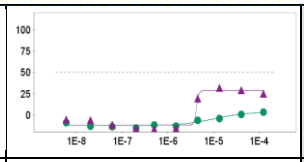	>122	31.8 ± 1.7	>122	3.1 ± 0.4
SR-01000276602-2	1	2207202	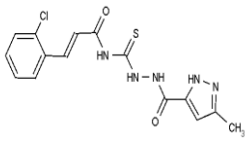	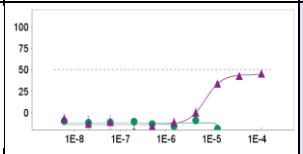	>122	45.1 ± 4.3	>122	-8.8 ± 1.3
SR-01000085984-2	15	843016	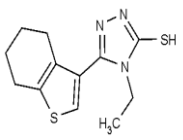	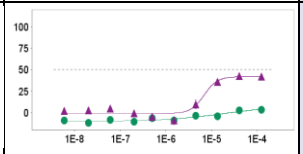	>122	42.3 ± 2.2	>122	3.6 ± 0.9
SR-01000360356-2	2	3132648	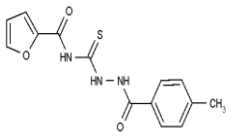	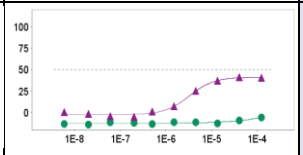	>122	41.5 ± 2	>122	-5.4 ± 1.5
SR-01000718277-1	2	5108935	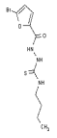	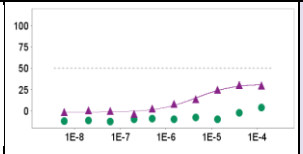	>122	30.5 ± 4	>122	3.7 ± 0.3
SR-01000709827-1	49	5399788	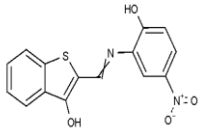	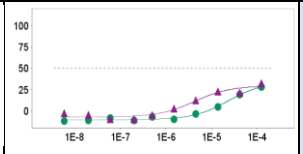	>122	32.6 ± 2.2	>122	27.9 ± 1.3
SR-01000886362-1	10	696254	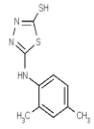	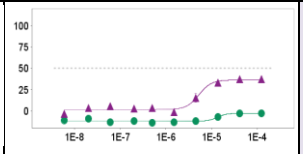	>122	37 ± 3.7	>122	-2.6 ± 3.9
SR-01000076066-4	9	719408	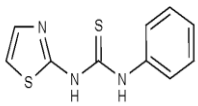	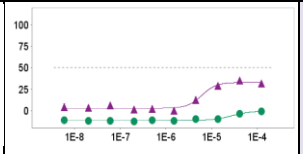	>122	35 ± 0.7	>122	-0.8 ± 1.7
SR-01000902281-1	51	387183	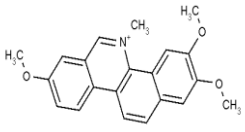	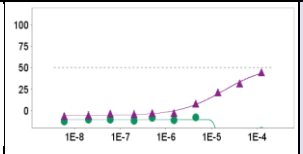	>122	44.3 ± 2.1	>122	-8 ± 1.6
SR-01000878821-1	81	241137	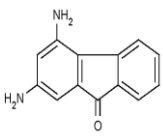	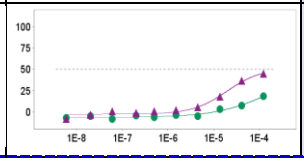	>122	44.6 ± 1.6	>122	18.2 ± 1.3

SR-01000834950-1	51	24818768	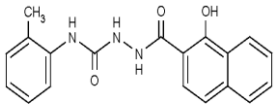	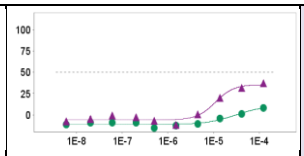	>122	37 ± 0.1	>122	8.4 ± 1.2
SR-01000882339-1	33	5469532	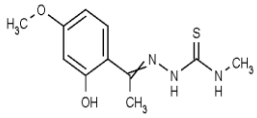	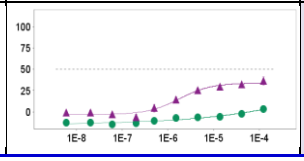	>122	36.4 ± 5.1	>122	3.6 ± 1.3